Modeling, Control, and Implementation of Compact Multilevel Converters for Power Quality Applications

by

Amirabbas KAYMANESH

MANUSCRIPT-BASED THESIS PRESENTED TO ÉCOLE DE TECHNOLOGIE SUPÉRIEURE IN PARTIAL FULFILLMENT FOR THE DEGREE OF DOCTOR OF PHILISOPHY
Ph. D.

MONTRÉAL, DECEMBER 13TH, 2021

ÉCOLE DE TECHNOLOGIE SUPÉRIEURE
UNIVERSITÉ DU QUÉBEC

BOARD OF EXAMINERS

THIS THESIS HAS BEEN EVALUATED

BY THE FOLLOWING BOARD OF EXAMINERS

Mr. Ambrish Chandra, Thesis Supervisor
Department of Electrical Engineering, École de technologie supérieure

Mr. Mohammad Jahazi, President of the Board of Examiners
Department of Mechanical Engineering, École de technologie supérieure

Mr. Maarouf Saad, Member of the jury
Department of Electrical Engineering, École de technologie supérieure

Mr. Akshay Kumar Rathore, External Evaluator
Department of Electrical and Computer Engineering, Concordia University

THIS THESIS WAS PRENSENTED AND DEFENDED

IN THE PRESENCE OF A BOARD OF EXAMINERS AND THE PUBLIC

ON DECEMBER 8TH, 2021

AT ÉCOLE DE TECHNOLOGIE SUPÉRIEURE

ACKNOWLEDGMENT

I cannot begin to express my thanks to my supervisor, Professor Ambrish Chandra, for the deep trust he put in me and the freedom of action he afforded me. His unending support, tremendous experience, priceless comments, and constructive recommendations have contributed to my continued development as a scientist.

As a member of the ÉTS GREPCI group, I have had a unique opportunity of collaborating with several great researchers who played a decisive role in the success of this project. A special thanks goes to them.

I would like to also express my deepest appreciation to the members of my Ph.D. committee who devotedly accepted to review this thesis.

Last but not least, I would like to extend my deepest gratitude to my family: my parents Mitra Yazdizadeh and Abolfazl Kaymanesh, for their unconditional love, lifelong support, and encouragement.

Modélisation, contrôle et implementation des convertisseurs compacts multiniveaux pour des applications de qualité de l'énergie

Amirabbas KAYMANESH

RÉSUMÉ

Pour garantir à tous l'accès à une énergie abordable, fiable et moderne, il est d'une grande importance d'accroître la pénétration des énergies renouvelables dans le réseau électrique. Par conséquent, les défis liés à la qualité de l'énergie doivent être considérés avec prudence. Pour cette raison, l'objectif principal de cette thèse est de développer différentes topologies de convertisseurs multiniveaux à haute densité de puissance ainsi que les contrôleurs nécessaires pour améliorer la qualité de l'énergie dans les systèmes électriques de manière efficace et fiable.

Tout d'abord, un compensateur synchrone statique basé sur des cellules U compactées modifiées à sept niveaux (MPUC7), soit (MPUC7-STATCOM), avec un contrôle prédictif (AFCS-MPC) est introduit. Par rapport à un compensateur synchrone statique basé sur un pont en H en cascade (CHB) à sept niveaux, la configuration proposée a un nombre de composants actifs/passifs exceptionnellement réduit, et le contrôle AFCS-MPC conçue par MPUC7-STATCOM est également simplifié. Le fonctionnement en mode Boost et la tension nominale plus basse des composants peuvent également être mentionnés comme qualités du MPUC7-STATCOM. De plus, les facteurs de pondération de l'AFCS-MPC proposé sont réglables automatiquement en temps réel.

Deuxièmement, une nouvelle configuration d'un ressort électrique basée sur l'onduleur modifié à cinq niveaux (MPUC5) est introduite pour atténuer les harmoniques et les fluctuations de tension à divers points du réseau en présence de sources d'énergies renouvelables. De plus, le principe de fonctionnement, la procédure de conception et la configuration du ressort électrique basé sur MPUC5, soit (MPUC5-ES), sont présentés. Un contrôleur simple et efficace, sans boucle de contrôle supplémentaire pour réguler les tensions du bus CC, a également été conçu et appliqué au MPUC5-ES.

Troisièmement, une configuration de ressort électrique à condensateur multiniveau à haute densité de puissance (ES-1) basée sur un convertisseur de cellules U à sept niveaux modifié (MPUC7), soit (MPUC7-ES1), est présentée. Une nouvelle stratégie de contrôle basée sur la commande prédictive (FCS-MPCC) est également proposée pour l'application MPUC7-ES1. Cet algorithme est conçu pour prédire le comportement du système pour tous les vecteurs de commutation possibles sur la base des modèles discrets de MPUC7-ES1 qui est développé pour la première fois. Par rapport aux méthodes de contrôle linéaire ES-1 conventionnelles, la stratégie proposée présente des avantages clés, notamment la prise en compte des modèles

dynamiques du convertisseur ES-1, elle ne nécessite pas de modulateur et possède une fréquence de commutation inférieure.

Quatrièmement, afin de fournir de l'énergie aux charges sensibles avec un niveau de fiabilité et de qualité amélioré, une topologie compacte à ressort électrique à batterie (ES-2), fondée sur l'onduleur Packed E-Cell (PEC) et sur sa stratégie de contrôle basée sur un réseau de neurones artificiels (RNA), est introduite. Du point de vue de la fiabilité, l'ES-2 basé sur le PEC (PEC-ES2) a la capacité de fonctionner instantanément de neuf à cinq niveaux en cas de défaut sur l'un des commutateurs bidirectionnels. En ce qui concerne la qualité de l'énergie, par rapport aux topologies ES-2 à demi-pont ou à pont complet, pour le PEC-ES2 la tension des commutateurs est diminuée de moitié, le contenu harmonique est inférieur dans le courant et la tension de sortie, la fréquence de commutation est considérablement plus faible, des applications de puissance plus élevée sont possibles, etc. Le contrôleur intelligent proposé basé sur un RNA peut également régler et stabiliser indépendamment à la fois la tension du réseau et le facteur de puissance de la charge réactive avec des performances dynamiques améliorées.

Les opérations en régime permanent et dynamique du ressort électrique multiniveau compact introduit et des topologies STATCOM et les techniques de contrôle proposées sont également illustrées par des simulations approfondies et des résultats expérimentaux.

Mots-clés: ressort électrique, STATCOM, convertisseur multiniveaux, MPUC5-ES, MPUC7-STATCOM, PEC-ES2, MPUC7-ES1, qualité de l'énergie, contrôle prédictif, RNA.

Modeling, control, and implementation of compact multilevel converters for power quality applications

Amirabbas KAYMANESH

ABSTRACT

To ensure access to affordable, reliable, and modern energy for all, increasing the penetration of renewable energies into the electricity grid is of great importance. Consequently, power quality-related challenges should be considered prudently. Therefore, the focal goal of this thesis is to develop various high-power-density multilevel converter topologies and the required controllers for improving the power quality of electrical systems efficiently and reliably.

First, a seven-level modified packed U-cell (MPUC7) based static synchronous compensator (MPUC7-STATCOM) with an autotuned finite control-set model predictive control (AFCS-MPC) is introduced. In comparison with a seven-level cascaded H-bridge (CHB) based STATCOM not only, the proposed configuration has exceptionally reduced active/passive component count, but also MPUC7-STATCOM designed AFCS-MPC control method complexity is attenuated meaningfully. Boost-mode operation and low voltage rating of the components can be also mentioned as the merits of the MPUC7-STATCOM. Moreover, the weighting factors of the proposed AFCS-MPC are tunable automatically and effectively in real-time.

Second, a novel configuration of electric spring based on the modified five-level packed u-cell (MPUC5) inverter for mitigating harmonics and voltage fluctuations at various points of a grid with unstable generated power from distributed renewable energy sources is introduced. Moreover, operation principles, design procedure, and configuration of the MPUC5-based electric spring (MPUC5-ES) are presented. A simple and yet efficient controller without any extra control loop for regulating DC bus voltages has been also designed and applied to MPUC5-ES.

Third, a high-power-density multilevel capacitor-based electric spring (ES-1) configuration with boost-mode operation based on a seven-level modified packed U-cell converter (MPUC7-ES1) is presented. A novel control strategy based on finite control-set model predictive current control (FCS-MPCC) is also proposed for MPUC7-ES1 application. This algorithm is designed to predict the system behavior for all the conceivable switching vectors based on the discrete models of MPUC7-ES1 that is developed for the first time. Comparing to the conventional ES-1 linear control methods, the proposed strategy has key merits including considering the dynamic models of ES-1 converter, not requiring a modulator, and lower switching frequency.

Fourth, aiming at delivering power to sensitive loads with an enhanced level of reliability and quality, a compact multilevel battery-based electric spring (ES-2) topology, founded on the Packed E-Cell (PEC) inverter, and its respective artificial neural network (ANN) based control strategy are introduced. From the reliability point of view, the PEC-based ES-2 (PEC-ES2) has the capability of instant nine to five-level operation under its bidirectional switch faulty condition. Regarding the power quality, in comparison with the half or full-bridge ES-2 topologies, PEC-ES2 has halved voltage rating switches, lower harmonic content in its output current and voltage, considerably lower switching frequency, higher power applications, etc. The proposed intelligent ANN-based controller can also tune and stabilize both the grid voltage and responsive load setup power factor independently and instantly with improved dynamic performance.

Steady-state and dynamic operations of the introduced compact multilevel electric spring and STATCOM topologies and the proposed control techniques are also illustrated through extensive simulation and experimental results.

Keywords: electric spring, STATCOM, multilevel converter, MPUC5-ES, MPUC7-STATCOM, PEC-ES2, MPUC7-ES1, power quality, model predictive control, ANN.

TABLE OF CONTENTS

Page

LIST OF TABLES

Page

LIST OF FIGURES

Page

LIST OF ABREVIATIONS

ABC	Artificial Bee Colony
AC	Alternative Current
ANN	Artificial Neural Network
CHB	Cascaded H-Bridge
DC	Direct Current
DSM	Demand Side Management
DSP	Digital Signal Processor
ES	Electric Spring
FC	Flying Capacitor
FPGA	Field Programmable Gate Array
MMC	Modular Multilevel Converter
MPC	Model Predictive Control
MPUC	Modified Packed U-Cell
NPC	Neutral Point Clamped

PCC	Point of Common Coupling
PEC	Packed E-Cell
PI	Proportional Integral
PLL	Phase-locked loop
PUC	Packed U-Cell
PWM	Pulse Width Modulation
RCD	Radial-Chordal Decomposition
SHE	Selective Harmonic Elimination
STATCOM	Static VAR Compensator
SVM	Space Vector Modulation
THD	Total Harmonic Distortion

INTRODUCTION

Most climate scientists believe that human influence has been the main cause of the current global warming trend through the expansion of the greenhouse effect (Pachauri, Mayer, & Intergovernmental Panel on Climate Change, 2015). It is unfortunate but true that the burning of fossil fuels like coal and oil has dramatically increased the concentration of heat-trapping greenhouse gases into the atmosphere over the last century. There are many negative effects of global warming, including, but not limited to, more frequent severe weather, shifting wildlife populations and habitats, rising sea levels, and higher wildlife extinction rates. The most vital solution is reducing the demand for fossil fuels by increasing the penetration of renewable energies like solar, wind, biomass, and geothermal into power systems. It is worth mentioning that as of 2017, renewable energy sources including hydropower accounted for an estimated 25% of the global power generation mix (*World Energy Outlook-2017*, 2017). However, achieving the goal of having a world powered by wind, water, and sunlight has certain challenges to the reliability, stability, and power quality of the bulk power system.

Since generated power by the non-dispatchable renewable energy resources fluctuates, they do not correlate with consumer load demand in real-time. Therefore, power quality concerns such as voltage stability need to be considered. Regarding mitigating different power quality issues, recently, through the application of power electronics to power systems, various real-time methods have been proposed. In this regard, the static synchronous compensator (STATCOM) and electric spring (ES) technologies are of great importance for mainly compensating reactive power accurately and instantly. Primarily, two-level voltage source converters have been employed as single-phase STATCOM and ES. Nevertheless, in comparison to these conventional configurations, multilevel ES/STATCOM topologies such as cascaded H-bridge (CHB) (Ge & Gao, 2018), flying capacitor (FC) (Shukla, Ghosh, & Joshi, 2007), and neutral point clamped (NPC) (Chivite-Zabalza, Izurza-Moreno, Madariaga, Calvo, & Rodríguez, 2013) can offer crucial merits. Lower switching frequency, improved electromagnetic interference and *dv/dt*, enhanced power quality performance that is due to the quasi-sinusoidal voltage and current waveforms, and higher efficiency are just some of them. However,

requiring an augmented number of active/passive components, complexity, and being bulky/costly are considered as their demerits.

Motivation and Challenges

Considering the mentioned issues, various compact multilevel converters have been introduced by researchers for a wide range of power system applications. Among the conventional and recently introduced multilevel voltage source converters, Packed U-Cell (PUC) based bidirectional topologies such as seven-level modified PUC (MPUC7) and nine-level Packed E-Cell (PEC9) have numerous encouraging advantages (Kaymanesh, Chandra, & Al-Haddad, 2021). Requiring the least possible number of independent/dependent dc sources, reduced number of passive/active components, availability of extra switching combinations, lower voltage stress, high reliability concerning their multilevel operation, and noticeable dynamic performance during intensive transients are some of the main merits. Consequently, these high-power-density multilevel converters are suitable options for high-power low/medium voltage industrial applications. Although by far these topologies have been employed for different applications like renewable energies integration (Vahedi, Sharifzadeh, & Al-Haddad, 2018), they have not been analyzed and developed for ES and STATCOM utilizations yet.

Therefore, to diminish the size and cost of multilevel ES/STATCOM converters with an improved complexity as well as having enhanced efficiency, investigating configurations that have the capability of generating more voltage levels with the least possible component count is key. Besides, by considering the dynamic models and nonlinearities of these novel ES/STATCOM multilevel configurations, multifunctional control methods such as finite control set model predictive control (FCS-MPC) should be designed and applied to them to support their superior steady-state and dynamic performance. Instantaneous and accurate regulation of the auxiliary capacitors' voltages with reduced voltage ripples as well as reducing the switching frequency are also some of the important challenges. Nonetheless, it should be considered that increased complexity and computational burden are unfavorable features for a controller, especially for industrial utilizations.

Research Objectives

The main objective of this thesis is focused on mathematical modeling, control, simulation, and real-time implementation of compact multilevel converters for single-phase electric spring and STATCOM applications to improve the power quality of a weak electrical system.
The sub-objectives of this thesis are highlighted as:

Proposing and implementing high-power-density multilevel topologies for capacitor-based ES (ES-1), battery-based ES (ES-2), and STATCOM applications with features such as reduced component count, high-power quality performance, and boost-mode operation;

Developing a simple but multifunctional control method for independent and concurrent mitigation of both harmonics and voltage fluctuations of a critical load in a weak power system using a compact multilevel capacitor-based ES;

Designing novel model predictive based nonlinear control approaches for the proposed high-power-density multilevel STATCOM and ES-1 configurations focused on improving voltage stability of power systems;

Development of a multifunctional intelligent controller and a modulation technique for the introduced compact multilevel ES-2 topology with the main goal of stabilizing voltage and power factor correction concurrently and independently with enhanced reliability and transient operation in an electrical grid with high penetration of renewable energy resources.

Methodology

The employed methodology for achieving the objectives of this thesis is dividable into five main stages:

Literature review: First and foremost, to form a strong basis for high-quality, innovative, and impactful research, numerous recently published exemplary articles mainly focused on different types and features of multilevel converters, as well as various versions of currently available ES/STATCOM topologies and controllers, have been selected, thoroughly analyzed, and simulated. It is worth mentioning that due to the importance of this step, it lasted until the end of the Ph.D. program.

Operation principles: Based on the mentioned objectives, operating principles, including detailed designs and configurations, of the proposed ESs and STATCOM are analyzed and presented. The design process mainly consists of calculating the independent and/or dependent dc links voltages, amounts of the inductive and/or capacitive components of the required output filters, and capacitance values of auxiliary capacitors. On the other hand, regarding the proposed ES/STATCOM configurations, switching states, employed modulation techniques, required semiconductor switches, and their current and voltage ratings, and dc sources are all clarified. Moreover, thorough comparisons with the already available technologies have been done.

Mathematical modeling: Considering designing and developing the required controllers, the mathematical modelings of the introduced ES/STATCOM configurations have been performed. Consequently, their dynamic models and nonlinearities have been considered in the designed advanced controllers.

Simulation: In order to extensively analyze and verify the steady-state and dynamic performance of the developed ES/STATCOM configurations and controllers in a safe and efficient manner, MATLAB/Simulink, as a block diagram multi-domain environment, has been employed for simulations.

Experimental setup: To experimentally illustrate the operation and viability of the proposed ES/STATCOM multilevel topologies and controllers, experimental results are also presented. In the experiments, a 28-amp three-phase variable autotransformer (480V ac input to 0-560V

ac output voltage) has been used as a controlled voltage source. Regarding running the designed controllers with a fixed sampling time in real-time, MicroLabBox (DS1202), which is a compact rapid control prototyping (RCP) system, has been also utilized. Moreover, high current/voltage measurements (OP8662), gate drivers, an isolation card, a power analyzer, and an oscilloscope have been employed. Besides, using IGBT (FGA30N60LSD) and MOSFET (C3M0120090D) switches, prototypes of the proposed compact multilevel ESs/STATCOM are implemented.

Thesis Contribution

The key contributions of this thesis are highlighted below briefly.

A new seven-level STATCOM topology (known as MPUC7-STATCOM) with promising features such as being compact, high-power quality performance, improved complexity, boost-mode operation, and the reduced active/passive component count is proposed.

An FCS-MPC-based controller with reduced complexity/computational burden is designed and applied to MPUC7-STATCOM. Employing the designed controller results in fast regulation of the capacitors' voltages with improved overshoots and settling times especially during transients and availability of parametric mismatches.

An intuitive and simplified online weighting factors autotuning method for the designed model predictive-based MPUC7-STATCOM controller is developed.

In comparison to the MPUC5-based STATCOM (Vahedi, Dehghanzadeh, & Al-Haddad, 2018), although the size of utilized capacitors is reduced, not only voltage distortion of these capacitors is decreased but also the power quality characteristics of the generated compensation voltage and current have been improved. So, the size/cost of the required output filter is also reduceable. MPUC7-STATCOM comparison with the single-phase seven-level CHB STATCOM, as well as its merits, are also presented.

A novel five-level reduced component counts ES-1 converter topology has been proposed. This five-level modified packed u-cell (MPUC5) based ES-1 (MPUC5-ES) improves the operations and power quality characteristics of a capacitor-based electric spring from various points of view. For instance, MPUC5-ES has a boost mode operation with a halved voltage at dc links and reduced/fixed switching frequency.

The operation principles and systematic design of an MPUC5-based smart load have been presented.

A simplified control method and a modulator have been developed for mitigating both harmonics and voltage fluctuations of a critical load simultaneously in a weak electrical grid with high penetration of renewable energies using the introduced MPUC5-ES.

Voltage/power regulation of the introduced five-level ES-1 employed auxiliary capacitors are integrated into the designed modulation technique. This technology is developed for capacitor-based electric spring applications for the first time.

For the first time, a five-level electric spring using capacitors as its energy storage element has been proposed for mitigating both harmonics and voltage fluctuations simultaneously.

A seven-level capacitor-based electric spring titled ‘MPUC7-ES1’ with boost mode performance is proposed. This highly compact seven-level capacitor-based electric spring employs only six semiconductor switches and two reduced-size capacitors.

Concerning demerits of existing ES-1 linear proportional-integral (PI) controllers, a nonlinear hybrid controller based on finite control set model predictive current control (FCS-MPCC) with a controlled switching frequency is designed and proposed. In comparison to MPUC5-ES (Kaymanesh & Chandra, 2020), the dc-link capacitors’ dynamics and converter/output filter nonlinearities are considered in the controller design. So, each one of the capacitors is independently modifiable to the desired voltage level. Consequently, not only the power

density of MPUC7-ES1 topology will be improved but also it can be operational in a seven-level mode with an even more improved power quality performance.

The MPUC7-ES1 state-space average model is developed and presented.

Concerning the inherent topological demerits of the two-level battery-based electric spring configurations, an intelligent compact nine-level PEC-based ES-2 (PEC-ES2) is proposed. In addition to the general merits of utilizing a compact multilevel inverter as ES-2, the proposed PEC-ES2 has dedicated advantages. First, PEC-ES2 has the capability of five-level operation under faulty bidirectional power switch conditions. Second, PEC-ES2 requires the least possible number of components as a nine-level high power density ES-2.

Adjustment of the developed PEC-ES2 dc-link voltage does not compel an intricate controller and is achieved using an active voltage tuning method integrated into the proposed hybrid PEC-ES2 modulator with only one voltage sensor.

Design and operating principles of the introduced PEC-ES2 are presented.

A novel multifunctional ES-2 controller based on artificial neural network (ANN) and radial-chordal decomposition (RCD) theory is proposed for concurrent and independent regulation of both sensitive loads (SLs) voltage and responsive load (RL) power factor with an enhanced transient operation.

Thorough comparative studies among the proposed ES-1, ES-2, and STATCOM compact multilevel topologies and controllers and the existing configurations and control methods have been performed.

Extensive simulations and real-time implementations of all the developed ES and STATCOM configurations and controllers have been done.

The results of this thesis have been published in four peer-reviewed IEEE journals. The first journal paper titled ‘Electric Spring Using MPUC5 Inverter for Mitigating Harmonics and Voltage Fluctuations’ is published in IEEE Journal of Emerging and Selected Topics in Power Electronics (Kaymanesh & Chandra, 2020). The second journal paper titled ‘Model Predictive Control of MPUC7-Based STATCOM Using Autotuned Weighting Factors’ is published in IEEE Transactions on Industrial Electronics (Kaymanesh, Chandra, et al., 2021). The third journal paper titled ‘PEC Inverter for Intelligent Electric Spring Applications Using ANN-Based Controller’ is published in IEEE Journal of Emerging and Selected Topics in Industrial Electronics (Kaymanesh, Babaie, Chandra, & Al-Haddad, 2021b). The fourth and last journal paper titled ‘Model Predictive Current Control of Multilevel Smart Load Based on MPUC7 Converter’ is published in IEEE Access (Kaymanesh, Babaie, Chandra, & Al-Haddad, 2021a). In addition, the results of this thesis have been presented more than eleven times at various well-known prestigious international conferences such as the 2020 and 2021 IEEE Industry Applications Society Annual Meeting, IECON 2020 The 46th Annual Conference of the IEEE Industrial Electronics Society, etc.

Thesis Outline

This thesis is divided into five main chapters. CHAPTER 1 is focused on presenting a thorough literature review on topologies and controllers of various generations of currently available STATCOMs and electric springs. Considering improving voltage stability of single-phase power systems, a new seven-level high-power density STATCOM configuration based on MPUC7 converter with an autotuned finite control-set model predictive control is proposed and experimentally validated in CHAPTER 2. CHAPTER 3 presents a novel capacitor-based electric spring topology employing MPUC5 converter, as well as its simplified controller and modulator, for mitigating harmonics and voltage variations of critical loads available in a weak power system. In this chapter, simulation and experimental results are also presented to validate the introduced five-level ES-1 and its controller. CHAPTER 4 develops and proves the viability of a finite control set model predictive current control of a multilevel smart load based on an MPUC7 converter exhaustively. CHAPTER 5 mainly covers the mathematical

modeling, development, simulations, and experimental validation of an intelligent battery-based electric spring using a PEC converter. The PEC-ES2 ANN-based control strategy and hybrid modulation technique are also detailed in this chapter. Finally, concluding remarks and some ideas regarding future works are also presented.

CHAPTER 1

LITERATURE REVIEW OF STATCOMS AND ELECTRIC SPRINGS

1.1 Introduction

There are various definitions of electric power quality (PQ) in numerous articles and books. However, it is commonly defined as a benchmark to show how much voltage, current, and/or frequency of an electrical system conform to established standards by technical organizations like the Institute of Electrical and Electronics Engineers (IEEE) (Singh, Chandra, & Al-Haddad, 2014). Generally, poor power quality performance will result in malfunction or even failure of both utility and consumer electrical equipment. More importantly, the loss of productivity in industries and businesses that can be directly resulted from these equipment failures should be also considered. Consequently, analyzing and mitigating power quality problems is critically important. There are various causes behind the power quality problems in electrical systems, including but not limited to lightning strikes, severe weather, large loads ON-OFF, nonlinear loads, unbalanced loads or utility supplies, faults, and equipment failure. As a result, some of the major power quality issues at the point of common coupling (PCC) are voltage and frequency fluctuations, harmonics, and low power factors.

The majority of these power quality issues, which are propagatable to other parts of the network, can be originated from both utilities and consumers. In this regard, on the one hand, it is the utilities' responsibility to provide high-quality power for consumers. On the other hand, consumers should not cause distortions that can have negative impacts on other users. Therefore, considering mitigating power quality issues in the electrical system, several techniques and equipment have been proposed and employed. Passive components including reactors and capacitors, passive/active/hybrid filters with various series and parallel combinations, shunt-mounted flexible AC transmission system (FACTS) equipment such as static VAR compensator (SVC), static synchronous series compensator (SSSC) and STATCOM, and demand-side management techniques like energy storage system and electric

spring are just some of them. Among these methods, STATCOM and, more recently, electric spring, which are power electronics-based approaches, have the main merits of being relatively cost-effective, accurate, instant, multifunctional, and real-time. Hence, various aspects of these reactive power compensation techniques have been investigated comprehensibly by engineers and researchers. Correspondingly, different types of STATCOM and electric spring topologies, controllers, and applications have been proposed and developed for low and medium-voltage microgrids and power systems.

Recently, due to poor PQ operation and inherent topological demerits of conventional two-level STATCOM and electric spring configurations, they are being replaced by multilevel ones. So, utilization of these techniques for higher power applications can be a more viable option. By far, different two-level and multilevel STATCOM and ES structures have been proposed where each one of them has its specific merits and demerits which make it more suitable for a particular operation. Classical multilevel converters such as CHB (Nasiri, Farhangi, & Rodríguez, 2019) and NPC (Kaymanesh, Rezkallah, Saeedi, & Chandra, 2020) can be also employed as STATCOM or ES. Nonetheless, increased component count and complexity are two major issues of these structures. Thus, the trend should be developing novel compact multilevel STATCOM and ES topologies that have improved power quality characteristics with the least plausible components. Regarding the development of high-power-density STATCOM and ES configurations, their control methods should be also taken into account as a result of their considerable impact on both steady-state and dynamic operation of the system. On the one hand, considering dynamic models of a compact STATCOM/ES multilevel configuration in its controller is key. On the other hand, increased complexity and computational burden are not favorable features of a controller, especially for industries. So, it is also required to move toward intuitive and simplified nonlinear controllers rather than linear ones. Finally, in view of STATCOM and ES applications, the multifunctional operation of these real-time reactive power compensators increases the reliability and efficiency of the electrical system. Accordingly, to have a thorough understanding of already available STATCOM and ES topologies, controllers, and applications, in this chapter, an extensive literature review is done.

1.2 STATCOM Converter Configurations, Controllers, and Applications

STATCOM is a power electronics-based shunt-type FACTS equipment designed to enhance voltage stability, increase the transmission capability of ac lines, and improve the power factor through injecting/absorbing reactive power accurately and instantly. Generally, it is made up of a converter with capacitors as the energy storage components on its dc side, a coupling inductive filter on its ac side, and a controller. A wide range of two-level/multilevel topologies, linear/nonlinear controllers, and monofunctional/multifunctional applications have been proposed for STATCOM converters. Some of them are reviewed as follows.

1.2.1 Full-Bridge STATCOM

A single-phase full-bridge STATCOM topology is introduced recently. As can be seen in Figure 1.1, this two-level STATCOM consists of a capacitor-based full-bridge converter and an inductive output filter (Isobe, Shiojima, Kato, Hernandez, & Shimada, 2016). Normally, for generating reactive power, produced voltage by a STATCOM converter should be higher than the grid voltage. Accordingly, the minimum voltage rating of the required capacitor and semiconductor switches in this topology should be equal to the peak value of its dc-link voltage. The two-level waveform of the generated compensation voltage, which has noticeably high harmonics contents, is yet another demerit of this STATCOM topology. However, employing a reduced-size film capacitor and improved switching loss are the merits of this proposed full-bridge STATCOM. A PI-based controller with a novel modulator and capacitor voltage regulator is also developed in this work. Finally, it should be noted that in this work steady-state performance of the proposed STATCOM topology and controller is focused and their transient characteristics are not investigated properly.

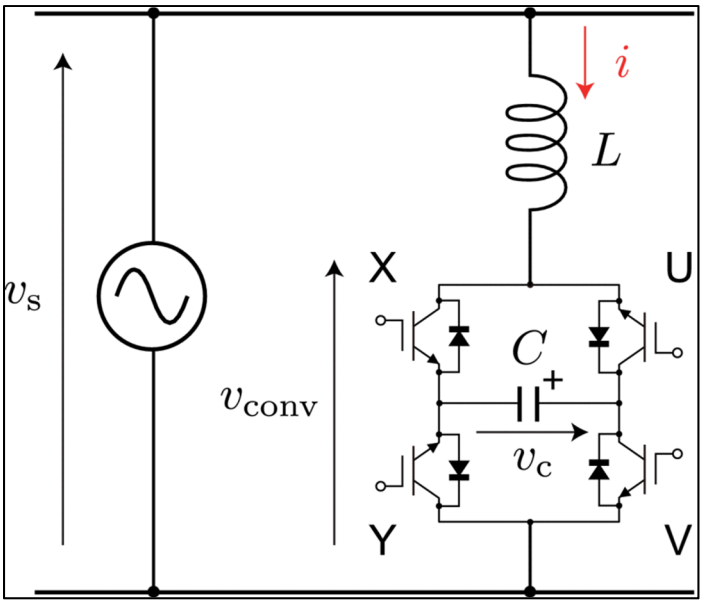

Figure 1.1 Topology of a full-bridge STATCOM
Taken from Isobe (2016)

1.2.2 Cascaded H-bridge Multilevel STATCOMs

Due to its modularity, the possibility of fault-tolerant operation, structural simplicity, transformerless operation, and extensibility, the cascaded H-bridge converter has been the most common multilevel topology employed as STATCOM. Generally, CHB topology for applications like renewable energy integration requires several isolated dc sources which can be costly, complicated, and bulky. However, for STATCOM utilization this issue is also resolved as these isolated dc sources are replaced by capacitors as the passive energy storage elements. Figures 1.2 and 1.3 illustrate a schematic diagram of a three-phase CHB-based STATCOM and the structure of each H-bridge cell, respectively (Sajadi, Iman-Eini, Bakhshizadeh, Neyshabouri, & Farhangi, 2018). Capacitive dc-links voltage balancing, fault-tolerant performance, reduction of switching losses and capacitor voltage ripple, reducing the size of the required capacitors, asymmetric performance, selective harmonic mitigation, and developing simplified nonlinear controllers are some of the main focuses of already available works on CHB-based STATCOMs, which are described below.

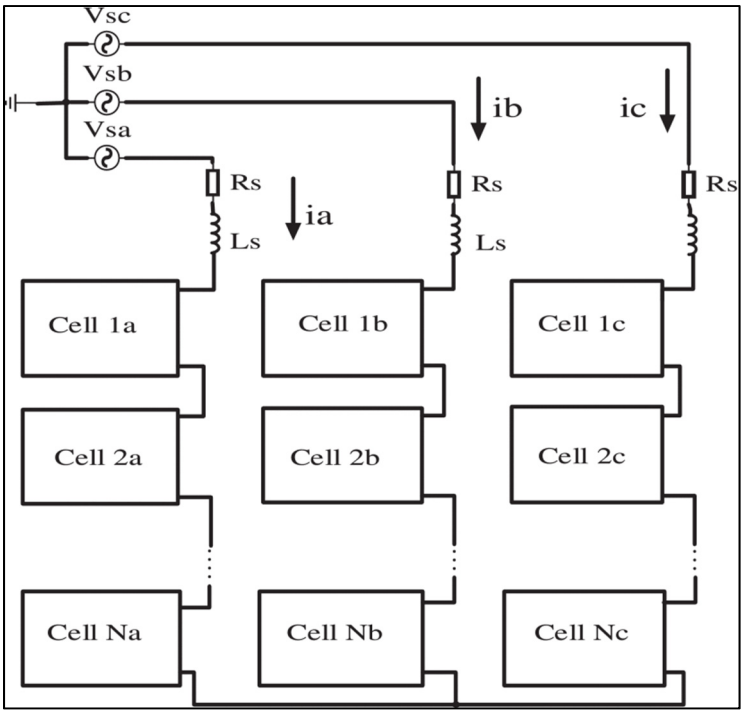

Figure 1.2 A three-phase CHB-based STATCOM
Taken from Sajadi (2018)

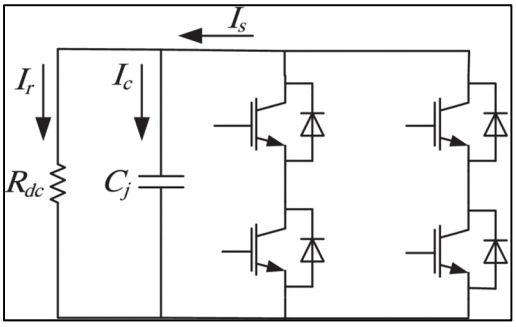

Figure 1.3 Each cell in Figure 1.2
Taken from Sajadi (2018)

1.2.2.1 Cascaded H-Bridge STATCOM Capacitive Dc-Links Voltage Balancing

In a CHB-based STATCOM topology, it is important to keep the dc side voltages of all the cells balanced. However, the power losses of different H-bridge cells are not identical. In this regard, demanded active power of each cell should be equal to its power losses. Consequently, to control each dc-link voltage of a CHB STATCOM independently, a novel voltage balancing

approach has been proposed (Barrena, Marroyo, Rodriguez Vidal, & Torrealday Apraiz, 2008). This method not only resolves the issues related to the capacitors' voltage balancing but also distributes the required reactive power among all the employed H-bridge cells in an equal manner. Control loops of active and reactive power of the proposed multilevel STATCOM are demonstrated in Figure 1.4. Besides, a schematic of the designed method for regulating active power distribution is presented in Figure 1.5 (Barrena et al., 2008). It should be also noted that this method can be operational with any modulation method.

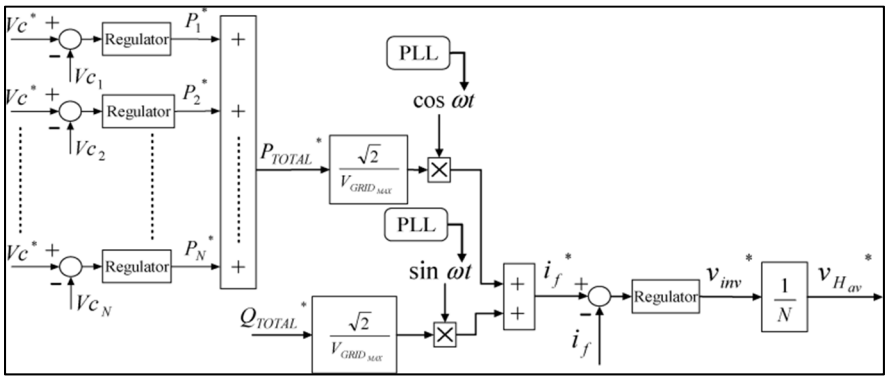

Figure 1.4 Control loops of a STATCOM active/reactive power
Taken from Barrena (2008)

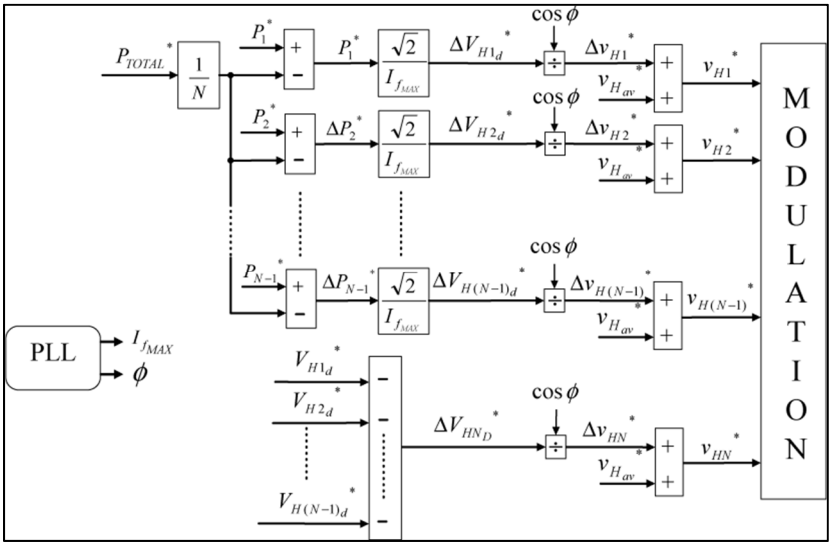

Figure 1.5 Schematic of the active power distribution method
Taken from Barrena (2008)

On the other hand, as a result of coupling phenomena, the operation of distinct voltage controllers, which balance dc links voltages individually, can have negative effects on the rest of the controller subsystems, namely the output current controller and the group voltage controller. Consequently, authors in (Farivar, Hredzak, & Agelidis, 2016) have proposed a decoupled controller suitable for single-phase and three-phase CHB-based STATCOMs. Based on this novel method, two main decoupling circumstances are defined. Firstly, the summation of the squares of the dc-link voltages in the cluster voltage regulator subsystem should be fixed. Second, the summation of the applied changes by the separate voltage controllers to the cells' output voltages must be equal to zero. The diagram of the introduced decoupled control technique is depicted in Figure 1.6. Finally, the dynamic operation of the proposed decoupled controller is demonstrated experimentally using a prototype of a single-phase seven-level CHB STATCOM.

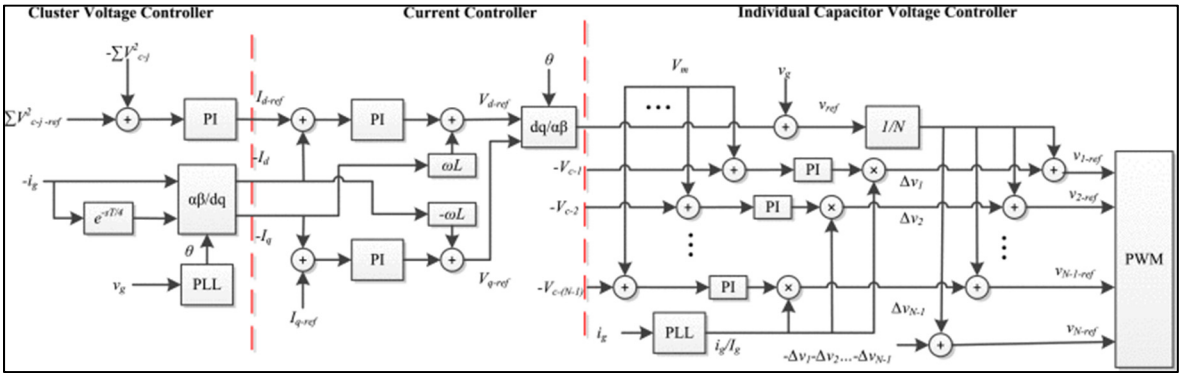

Figure 1.6 Diagram of a CHB-based STATCOM decoupled control technique
Taken from Farivar (2016)

1.2.2.2 Cascaded H-Bridge STATCOM Fault-Tolerant Operation

Failed performance of a STATCOM topology will jeopardize the power quality and stability of an electrical power system. As a direct result of an increased number of passive and active components employed in a CHB-based STATCOM especially for medium voltage higher power applications, it is critical to analyze the reliability of this converter topology. Therefore, several fault-tolerant strategies have been proposed in the literature. In (Song & Huang, 2010), it is proposed to employ one extra H-bridge cell in each phase as a backup. To increase the

system reliability, these available redundancies in the H-bridge cells of CHB-based STATCOM configuration are then utilized. Consequently, as an instance, a five-level CHB STATCOM with the extra cells in a normal performance will be operational as a seven-level topology. However, as illustrated in Figure 1.7 in the case of failure, the problematic cells will be bypassed and the system will continue its performance with a five-level output voltage waveform. Moreover, Figure 1.8 demonstrates a simplified scheme of the developed controller and the employed CHB-based STATCOM converter model. Considering both steady-state and transient operations, this introduced method is validated for both five-level and seven-level three-phase CHB STATCOM applications. It can be also employed for topologies with even more voltage levels. Nonetheless, two points should be also considered. First, an amplified number of components increases the chance of failures inevitably. Second, the increased volume, cost, and complexity of this multilevel STATCOM topology is a critical issue that cannot be ignored.

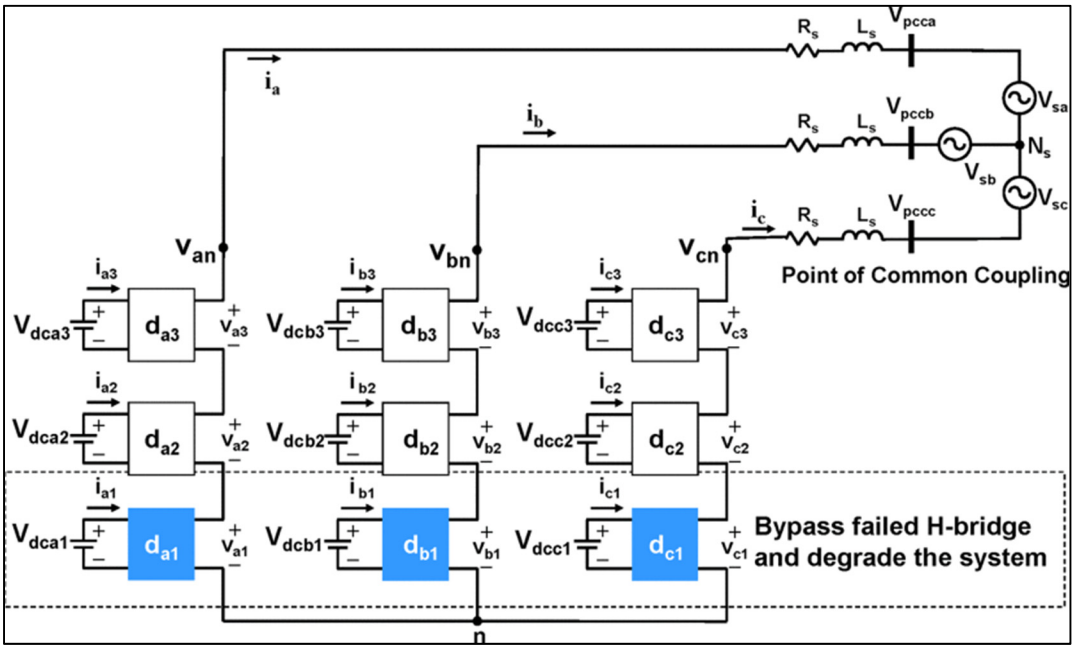

Figure 1.7 Schematic of a five-level CHB STATCOM with the extra cells
Taken from Song (2010)

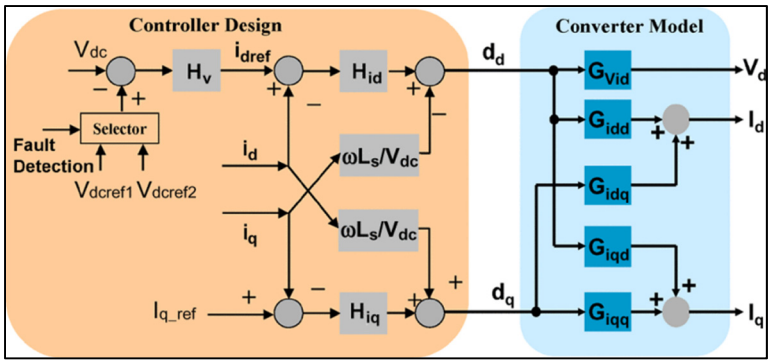

Figure 1.8 CHB STATCOM controller with fault-tolerant
Taken from Song (2010)

1.2.2.3 Reduction of Switching Loss/Capacitor Voltage Ripple of CHB STATCOM

High switching loss is in direct connection with the reduced operational efficiency of a CHB-based STATCOM. Moreover, capacitor voltage ripple has negative effects on the capacitor's lifetime, and increased size capacitors will be also required. These are critical issues that should be considered to improve the efficiency, reliability, and power density of any multilevel STATCOM configuration. Consequently, in (Townsend et al., 2013), it is proposed that extra switching vectors available in a CHB STATCOM converter make it possible to tradeoff among harmonics content of the generated voltage, losses due to switching, and voltage ripple of the capacitors. To effectively optimize this tradeoff, by using novel heuristic mathematical models, a nonlinear model predictive control (MPC) method is designed and developed. The stability of this MPC-based controller has been also proven. In comparison to a conventional space vector modulation (SVM), it should be mentioned that although the SVM technique can effectively control the switching frequency even better than the introduced controller, it has negative impacts on the dc-links capacitors lifetime. Furthermore, it is proven that this MPC-based method has superior performance compared with the PWM approach which is extensively employed by industries. However, the computational burden and complexity of the developed controller for CHB-based STATCOM application is still an unsolved problem. A simplified schematic of this controller is illustrated in Figure 1.9.

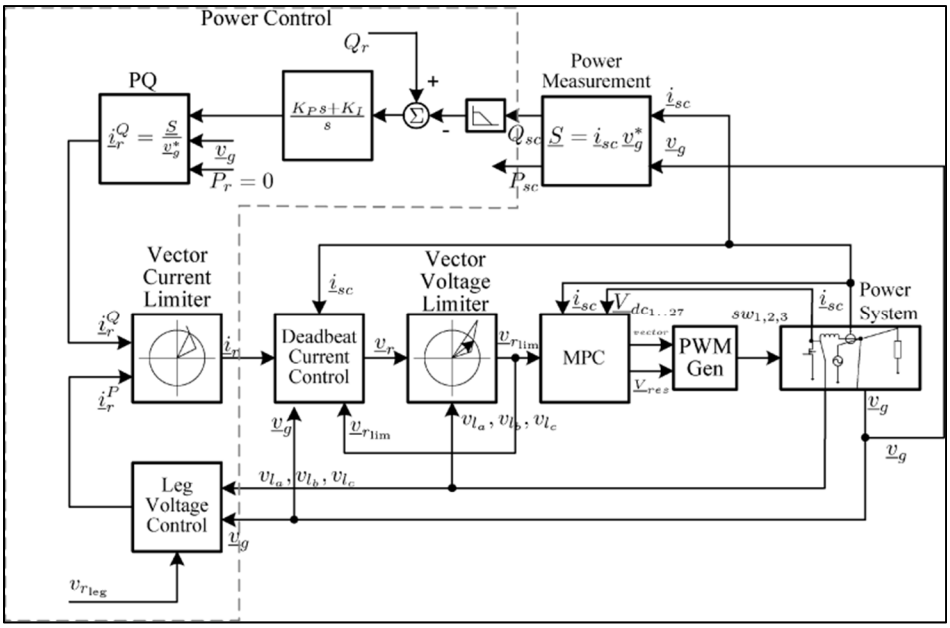

Figure 1.9 Illustration of MPC controller applied on a CHB STATCOM
Taken from Townsend (2013)

1.2.2.4 Reducing the Size of CHB-Based STATCOM Capacitors

Recently electrolytic capacitors are being replaced by film capacitors which are considered more reliable options. However, at the same capacitance value, film capacitors are relatively bulkier. This limits film capacitors utilizations especially for multilevel converters. From this perspective and considering reducing the required capacitance value, an innovative CHB-based STATCOM system has been proposed (Farivar, Townsend, Hredzak, Pou, & Agelidis, 2017). The main idea is to develop a multilevel STATCOM system that can be functional even with highly increased voltage ripples on dc links capacitors. However, the augmented amount of voltage ripples should be almost the same as the calculated theoretical limits. Therefore, in contrast with conventional STATCOM systems, this amplified voltage ripple makes it possible to improve the power density of a CHB-based STATCOM by reducing its capacitors' cost and volume. Another feature of this multilevel STATCOM system is its V-I asymmetric characteristic that is particularly suitable for reactive power compensation equipment. In this regard, the operational range of this introduced CHB-based STATCOM system expressed as per-unit is illustrated in Figure 1.10. A controller with a high bandwidth is also designed for

this CHB STATCOM with reduced capacitance value to effectually tune the dc links voltages even during severe transient operation, which is shown in Figure 1.11. By this system, the voltage stress on the switching components will be also lower that also has a positive impact on the system's reliability. Finally, it has been experimentally proven that, first, through the proposed CHB STATCOM system, although the harmonics content of generated current is improved, the size of the employed capacitors is decreased by about 80% compared with classical designs. Second, this system can be operational even with more than 90% voltage ripples on the dc links capacitors.

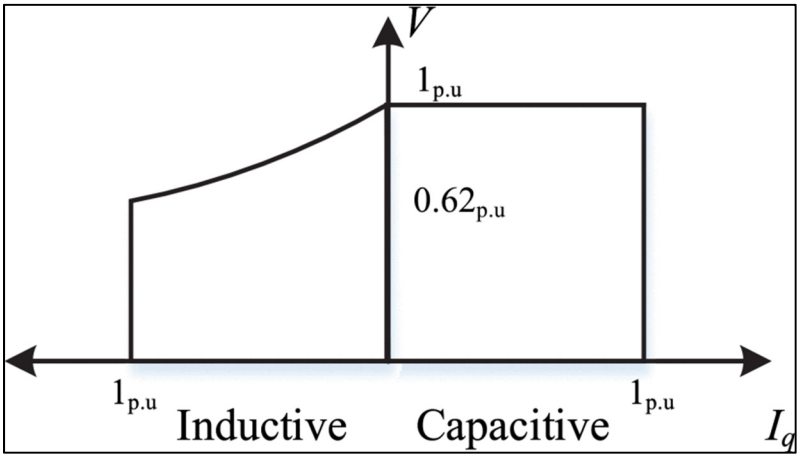

Figure 1.10 CHB-based STATCOM operation range
Taken from Farivar (2017)

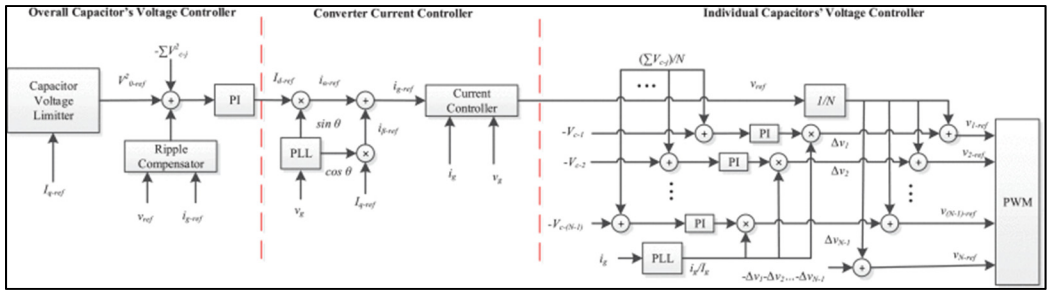

Figure 1.11 Control diagram of a CHB STATCOM with reduced capacitance
Taken from Farivar (2017)

1.2.2.5 Asymmetric CHB-Based STATCOM

A CHB-based STATCOM that has an equal voltage value at its capacitive dc links is known as symmetric topology. In this configuration, for achieving a lower harmonic content in the generated compensation voltage/current waveform, two main methods have been employed. First, the number of H-bridge cells should be increased to generate more voltage levels. Second, the switching frequency should be boosted. Considering the first method, the main issues are higher cost/volume and reduced reliability. Through the second approach, the system will have a decreased efficiency due to a higher switching loss. To address these problems, by choosing unequal amounts for the capacitive dc links, it will be possible to enhance the number of voltage levels. Accordingly, without requiring more passive and active components, the power quality operation of the system will be improved. Moreover, in this configuration, modules with higher dc-link voltage have lower commutation frequency and vice versa. This also leads to lower commutation loss and consequently better efficiency. In the literature, this CHB STATCOM topology is known as asymmetric. Principally, a controller designed for a CHB-based should have two main objectives: 1) tuning the voltages of the capacitive energy storage elements and 2) controlling the reactive power of the system. However, to achieve an asymmetric operation first objective should be focused on. Numerous methods have been proposed in the literature considering these control terms. As an instant, authors in (Sajadi et al., 2018) proposed to control the dc links voltages in an unequal manner through a novel modulation technique with selective harmonic mitigation capability. Besides, the system's reactive power is controlled by regulating the current in a decoupled manner. The diagram of this decoupled current control method for an asymmetric CHB-based STATCOM is depicted in Figure 1.12.

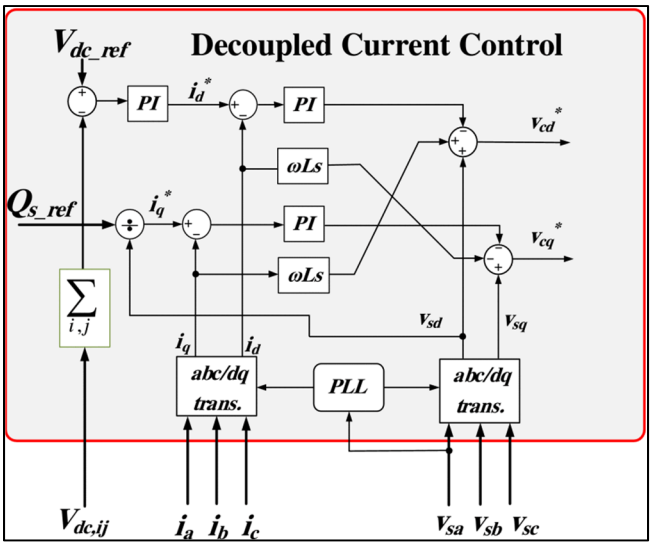

Figure 1.12 A decoupled current controller
Taken from Sajadi (2018)

1.2.2.6 Selective Harmonic Mitigation Approach for CHB STATCOM

To reduce the harmonics content of the generated voltage by a CHB-based STATCOM without increasing the number of employed H-bridge cells, the selective harmonic elimination (SHE) modulation approach is also proposed in the literature. Mostly, in selective harmonic elimination modulation methods, it is required to solve several equations with transcendental functions for numerous input conditions, which increases the complexity and computational burden. This limits the application of this modulator-based harmonic mitigation approach. To reduce the SHE modulation complexity, a new method is proposed to provide switching angles in a constant manner (Haw, Dahidah, & Almurib, 2014). As a result, in this method, it is not required to tiresomely manipulate switching angles that are calculated offline. But, this technique is dependent on having adjustable dc links voltages which are provided by dc-dc buck converters. Figure 1.13 demonstrates the structure of the proposed single-phase CHB-based STATCOM for five-level operation and its generated voltage waveform. Although the improved performance of this CHB-based STATCOM with an integrated buck converter in its H-bridge cells is demonstrated, the increased number of components and structural complexity are two main issues of this SHE technique.

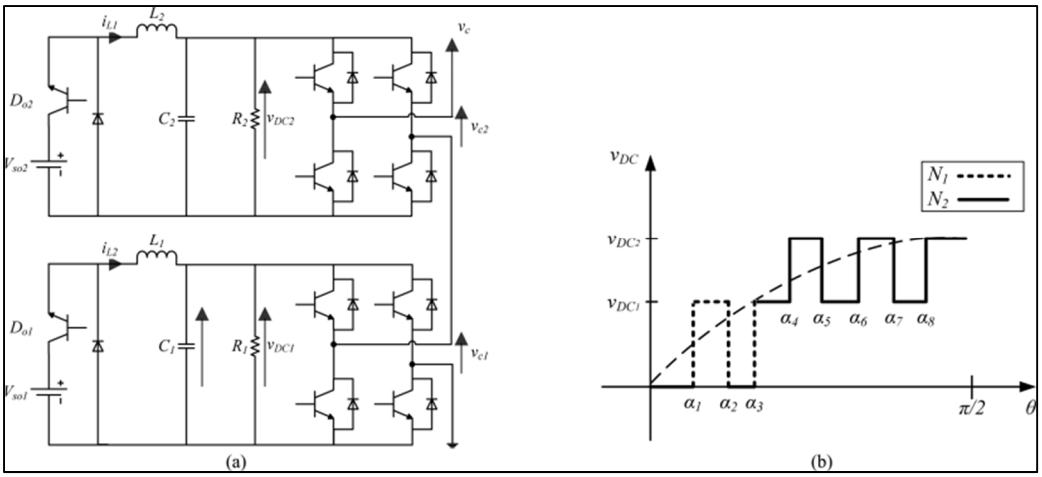

Figure 1.13 (a) A five-level CHB STATCOM and (b) SHE voltage waveform
Taken from Haw (2014)

1.2.2.7 Simplified Nonlinear Control Approach for CHB STATCOM

Mostly, for CHB-based STATCOM applications, over linear control methods, nonlinear ones have critical merits such as improved steady-state errors and dynamic performance. This is due to the fact that most of the nonlinear control methods consider the nonlinearities of the employed converter in their design. However, the increased computational burden and complexity of these methods are their main issues. Among various nonlinear control methods employable for CHB-based STATCOM application, model predictive control stands out due to its several advantages. Being multi-objective, optimizable operation, and intuitiveness are among these merits. Nonetheless, computational complexity and high execution time are still the main problems of this controller. Consequently, it has been extensively focused to improve the MPC algorithm complexity to polynomial functions for CHB-based STATCOM utilization in the literature (Y. Zhang, Wu, & Yuan, 2017). It is also suggested to implement the MPC method on a parallel combination of a digital signal processor (DSP) and a field-programmable gate array (FPGA) (Y. Zhang, Yuan, Wu, Yuan, & Zhou, 2020). As can be seen in Figure 1.14, converting the analog signals into digital ones (known as ADC) at the primary stage of the MPC algorithm and gate signals distribution at the final stage can be achieved using the FPGA. All the remaining control tasks such as the optimization process are implemented by the DSP. Therefore, in this parallel combination of FPGA and DSP, the execution time of the MPC

algorithm is merely dependent on the DSP. Accordingly, in order to improve the execution time of the MPC algorithm, the optimization process can be divided into low complexity and high complexity problems. Hence, in (Y. Zhang et al., 2020) as depicted in Figure 1.15 flowchart, FPGA has been also exploited for running the complicated part of the optimization process, which is the sorting task (related to the second algorithm). Through this method and employing an inexpensive combination of FPGA and DSP, it has been shown that an online MPC control technique can be employed for medium-voltage high power CHB-based STATCOM applications.

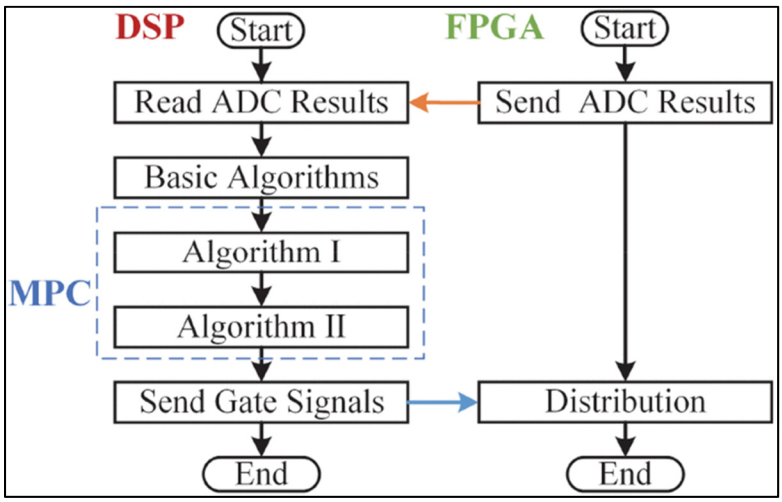

Figure 1.14 Conventional combination of DSP and FPGA
Taken from Zhang (2020)

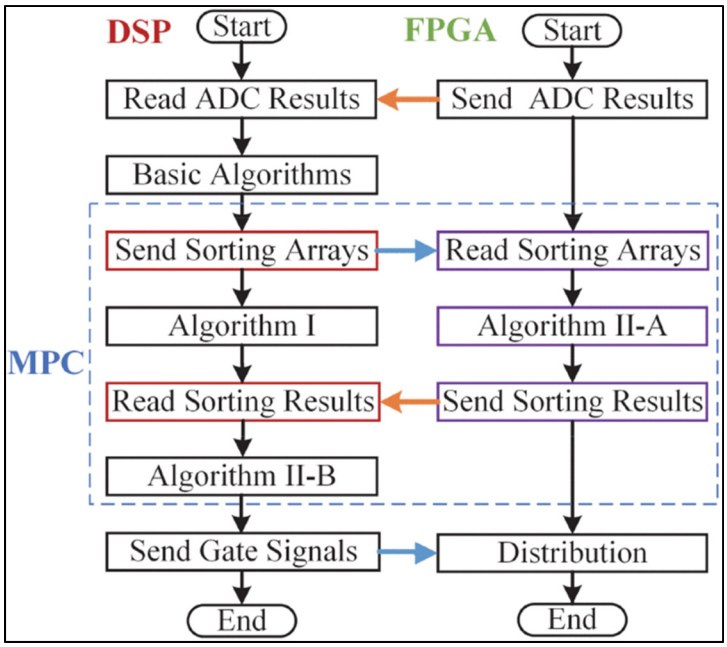

Figure 1.15 Improved combination of DSP and FPGA
Taken from Zhang (2020)

1.2.3 NPC-Based STATCOM

Figure 1.16 demonstrates a simplified structure of a three-level NPC (3L-NPC) based STATCOM (3L-NPC-STATCOM) connected to a power system (Saeedifard, Nikkhajoei, & Iravani, 2007). Compared with a two-level STATCOM, an NPC-based STATCOM topology has merits such as improved harmonic spectrum, reduced common-mode voltage, and higher voltage/power application. However, a highly increased number of components and complexity especially for higher voltage levels limit NPC applications. Besides, irregular distribution of switching (commutation) loss in switching devices that results in uneven thermal stresses is considered as one of the main demerits of this system. As a result, the degradation rate of switching components is different, which reduces the system reliability. Moreover, various operation modes result in diverse computation loss distributions in an NPC-based STATCOM configuration. Therefore, it would be also problematic to design a heat sink for this multilevel STATCOM configuration. Considering these commutation-related problems, a new modulation technique (known as semidipolar) has been developed for a 3L-NPC-STATCOM system (Zhou & Cheng, 2019). Furthermore, based on this modulator, a

controller is designed for balancing the active neutral point voltage. Nonetheless, it should be noted that employing this semidipolar modulator will impose a tradeoff between the harmonics content of the generated current and the commutation loss distribution operation.

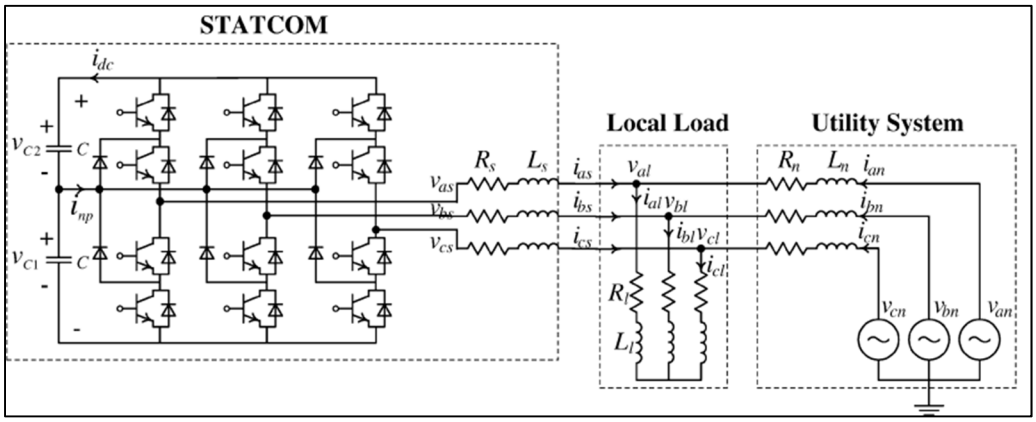

Figure 1.16 Diagram of a three-level NPC based STATCOM
Taken from Zhou (2019)

1.2.4 MMC-Based STATCOMs

Among various multilevel converter structures, modular multilevel converter (MMC) has recently gained a lot of attention for medium/high-voltage applications. The MMC structure is founded on the idea of connecting several lower-voltage cells, such as half-bridge or full-bridge cells, known as submodules in a cascaded manner to obtain the desired voltage level. Modular structure, extensibility, and availability of inherent redundancy are among the main merits of this topology (Cupertino, Pereira, Seleme, & Teodorescu, 2020). Considering these features, MMC has been also developed for medium/high-voltage STATCOM implementations. As depicted in Figure 1.17, single-star bridge cell (a), double-star bridge cell (c), single-delta bridge cell (b), and double-star chopper cell (c) are the main configurations of the MMC available in the literature (Cupertino, Farias, Pereira, Seleme, & Teodorescu, 2019). The first and second configurations are not favorable candidates for STATCOM applications due to respective disadvantages of the higher number of components and lacking circulating current. However, single-delta bridge and double-star chopper cells have circulating current and are consequently considered as suitable candidates for STATCOM implementations. In

this regard, these two MMC topologies have been compared from various aspects, including structural differences, energy storage requisites, dynamic performances, etc (Cupertino et al., 2019). As a result, it has been demonstrated that regarding requiring lower size energy storage elements, single-delta bridge cell topology has a superior characteristic. Besides, during the compensation of positive sequence currents, power losses in this topology are improved. On the other hand, regarding the losses and current rating during compensation of negative sequence components, the double-star chopper cell has an improved operation. In the end, regarding conditions with unbalanced voltage in weak grids, it is proposed to employ a double-star chopper cell topology as it has enhanced operation.

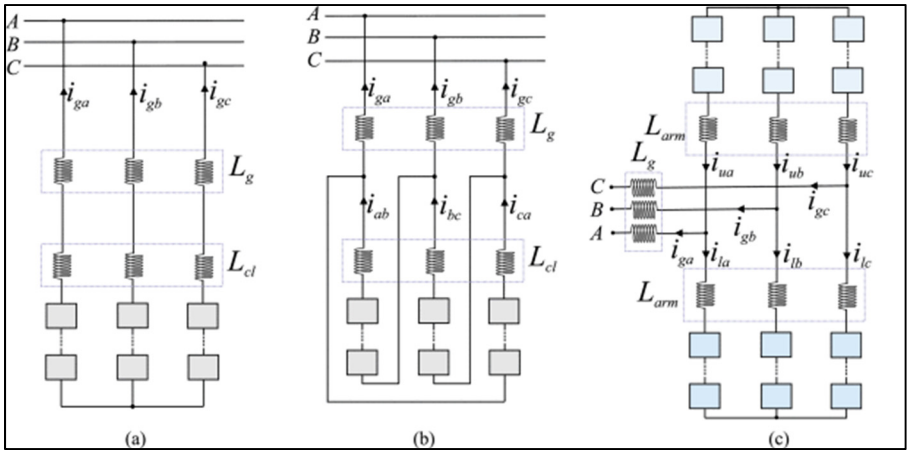

Figure 1.17 Available configurations of the MMC
Taken from Cupertino (2019)

1.3 ES Converter Configurations, Controllers, and Applications

Many researchers have been working toward investigating solutions for increasing the penetration of renewable energies into power systems without compromising on power quality. Among all the reported methods, demand-side management (DSM)-based techniques are of great importance and various applications of DSM can be found in the literature. Some of the existing approaches and technologies are (Zheng, Hill, Song, Zhao, & Hui, 2020), (C.-K. Lee, Liu, Tan, Chaudhuri, & Hui, 2020):

Energy consumption scheduling: In this approach for flattening the demand curve, the usage times for consumer appliances would be optimally scheduled. However, it would only be practical to shape the load profile in terms of days or hours. Besides, these appliances should be connected to remote communication and information systems like the Internet. Consequently, the power systems will be even more prone to cyber-security problems.

Load control by real-time pricing (RTP): This method aims to encourage customers to reduce their consumption or shifting their electricity usage during peak periods in response to time-based rates. Thus, in RTP the price of electricity would change based on the cost of power generation. Nonetheless, this method has also some disadvantages that need to be considered. Firstly, like the first solution, it cannot cope with the real-time imbalances of power generation and load demand. Secondly, costly electricity smart meter devices that can send and receive information are needed to be employed. Last but not least, it could be difficult for consumers to respond to price changes on an hourly basis.

Use of energy storage systems: The idea behind using energy storage systems such as pumped storage hydropower, electric batteries, and flywheels is to increase energy consumption when the generation is more than demand, and vice versa. However, it should be also considered that although these storage systems can help to achieve real-time power balance, their round-trip efficiency, capital investment, and space requirements are still debatable.

Direct load control (DLC): To manage the demand of consumers at the time of the peak demand, through direct load control programs, the utility would be able to remotely control the energy consumption of certain loads such as air conditioners or water heater systems. Nonetheless, the implementation of DLC programs could be interrupting and cause inconvenience, especially for residential consumers. Furthermore, this solution requires both remote communication systems and smart metering devices that not only increase the cost but also decrease the reliability of the power grid.

Electric Spring: After over three centuries, the mechanical spring concept has been extended to power systems just recently. The idea of electric spring has been proposed as a real-time novel power electronics-based demand-side management technology. It has been mainly designed with the aim of instant regulation of the voltage at various points of an electrical grid with high penetration of intermittent renewable energy sources independent of any communication systems. Therefore, ES has a great potential for improving power quality in future power systems efficiently and reliably. In this regard, ES distributed in a power system can have three main functions: 1) providing support for mains voltage, 2) storing electric energy, and 3) dumping electric oscillations (Hui, Lee, & Wu, 2012). Although electric spring technology has undeniable similarities to previous reactive power controllers such as STATCOM and static VAR compensator (SVC), it has fundamental differences. Firstly, the control paradigm of an ES is completely different. To be specific, it utilizes an input-feedback and input-voltage control as shown in Figure 1.18 (Hui et al., 2012). Secondly, it not only controls reactive power but also alters the active power consumption of its series-connected load (C. K. Lee, Chaudhuri, & Hui, 2013). To clarify this, loads available in an electrical grid can be classified as critical and non-critical. Critical loads such as data centers require stable and high-quality power at their terminals. However, the voltage and power of the non-critical loads like public lighting systems can fluctuate to some extends (C.-K. Lee et al., 2020). Non-critical loads, which are connected in series with ES, as depicted in Figure 1.19 (Tan, Lee, & Hui, 2013), will be converted into a new generation of smart loads. These smart loads can dynamically modify their power consumption regarding the amount of generated active/reactive power. Thirdly, it can be installed in all the residential, commercial, and industrial areas and spread all over the bulky power systems for decentralizing power quality control.

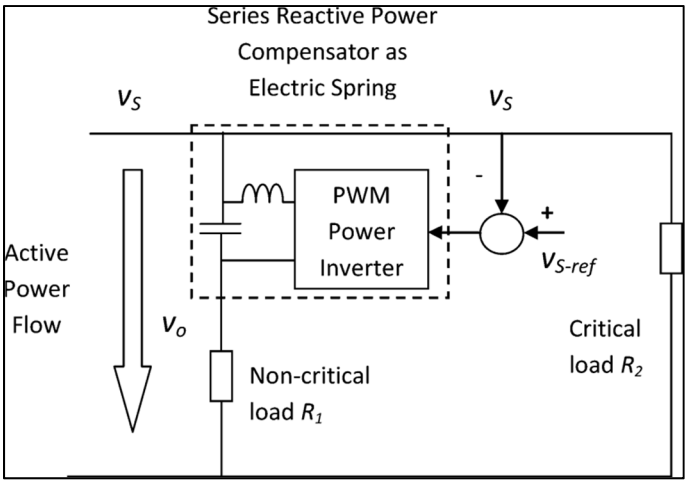

Figure 1.18 Simplified schematic of an ES
Taken from Hui (2012)

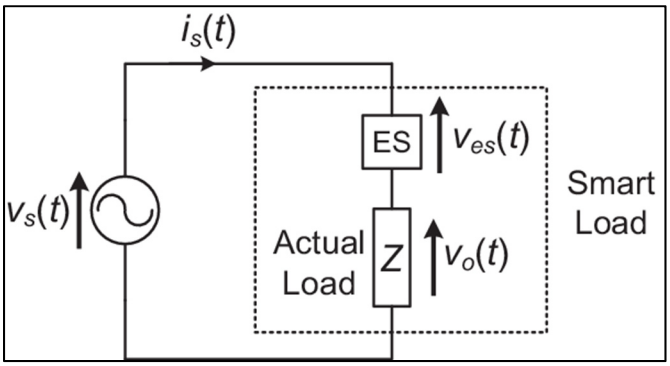

Figure 1.19 ES embedded in a smart load setup
Taken from Tan (2013)

By far, various versions of ES technologies, controllers, and applications have been introduced and developed in the literature. Some of them are reviewed as follows.

1.3.1 Capacitor-Based ES

The first version of ES (ES-1) mostly consists of one or two bulky auxiliary capacitors and a half-bridge or full-bridge converter. To reduce harmonics of the generated two-level voltage waveform to tolerable levels, a passive LC filter should be also employed. Figure 1.20 illustrates a simplified scheme of a half-bridge-based ES-1 (C. K. Lee, Chaudhuri, & Hui, 2013). As can be seen, ES-1 should be connected in series with a non-critical load which can

be resistive, inductive, or capacitive. As capacitive energy storage elements (capacitors) are employed in ES-1, it compensates for reactive power directly. By controlling the dc-link electric field dynamically, the electric spring injects a tuned magnitude of voltage in both directions (positive or negative) to regulate its input voltage and alter its output voltage. The ES-1 output voltage is the non-critical load input voltage. Therefore, ES-1 can also compensate for active power indirectly. The main advantage of this first version of ES in comparison to other generations is its structural simplicity for improving voltage and/or frequency stability in the power system.

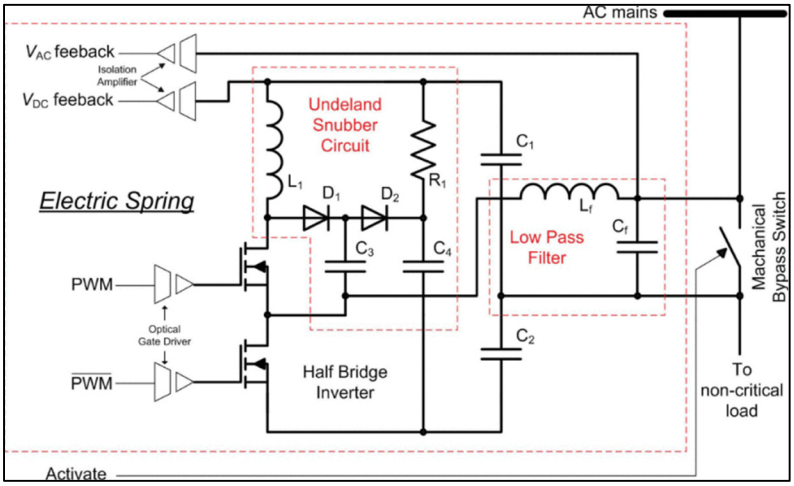

Figure 1.20 Simplified scheme of a half-bridge-based ES-1
Taken from C. K. Lee (2013)

In (C. K. Lee & Hui, 2013), it is highlighted that in grids with a high percentage of renewable energies, using a battery-based energy storage system is a costly solution for balancing demanded and generated powers. Therefore, through extensive theoretical and experimental results, it has been proven that employing the capacitor-based electric spring in a sample 90-kVA electrical grid with an unstable PCC voltage can effectively reduce the required energy storage capacity for mitigating power imbalances and stabilizing the critical load(s) voltage. A detailed hardware circuit of a single-phase half-bridge ES-1 with a novel Undeland snubber has been also reported in (C. K. Lee, Chaudhuri, & Hui, 2013). As seen in Figure 1.21, in this work, a dual-loop PI-based controller with the main aim of compensating reactive power while tuning the ES-1 dc-link voltage has been also implemented and applied to the proposed two-

level topology. On the other hand, the first attempt to experimentally prove the effectiveness of a group of distributed ES-1s (three 1-kVA prototypes) to stabilize a relatively small-sized electrical grid without any communications infrastructure was reported in (C. K. Lee, Chaudhuri, Chaudhuri, & Hui, 2013). In this work, all the employed ES-1s were able to participate in voltage stabilization of the system based on their installation locations. In this regard, a droop control method has been proposed for ES-1 applications. A diagram of this method can be also seen in Figure 1.22. Nevertheless, to effectively demonstrate the performance of several numbers of these capacitor-based distributed voltage/frequency control devices in large-scale electrical grids, extensive simulation-based analyses should be performed. Consequently, in (Chaudhuri, Lee, Chaudhuri, & Hui, 2014) and (T. Yang, Liu, Chen, Yan, & Hui, 2018), simple yet relatively accurate ES-1 dynamic averaged models are proposed and validated, which can be employed for voltage/frequency stability simulation-based studies.

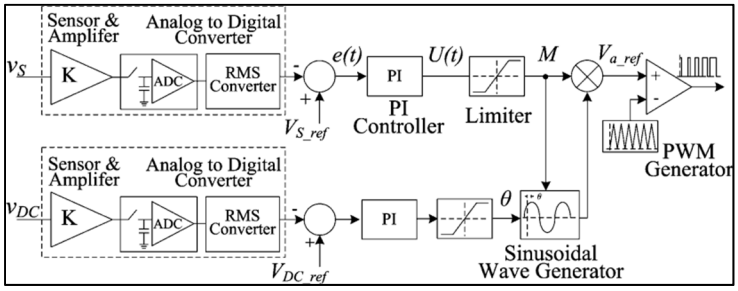

Figure 1.21 Dual-loop PI-based ES-1 controller
Taken from C. K. Lee (2013)

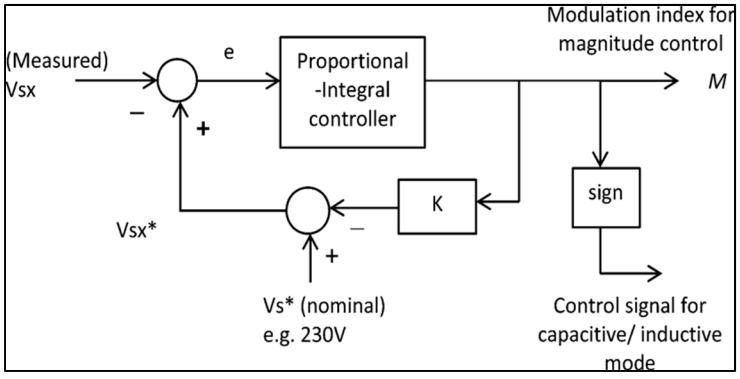

Figure 1.22 Droop control method for ES-1 applications
Taken from C. K. Lee (2013)

Comparing the operation and effectuality of a centralized STATCOM installed on the medium voltage side and a group of distributed ES-1s mounted on the low voltage side in various case scenarios is the focus of (Luo et al., 2015). The results of this comparison have proved that although ES-1s collectively required lower amounts of capacitive energy storage, they can achieve enhanced performance regarding the regulation of the mains voltage with improved reliability. As mentioned earlier, ES-1 is capable of direct compensation of merely reactive power. However, by tuning a non-critical load voltage, which is a voltage-dependent load, its demanded active power can be also altered. Based on this fact, in (Akhtar, Chaudhuri, & Ron Hui, 2015), PCCs frequency control is prioritized over controlling the critical load voltage and the effectiveness of ES-1 in this regard has been also proven. The scheme of the respective designed controller can be also seen in Figure 1.23. Finally, verifying the effectiveness of ES-1 technology, as well as proposing the required control methods, for improving the flicker phenomenon and enhancing the performance of an ac microgrid particularly after occurring severe natural disturbances (such as lightning) are the main focuses of (Sharma et al., 2017) and (Liang, Hou, Hill, & Hui, 2018), respectively.

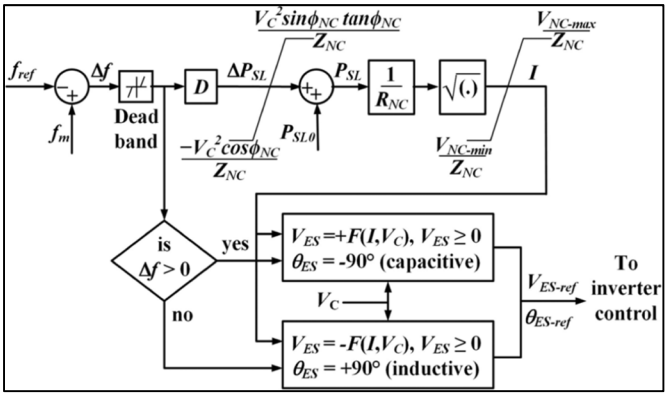

Figure 1.23 ES-1 frequency control loop structure
Taken from Akhtar (2015)

1.3.2 Battery-Based ES

As depicted in Figure 1.24, to extend the operating range and capabilities of ES-1, instead of capacitors, batteries can be employed as energy storage elements (J. Chen, Yan, Yang, Tan, & Hui, 2019). In this regard, the second version of Electric Spring (ES-2) is introduced and

developed. Therefore, ES-2 can be employed for direct compensation of not only reactive power but also active power. As a result, both the mains voltage and frequency of the system can be stabilized independently and instantly. Besides, ES-2 can have also other applications such as improving power factors and compensating loads (C.-K. Lee et al., 2020). So far, due to its versatile and multifunctional operation, ES-2 has been the most employed and developed electric spring technology. In (Tan et al., 2013), authors have managed to investigate steady-state operations and control fundamentals of the ac battery-based ES for instantaneous compensations of active and/or reactive powers regarding various types of loads (resistive, capacitive, and inductive). To support the respective theoretical framework, extensive mathematical equations have been also provided. Besides, all the introduced ES-2 compensation modes (eight plausible modes) have been extensively analyzed and confirmed through experimental results.

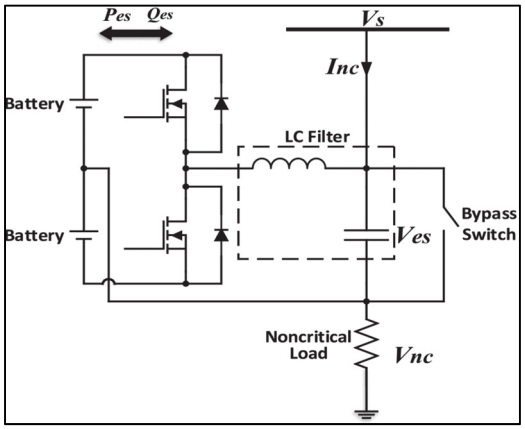

Figure 1.24 Diagram of the ES-2
Taken from Chen (2019)

Several control methods have been proposed for ES-2 applications. In (Q. Wang, Cheng, Chen, & Wang, 2015), based on a new δ control concept, an ES-2 controller was proposed for power factor improvement and regulating the grid voltage. In this technique, as can be seen in Figure 1.25, a proportional resonant (PR) controller as an outer voltage control loop and a proportional controller as an inner current control loop are designed and employed. By a δ-based controller, ES-2 operation modes considering various grid voltages can be defined and applied automatically. However, this method requires several parameters of the electrical system,

including characteristics of the critical/non-critical loads and transmission line. This is not a favorable feature, especially for practical implementations. On the other hand, to regulate the input active and reactive powers and by utilizing the synchronous reference frame control known as DQ rotating frame, another ES-2 control approach is proposed (Q. Wang, Cheng, Jiang, Zuo, & Buja, 2018). This method has two main advantages. First, it can decouple the active and reactive power control. Second, its operation does not require any information from the system. However, this method employs more than three PI controllers. So, tuning its PI coefficients will be a tedious task. Among the introduced ES-2 controllers, due to merits such as supporting ES-2 multifunctional operation, simplicity, and capability of direct/simultaneous control of smart load setup active and reactive powers, a radial-chordal decomposition (RCD) based control method stands out (Mok, Tan, & Hui, 2016). By employing this method, the voltage and power angle of an ES-2-based smart load can be controlled in a decoupled manner intuitively. Consequently, through a single ES-2, the power factor of the smart load setup and critical load voltage stability are improvable independently and instantaneously. An illustration of this controller is also presented in Figure 1.26. As can be seen, merely one closed-loop PI controller is required which makes it a suitable option for industrial applications. This RCD controller technique has been also validated both mathematically and experimentally.

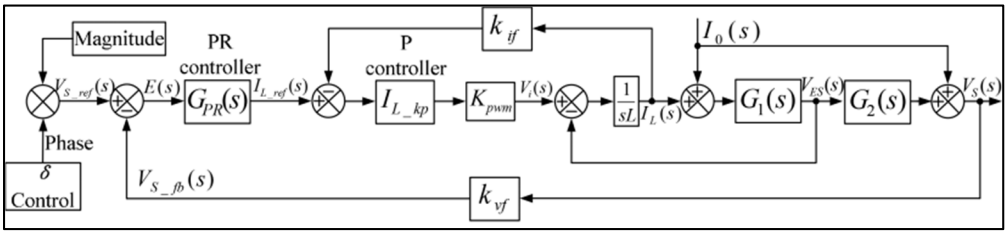

Figure 1.25 Control loops of ES-2 controller based on δ concept
Taken from Q. Wang (2015)

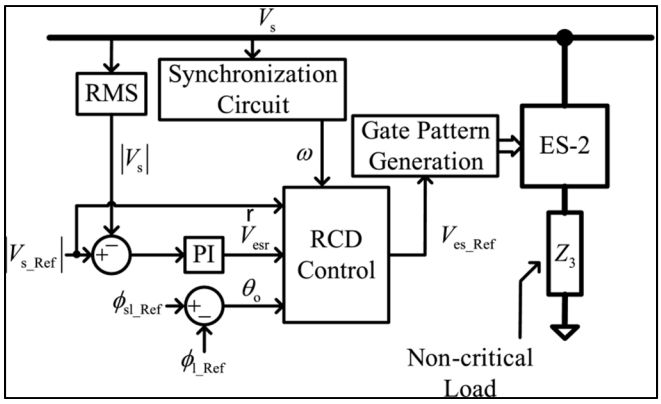

Figure 1.26 ES-2 RCD-based controller diagram
Taken from Mok (2016)

As mentioned earlier, the multifunctionality of ES-2 for mitigating power quality issues of electrical systems is one of its main merits. So, by taking advantage of ES-2 four-quadrant performance, in addition to alleviating voltage and frequency fluctuations in a power system, ancillary services such as harmonics mitigation and power factor correction can be also achieved. Correspondingly, to support this capability of ES-2, respective operation principles and a PI-based current controller have been proposed and validated (Yan, Tan, Lee, Chaudhuri, & Hui, 2017).

1.3.3 Back-to-Back ES

In comparison to ES-1 and ES-2 in addition to the series converter, the third version of the electric spring (ES-3) has also a bidirectional ac-to-dc shunt converter (coupled with the grid) in a back-to-back configuration. As illustrated in Figure 1.27, although ES-3 (also known as back-to-back ES (ES-B2B)) does not have any battery/capacitor-based energy storage system, it has the ability to compensate both active and reactive power independently with an extended operating range (Akhtar, Chaudhuri, & Hui, 2017). As an instance, the operating range of an ES-3 in comparison to ES-1 is presented in Figure 1.28 (Yan, Lee, et al., 2017). Furthermore, without having battery physical limitations, ES-3 has an enhanced performance that is of great importance. In this configuration, the series converter has the responsibility of controlling the magnitude and phase angle of the compensation voltage in series with a non-critical load. On

the other hand, the shunt converter's responsibility is to maintain the dc voltage across the dc-link between two converters constant. So, active power compensation, which is achieved through the series converter, can be supported (Akhtar et al., 2017). One of the main disadvantages of the third version of ES is requiring an isolation transformer for decupling the employed converters (Yan, Lee, et al., 2017). Nonetheless, recently, it has been proven that by employing a three-phase converter topology, this problem can be also solved (H. Liu, Ng, Lee, & Ron Hui, 2020).

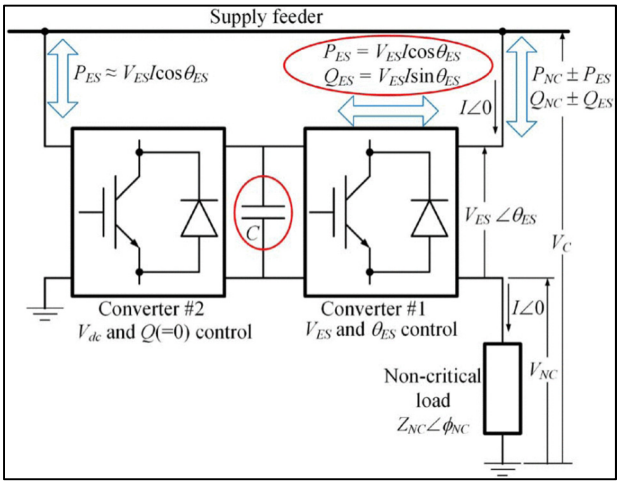

Figure 1.27 Third version of Electric Spring
Taken from Akhtar (2017)

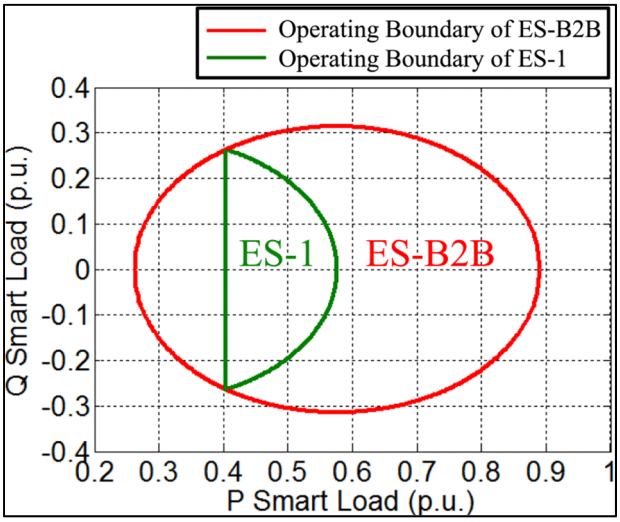

Figure 1.28 ES-3 and ES-1 operating ranges
Taken from Yan (2017)

1.3.4 Hybrid ES with Renewable Energy

One of the recently introduced versions of electric spring technology known as hybrid ES integrates distributed renewable energy resources such as photovoltaic (PV) panels into its configuration as the dc source. Accordingly, without requiring any electric battery on its dc side, hybrid ES can achieve active and reactive power control in a simultaneous, direct, and decoupled manner. Furthermore, it enables the delivery of maximum harvested PV power to the system at the same time. Consequently, a separated interfacing inverter will not be required. Besides, in this topology, it is not required to consider various states of a battery such as state of charge (SoC) and state of health (SoH) in the controller design. Nonetheless, in this system intermittency problem of the integrated renewable energy sources should be considered. A simplified circuit diagram of a hybrid ES is depicted in Figure 1.29 (T. Yang et al., 2019).

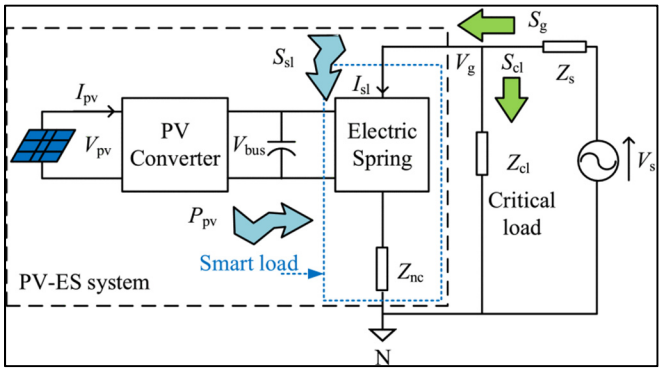

Figure 1.29 Circuit diagram of a hybrid ES
Taken from Yang (2019)

1.3.5 Three-Phase ES

Due to the enhanced power density of a three-phase circuit in comparison to a single-phase one, it is employed for distributing high amounts of power. Nevertheless, by having a combination of single-phase and three-phase loads like available loads in residential buildings, the load will be unbalanced. Therefore, three-phase ES has been introduced mainly for mitigating voltage instabilities and power imbalances in three-phase electrical systems such as high-rise residential buildings. It should be connected in series with non-critical loads to realize

demand-side management. As depicted in Figure 1.30 (Yan, Tan, Lee, Chaudhuri, & Hui, 2015), a three-phase ES configuration comprises a three-phase converter, battery packs on its dc link, and a lowpass filter in the output of each leg. Besides, three-phase ES has been also developed for mitigating zero and negative-sequence currents in an unbalanced power system (Mok, Ho, Tan, & Hui, 2017). Moreover, by taking advantage of the multifunctionality of ES technology, three-phase ES can be utilized for more applications like harmonics reduction (Yan et al., 2018).

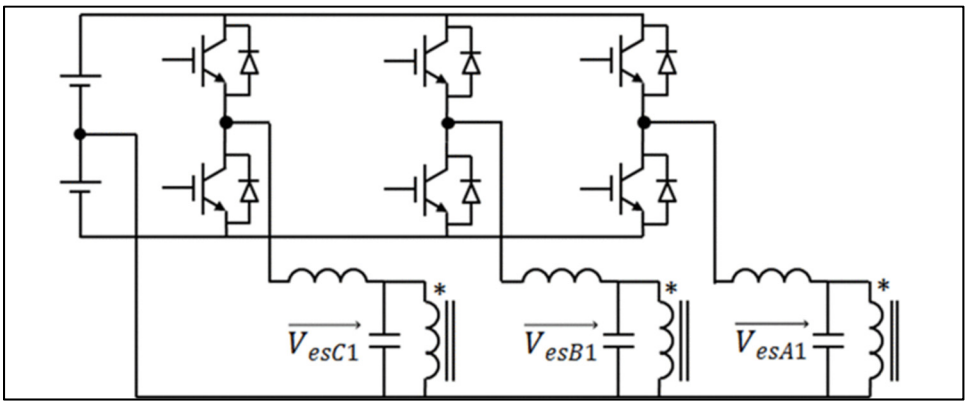

Figure 1.30 Topology of a three-phase ES
Taken from Yan (2015)

1.3.6 DC ES

Recent development in power electronics technologies has renewed interest in employing dc microgrids. A dc microgrid has some important advantages over an ac one, which can significantly improve an electrical system's efficiency and reliability. More convenience in the integration of renewable energy resources without depending on dc-ac conversion systems and not requiring frequency synchronization are some of them (M.-H. Wang, Yan, Tan, & Hui, 2018). However, similar to ac grids, variable load demands and high penetration of integrated intermittent PV systems in a dc microgrid can cause critical power quality problems such as voltage stability and power imbalance. Accordingly, the electric spring concept is developed for dc microgrids and a DC ES has been introduced. It has been proven that by employing DC ES technology in a dc microgrid all the mentioned power quality issues can be mitigated in an

online, effective, and efficient manner (Mok, Wang, Tan, & Hui, 2017). A simplified schematic diagram of a DC ES installed in a basic dc microgrid is presented in Figure 1.31. As illustrated, a DC ES setup is mainly made up of a bidirectional dc-dc converter and a battery as its energy storage element. It should be also connected in series with a non-critical load to tune its demanded power dynamically.

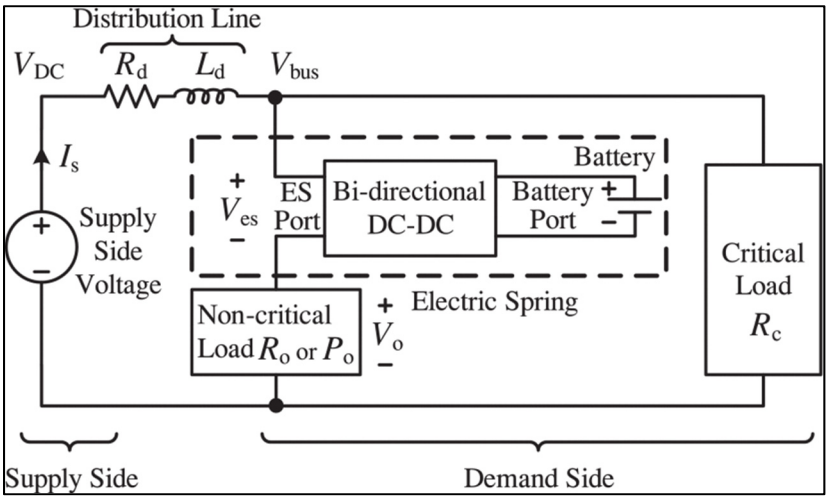

Figure 1.31 Diagram of a DC ES integrated into a microgrid
Taken from Mok (2017)

1.4 State of the Art and Originality of the Research

As can be noted from the available literature, as a response to the low power quality performance of two-level STATCOM configurations, multilevel STATCOMs based on different conventional topologies such as CHB and NPC have been developed. Common merits of these multilevel STATCOMs include but are not limited to reduced commutation frequency, improved harmonic components of the generated voltage/current, and lower voltage stress on the switching devices/auxiliary capacitors. However, the highly increased number of passive and active components (auxiliary capacitors and switches), being costly and bulky, and requiring highly complex controllers with noticeable computational burdens are some of their main demerits, which should be considered. On the other hand, considering the developed and reported ES technologies, mostly half-bridge and full-bridge topologies are employed as the ESs' converters. However, from both power quality and reliability points of view, these two-

level ESs are not favorable options, specifically for higher power industrial or commercial implementations. Besides, mostly, linear PI-based controllers are applied to various generations of ES (C. K. Lee, Chaudhuri, & Hui, 2013). Although PI-based controllers can be implemented more conveniently, neglecting the converter nonlinearities and dynamics models, which results in poor dynamic performance, and requiring a modulation technique are among their shortcomings. High switching frequency, lack of boost mode and fault-tolerant operations, high harmonic voltage/current content, and requiring bulky capacitors/output lowpass filters are yet other disadvantages of already available ES systems. In addition, the multifunctional operation of ES technologies increases system efficiency. But, due to the limited number of available works on multifunctional ESs, it is also required to perform more focused research on the multifunctionality aspect of ES technologies (M. Wang, He, Xu, Dong, & Lei, 2021). Considering all these merits and demerits of the introduced STATCOMs and ESs, it is clear that there are still several challenges that need to be considered to improve their performances from various aspects.

The high-power density multilevel converters are being developed as appropriate configurations for different single/three-phase power systems applications. Decreased number of switching vectors, reduced component counts, improved size and cost, and more reliable operation are some of the advantages of compact multilevel converters over conventional multilevel topologies. Recently, a novel compact bidirectional multilevel inverter configuration founded on a seven-level packed U-cell (PUC7) is proposed (Ounejjar, Al-Haddad, & Gregoire, 2011). It is made up of a single dc source, merely three pairs of complementary switching devices, and one auxiliary capacitor. Due to the significantly reduced number of switches in this seven-level topology, there are not enough redundant switching states to modify its capacitor voltage integrated into the modulation technique. However, by decreasing the levels of the generated voltage (from 7 to 5) and employing the resulted extra switching vectors, authors in (Vahedi, Labbé, & Al-Haddad, 2016) have managed to tune the auxiliary capacitor’s voltage without using a separated controller integrated into the modulator in an open-loop/sensorless manner. Hence, a five-level PUC-based inverter (PUC5) has been presented. Considering its favorable topological merits, PUC5

has gained a lot of attention from both academia and industry. Accordingly, several types of PUC-based multilevel topologies like five-level modified PUC (MPUC5) (Vahedi, Shojaei, Dessaint, & Al-Haddad, 2018), seven-level modified PUC (Vahedi, Sharifzadeh, et al., 2018), and nine-level packed E-cell (Sharifzadeh & Al-Haddad, 2019) have been introduced and developed in stand-alone or grid-connected modes. Nonetheless, these compact PUC-based multilevel configurations have not been yet modeled, controlled, and implemented for STATCOM or ESs multifunctional applications.

1.5 Conclusion

Lately, as a result of the increased importance of power quality problems, various types of STATCOM and ES technologies have been extensively developed and employed for mitigating a wide range of power quality issues in power systems. For high/medium power/voltage applications, on the one hand, regarding the proposed two-level (half-bridge or full-bridge) ESs and STATCOM configurations, inherent poor power quality characteristics such as increased harmonics of the generated compensation voltage and high voltage stress on the passive/active components are the main issues. On the other hand, in the literature, these problems are addressed mainly at the expense of noticeably increasing the size/cost, complexity, and component count of the STATCOM/ES systems by employing classical multilevel topologies (as an instance CHB). Besides, developed controllers for these multilevel STATCOM/ES configurations with amplified numbers of dependent and independent dc links and switching vectors are also complex with high computational burdens. Considering these issues, the need for developing high power density multilevel converters and the required simplified nonlinear controllers with improved steady-state and dynamic operations for the STATCOM and ESs applications suitable for both low and medium voltage systems is clear.

CHAPTER 2

MODEL PREDICTIVE CONTROL OF MPUC7-BASED STATCOM USING AUTOTUNED WEIGHTING FACTORS

Amirabbas Kaymanesh [a], Ambrish Chandra [a] and Kamal Al-Haddad [a],

[a] Department of Electrical Engineering, École de Technologie Supérieure,
1100 Notre-Dame West, Montreal, Quebec, Canada H3C 1K3

Paper published in *IEEE Transactions on Industrial Electronics*, April 2021

Abstract

A seven-level modified packed U-cell (MPUC7) based static synchronous compensator (MPUC7-STATCOM) with an autotuned finite control-set model predictive control (AFCS-MPC) is introduced in this article. MPUC7-STATCOM is a compact four-quadrant cascaded topology that comprises merely six switches and two isolated dc capacitors. Thus, in comparison with a seven-level cascaded H-bridge (CHB) based STATCOM not only, the proposed configuration has exceptionally reduced active/passive component count, but also MPUC7-STATCOM designed AFCS-MPC control method complexity is attenuated meaningfully. Boost-mode operation and low voltage rating of the components can be also mentioned as the merits of the MPUC7-STATCOM. Using the proposed AFCS-MPC, nonlinearities of the MPUC7 converter have been considered and both capacitors' voltages are directly regulatable at different desired amounts accurately. Moreover, the weighting factors of the proposed AFCS-MPC are tunable automatically in real-time. Consequently, MPUC7-STATCOM has a desirable dynamic operation and its capacitors' values are reduced. Provided simulation and experimental results validate the viability of the MPUC7-STATCOM topology and robustness of the designed AFCS-MPC method as well as its steady-state and dynamic operation.

2.1 Introduction

With the ambition of having a low-carbon energy sector in future, the acceleration of the renewable energy integration rate is unavoidable. Consequently, power quality-related challenges such as voltage sag/swell should be considered prudently. The static synchronous compensator (STATCOM), as a shunt-mounted flexible AC transmission system (FACTS) equipment, is of great importance for stabilizing voltage and power factor correction (PFC) through primarily instant and accurate reactive power compensation in the power system. Recently, classical two-level STATCOM converters are being substituted by multilevel topologies. In comparison, multilevel STATCOM configurations such as cascaded H-bridge (CHB) (Y. Zhang et al., 2020) and neutral point clamped (NPC) (Zhou & Cheng, 2019) can offer pivotal advantages such as lower switching frequency, electromagnetic interference and dv/dt, enhanced power quality performance due to the quasi-sinusoidal voltage and current waveforms, higher efficiency, etc. Nonetheless, an augmented number of active/passive components, complexity, and being bulky/costly are considered as their demerits. For attenuating the impact of these issues, a five-level modified packed U-cell (MPUC5) converter was firstly introduced by Nami in 2013 (Nami, Wang, Dijkhuizen, & Shukla, 2013). Since then, it has been employed for various applications in mostly distributed energy systems, including active power filter (Vahedi, Shojaei, et al., 2018), (Babaie, Sharifzadeh, & Al-Haddad, 2020), grid-connected photovoltaic (PV) utility interface (Vahedi, Sharifzadeh, et al., 2018), capacitor-based electric spring (Kaymanesh & Chandra, 2020), battery-based electric spring (Kaymanesh, Babaie, Tidjani, Chandra, & Al-Haddad, 2020), and dual-output rectifier (Vahedi & Al-Haddad, 2016a).

In addition, a novel five-level STATCOM topology founded on the MPUC5 has been proposed lately (Vahedi, Dehghanzadeh, et al., 2018). In (Vahedi, Dehghanzadeh, et al., 2018), via exploiting the availability of additional switching states, voltage and power balancing of both isolated capacitors is integrated into the modulator. Boost transformerless operation, reduced number of components and lower voltage rating of the utilized power switches are also other distinctive features of the introduced MPUC5-based STATCOM. However, the designed linear

cascade proportional-integral (PI) control technique in (Vahedi, Dehghanzadeh, et al., 2018) has critical frailties that should be overcome. The first issue is having two closed-loop controllers (outer/inner) with different dynamic response times that require precise and tedious adjustment of at least four PI coefficients. Secondly, by this method, capacitors' voltages are regulatable merely at the same value. Nevertheless, fixing the second capacitor voltage value to half of the first one can lead to even more reduction in the generated compensation voltage/current total harmonic distortion (THD) by a seven-level MPUC-based STATCOM (MPUC7-STATCOM) operation. Consequently, more reduction in the size and cost of the required output filter inductor will be plausible. Finally, the dynamic model and nonlinearities of the MPUC5 converter have not been considered in the above-mentioned control method.

The recent and rapid advancement of microprocessors with significant calculation power has made the evolution from conventional linear control methods to more developed nonlinear controllers conceivable. This opens up more opportunities for power electronics technology. Among numerous nonlinear control approaches for power converters such as sliding mode control (SMC) (Shen et al., 2020) and Lyapunov control (Gavagsaz-Ghoachani et al., 2019), model predictive control (MPC) has been focused in the literature tremendously (X. Liu, Wang, & Peng, 2019). The superior dynamic operation, the inclusion of the exact converter model, and intuitive multi-objective constrained optimization capability are the main motives behind MPC popularity among researchers focused on multilevel converters. To explain MPC modus operandi, it is worth mentioning that through using explicit mathematical models of the converter, control objectives should be articulated in a cost function that should be minimized. This minimization procedure is a benchmark for obtaining the required control signal in the following sampling time. Therefore, all the control aims are achievable concurrently (Abughalieh & Alawneh, 2019).

Continuous control-set model predictive control (CCS-MPC) and finite control-set MPC (FCS-MPC) are the chief methodologies of the MPC for multilevel converters. On the one hand, using CCS-MPC, multilevel power converters can be controlled indirectly, by generating a continuous control signal. This is achievable by nullifying the cost function's derivative. In the

next step, via various modulation techniques, required analogue switching signals are synthesizable. On the other hand, in FCS-MPC known as direct MPC, by taking advantage of the fact that in a multilevel converter switching combinations are limited, the optimization problem is solvable more conveniently. In this case, the selection of a proper switching sequence of a multilevel converter is done directly by solving the cost function for all the possible sequences and one that provides a minimized cost will be selected. The key merits of this methodology are that, firstly, the control signals are generated directly, secondly, the optimization problem is relatively straightforward and, finally, the utilization of any modulation technique is not required (Donoso et al., 2018).

However, accurate adjustment of the FCS-MPC cost function's weighting factors is key regarding its operation and robustness as a controller with multiple objectives. Conventionally, various trial-and-error-based techniques have been employed for tuning weighting coefficients in a static manner (Karamanakos & Geyer, 2020). Nevertheless, the shared drawback of these empirical techniques is their poor performance/robustness during transients and under the availability of mismatches in parameters. Consequently, several researches have been oriented toward proposing methods for online adjustment of cost function’s weighting factors in FCS-MPC for converters automatically. In (Babaie, Sharifzadeh, Mehrasa, Chouinard, & Al-Haddad, 2021), a multi-objective algorithm based on Artificial Bee Colony (ABC) is introduced. Various real-time modification approaches employing fuzzy have been also proposed (X. Liu et al., 2019), (Villarroel et al., 2013). These ABC and fuzzy-based techniques have promising operations. But, they are multifaceted methods with increased computational burdens. In (Caseiro, Mendes, & Cruz, 2019), weighting coefficients are calculated dynamically at each sampling time in continuous relation with the available errors regarding the control objectives. Although this method has acceptable performance, as several extra parameters should be defined, it has an increased complexity especially for multilevel converters with more control objectives. It should be noted that boosted complexity and computational burden are unfavorable features for a controller, especially for industrial applications.

With this regard, recently, in (Li, Zhang, Shadmand, & Balog, 2017), a simplified automatic tuning method is presented for weighting factors in the model predictive control of a single-phase H-bridge inverter to make the transition between grid-connected and autonomous operation modes as seamless as possible. This autotuning technique is also enhanced for a capacitor less three-phase STATCOM based on a 3×3 matrix converter by Shadmand in (Shadmand, Jain, & Balog, 2019). It has the merits of online optimum weighting factors regulation in each sampling time and being vigorous against existing system uncertainties. Furthermore, not only it does not require unfavourable complex computations, but also it is a very intuitive technique. Consequently, in this article, this method is extended and developed for a single-phase multilevel converter MPC-based controller with three control objectives (rather than two) including two auxiliary capacitors' voltages for the first time.

Hence, this article develops and employs a nonlinear control technique based on the autotuned FCS-MPC (AFCS-MPC) to propose a novel seven-level MPUC-Based STATCOM configuration. Comparing with the already introduced MPUC5-based STATCOM (Vahedi, Dehghanzadeh, et al., 2018), in this nonlinear control method, two closed-loop PI controllers, four triangular pulse-width modulation (PWM) carriers and the switching states table are all eliminated and replaced by a real-time constrained optimization problem including cost function with online auto adjustable weighing factors and mathematical discrete models. Through utilizing the presented AFCS-MPC for the MPUC7-STATCOM, not only the dynamic performance is amended but also various objectives are achievable, specifically instant and autonomous regulation of the capacitors' voltages and injected compensation current. Notice that although high computational burden can be considered as a hindrance, AFCS-MPC computational complexity and execution time for the MPUC7-STATCOM as a seven-level converter with the least possible number of components and switching conditions, in comparison with a seven-level CHB STATCOM, as an instance, that has several more switching states, switching redundancies and dc-links (Nasiri et al., 2019), (Y. Zhang et al., 2017), is insignificant. The practicability and performance of the presented MPUC7-STATCOM and controller are also validated experimentally in real-time.

Major novelties of this article are highlighted as follow:

1. A new multilevel STATCOM topology with features such as being compact, high-power quality performance, boost-mode operation and the reduced component count is proposed. Besides, an MPC-based controller with online auto-tunable weighting factors and reduced complexity and the computational burden is designed and applied to this configuration for the first time.
2. Employing the designed controller results in fast regulation of the capacitors' voltages with an improved overshoot and settling times especially during transients and availability of parametric mismatches.
3. In comparison to the MPUC5-based STATCOM, although the size of utilized capacitors is reduced, not only voltage distortion of these capacitors is decreased but also power quality characteristics of the generated compensation voltage and current have been improved. So, the size/cost of the required output filter is also reduceable. MPUC7-STATCOM comparison with the single-phase seven-level CHB STATCOM as well as its merits are also presented.
4. Implementation of a single-phase STATCOM based on the modified packed U-cell configuration has been done.

In the following, Section 2.2 introduces MPUC7-STATCOM configuration and presents analyzation of its properties. Section 2.3 presents a detailed comparative study of the multilevel STATCOM configurations. The applied autotuned finite control-set model predictive control technique is presented in Section 2.4. Moreover, Sections 2.5 and 2.6 present the simulation and experimental results of the MPUC7-STATCOM performances, respectively. Finally, in Section 2.7, the conclusion is provided.

2.2 MPUC7-STATCOM Configuration

To diminish the size and cost of multilevel converters as well as having improved efficiency, investigating configurations that have the capability of generating more voltage levels with the least possible component count is key. Given this, a single-phase MPUC7-STATCOM configuration, as a credible alternative for the MPUC5-based STATCOM and seven-level

CHB STATCOM, is introduced. The MPUC7-STATCOM as a compact four-quadrant cascaded topology is depicted in Figure 2.1. As seen, two back-to-back crossed-connected half-bridge cells constitute this configuration. Regarding various switching combinations presented in Table 2.1, MPUC7-STATCOM topology can generate up to seven voltage levels (0, ±E, ±2E, ±3E) in its output (V_{ab}). It consists of only six semiconductor switches and two dc capacitors. To achieve seven-level voltage waveform operation, capacitors' voltages, V_{C1} and V_{C2}, should be regulated at 2E and E, respectively. Concerning employed switches' voltage ratings, S_b and S_e should withstand 3E. Besides, S_a and S_d should have a voltage rating of 2E, while S_c and S_f voltage rating is merely E.

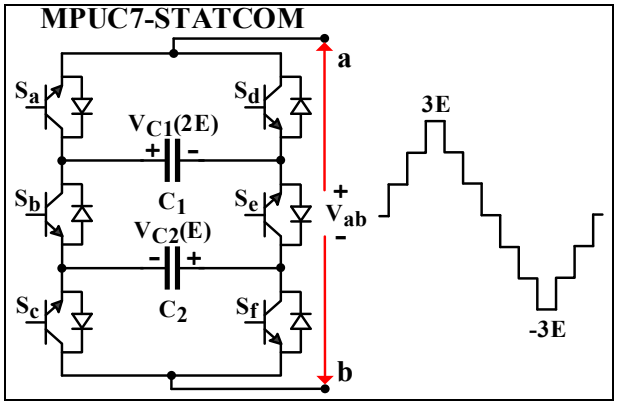

Figure 2.1 MPUC7-STATCOM configuration

Table 2.1 MPUC7-STATCOM switching states

States	S_a	S_b	S_c	Vab	Voltage Level
1	1	0	1	$V_{C1}+V_{C2}$	3E
2	1	0	0	V_{C1}	2E
3	0	0	1	V_{C2}	E
4	0	0	0	0	0
5	1	1	1	0	0
6	1	1	0	$-V_{C2}$	-E
7	0	1	1	$-V_{C1}$	-2E
8	0	1	0	$-V_{C1}-V_{C2}$	-3E

Another critical quality of the MPUC7-STATCOM topology is that its maximum value of the generated compensation voltage (3E) is the summation of both auxiliary capacitors' voltages. This boost-mode operation makes it possible for the dc links (C_1 and C_2) and four of the six switches (S_a, S_c, S_d, and S_f) to have voltage ratings notably smaller than the MPUC7-STATCOM output voltage maximum value. Therefore, relatively small-sized capacitors can be utilized to provide the required maximum voltage value in the STATCOM output. This is one of the structural merits of the proposed topology over two-level-based STATCOM configurations that is interesting for the proliferation of this single-phase STATCOM topology in higher voltage level applications. Operation of MPUC7-STATCOM switches S_a, S_b, and S_c are also complementary to S_d, S_e, and S_f, respectively. By having capacitors as its energy storage elements, MPUC7-STATCOM is designed to mainly and directly compensate reactive power. However, it is also capable to exchange required active power with the grid for charging/discharging the employed capacitors. Therefore, on average, the active power should be controlled continuously to about zero. Yet, it can fluctuate around zero to compensate for system losses.

2.3 Multilevel STATCOM Configurations Comparative Study

Regarding the required active/passive components and generated voltage level, comparison results among MPUC7-STATCOM, MPUC5-based STATCOM, and well-known seven-level single-phase converter topologies, which can be also employed as STATCOM, such as CHB, NPC, and Flying Capacitor (FC) are presented in Table 2.2. As is clear, in the introduced STATCOM topology the minimum number of both passive and active components has been used for generating a seven-level compensation voltage. Consequently, MPUC7-STATCOM can be considered as the most efficient, compact, and cost-effective seven-level configuration. It should be also noted that regarding the single-phase STATCOM application, NPC and FC have not been reported for seven-level operation in the literature. So, although these configurations are mentioned in Table 2.2, they are not compared with the proposed topology in more detail.

Table 2.2 Comparison of Multilevel STATCOM Topologies

STATCOM Type	Capacitor	Diode	Switch	Voltage Level
CHB	3	0	12	7
NPC	6	10	12	7
FC	15	0	12	7
MPUC5	2	0	6	5
Proposed MPUC7	2	0	6	7

2.3.1 Comparison with MPUC5-based STATCOM

One of the main differences between the proposed topology and the MPUC5-based STATCOM is their desired capacitors' voltages. To be clearer, for having the same maximum amount of output voltage (3E), voltages of the capacitors should be fixed at the same value of 3/2E. So, a five-level operation that perceptibly contains more harmonic content is conceivable. Hence, MPUC5-based STATCOM generated current has also higher THD. Besides, in the MPUC5-based STATCOM, through the employed PI-based control method (Vahedi, Dehghanzadeh, et al., 2018), merely the output current is controlled and by using available additional switching states, voltages of both capacitors are regulatable only at the same value. Consequently, as the employed controller is not dependent on the converter dynamic models and charging and discharging of the capacitors is reliant on the required compensation current, voltage distortion on the capacitors is relatively high. Therefore, MPUC5-based STATCOM needs comparatively larger auxiliary capacitors. On the other hand, through the superior operation of the designed AFCS-MPC, voltages of the capacitors are controlled directly and their dynamic models have been also considered. Therefore, employed capacitors' values and their voltage distortion are reduced at the same time in the MPUC7-STATCOM. This reduces the total size and cost of the converter and improves its efficiency.

2.3.2 Comparison with Seven-level CHB-STATCOM

On the other hand, to make a comparison between topologies of the single-phase MPUC7-STATCOM and a seven-level CHB-STATCOM as one of the most appealing multilevel STATCOM configurations, which is illustrated in Figure 2.2, the following points are to be noted: 1) the number of the required power switches is reduced from 12 in the CHB-STATCOM topology to only 6 switches, 2) instead of three isolated capacitors, in the MPUC7-STATCOM only two capacitors are required, 3) there are 3^3 switching states in a seven-level CHB-STATCOM, however, merely 7 switching combinations are available in the proposed topology. Consequently, a reduced number of components in the MPUC7-STATCOM results in improved reliability, size, and cost immensely as well as higher efficiency. Besides, a reduced number of dc links and switching states decreases the nonlinearities of the STATCOM model. This is the key reason that in comparison with the single-phase seven-level CHB-STATCOM, designed AFCS-MPC controller complexity and computational burden are alleviated significantly.

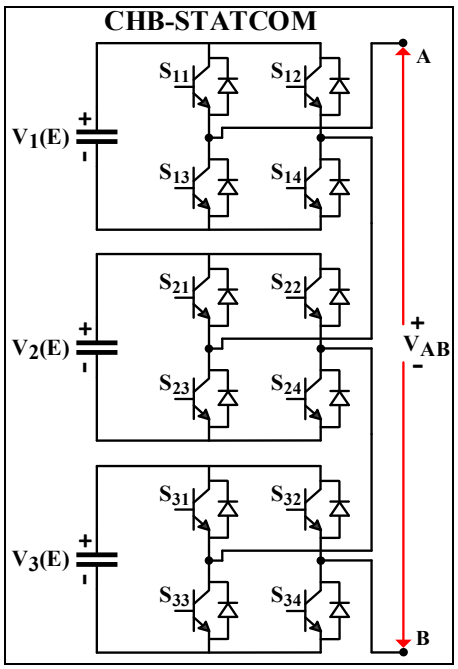

Figure 2.2 CHB-STATCOM

2.4 Proposed Autotuned Finite Control-Set Model Predictive Control

Although auspicious features of the MPUC7-STATCOM topology have been exhibited, three focal control objectives are required to be achieved for ensuring its proper performance. These objectives are the grid current (Is), first capacitor voltage (V_{C1}), and second capacitor voltage (V_{C2}). For simplifying computations, all of the semiconductor switches are deemed to be ideal and merely have ON or OFF states. Besides, there is a requirement for defining two additional variables (S_1 and S_2) to make the application of power switches' ON/OFF states into the calculations more straightforward. Thus, S_1 and S_2 are calculatable as follows:

$$S_1 = S_a - S_b \tag{2.1}$$

$$S_2 = S_b - S_c \tag{2.2}$$

All of the possible states' variables of MPUC7-STATACOM based on the S_1 and S_2 are presented in Table 2.3. Notice that, inasmuch as there are two switching states for the zero-voltage level, seven of the eight plausible switching combinations of the MPUC7-STATCOM presented in Table 2.1 are considered in the controller design. The seven-level compensation voltage (V_{ab}), generated by the MPUC7-STATCOM, is also calculatable as below:

$$V_{ab} = S_1 \times V_{C1} - S_2 \times V_{C2} \tag{2.3}$$

Table 2.3 Revised MPUC7-STATCOM Switching States

States	S_1	S_2	Vab	Voltage Level
1	1	-1	$V_{C1}+V_{C2}$	3E
2	1	0	V_{C1}	2E
3	0	-1	V_{C2}	E
4	0	0	0	0
5	0	1	$-V_{C2}$	-E
6	-1	0	$-V_{C1}$	-2E
7	-1	1	$-V_{C1}-V_{C2}$	-3E

Regarding the voltages of both first and second capacitors (V_{C1} and V_{C2}), we have:

$$I_1 = C_1 \times \frac{dV_{C1}}{dt} = -S_1 \times I_s \tag{2.4}$$

$$\mathrm{I}_2 = C_2 \times \frac{dV_{C2}}{dt} = S_2 \times I_s \tag{2.5}$$

here, I_1, I_2, C_1, and C_2 are the currents and capacitances of the first capacitor and the second capacitor, respectively. By utilizing the well-known Euler forward estimation presented in (2.6) and (2.7), for the sampling time of T_S, auxiliary capacitors' voltages predictive models ($\mathrm{V_{C1}(k+1)}$ and $\mathrm{V_{C2}(k+1)}$) are calculatable based on (2.8) and (2.9) as follows:

$$\frac{dV_{C1}}{dt} = \frac{V_{C1}(k+1) - V_{C1}(k)}{T_s} \tag{2.6}$$

$$\frac{dV_{C2}}{dt} = \frac{V_{C2}(k+1) - V_{C2}(k)}{T_s} \tag{2.7}$$

$$V_{C1}(k+1) = -\frac{S_1 \times T_s}{C_1} \times I_s(k) + V_{C1}(k) \tag{2.8}$$

$$V_{C2}(k+1) = \frac{S_2 \times T_s}{C_2} \times I_s(k) + V_{C2}(k) \tag{2.9}$$

After achieving predictive models of the capacitors' voltages, the grid's current predictive model ($I_s(k+1)$) is still required. In this regard, MPUC7-STATCOM dynamic model is described by the below differential calculation.

$$V_{ab} = V_s + r_f \times I_s + l_f \times \frac{dI_s}{dt} \tag{2.10}$$

here, r_f and l_f represent resistance and inductance of the MPUC7-STATCOM output inductive filter, respectively. Besides, V_s defines the ac voltage of the grid. Another time, by employing the Euler forward approximation, the grid current (I_s) can be also calculated as below:

$$\frac{dI_s}{dt} = \frac{I_s(k+1) - I_s(k)}{T_s} \tag{2.11}$$

Considering (2.10) and (2.11), the grid's current predictive model ($I_s(k+1)$) can be written based on (2.12).

$$I_s(k+1) = \left(1 - \frac{r_f \times T_s}{l_f}\right) \times I_s(k) + \frac{T_s}{l_f} \times (V_{ab}(k) - V_s(k)) \tag{2.12}$$

Regarding the capacitors' voltages and the grid's current calculated predictive models, the cost function of the MPUC7-STATCOM AFCS-MPC (g(k+1)) is designable as follows,

$$g(k+1) = \alpha_1 \times \frac{1}{I_{sn}} \left| I_s(k+1) - I_{sref} \right| + \alpha_2 \times \frac{1}{V_{C1n}} \left| V_{C1}(k+1) - V_{C1ref} \right| + \alpha_3 \times \frac{1}{V_{C2n}} \left| V_{C2}(k+1) - V_{C2ref} \right| \quad (2.13)$$

where, V_{C1ref}, V_{C2ref}, and I_{sref} denote first and second capacitors' reference voltages (2E and E) and the reference of the grid's current, respectively. V_{C1n}, V_{C2n}, and I_{sn} represent the nominal amounts for the first and second capacitors' voltages and the grid's current that are used for normalizing the employed quantities. Besides, α_1, α_2, and α_3 are the autotuned weighting factors that will be defined.

To explain the weighting factor's impact and importance two main points should be considered. First, as cost function includes multiple control objectives, via weighting factors and regarding the tolerable difference between the predictive models and their respective references, these control objectives can have different prioritizations. As an instance, if in (2.13) the difference between $I_s(k+1)$ and I_{sref} is higher than its permissible value, by increasing α_1, this control objective will be prioritized in relation to other control aims and appropriate switching states will be selected with this consideration. Second, combining control targets with various nature such as different magnitudes and units (voltage, current, switching losses, etc.) in a cost function necessitates the employment of weighting factors. Therefore, optimum operation of the FCS-MPC is in direct connection with the accurate adjustment of its cost function's weighting factors. As mentioned, various empirical approaches can be employed for tuning weighting factors in a static manner (Karamanakos & Geyer, 2020), which have promising results during the steady-state operation of the system. However, due to the availability of numerous transients and parametric mismatches, there is a need for utilizing a method based on an online selection of weighting factors in an automated manner.

To accommodate online and automated adjustment of optimal weighting factors in this article,

these coefficients are selected based on the achieved predicted errors of the control terms. So, in each T_S, divergences between the control objectives and their references, which are already calculated in (2.13), are required. Consequently, (2.13) should be splitted as below,

$$g_1 = \frac{1}{I_{sn}} \left| I_s(k+1) - I_{sref} \right| \tag{2.14}$$

$$g_2 = \frac{1}{V_{C1n}} \left| V_{C1}(k+1) - V_{C1ref} \right| \tag{2.15}$$

$$g_3 = \frac{1}{V_{C2n}} \left| V_{C2}(k+1) - V_{C2ref} \right| \tag{2.16}$$

Besides, g_1, g_2, and g_3 should be calculated regarding the seven plausible switching combinations (i=1-7). Next, the minimum amounts of the calculated $g_1(i)$, $g_2(i)$, and $g_3(i)$ should be chosen as follow:

$$\tau_1 = min\ g_1(i) \tag{2.17}$$

$$\tau_2 = min\ g_2(i) \tag{2.18}$$

$$\tau_3 = min\ g_3(i) \tag{2.19}$$

Now, τ_1, τ_2, and τ_3, which are the respective selected minimum values of the calculated $g_1(i)$, $g_2(i)$, and $g_3(i)$ for all the seven switching states should be compared with the permissible errors of the control aims concerning the system constraints.

$$\tau_1 \leq \varepsilon_1 \rightarrow \alpha_1 = \gamma \tag{2.20}$$

$$\tau_2 \leq \varepsilon_2 \rightarrow \alpha_2 = \gamma \tag{2.21}$$

$$\tau_3 \leq \varepsilon_3 \rightarrow \alpha_3 = \gamma \tag{2.22}$$

where, ε_1, ε_2, and ε_3 define the tolerable tracking errors of the control purposes (g_1, g_2, and g_3). In this article, the importance of employing reduced size auxiliary capacitors has imposed a tradeoff with the current control objective. With this regard and concerning reducing the capacitors' voltage ripple, permissible error for capacitors' voltages is defined below 5% of their desired voltage values. Besides, permissible error for the current control objective is selected below 10% of the maximum value of the injected current (Kolluri, Gorla, & Panda, 2020). Moreover, γ is a determined coefficient. To determine the value of γ, it should be considered that the defined control objectives have different variables' nature. As an instance, when the maximum value of the required current is around 11.8 A and the first capacitor's voltage is almost 133.3 V, the current error can be much smaller than the error of the first capacitor's voltage. This renders having a cost function with control objectives that are not equally important. In this regard, as can be noted from (2.13), the cost function has been normalized to have variables with the same degree of importance. As a consequence of having normalized control objectives, which are significant equally, as a beginning point γ should be equal to 1. However, if any of the (2.20), (2.21), and (2.22) is unsatisfied, for prioritization of the unfulfilled control objectives, a bigger amount for the corresponding weighting factors must be chosen as follow:

$$\tau_1 \leq K \times \varepsilon_1 \rightarrow \alpha_1 = K \times \gamma \tag{2.23}$$

$$\tau_2 \leq K \times \varepsilon_2 \rightarrow \alpha_2 = K \times \gamma \tag{2.24}$$

$$\tau_3 \leq K \times \varepsilon_3 \rightarrow \alpha_3 = K \times \gamma \tag{2.25}$$

here, $K \in \{1, 2, \dots, N\}$. In each sampling time, α_1, α_2, and α_3 are selected regarding the quantities of τ_1, τ_2, and τ_3, respectively. Therefore, these achieved real-time tuned weighting factors are applicable to (2.13) for the next sampling period.

To have a better notion of the proposed AFCS-MPC, a flowchart of this MPUC7-STATCOM non-linear controller is illustrated in Figure 2.3. As seen, it contains two main loops. Through the external loop, which should be performed each sampling time (k), the variables of $I_s(k)$, $V_s(k)$, $V_{C1}(k)$, and $V_{C2}(k)$ are measured and send to the controller. On the other hand, in the internal loop that contains weighting factors autotuning subdivision, for achieving the optimal values, the calculations of V_{ab}, $V_{C1}(k+1)$, $V_{C2}(k+1)$, and $I_s(k+1)$, based on (2.3), (2.8), (2.9), and (2.12) correspondingly, should be done for all the plausible switching combinations. Based on these achieved amounts, $g_1(i)$, $g_2(i)$, and $g_3(i)$ will be also calculated and, as explained before, the weighting factors selection process is performed. As the next step, regarding (2.13) and by taking advantage of the discrete feature of the MPUC7 converter, S_1 and S_2 that result in a minimized amount of g(k+1) are selected. After determining the switching state number by employing Table 2.3 and the achieved S_1 and S_2, with regard to Table 2.1, switching signals will be generated and directly transferred to the MPUC7-STATCOM switches. Figure 2.4 also depicts a simplified schematic of the presented AFCS-MPC for the MPUC7-STATCOM application. As can be seen, for compensation of merely reactive power, the arbitrarily chosen reference grid current (I_{sref}) should have $\pi/2^{\circ}$ phase difference with the grid voltage (V_s).

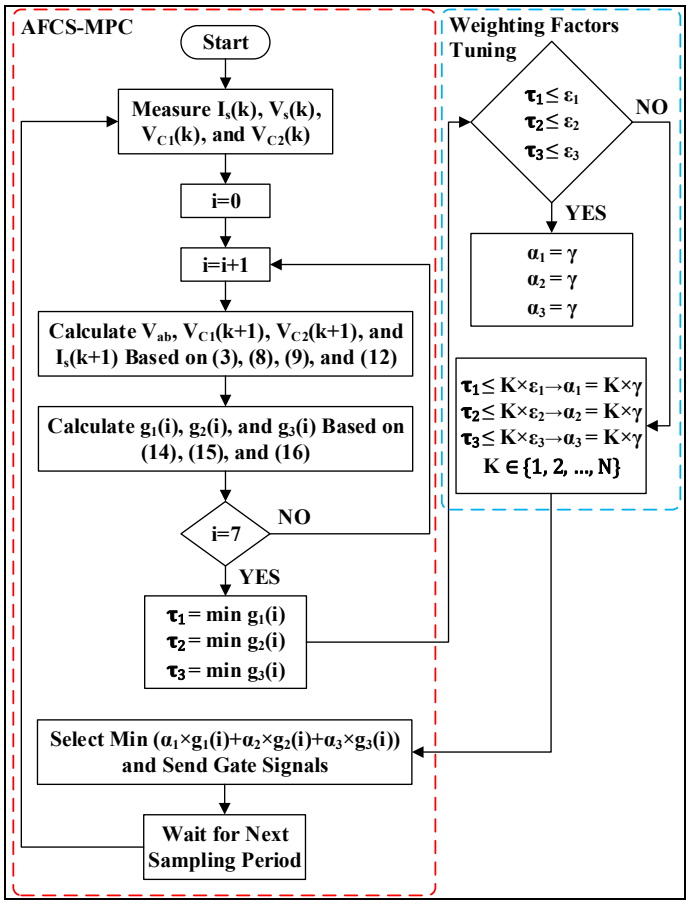

Figure 2.3 MPUC7-STATCOM controller flowchart

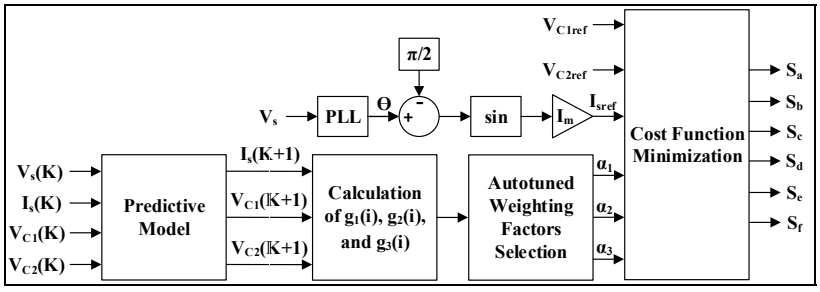

Figure 2.4 Simplified illustration of the designed AFCS-MPC

2.5 Simulation Results

Utilizing the SimPowerSystems toolbox of MATLAB, a simulated system comprising the proposed MPUC7-STATCOM as depicted in Figure 2.5 is designed. Besides, specifications of this Simulink-based system are presented in Table 2.4. All the simulation parameters are

selected as the same values considered in (Vahedi, Dehghanzadeh, et al., 2018) excluding the dc capacitors amounts and voltages. By utilizing the designed AFCS-MPC, it has been possible to decrease the values of C_1 and C_2.

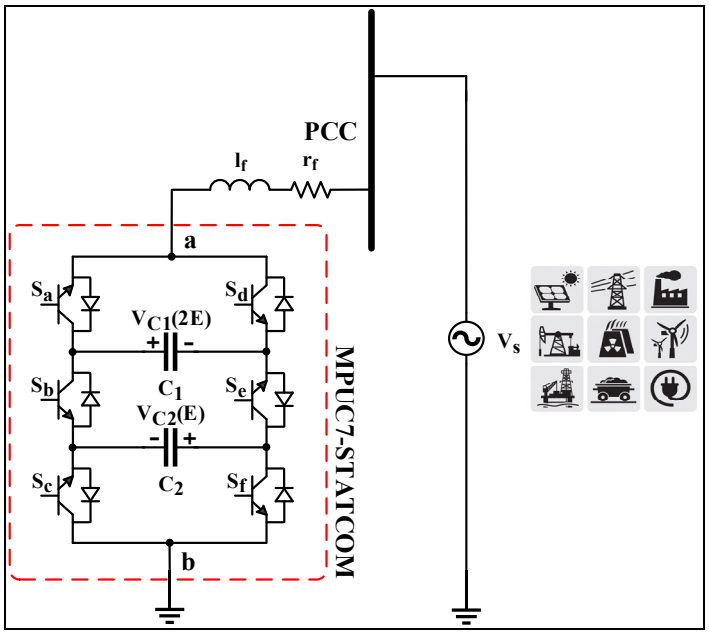

Figure 2.5 Diagram of the simulation/experimental

Table 2.4 Parameters of the simulation setup

RMS Voltage of Grid (V_s)	120 V
Grid Frequency (F)	60 Hz
Output Filter Inductance (l_f)	2.5 mH
Output Filter Resistance (r_f)	0.1 Ω
Maximum Value of Output Voltage (3E)	200 V
First Capacitor DC Voltage ($V_{C1} = 2E$)	133.3 V
Second Capacitor DC Voltage ($V_{C2} = E$)	66.7 V
First Capacitor Capacitance (C_1)	2000 µF
Second Capacitor Capacitance (C_2)	2000 µF

2.5.1 Comparison Between MPUC7-STATCOM and MPUC5-based STATCOM

To make a valid performance comparison between the MPUC5-based STATCOM (Vahedi, Dehghanzadeh, et al., 2018), and the introduced MPUC7-STATCOM, firstly, the steady-stated operation results of the MPUC7-STATCOM at approximately 1 kVAr ($I_m = 11.8$ A) are focused. In this regard, Figure 2.6 illustrates the recorded measurements of this simulation test. As can be seen, instead of the five-level, the generated compensation voltage has a seven-level performance. This results in a lower THD of the generated voltage and consequently superior power quality performance. In addition, the grid current has $\pi/2^{\circ}$ phase difference with the generated voltage to compensate mainly reactive power. Moreover, V_{C1} and V_{C2} are successfully fixed at around their desired values (133.3 V and 66.7 V). On the other hand, although smaller capacitors have been employed in this work in comparison with (Vahedi, Dehghanzadeh, et al., 2018), voltage distortion on the capacitors is reduced from around 10% in (Vahedi, Dehghanzadeh, et al., 2018) to almost 5%. This improvement is mainly the result of controlling the capacitors' voltages directly through the designed AFCS-MPC. The other important point is that the consumed amount of active power, which is mostly due to the converter losses and voltage/power balance of the capacitors, is reduced from around 15 W in (Vahedi, Dehghanzadeh, et al., 2018) to less than 5 W. Nonetheless, as desired, the produced reactive power is stabilized at around 1 kVAr.

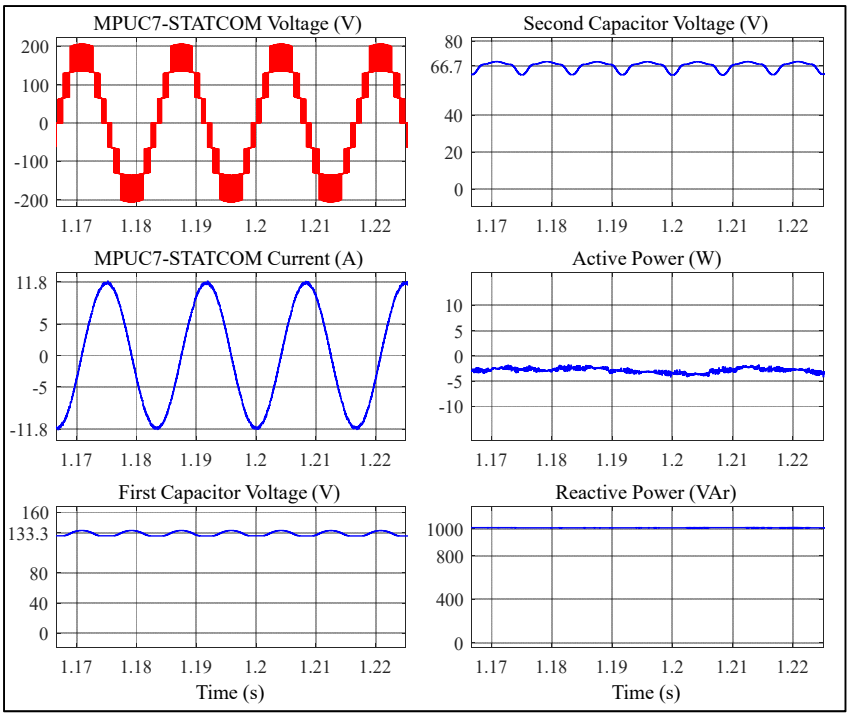

Figure 2.6 Simulation results at 1 kVAr

The harmonic spectrum analysis of the MPUC7-STATCOM injected current during the aforementioned simulation is indicated in Figure 2.7. As depicted, the THD content is merely 1.6% which is less than half of the harmonic content of the injected current during the same circumstances and output filter inductor using an MPUC5-based STATCOM (Vahedi, Dehghanzadeh, et al., 2018). This is a direct result of the MPUC7-STATCOM seven-level operation. It should be also considered that, while comparing to the MPUC5-based STATCOM proposed in (Vahedi, Dehghanzadeh, et al., 2018), MPUC7-STATCOM has enhanced power quality operation, it employs auxiliary capacitors with reduced capacitance values. This confirms the improved power density, size, and cost of the proposed MPUC7-STATCOM topology. On the other hand, for demonstration of the MPUC7-STATCOM dynamic operation, firstly, by instant reduction of I_m from 11.8 A to 5.9 A the reactive power generation is decreased from roughly 1 kVAr to approximately 0.5 kVAr suddenly. Secondly, by increasing I_m from 5.9 A to 11.8 A, the reactive power generation is increased from around 0.5 kVAr to almost 1 kVAr instantly. As demonstrated in Figures 2.8 and 2.9, after these transients, the capacitors' voltages have been kept at the required values successfully. Moreover, the seven-

level waveform of the MPUC7-STATCOM voltage is acceptable during both of these sudden transients. However, as expected, the injected current and reactive power have been reduced and increased instantly within just one cycle, respectively.

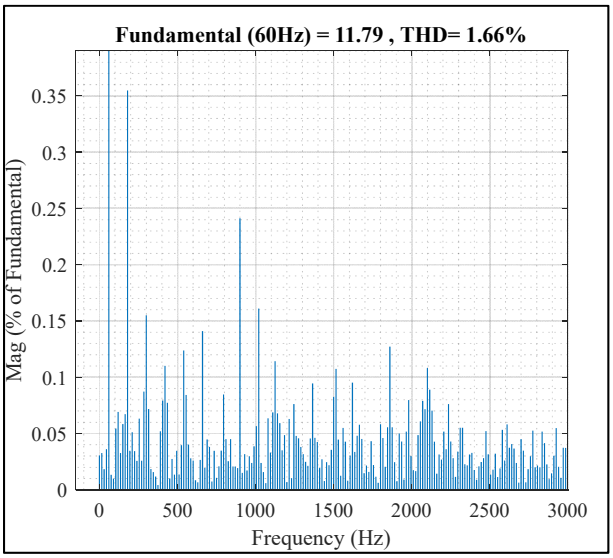

Figure 2.7 Injected current harmonic analysis

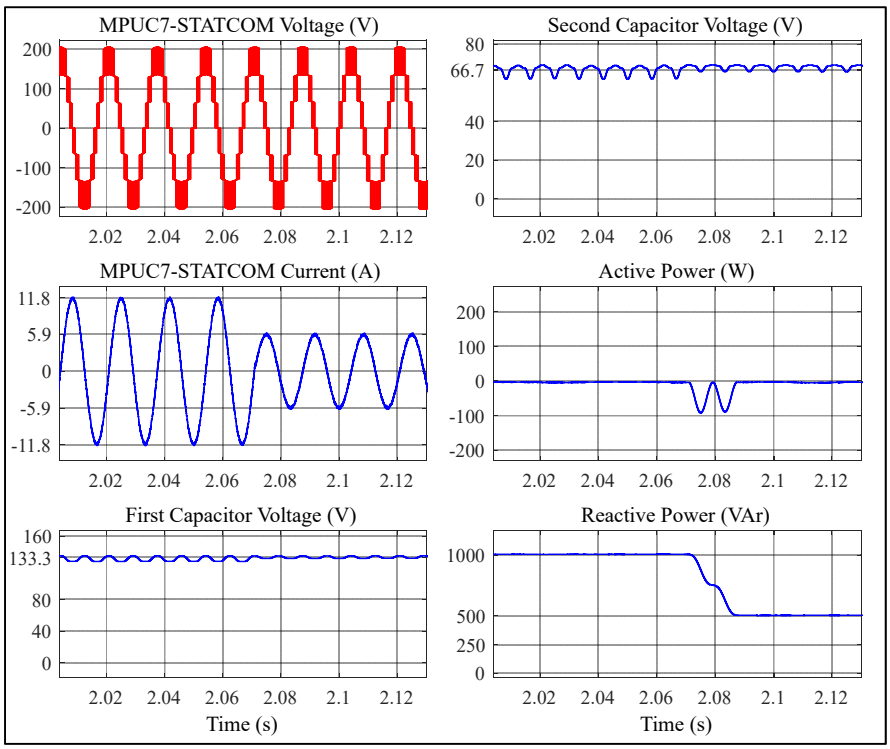

Figure 2.8 Reactive power reduction from 1 kVAr to 0.5 kVAr

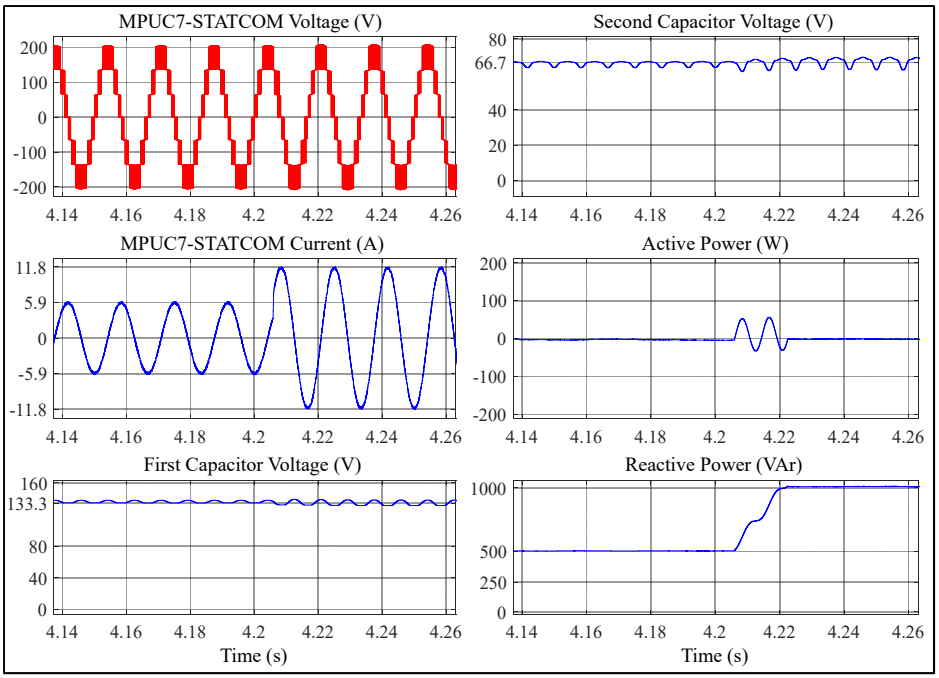

Figure 2.9 Increasing the reactive power from 0.5 kVAr to 1 kVAr

2.5.2 Comparison Between AFCS-MPC and the Conventional FCS-MPC

In order to demonstrate the superior operation of the proposed AFCS-MPC for the MPUC7-STATCOM, its dynamic performance and computational burden during the converter start-up have been compared with the conventional FCS-MPC with fixed weighting factors ($\alpha_1 = 1.5, \alpha_2 = 1.2$, and $\alpha_3 = 1.85$). Firstly, for comparing the start-up transient performance of the proposed AFCS-MPC with the conventional FCS-MPC with fixed weighting coefficients, Figure 2.10 illustrates the measured parameters of the system during MPUC7-STATCOM start up for roughly 1 kVAr operation. It should be also mentioned that the model capacitance values of the capacitors in both controllers have been changed to 3000 μF to apply parametric mismatches. As can be noted, although there is an unstable condition, as well as harsh mismatches available in the system, both overshoots and settling times of the capacitors' voltages, are improved significantly by the proposed controller. Moreover, to show the real-time auto-adjustment performance of the designed AFCS-MPC, as an instance, Figure 2.11 depicts three-dimension curve of the second capacitor's voltage tracking errors ($|V_{C2}(k+1) - V_{C2ref}|$) based on the related weighting factor (α_3) and time during this simulation. Presented

results prove the online and automated adjustment of weighting factors based on the calculated tracking errors of the related control goal.

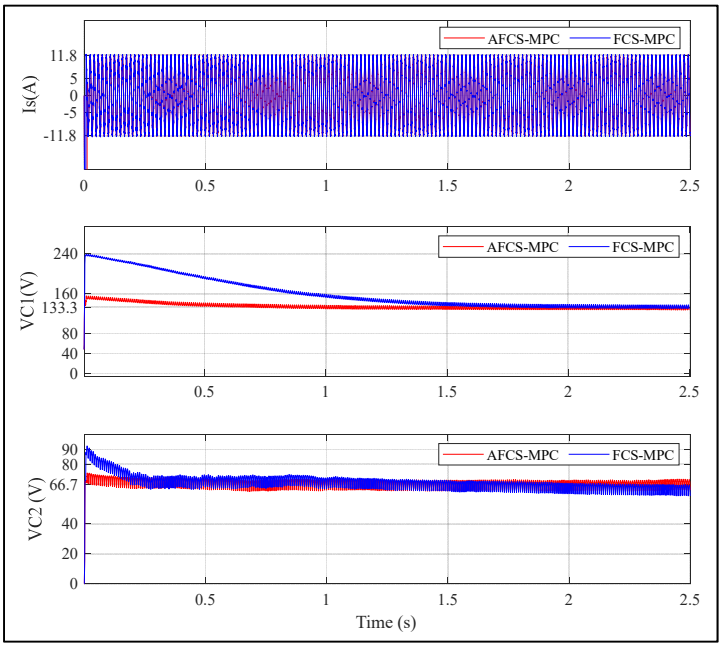

Figure 2.10 Measurements during start up
with the conventional FCS-MPC and AFCS-MPC

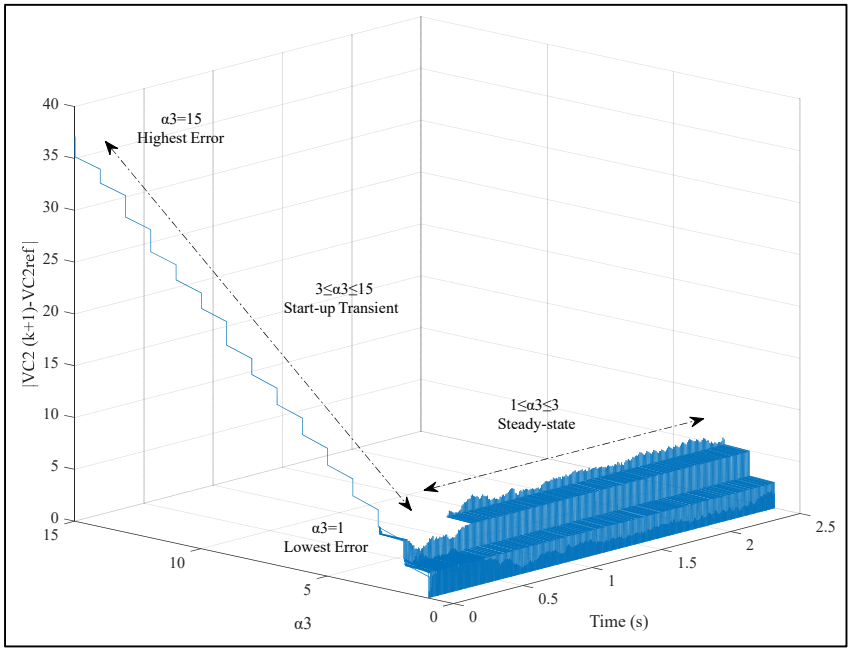

Figure 2.11 V_{C2} tracking errors based on autotuned α_3 and time

On the other hand, to compare their computational costs, both of these controllers have been applied to the MPUC7-STATCOM. During the start-up and with a sampling time of 20 µs, execution times of the controllers are measured for a period of 0.2 s. As illustrated in Figure 2.12, the average execution time of the conventional FCS-MPC is at about 3.32 µs. However, AFCS-MPC average execution time is increased to roughly 3.56 µs. As is clear, on average there is only around a 7.2% increase in the computational burden of the proposed control method that proves its practicality. This is mainly due to the fact that the main parameters employed for real-time auto-adjustment of the weighting coefficients are control objectives' tracking errors which are already calculated in (2.13). This demonstrates that AFCS-MPC for MPUC7-STATCOM is a computationally efficient controller.

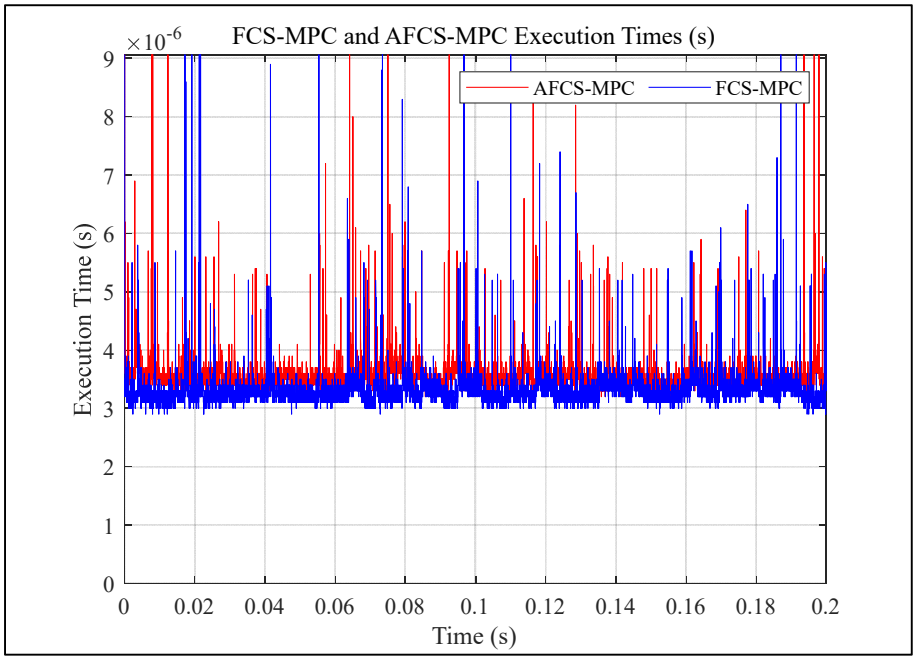

Figure 2.12 Execution times of FCS-MPC and AFCS-MPC

2.6 Experimental Results

This section is mainly devoted to demonstrating the steady-state and transient operation of the introduced MPUC7-STATCOM in addition to its feasibility experimentally. Accordingly, exploiting six insulated-gate bipolar transistor (IGBT) switches (FGH30N60LSD) and two dc

capacitors, a laboratory prototype of the MPUC7-STATCOM has been implemented. Moreover, the designed AFCS-MPC algorithm is applied to this MPUC7-STATCOM prototype by a MicroLabBox dSPACE 1202 control board and associated channels of I/O in real-time with a static sampling time of 50 µs. Using dSPACE analog-to-digital converter (ADC) cards, measured signals of $I_s(k)$, $V_s(k)$, $V_{C1}(k)$, and $V_{C2}(k)$ via OPAL-RT high voltage and current monitoring interface (OP8662), are also sampled and transferred to the MicroLabBox in an online manner. It should be also mentioned that using OPAL-RT voltage/current probe, the range of measured parameters will be converted to merely ±10 V voltage signals that are manageable and readable by the real-time controller's inputs. The schematic design of the prepared experimental setup and its picture are illustrated in Figures. 2.5 and 2.13, respectively. Additionally, the parameters of this MPUC7-based laboratory arrangement are the same as the simulation system presented in Table 2.4.

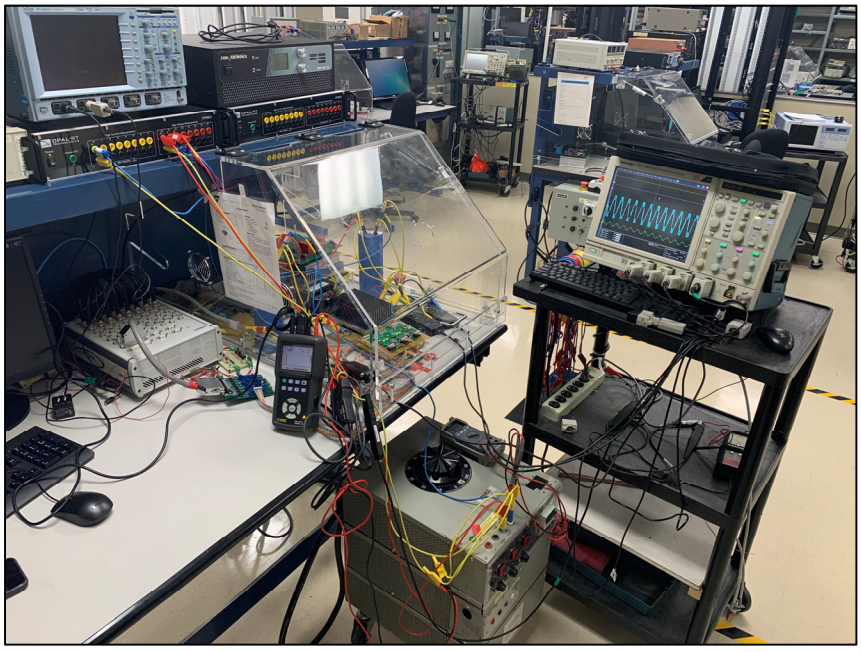

Figure 2.13 Experimental setup picture

As above-mentioned, the main objective of the MPUC7-STATCOM is to maintain the point of common coupling (PCC) voltage stability through instant reactive power compensation. Hence, initially, to confirm the MPUC7-STATCOM performance in steady-state, Figures 2.14 and 2.15 depict measured parameters of the system when grid-connected MPUC7-STATCOM

operates, as an instance, at around 0.5 kVAr. This means that the maximum value of the grid current reference (I_m) is set at about 5.9 A. As Figure 2.14 shows, although the maximum value of the MPUC7-STATCOM produced voltage is 200 V (3E), V_{C1} and V_{C2} are controlled at around 133.3 V (2E) and 66.7 V (E), respectively. Therefore, MPUC7-STATCOM boost-mode operation competence can be proven. Besides, as seen, regarding the defined permissible error for capacitors' voltages, the voltage distortion of capacitors is merely at around 5%. Moreover, as is clear in Figure 2.15, the grid's current waveform leads the grid and MPUC7-STATCOM voltages by about $\pi/2^{\circ}$ for compensating primarily reactive power. Nonetheless, MPUC7-STATCOM consumes an insignificant value of active power mainly for fixing the auxiliary capacitors' voltages to their desired values and switching losses. Furthermore, due to the accurate regulation of the capacitors' voltages with tolerable ripples through the proposed AFCS-MPC, the seven-level waveform of the generated compensation voltage by the MPUC7-STATCOM is acceptable.

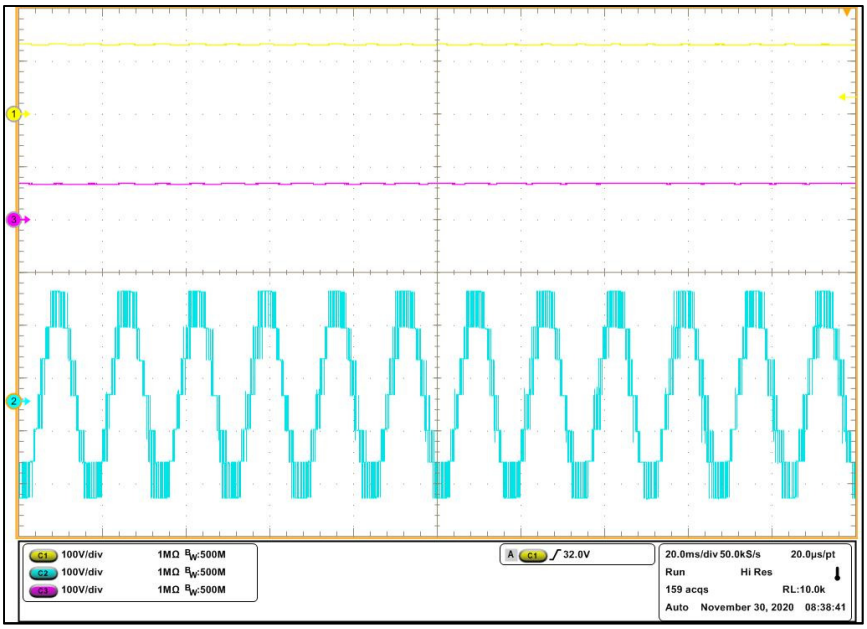

Figure 2.14 From top to bottom, V_{C1}, V_{C2}, and V_{ab} during steady-state 0.5 kVAr operation

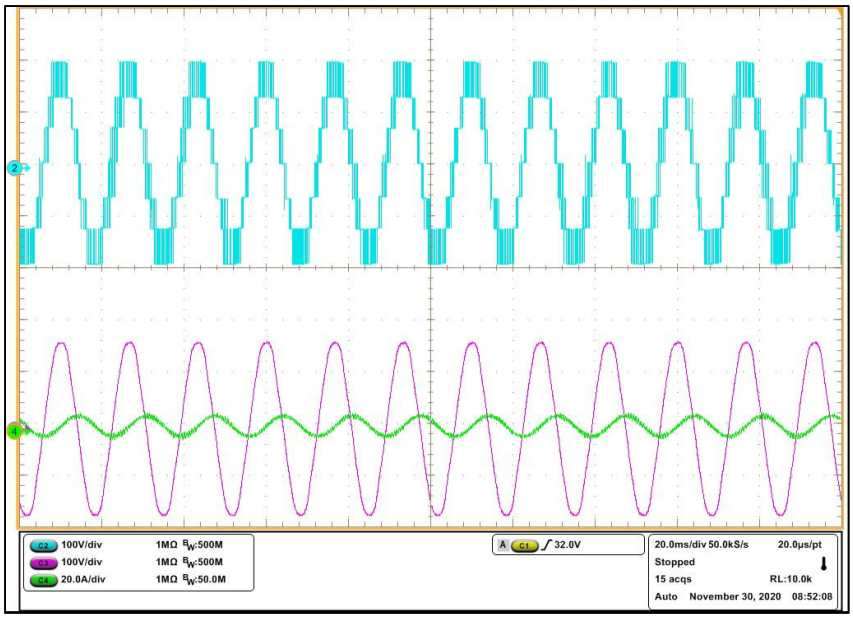

Figure 2.15 From top to bottom, V_{ab}, V_S, and I_S during steady-state 0.5 kVAr operation

With regard to the MPUC7-STATCOM dynamic performance illustration, firstly, MPUC7-STATCOM generated reactive power is decreased from about 1 kVAr to almost 0.5 kVAr instantly. Secondly, it is increased from roughly 0.5 kVAr to around 1 kVAr. So, 50% reduction and 100% amplification in the MPUC7-STATCOM injected reactive power have been tested. Recorded waveforms of these tests are presented in Figures 2.16 and 2.17. As can be noted, during both of these sudden reactive power changes, as a result of MPUC7-STATCOM's superior dynamic operation, although the maximum values of the grid current are reduced and increased instantly, the capacitors' voltages are effectively and simultaneously kept stable at their wanted amounts. Consequently, the seven-level waveform of the generated compensation voltage is satisfactory throughout these significant transients. On the other hand, using a power analyzer, THD analysis of the MPUC7-STATCOM current throughout 1 kVAr operation can be seen in Figure 2.18. The injected current THD is around 3.7% that satisfies the IEEE 1547 standard requirement. Furthermore, to investigate the robustness of the designed AFCS-MPC for the MPUC7-STATCOM against the availability of the parametric mismatches, model capacitance values of C_1 and C_2 in the real-time controller have been changed from 2000 µF to 3000 µF. Figure 2.19 provides the measured and recorded harmonic

analysis of the MPUC7-STATCOM current throughout 1 kVAr operation in this case. As can be seen, even during the presence of severe parametric mismatches, measured THD is still less than 5%.

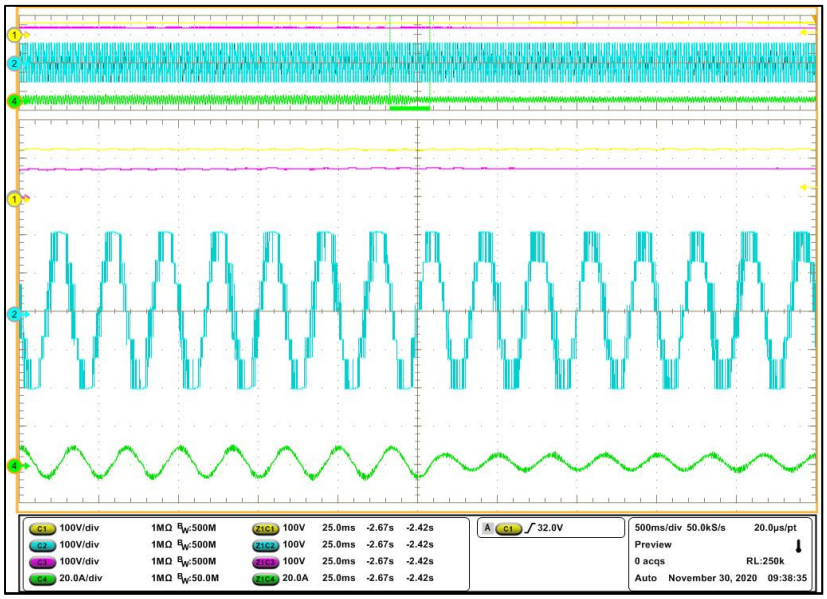

Figure 2.16 From top to bottom, V_{C1}, V_{C2}, V_{ab}, and I_S during instant reduction of the compensated reactive power

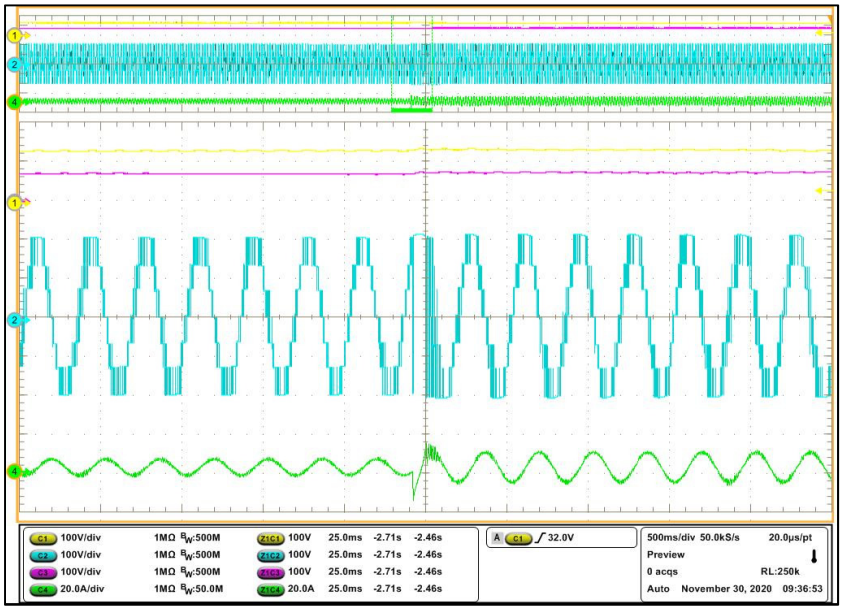

Figure 2.17 From top to bottom, V_{C1}, V_{C2}, V_{ab}, and I_S during instant amplification of the reactive power

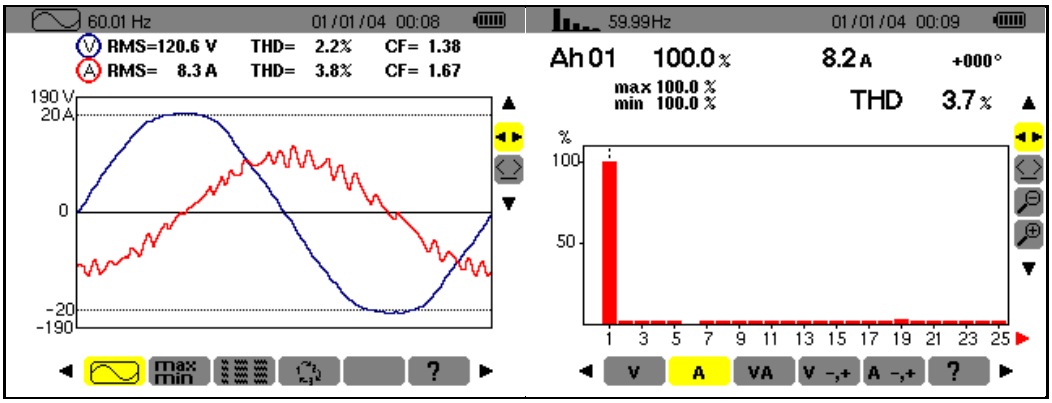

Figure 2.18 Power analyzer results of the injected current THD analyzation

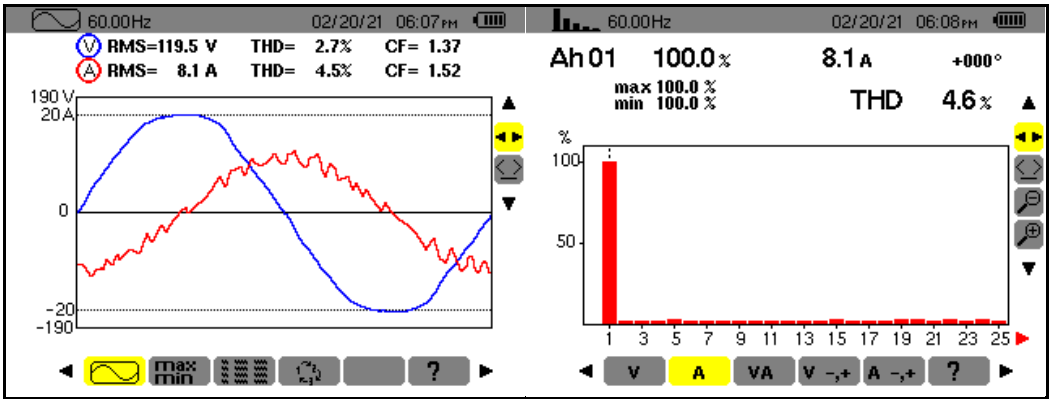

Figure 2.19 Power analyzer results of the injected current
THD analyzation under availability of the parametric mismatches

Finally, it is clear that achieved experimental results are in accordance with the simulation tests and a higher amount of injected current THD in the experimental results is mainly due to the higher sampling time of the real-time controller.

2.7 Conclusion

This article presents a compact single-phase MPUC7-STATCOM topology and its particular auto tunable FCS-MPC method for the first time. Previously, in the five-level MPUC5-based STATCOM, by utilizing a linear PI-based controller, only the grid current was controllable in a closed-loop manner and capacitors' voltages were regulated at only the same value through the extra switching states. However, regulation of the MPUC7-STATCOM capacitors'

voltages and injected compensation current accurately and autonomously using only a single control loop are made possible by the objective constrained optimization with auto-adjusted weighing factors competence of the designed AFCS-MPC. Subsequently, although both of these STATCOM configurations have the same component count, seven-level operation with reduced-size capacitors is realizable via the introduced MPUC7-STATCOM. Furthermore, PI-coefficients adjustment is not required and a dynamic model of the MPUC7 converter has been also considered. On the other hand, in comparison with a CHB-STATCOM, MPUC7-STATCOM has two pivotal merits. First, the number of required switches is halved and only two isolated dc capacitors are employed. Secondly, its AFCS-MPC control algorithm is less complex as a result of having a lower number of active/passive components, switching states, and control objectives. By the presented extensive simulation and experimental results, MPUC7-STATCOM feasibility and operation are also confirmable effectively. Finally, the proposed STATCOM topology can also be a superior candidate for replacing the three-phase seven-level CHB-STATCOM.

CHAPTER 3

ELECTRIC SPRING USING MPUC5 INVERTER FOR MITIGATING HARMONICS AND VOLTAGE FLUCTUATIONS

Amirabbas Kaymanesh [a] and Ambrish Chandra [a],

[a] Department of Electrical Engineering, École de Technologie Supérieure,
1100 Notre-Dame West, Montreal, Quebec, Canada H3C 1K3

Paper published in *IEEE Journal of Emerging and Selected Topics in Power Electronics*,
October 2020

Abstract

This paper introduces a novel configuration of electric spring based on the modified five-level packed u-cell (MPUC5) inverter for mitigating harmonics and voltage fluctuations at various points of a grid with unstable generated power from distributed renewable energy sources. Immanent merits of the proposed configuration include, but are not limited to, halved DC links voltages, boost mode operation, possibility of higher power applications, smooth five-level voltage waveform with low total harmonic distortion (THD) index, the smaller size of output low pass filter, and low switching frequency. The operation principles, design procedure, and configuration of the MPUC5-based electric spring (MPUC5-ES) are also presented. Besides, a simple and yet efficient controller without any extra control loop for regulating DC bus voltages has been proposed. Finally, the introduced multilevel electric spring is tested through extensive simulation and experimental studies to confirm its dynamic and steady-state performances in various operation modes in a weak grid fed by both conventional and intermittent renewable energy sources.

3.1 Introduction

In order to ensure access to affordable, sustainable, and modern energy for all, increasing the penetration of inverter-based renewable distributed energy resources such as solar power into the electricity grid is of great importance. As of 2019, renewable energy sources including hydropower accounted for an estimated 17.3% primary energy supply of the Canada power generation mix (Canada, 2017). However, achieving the goal of having a world powered by wind, water and sunlight has certain challenges to the stability and reliability of operation of the bulk power system. In order to encounter these issues, electric spring (ES) has been proposed as a modern demand response management technology (Hui et al., 2012). It has been mainly designed with the aim of regulating the voltage at various points of the grid with high penetration of intermittent renewable energy sources by merely reactive power compensation. Therefore, power electronic-based electric spring could have a pivotal role in stabilizing power grids with high penetration of nonsynchronous generators in the future. By far, various versions of ESs have been reported in several papers.

Chi Kwan and Shu Yuen (C. K. Lee & Hui, 2013) have proved that employing electric spring can reduce the needed energy storage capacity for stabilizing the grid. Steady-state analysis and control principle of the ES have been reported in (Tan et al., 2013). Hardware and control implementation of an ES have been done for the first time in (C. K. Lee, Chaudhuri, & Hui, 2013). Authors in (Chaudhuri et al., 2014) and (T. Yang et al., 2018) have managed to present a dynamic model of an ES that can be employed for voltage and frequency control analyzations. Most recently, in (Q. Wang et al., 2018) and (Zheng, Hill, Meng, & Hui, 2017) new control schemes for both active and reactive power of different types of ESs have been proposed. In all the reported works, half-bridge or full-bridge voltage source inverters have been employed as ES. However, in comparison to these conventional topologies, multi-level inverters (MLI) have numerous advantages such as higher power application, lower switching frequency and losses, better power quality performance, improved total harmonic distortion (THD), less voltage stress on the power semiconductor devices, lower electromagnetic interface, reduced size of output LC filter etc.

The cascaded H-bridge, flying capacitor and neutral point clamped inverters are considered classical multi-level configurations that can be employed as ES. However, these topologies for producing a higher number of output voltage levels have disadvantages such as an increased number of independent DC sources, switches and capacitors (Gautam, Kumar, & Gupta, 2018). In addition, for utilizing classical multilevel inverters as the first version of ES, which exchanges only reactive power with the system, a complex external controller is required to balance the voltage of energy storage elements. Recently, modified five-level packed U-cell converter so-called MPUC5 with a novel characteristic of balancing power and voltage of the DC capacitors through redundant switching states has been introduced in (Vahedi & Al-Haddad, 2016a) as an active buck power factor corrector rectifier. In (Vahedi, Shojaei, et al., 2018), authors have also managed to employ MPUC5 configuration as an active power filter. This topology is operational at no-load conditions, which makes it a suitable option for ES application.

In comparison to the progress of various controller methods applied on ES, there are few works with the focus on the topology of the ES itself. Therefore, in this work, MPUC5 topology has been introduced as an electric spring for the first time. Besides, a control method has been also proposed for mitigating both harmonics and voltage fluctuations using a five-level type of ES with MPUC5. Exploiting MPUC5 configuration as an ES will result in the following improvements.

1. Proposed ES operates in boost mode with a halved voltage at DC links, which makes the application of ES for higher power/voltage levels a plausible option.
2. The value of THD is decreased at the output of the MPUC5-based ES (MPUC5-ES) due to the symmetrical five-level waveform of the generated voltage. This also results in less current harmonics, which leads to a reduced size of output low pass LC filter.
3. The switching frequency is notably lower and thus losses in switches will be reduced and total efficiency is higher.
4. It has a promising dynamic performance in various operation conditions.

5. Semiconductor switches in MPUC5-ES configuration endure lower voltage stress in comparison to conventional ES and the voltage and power rating of the employed components are lower.

The main contributions of this work are also highlighted below briefly.
1. A multilevel topology as ES has been proposed which improves the operation and power quality characteristics of electric spring from various points of view.
2. The systematic design of a multilevel smart load has been presented for the first time.
3. Although harmonics mitigation employing ES technology has been recently proposed in (Q. Wang, Cheng, & Jiang, 2016) and (Yan, Tan, et al., 2017), in (Q. Wang et al., 2016) a current source inverter based on a full-bridge configuration is utilized as an ES and in (Yan, Tan, et al., 2017) a battery-based ES founded on a half-bridge topology is employed for harmonics suppression. To the best of our knowledge, it is the first time that a five-level electric spring using capacitors as its energy storage elements for mitigating both harmonics and voltage fluctuations has been proposed.

In detail, this paper is organized as follows. In section 3.2, operating principles as well as the design procedure of an MPUC5-based electric spring are presented. Configuration and voltage balancing method of the proposed MPUC5-ES have been described in section 3.2. The proposed controller algorithm and design are the focus of section 3.4. Section 3.5 discusses simulation and experimental results and analyzation of the introduced MPUC5-ES extensively. Finally, the conclusion is gotten in section 3.6.

3.2 Operating Principles and Design of the MPUC5-Based ES

Loads in power systems can be separated into two main different categories namely, critical and noncritical. Contrary to critical loads (CLs), noncritical loads (NCLs) such as street lighting systems can endure some extend of voltage fluctuations with relatively lower power quality. An NCL connected in series with an ES will be converted into a new generation of smart load (SL). These so-called SLs not only can stabilize the point of common coupling

(PCC) voltage with high power quality but also modify their power consumption with the availability of the generated renewable energy (Hui et al., 2012). These electric springs can be mounted in all residential, commercial and industrial areas and spread all over the bulk power system for decentralizing stability control in the near future.

Figures 3.1 and 3.2 depict the circuit diagram of the proposed ES in an SL setup and its vector diagram for PCC voltage regulation, respectively. As illustrated in Figure 3.1, two main categories of the loads are connected to a weak grid with a fluctuating distorted PCC voltage due to unstable produced power by distributed renewable energies. The proposed MPUC5-based ES is connected in series with the NCL to set up a multi-level SL configuration. It is worth mentioning that the NCL might be also a group of electrical devices that can endure voltage fluctuation in the same range. The SL setup is in parallel with a CL that is highly sensitive to the voltage variations and demands a constant amount of power with high quality such as electronic devices. Based on the vector scheme of the MPUC5-based ES depicted in Figure 3.2, the PCC voltage is the vector summation of the MPUC5-based electric spring output voltage and the NCL voltage. Thus, NCL voltage in the inductive mode will be reduced and conversely, through the capacitive mode will be increased.

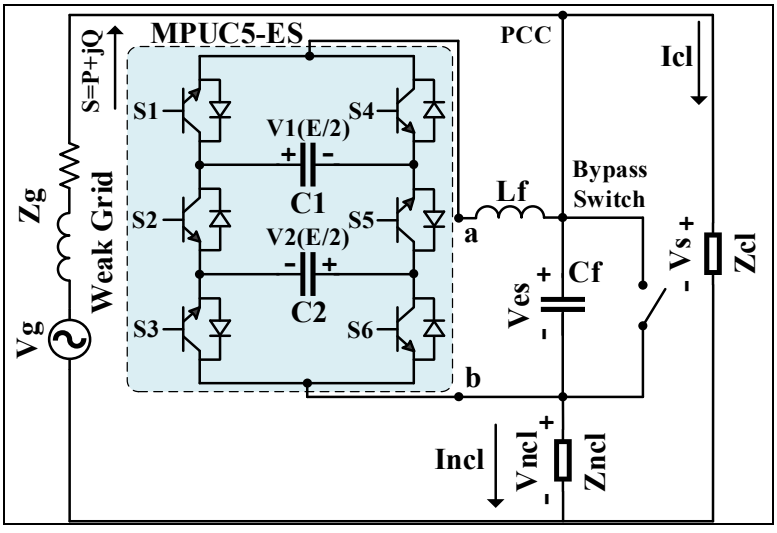

Figure 3.1 MPUC5-ES circuit in the SL setup

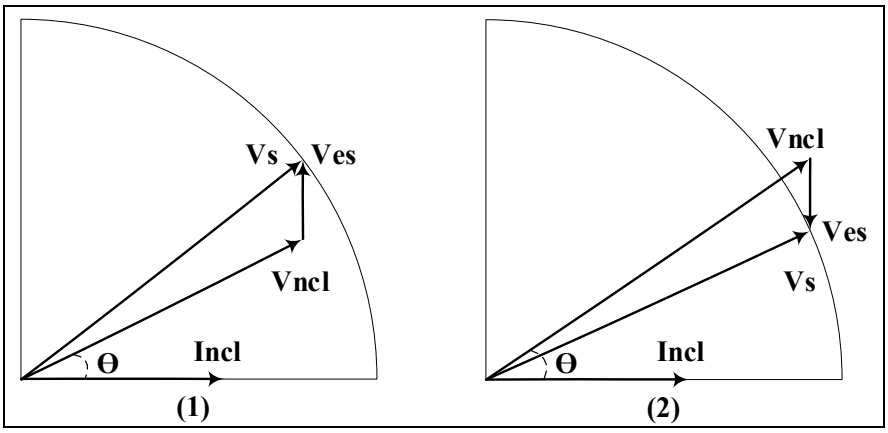

Figure 3.2 Vector scheme of the MPUC5-based ES with
an inductive NCL (1) inductive operation (2) capacitive operation

As mentioned, a CL demands high-quality power, therefore, the application of the MPUC5-ES can be extended to also reduce the THD of a distorted PCC voltage. For effectively mitigating CL harmonics, MPUC5-ES should also generate the harmonics component of the PCC voltage.

3.2.1 Operating Principles

The equation of the instantaneous PCC distorted voltage ($V_s(t)$) can be expressed as below.

$$V_s(t) = \sum_{n=1}^{\infty} V_n \, sin(n\omega t + \varphi_n) \tag{3.1}$$

here, n is the order of harmonic, V is the peak amount of voltage, ω denotes fundamental angular frequency, and φ_n is the respective phase angle. Employing Fourier analysis, (3.1) can be decomposed as below,

$$V_s(t) = V_1 \, sin(\omega t + \varphi_1) + \sum_{n=2}^{\infty} V_n \, sin(n\omega t + \varphi_n) \tag{3.2}$$

Therefore, for improving the power quality of the PCC voltage, and based on the instantaneous voltage equation of this system (3.3), MPUC5-ES by producing the harmonics components of the PCC voltage will be able to reduce the THD of the CL voltage effectively.

$$V_s(t) = V_{ncl}(t) + V_{es}(t) \tag{3.3}$$

On the other hand, based on the MPUC5-based ES vector diagram for both inductive and capacitive operation, the PCC voltage (V_s) can be also expressed as

$$V_s^2 = (V_{ncl}\, cos\, \Theta)^2 + (V_{ncl}\, sin\, \Theta \pm V_{es})^2 \tag{3.4}$$

where Θ denotes the angle of power factor (PF) of the NCL and V_{ncl} and V_{es} are NCL and MPUC5-ES voltages, respectively. Besides, as can be seen in Figure 3.2, for the inductive operation of the SLs, injected compensation voltage by the MPUC5-ES is positive and for the capacitive operation, V_{es} is negative. By solving (3.4), for the NCL voltage we have

$$V_{ncl} = \pm V_{es}\, sin\, \Theta \pm \sqrt{V_{es}^2\, sin\, \Theta^2 - V_{es}^2 + V_s^2} \tag{3.5}$$

As can be noted form (3.5), NCL voltage is dependent on both of the PCC and MPUC5-ES voltages. Thus, by adjusting the MPUC5-ES voltage and consequently modifying the NCL voltage, the active and reactive power of the NCL can be modified based on the generated power of the available renewable energy sources in the grid in order to stabilize the power system. This flexibility in the demanded power is the main reason for considering this setup as a multilevel smart load. Consequently, current, active power and reactive power of the smart load can be calculated based on (3.6) to (3.8), respectively (C. K. Lee, Chaudhuri, & Hui, 2013). It needs to be also clarified that for the sake of simplicity the power loss on the L_f is neglected and the ES is considered to be a controllable AC voltage source.

$$I_{sl} = \frac{V_{ncl}}{Z_{ncl}} = \frac{V_{ncl}}{\sqrt{R_{ncl}^2 + X_{ncl}^2}} \tag{3.6}$$

$$P_{sl} = V_{ncl} I_{sl} \cos\Theta = \frac{V_{ncl}^2 \cos\Theta}{Z_{ncl}} \tag{3.7}$$

$$Q_{sl} = V_{ncl} I_{sl} \sin\Theta + V_{es} I_{sl} = \frac{V_{ncl}^2 \sin\Theta + V_{ncl} V_{es}}{Z_{ncl}} \tag{3.8}$$

where $Z_{ncl} = R_{ncl} + jX_{ncl}$ defines the NCL impedance.

3.2.2 Design Procedure

For designing a multifunctional multi-level inverter-based SL firstly, the required reactive power produced by ES should be calculated based on (3.9). Furthermore, for the inductive operation of the MPUC5-based ES, Q_{es} has a positive sign and conversely for the capacitive operation, it should have a negative sign.

$$Q_{es} = \frac{\pm V_{es} V_{ncl}}{Z_{ncl}} \tag{3.9}$$

The current rating of the MPUC5-ES inverter MOSFET switches is dependent on the NCL rated current, which can be calculated by (3.6). Besides, the voltage rating of two switches namely S2 and S5 is the DC reference voltage of the inverter that can be determined by (3.10). However, four other switches endure half of the reference DC voltage of the inverter.

$$V_{DC} = \sqrt{2} V_{es} \tag{3.10}$$

The MPUC5-ES output voltage range is reliant on the allowable voltage fluctuation range of the NCL. Thus, for a resistive NCL and based on (3.2) V_{es} is obtained as

$$V_{es} = \sqrt{V_s^2 - V_{pncl}^2} \tag{3.11}$$

where V_{pncl} is the minimum permissible value of the non-critical load voltage, which could be different based on the NCL characteristics. For choosing the capacitors (C1 and C2) at the DC buses of the inverter, (3.12), as defined below, can be employed.

$$C_{1or2} = \frac{I_{peakncl} \times \Delta t_c}{V_{ripple}} \tag{3.12}$$

here V_{ripple} is a permissible ripple of the voltage of the capacitor, $I_{peakncl}$ is the peak current of NCL and Δt_c is the duration of charging and discharging of the capacitors in each switching period. Finally, for the selection of the low pass output filter (3.13) and (3.14) as presented below can be used (Abarzadeh, Vahedi, & Al-Haddad, 2019).

$$L_f = \frac{V_{DC}}{8 \times (n-1) \times \Delta I_{ncl} \times fsw} \tag{3.13}$$

$$f_{cutoff} = \frac{1}{2\pi \times \sqrt{L_f C_f}} \tag{3.14}$$

where n is the number of voltage level, ΔI_{ncl} is the NCL acceptable ripple of current, which is normally 15% of nominal current, fsw is the switching frequency, and f_{cutoff} is the cutoff frequency of the low pass filter.

3.3 MPUC5-ES Configuration and its Voltage Balancing Method

Although various configurations such as half-bridge (C. K. Lee, Chaudhuri, & Hui, 2013) or full-bridge (Yuan, Feng, Tong, Yang, & Tang, 2019) single-phase power inverters can be employed as the first version of ES, in this paper, due to the promising characteristics of the MPUC5 topology, it has been employed for ES-based SL application for the first time. On the one hand, for instance, a full-bridge based electric spring (Yuan et al., 2019) consists of one bulky auxiliary capacitor and four switches. The maximum value of its output voltage is equal

to its DC link voltage. Consequently, if it is required to have a peak voltage of *E* in the output, the DC link voltage level should be also *E* in this topology. Furthermore, the switching frequency, which is proportional to the switching power losses, of this conventional configuration is as high as 20 kHz, and all the switches should withstand the DC link voltage with high *dV/dt*. Finally, it has a two-level voltage waveform with a THD of around 100% (Vahedi & Al-Haddad, 2016b).

On the other hand, as illustrated within the dashed rectangle in Figure 3.1, the proposed five-level ES configuration has six active semiconductor switches (S1, S2, S3, S4, S5, and S6) and two auxiliary capacitors as its energy storage elements (C1 and C2). As mentioned before, the current rating of the employed active switches is equal to the NCL current. The voltage rating of the two middle switches (S2, S5) is equal to the DC reference voltage (*E*). However, these can be low-frequency switches with switching frequency as low as the grid frequency (60 Hz). Nonetheless, the voltage rating of the rest of the switches (S1, S4, S3, S6) is half of the DC reference voltage (*E/2*). Although these four switches should be high-frequency switches, their switching frequency that is 2 kHz is meaningfully lower than the employed switches in the two-level-based electric spring. Thus, the proposed topology is more efficient with lower switching loss. Besides, from a switching cost point of view, if both of these topologies were designed regarding having switches with the same voltage rating, both of them would consist of eight switches (Vahedi & Al-Haddad, 2016b, p. 5), while the switching frequency of the MPUC5-ES is lower. Consequently, in this case, cheaper switches with the same voltage rating but lower switching rates can be employed. Therefore, the proposed topology is a superior substitute for conventional ES configurations at no extra cost.

Regarding the capacitors, although MPUC5-ES has two auxiliary capacitors, due to its boost mode operation capability, DC links' voltages are half of the peak value of the generated five-level voltage. In addition, with regard to the five-level waveform of the produced voltage by the MPUC5-ES, its THD content is significantly lower at around 26%. Thus, the size and cost of the required output low pass filter are also lower. Considering all the mentioned advantages, MPUC5-ES is a more efficient topology with lower power/voltage rating switches and superior

power quality characteristics. Consequently, due to the distributed nature of the ES in the power system, the proposed topology will be a superior substitute, especially on a large scale. Finally, it should be also mentioned that each couple of S1-S4, S2-S5, and S3-S6 are complimentarily switches.

Recently, in (Patil et al., 2017) and (Sundar, Philip, Tapasvi, Akash, & Hiraj, 2016) a three-level and five-level ES topologies based on the cascaded H-bridge multilevel inverter have been introduced, respectively. However, both of these configurations are introduced for a battery-based ES. Thus, for being employed as the first generation of electric spring, which employs capacitors instead of batteries as its energy storage element, a complex closed-loop control method is required for controlling the voltage and power of the capacitors. In addition, in order to compare the proposed three-level configuration in (Patil et al., 2017) with the MPUC5-ES, it should be mentioned that MPUC5-ES has a boost mode operation, better power quality characteristics due to its five-level performance, and switches in MPUC5-ES configuration endure lower voltage stress. On the other hand, regarding the five-level cascaded H-bridge ES introduced in (Sundar et al., 2016), although it has a five-level operation, this topology requires eight switches and two isolated DC sources that limit its application.

MPUC5-ES configuration is founded on the idea of balancing energy storage elements voltage and power without any complicated extra closed-loop controllers and by just using redundant switching states as presented in Table 3.1 (Vahedi & Al-Haddad, 2016a). Regarding Table 3.1, it should be noted that V_{ab} represents the voltage level in the output. Besides, ΔE_{C1} and ΔE_{C2} define chagrining (+) and discharging (-) of the first and the second capacitors, respectively. This is the first time that this technique has been employed for controlling the voltage of a multilevel electric spring auxiliary capacitors in an open-loop manner. As an example, by activating state number 2 when V1 is lower than V2, NCL current will flow into the C1 from a positive side, which means that this capacitor will be charged. However, C2 will be discharged at the same time. On the other hand, when V1 is higher than V2, by choosing state number 3, C1 will be discharged, however, C2 will be charged. Thus, through choosing proper switching states 2 or 3 and similarly 6 or 7, DC-links' voltages and powers of both

capacitors will be balanced. Consequently, the DC voltage on each of the energy storage elements will be half of the calculated reference DC voltage of the MPUC5-based ES. Therefore, one of the primary merits of this topology, which is halved DC-link voltage, is also achieved. It should be stressed out that inasmuch as MPUC5-ES is in series connection with an NCL, its energy storage elements can be charged as soon as non-critical load current flows through them.

Table 3.1 MPUC5-Based ES Switching States

States	**S_1**	**S_2**	**S_3**	**S_4**	**S_5**	**S_6**	**V_{ab}**	**ΔE_{C1}**	**ΔE_{C2}**
1	1	0	1	0	1	0	$V_1+V_2=E$	+	+
2	1	0	0	0	1	1	$V_1=E/2$	+	-
3	0	0	1	1	1	0	$V_2=E/2$	-	+
4	0	0	0	1	1	1	0	-	-
5	1	1	1	0	0	0	0	-	-
6	1	1	0	0	0	1	$-V_2=-E/2$	-	+
7	0	1	1	1	0	0	$-V_1=-E/2$	+	-
8	0	1	0	1	0	1	$-V_1-V_2=-E$	+	+

3.4 Implemented Controller

The proposed MPUC5-based ES simplified controller block diagram is depicted in Figure 3.3. All the parameters of the designed controller scheme are also presented in Table 3.2. This controller consists of two main separated parts. First, AC and DC voltage closed-loop proportional-integral (PI) controllers that are responsible for regulating the input voltage of the inverter (PCC voltage) and its DC buses, respectively. The second part is intended for harmonics mitigation of the CL voltage and current.

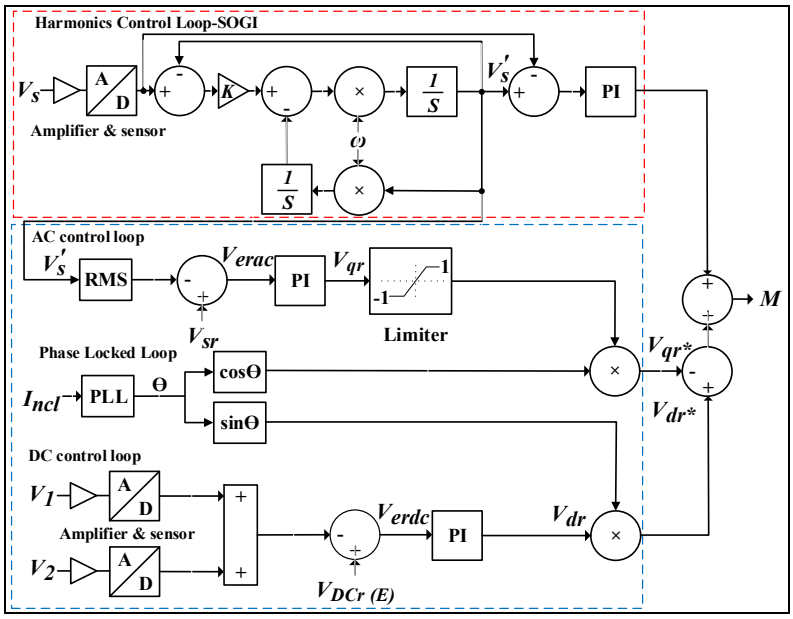

Figure 3.3 Schematic of the MPUC5-ES controller

Table 3.2 MPUC5-ES Proposed Controller Specifications

AC PI Controller		**DC PI Controller**		**Harmonic Controller**		
K_{PAC}	K_{IAC}	K_{PDC}	K_{IDC}	K_{Ph}	K_{Ih}	K
0.15	10	0.01	0.001	0.1	0.07	0.5

In the first part, as can be seen in the blue rectangle in Figure 3.3, in order to guarantee the input of this control loop is accurate and composed of the fundamental component, V_s' , which is the cleared PCC voltage (V_s), is compared with the root mean square (RMS) value of the reference voltage V_{sr}, which is $110\ V$, and the error will be attained based on (3.15).

$$V_{erac} = V_{sr} - V_s' \tag{3.15}$$

The obtained error (V_{erac}) is the input of the AC PI controller and its output is as below.

$$V_{qr} = (K_{PAC} + \frac{K_{IAC}}{s}) \times V_{erac} \tag{3.16}$$

where K_{PAC} and K_{IAC} are the proportional and integral gains of the AC proportional-integral controller. The V_{qr} is the reference amount of required reactive power from MPUC5-based ES in order to stabilize PCC voltage. On the other hand, based on (3.10), reference for the DC voltage in the DC control loop can be calculated. Moreover, voltages of the capacitors are sensed, sampled, and added together and the result is compared with the calculated reference DC voltage as below.

$$V_{erdc} = V_{DCr} - [V_1 + V_2] \tag{3.17}$$

where V_{DCr} denotes calculated reference DC voltage of the multilevel inverter and V_1 and V_2 are voltages of the capacitors C1 and C2, respectively. The acquired error (V_{erdc}) is the DC PI controller input for regulating DC voltage of the MPUC5-based ES inverter. Its output is as,

$$V_{dr} = (K_{PDC} + \frac{K_{IDC}}{s}) \times V_{erdc} \tag{3.18}$$

here K_{PDC} and K_{IDC} are the proportional and integral gains of the DC proportional-integral controller. V_{dr} denotes essentially the reference amount of the required active power from the MPUC5-ES inverter. It should be noted that the main purpose of this part of the controller is to stabilize PCC voltage and modify the required power by SL through exchanging merely reactive power with the grid. Nevertheless, mostly due to the power losses on switches, the MPUC5-ES also consumes a slight amount of active power.

In the next step, for calculating the reference of reactive power part of the ES voltage (V_{es}), it should have 90 degrees phase difference with the NCL current. On the other hand, the estimated reference of the required active power should be in-phase with the NCL current. Thus, NCL current is measured and sent to the Phase Locked Loop (PLL) to determine its phase angle. Therefore, for the active and reactive power components of the MPUC5-ES compensation voltage, we have the below formulas.

$$V_{qr*} = V_{qr} \times cos\,\theta \tag{3.19}$$

$$V_{dr*} = V_{dr} \times sin\,\theta \tag{3.20}$$

Finally, the first part of the modulation index (M_1) of the implemented controller can be expressed as follows:

$$M_1 = V_{dr*} - V_{qr*} \tag{3.21}$$

In the second part, the performance of harmonics elimination is highly dependent on the employed method for extracting the harmonic content of the CL voltage. Two main methods that can be used for detecting and damping all harmonic components of the PCC voltage are the Fast Fourier Transformation (FFT) and the Second Order Generalized Integrator (SOGI). Nevertheless, the first method has a longer computation time. Therefore, in this paper, the SOGI technique, which is suitable for systems with relatively low THD, is utilized with a faster estimation time (Hackl & Landerer, 2020). The structure of the employed SOGI is depicted in the red rectangle of Figure 3.3. Its closed-loop transfer function is as (Ciobotaru, Teodorescu, & Blaabjerg, 2006)

$$H(s) = \frac{V_s'}{V_s}(S) = \frac{K\omega S}{S^2 + K\omega S + \omega^2} \tag{3.22}$$

here, ω denotes the resonance frequency of the system, K is the value of damping factor, and V_s' is the cleared CL voltage. With regard to the damping factor selection, the bandwidth of the employed SOGI is proportionate to the selected value of K. In other words, the smaller amount of damping factor means more harmonic content of the CL voltage can be eliminated. However, the smaller amount of damping factor deteriorates the dynamic response time of the designed controller. Thus, there should be a trade-off considering these two aspects for damping factor selection. On the other hand, tuning of this system is realized in a frequency-dependent manner. Therefore, frequency fluctuations of the system with high penetration of

renewable energy sources might cause some problems. Consequently, adjustment of the ω has been achieved in an adaptive manner. To be clearer, the value of ω is adjusted through the frequency of the PCC voltage delivered by a PLL (Ciobotaru et al., 2006).

For mitigating the CL voltage harmonics, V_s' is compared with V_s and the resulted error signal is fed to a PI controller. The output of this control loop is as below,

$$M_2 = (K_{Ph} + \frac{K_{Ih}}{s}) \times (V_s' - V_s) \tag{3.23}$$

where, K_{Ph} and K_{Ih} are the proportional and integral gains of the employed proportional-integral controller and M_2 is the modulation index of the harmonic mitigation section. By far, it has been demonstrated that M_1 is computed with the aim of regulating the PCC voltage, while M_2 is calculated for mitigating the harmonic content of the distorted PCC voltage. In the end, for performing both of these tasks in real-time, as MPUC5-ES generated voltage should compensate PCC voltage fluctuations and contain its harmonics components the total modulation index (M) should be determined by adding both M_1 and M_2 as below,

$$M = M_1 + M_2 \tag{3.24}$$

It should be also mentioned that stabilizing the PCC voltage and mitigating its harmonic content are contradictory tasks. Besides, the harmonic content of the PCC voltage is transferred to the employed NCL. Therefore, there is a compromised operation regarding all the mentioned aspects. As a result, the proposed controller is suitable for systems with relatively low THD.

As can be seen in Figure 3.4, the output of the utilized controller will be a reference to the implemented modulation method. As explained in section 3.3, the voltage/power of the energy storage elements of the proposed MPUC5-ES is also balanced integrated into the utilized modulation technique in an open-loop manner. The exploited switching method has three main parts. In the first part, it has the typical four-level-shifted triangular carries and comparators

for implementing the phase disposition pulse width modulation (PDPWM) technique. In the second part, it includes logical operators for the AND and NOT operations. Finally, the last part is the switching states table based on Table 3.1.

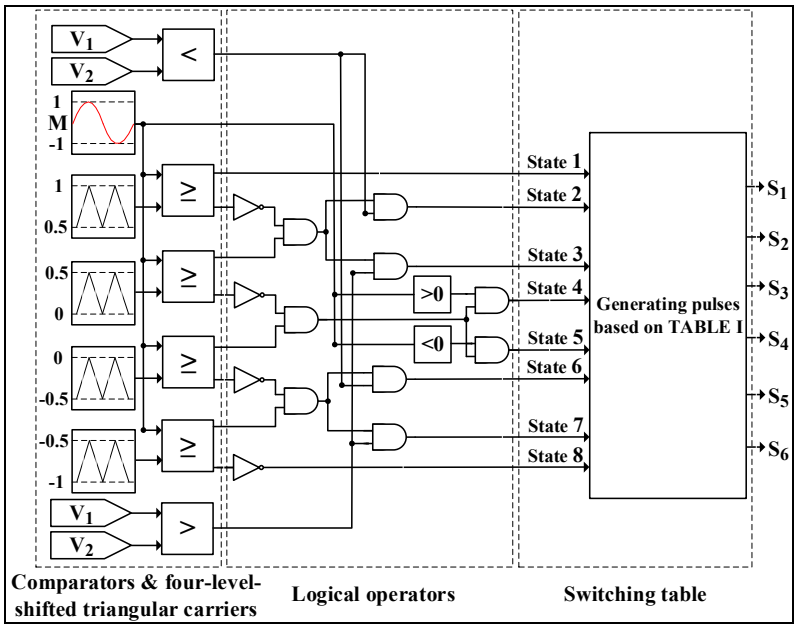

Figure 3.4 MPUC5-based ES switching pattern

3.5 Simulation and Experimental Results

3.5.1 Simulation Results

In MATLAB/SIMULINK, a weak power grid, fed by a single-phase ac source and a PUC5-based inverter as an unpredictable distributed renewable energy generator, has been modelled. Figure 3.5 illustrates the schematic of the simulated setup of the MPUC5-based electric spring and the grid structure. Besides, the complete specifications of the employed parameters are provided in Table 3.3. As can be seen, a resistive NCL is equipped with the MPUC5-ES as a five-level smart load. For emulating a renewable energy source, a PUC5 inverter in grid-connected mode has been also utilized. This inverter is capable of injecting various amounts of active and reactive power to the grid. As a result, the PCC voltage of the grid will be highly fluctuating (voltage sags and swells) around its nominal value, which is 110 V RMS (155.56

V peak). Details of the design of this inverter and its controller are presented in (Vahedi et al., 2016) comprehensively.

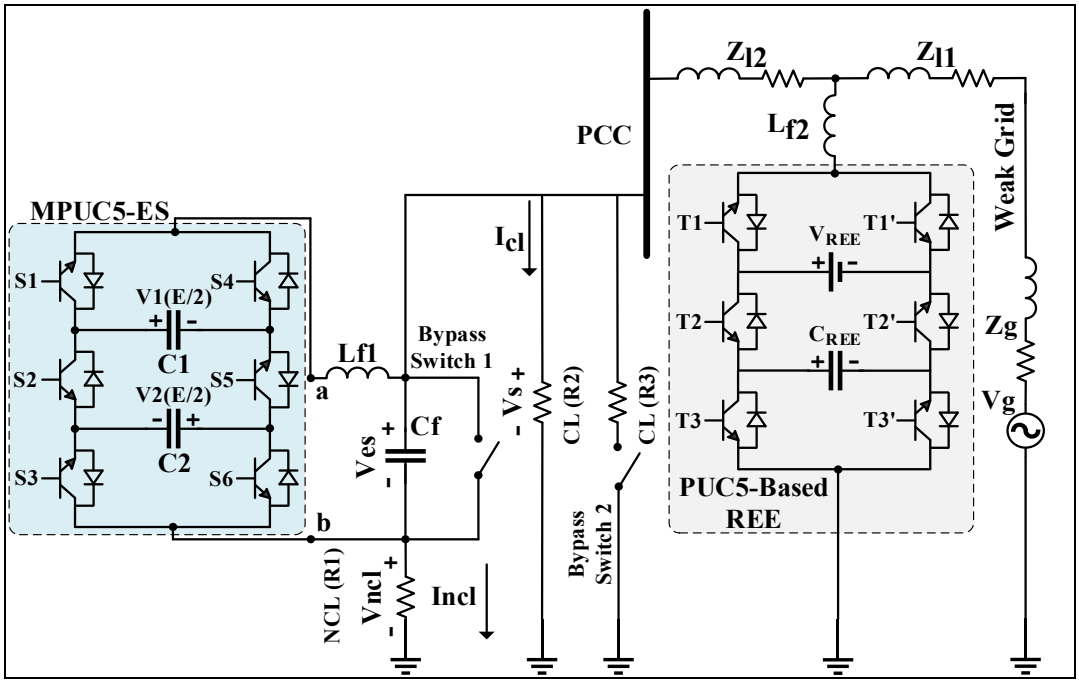

Figure 3.5 Simulation setup of MPUC5-ES and the grid structure

Table 3.3 Parameters of the Modeled System

AC Grid RMS Voltage (V_g)	110 V
Grid and switching Frequency (F_g), (F_{sw})	60 Hz, 2 kHz
Range of MPUC5-ES RMS Voltage (V_{es})	0 ~ 70 V_{ac}
Inductor of LC Filter of MPUC5-ES (L_{f1})	1.5 mH
Capacitance of LC Filter of MPUC5-ES (C_f)	35 µF
Output Filter Inductor of PUC5 (L_{f2})	4 mH
DC Voltage Reference (V_{DCr})	100 V
DC Bus Capacitance (C_1) and (C_2)	2200 µF
DC Bus Capacitance of REE (C_{REE})	2500 µF
DC Source Voltage of REE (V_{REE})	200 V
Source Impedance Z_g	0.49+j6.139 Ω
Distribution Line 1 Impedance Z_{l1}	0.1+j0.91 Ω
Distribution Line 2 Impedance Z_{l2}	0.1+j0.45 Ω
Non-critical load resistance R_1	25 Ω
Critical load resistances (R_2), (R_3)	25, 75 Ω

The sample time of the simulation is as low as 20 µs. Reference of the DC voltage controller has been arbitrary chosen to 100 V. This results in a halved amount of voltage on the DC capacitors, which is only 50 V. Thus, based on (3.7) the voltage range of the simulated multilevel ES would be around 0~70 Vac RMS. It should be noted that based on the permissible range of the voltage fluctuation tolerable by the noncritical load these amounts can be changed and recalculated. However, in this work, it is assumed that the minimum permissible value of the non-critical load voltage V_{pncl} can be as low as around 85 Vac RMS. Five different scenarios with and without harmonic control loop have been designed to prove the superiority of the dynamic and steady-state performance of the proposed MPUC5-based ES for stabilizing and improving power quality of the PCC voltage of the system with high penetration of unpredictable renewable energy.

3.5.1.1 MPUC5-ES Steady-States Modes Without Harmonic Control

The focus of this part is verifying the effectiveness of the proposed MPUC5-based ES in various steady-state operation modes for improving PCC voltage stability. Throughout the neutral mode, the generated and consumed power are almost balanced and the PCC voltage is at its nominal value. Consequently, the MPUC5-ES RMS voltage is around merely 1 V and the PCC and NCL voltages are almost equal. Measured waveforms of the system parameters during the neutral operation of the MPUC5-ES are shown in Figure 3.6.

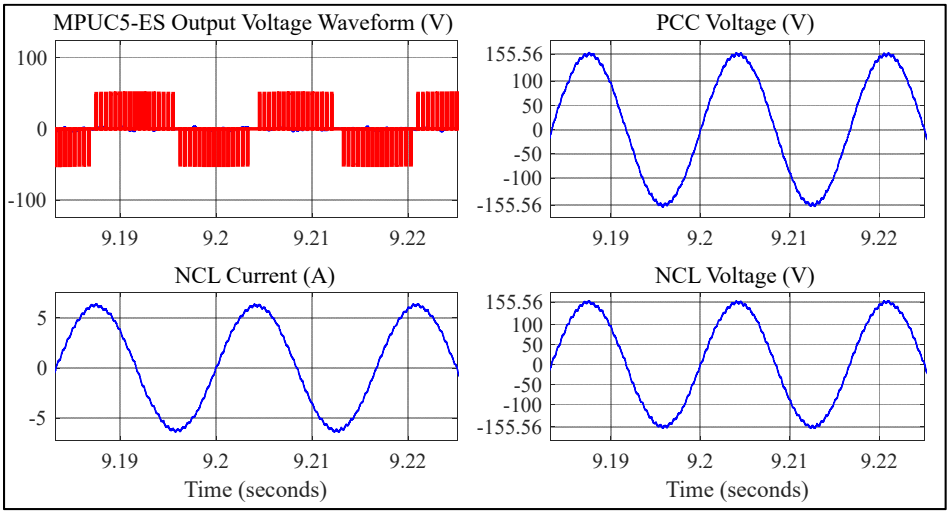

Figure 3.6 Waveforms during the steady-state neutral operation

Figures 3.7 and 3.8 illustrate MPUC5-ES five-level waveform and output voltage, NCL current and voltage, and PCC voltage during the inductive and capacitive operations, respectively. In order to compensate reactive power, as can be seen in Figure 3.7, during inductive operation, ES voltage is leading the NCL current by about 90 degrees. On the other hand, as illustrated in Figure 3.8, during the capacitive mode, the voltage of the MPUC5-ES is lagging the NCL current by roughly 90 degrees. Besides, the five-level waveform of the output voltage of the MPUC5-based ES is agreeable in both conditions as illustrated. In Figure 3.9, as an instance, the harmonic spectrum analysis of the MPUC5-ES injected five-level voltage during capacitive operation is also depicted. It shows that compared with conventional two-level inverters, utilizing the introduced configuration has improved the THD of the generated voltage from

around 100% (Vahedi & Al-Haddad, 2016b) to almost 26%. As a result, with a switching frequency of only 2 kHz, a relatively small-sized output filter is required.

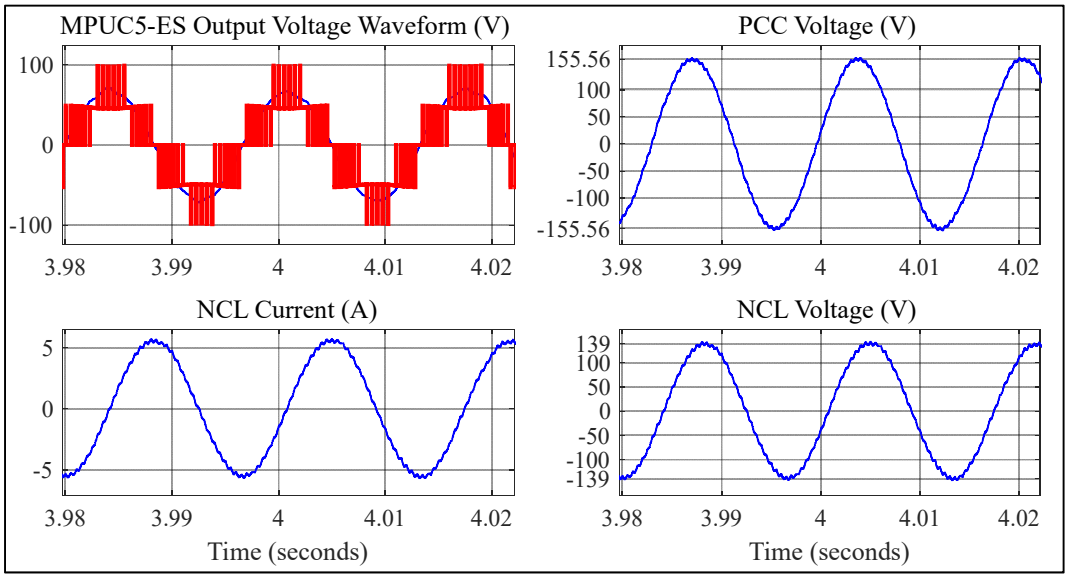

Figure 3.7 Waveforms during the steady-state inductive operation

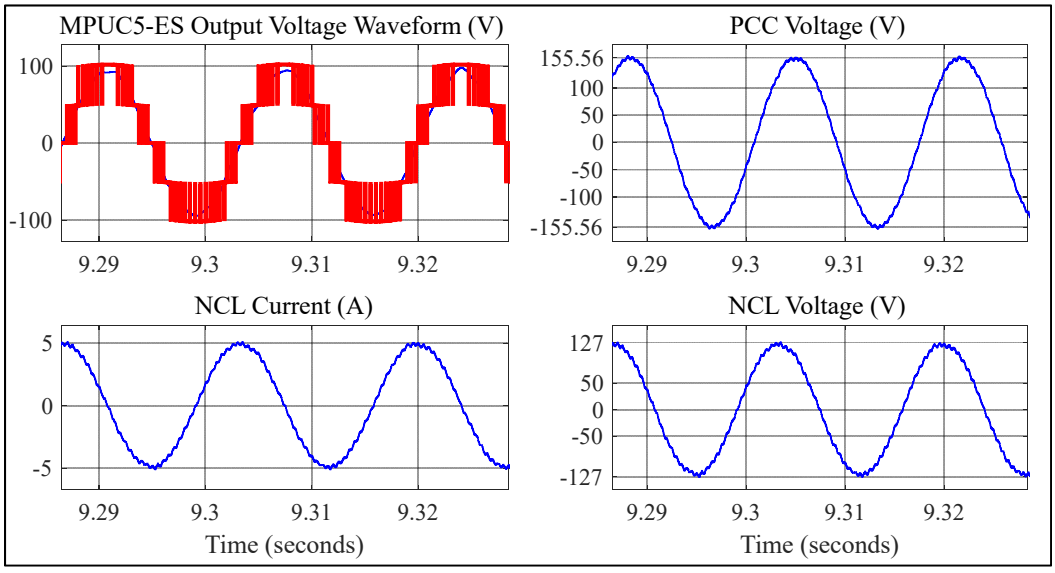

Figure 3.8 Waveforms during the steady-state capacitive operation

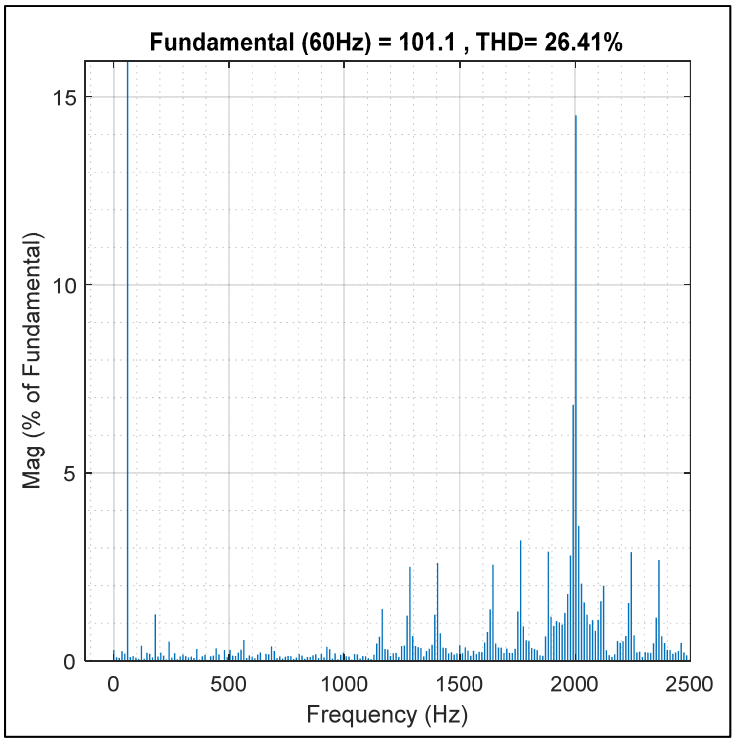

Figure 3.9 Voltage waveform FFT analysis

3.5.1.2 Waveforms in a Steady-States Mode with Harmonic Control

The focus of this part is to verify the performance of the proposed five-level electric spring and its controller with the harmonic control loop for improving both stability and power quality of the CL voltage in a steady-state mode. Therefore, the voltage of the grid is considered to be distorted as below,

$$V_{gh} = 155.56\,sin\,\omega t + 23.3\,sin\,3\omega t + 15.6\,sin\,5\omega t + 10.9\,sin\,7\omega t + 7.8\,sin\,9\omega t \quad (3.25)$$

Figures 3.10 and 3.11 illustrate the measured waveforms of this system, as an instance in a capacitive mode operation, without and with MPUC5-ES, respectively. As can be seen, the CL and NCL voltages' maximum value without MPUC5-ES is around 129 V (91.2 RMS V) with roughly 10% THD. However, after activating MPUC5-ES, through injecting the compensation voltage that is lagging the NCL current by roughly 90 degrees, the CL voltage is stabilized to

its nominal value. Besides, the power quality of the CL voltage waveform has been improved with only around 3% THD. FFT analyzations of the PCC voltage waveform without and with MPUC5-ES, in this case, are also presented in Figures 3.12 and 3.13, respectively. Finally, it is clear that the employed resistive NCL is drawing the harmonic components of the PCC voltage.

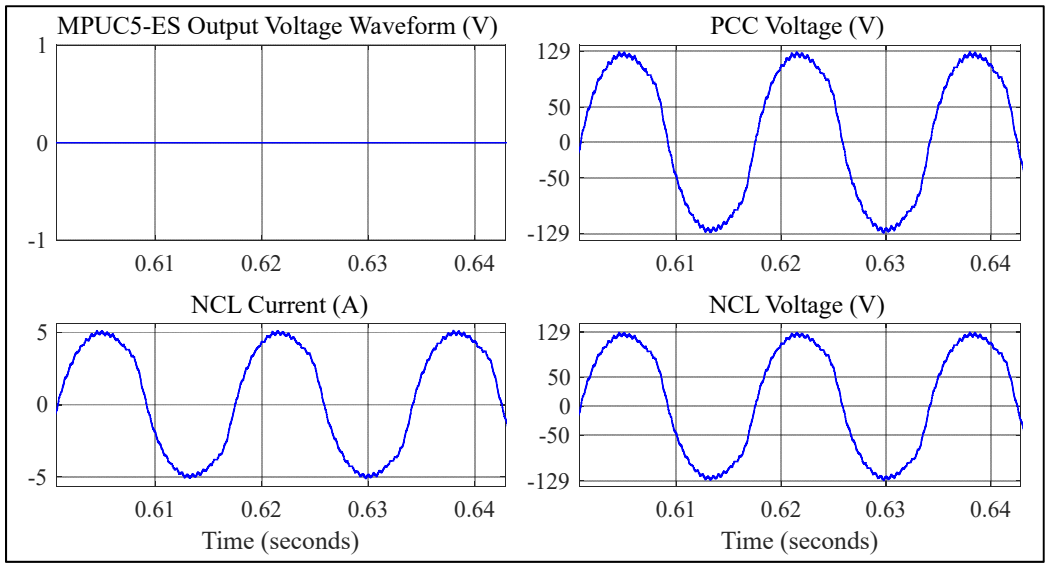

Figure 3.10 Steady-state waveforms with a distorted PCC and without MPUC5-ES

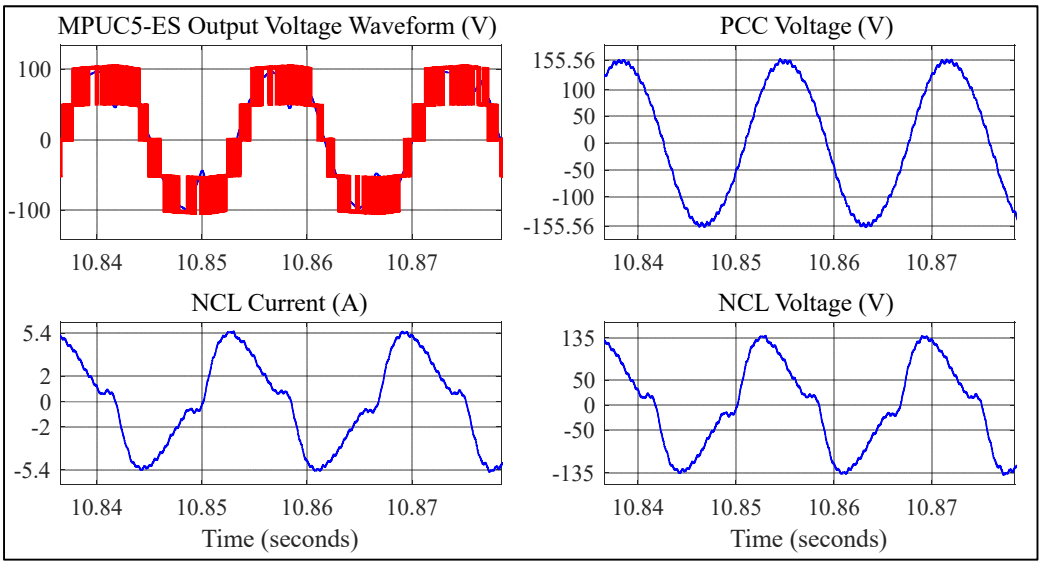

Figure 3.11 Steady-state waveforms of the system with a distorted PCC voltage with MPUC5-ES

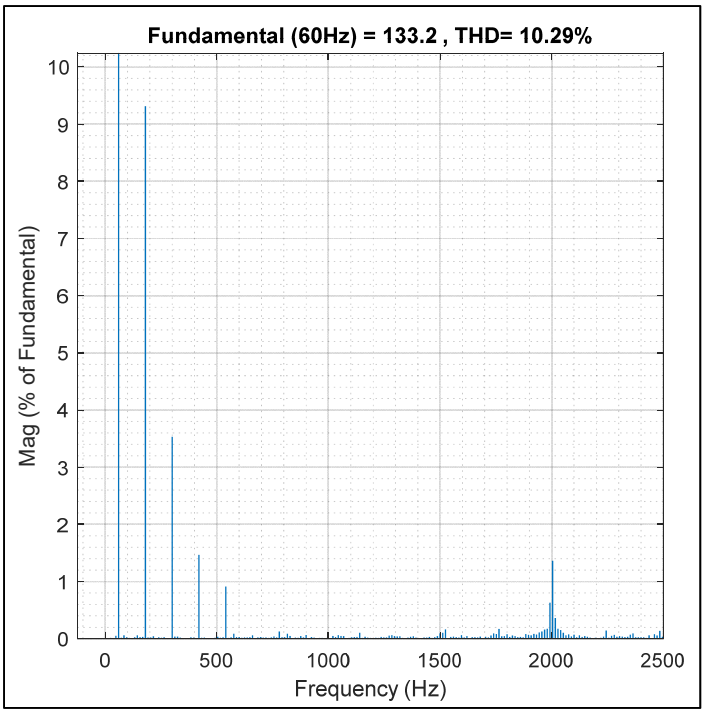

Figure 3.12 Distorted PCC voltage waveform FFT analysis without MPUC5-ES

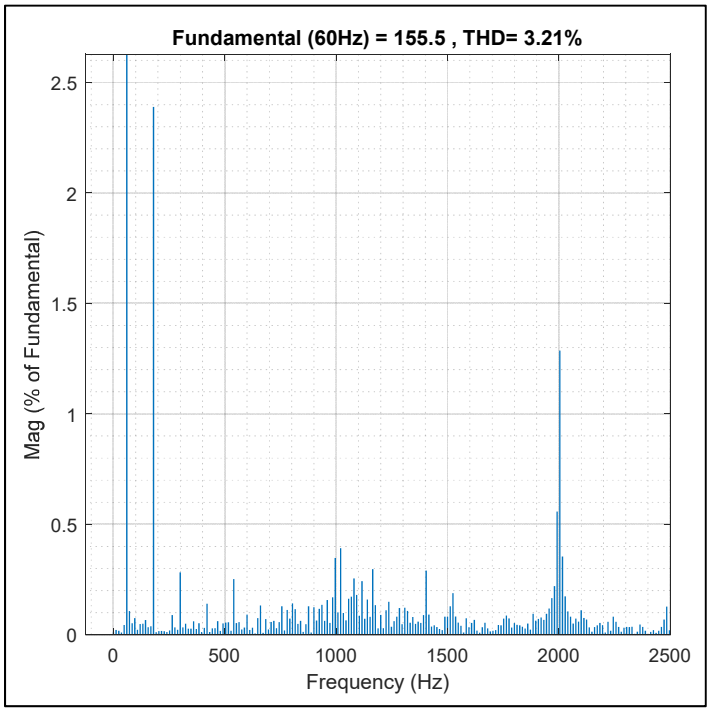

Figure 3.13 PCC voltage waveform FFT analysis with MPUC5-ES in capacitive mode

3.5.1.3 MPUC5-ES Response to the Fluctuation in the Injected Power

In this part of the simulation, the emulator of the renewable energy is injecting a fluctuating amount of active power to the grid. This simulation has been performed for a duration of 20 s. The same profile of injected active power to the grid is repeated each 10 s. During the first time, MPUC5-ES is activated and during the second time, it is deactivated through closing the bypass switch 1 at t=10 s. The measured RMS values of the PCC, MPUC5-ES, and NCL voltages, throughout the simulation time, can be also seen in Figure 3.14. In the first interval, due to the performance of the MPUC5-ES, the PCC voltage is effectively stabilized at the nominal value of 110 Vac RMS. On the other hand, during the second interval, due to the volatility of the injected active power, the PCC RMS voltage is varying from roughly 93.5 to 116 Vac. In fact, this is the voltage range of the designed MPUC5-ES based on the Electric Elasticity Limit (EEL) (Z. Zhang, Xie, Tong, & Gao, 2019). During both sag and swell conditions, MPUC5-ES has effectively alleviated the system overshoots and undershoots within just one cycle. Besides, even in the worst-case scenarios, voltage transients are less than 10% of the PCC nominal voltage, which is acceptable (Khamis, Zakzouk, Abdelsalam, & Lotfy, 2019).

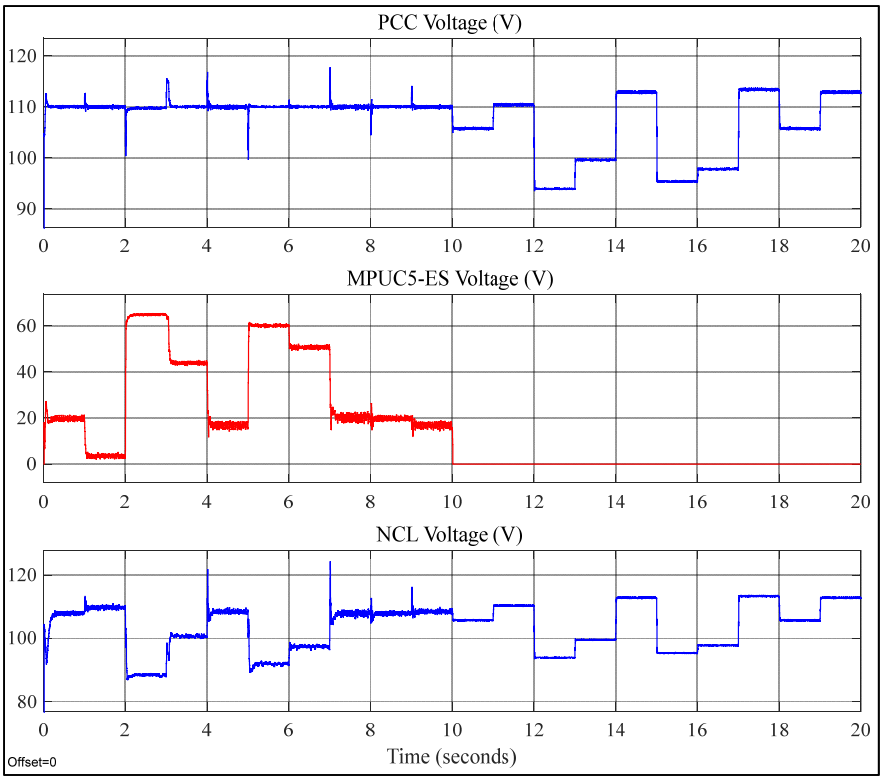

Figure 3.14 Measured RMS values due to the fluctuations in the injected active power

In Figure 3.15, the active and reactive power of the MPUC5-ES before and after closing the first bypass switch are shown. In almost all the conditions, the active power consumption of the implemented MPUC5-ES is around zero. However, during the first interval, proposed ES consumes a slight amount of active power mainly due to switching losses. On the other hand, during the under-voltage condition, it is providing reactive power to the grid and reducing the NCL voltage at the same time to support PCC voltage dynamically. However, during the over-voltage condition, it consumes reactive power from the grid to reduce the PCC voltage to its nominal value. As a result, based on (3.7) by varying the NCL voltage, the active power consumption of the NCL is adjusted based on the generated active power by the renewable energy source dynamically. Conversely, the CL consumed active power is kept constant effectively. Measured active power consumption of the NCL and CL throughout the experiment is also depicted in Figure 3.16.

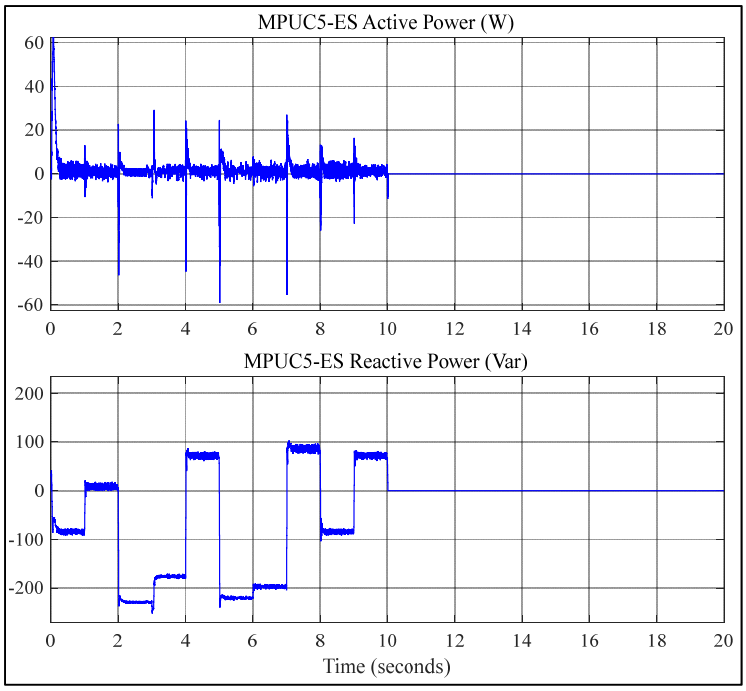

Figure 3.15 Active and reactive power of MPUC5-ES

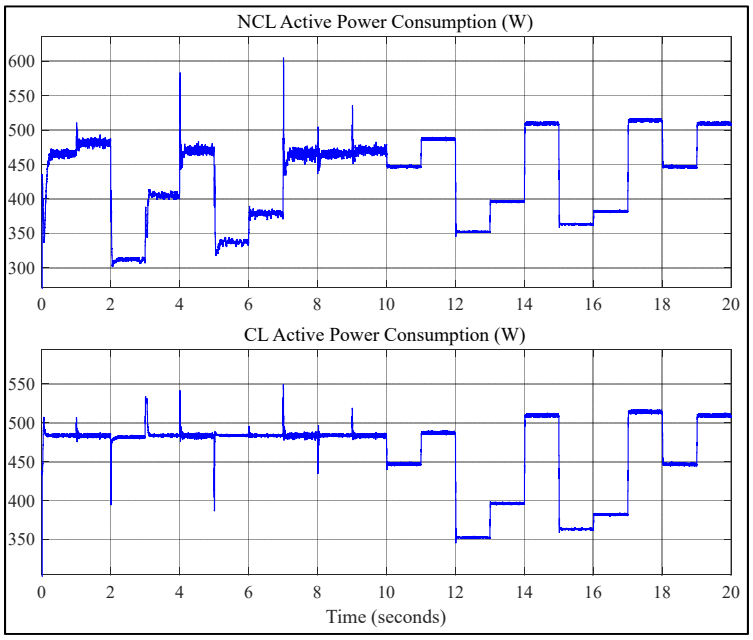

Figure 3.16 Active power consumption by NCL and CL

Figure 3.17 shows DC links' voltages namely V1 and V2 during this simulation. As can be seen, DC links' voltages are dynamically kept constant and equal to half of the reference DC

voltage during the simulation. This proves the effectuality of the implemented voltage balancing technique and its dynamic performance.

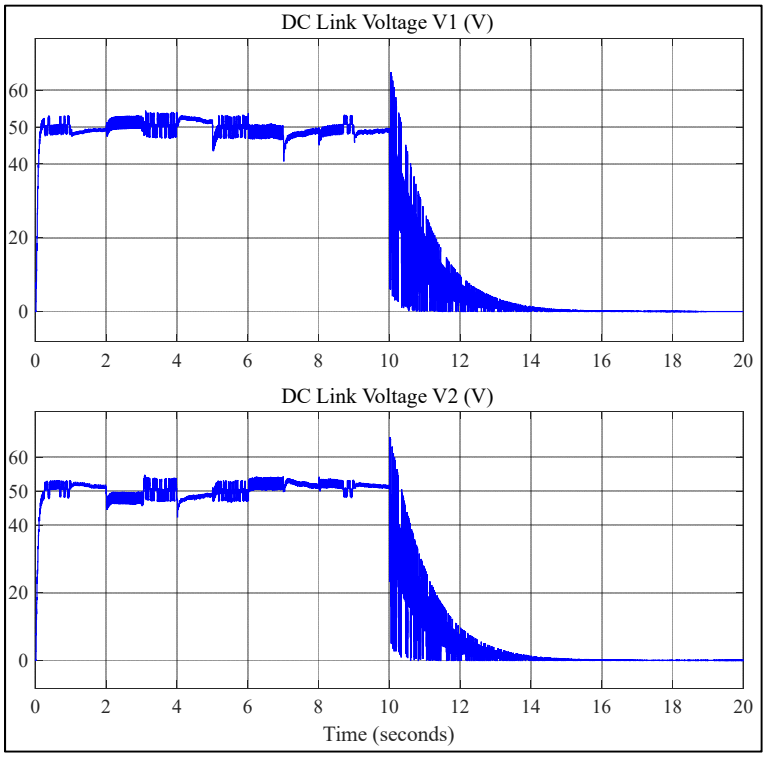

Figure 3.17 MPUC5-ES DC links voltages during fluctuation in the injected power

3.5.1.4 MPUC5-ES Dynamic Response to a CL Change

In this scenario, as an instance, during the inductive operation of the MPUC5-ES by closing the second bypass switch another critical load (R3) is suddenly inserted in parallel with the R2 at t=2.0 s. Consequently, the total resistance of the CLs is changed from 25 Ω to 18.75 Ω. Figure 3.18 illustrates the measured and recorded waveforms of the system during this simulation. It is obvious that the proposed ES successfully managed to keep the PCC voltage to its nominal value with high power quality. Besides, injected compensation voltage, without any noticeable transient, has instantly decreased. This is yet another proof for showing the superiority of the proposed MPUC5-ES dynamic performance.

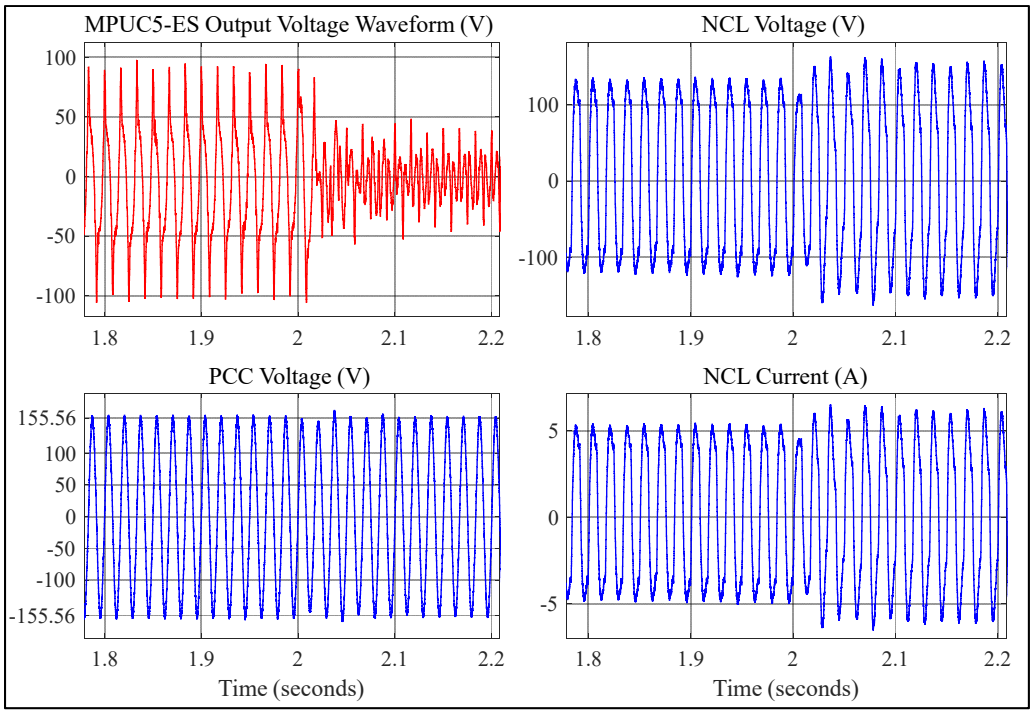

Figure 3.18 Waveforms of the system during a transient

3.5.1.5 Comparative study between MPUC5-ES and full-bridge ES

Here, in order to validate the merits of the MPUC5-ES, such as boost mode operation, lower THD and switching frequency, less voltage stress on switches and so on, in comparison with a conventional two-level full-bridge ES topology, in the simulated system with the same control method, MPUC5-ES has been replaced with a two-level full-bridge-based ES. It should be mentioned that all the parameters of this system are the same as the specifications presented in Table 3.3. However, as this time a conventional two-level ES topology is employed, the switching frequency and the capacitor's capacitance of the designed full-bridge ES are 20 kHz and 4400 µF, respectively (C. K. Lee, Chaudhuri, & Hui, 2013).

Firstly, for comparing the output voltage waveform and DC-link's voltage of the full-bridge-based ES with the proposed topology, Figure 3.19 illustrates the full-bridge ES two-level output voltage waveform and its DC-link voltage in comparison with the MPUC5-ES five-level output voltage waveform during a steady-state capacitive operation mode, as an instance.

As illustrated, the two-level ES DC-link voltage is as big as 100 V. However, as previously presented in Figure 3.17, the MPUC5-ES DC-links' voltages are equal to only 50 V with the same maximum value of the output voltage (100 V) that proves MPUC5-ES boost mode operation. In addition, harmonic analyzation of the two-level ES generated voltage is presented in Figure 3.20. As can be seen, in comparison with the MPUC5-ES harmonic spectrum analysis during the same experiment presented in Figure 3.9, the harmonic content of the generated voltage by the two-level ES increased to around 100 %. This proves the superior power quality performance of the proposed multilevel ES topology. Finally, in order to compare the voltage and switching frequency of the employed switches in both configurations, during the previous experiment, the voltage of one of the two-level ES switches and three switches of the MPUC5-ES have been measured and recorded that can be seen in Figure 3.21. It should be also mentioned that all the switches utilized in the full-bridge-based ES topology have the same voltage rating and switching frequency. Therefore, the voltage of only one switch of this configuration is presented. On the other hand, as in the MPUC5-ES topology S1-S4, S2-S5, and S3-S6 are complimentarily and each pair has switches with the same voltage rating, measuring the voltages of S1, S2, and S3 is sufficient for this comparison. Based on Figure 3.21, it is clear that although the voltage rating of S2 and the full-bridge-based ES switches are equal, the switching frequency of S2 is much lower at only 60 Hz. On the other hand, regarding S1 and S3, not only the voltage rating of these switches is only 50 V, which is half of the full-bridge-based ES switches, but also their switching frequency is around 2 kHz that is ten times lower.

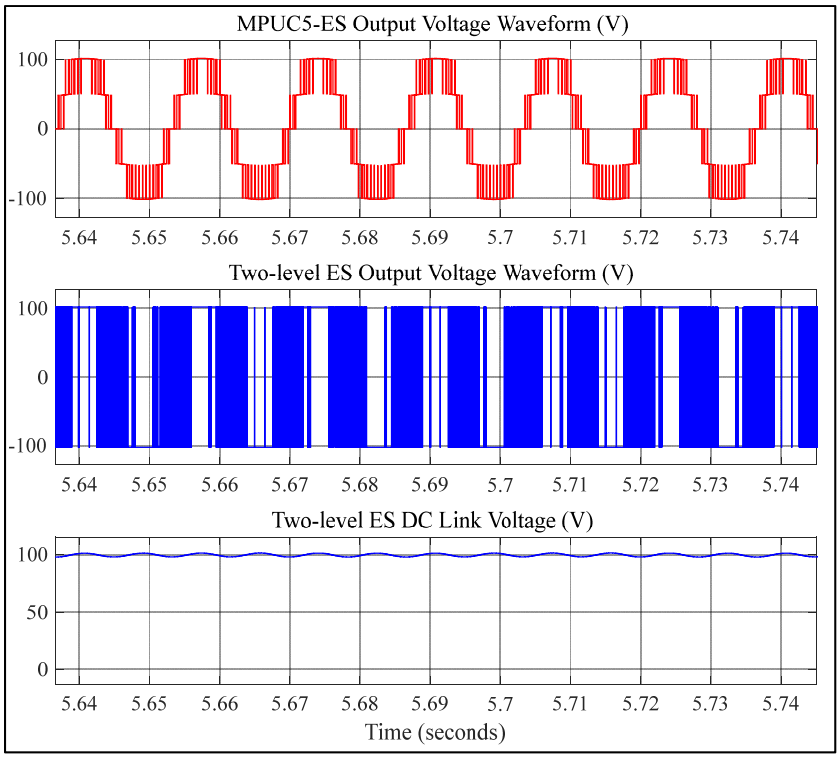

Figure 3.19 MPUC5-ES, ES, and ES DC-link voltages during the capacitive operation

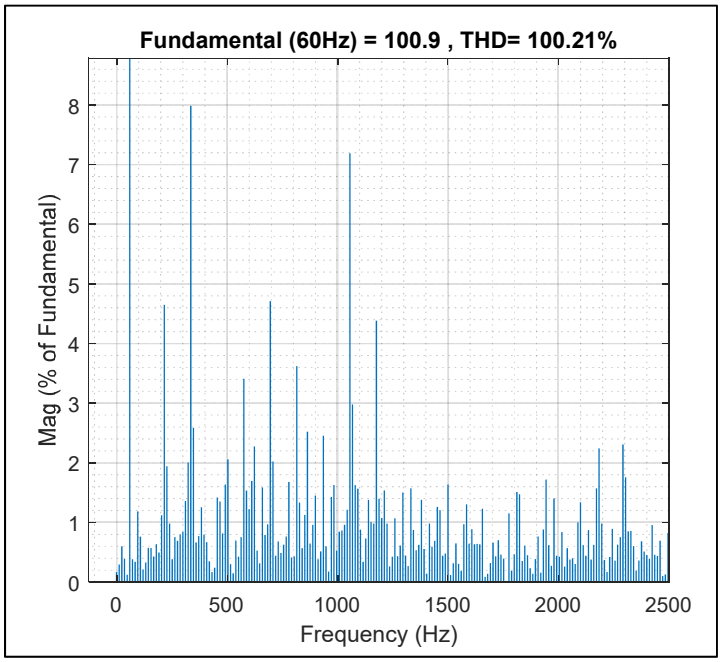

Figure 3.20 Two-level ES voltage FFT analysis

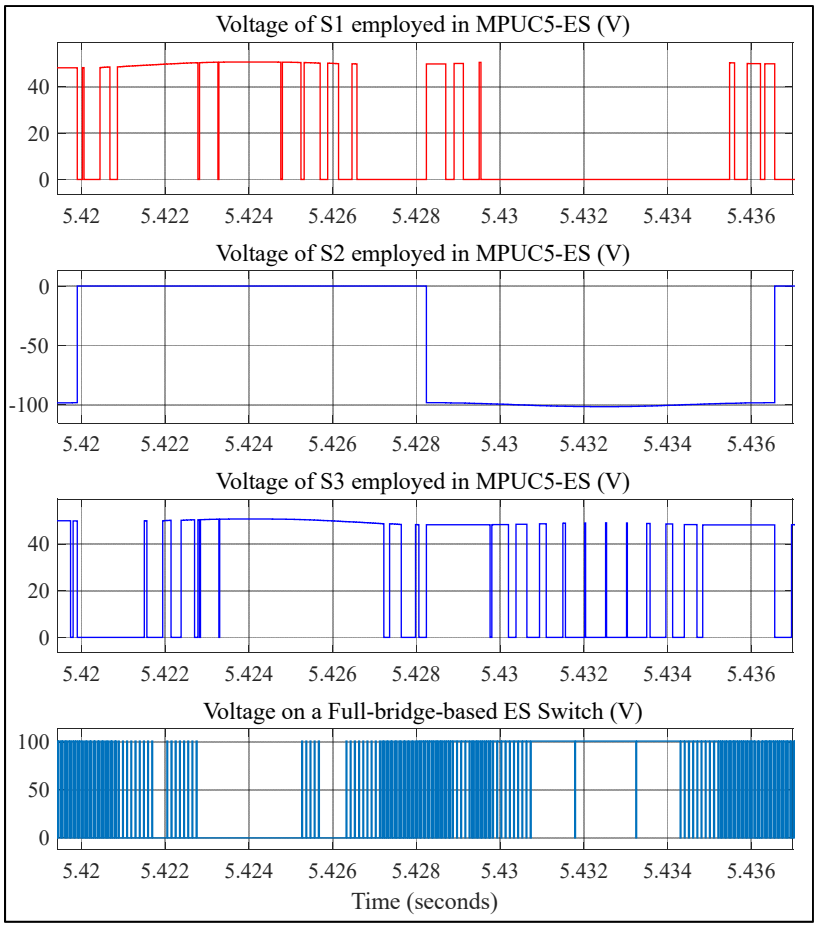

Figure 3.21 Voltage on one of the two-level ES switches and three switches of MPUC5-ES

3.5.2 Experimental Results

In order to verify the feasibility and steady-state and dynamic performance of the proposed configuration in various operation modes, using six MOSFET switches, a prototype of the MPUC5-ES inverter has been built. A dSPACE DS1104 controller board has been also used for implementing the control part of the SL in real-time. A variable single-phase AC power source emulator (V_g) in series with grid impedance as a relatively weak grid has been used for checking the steady-state and dynamic performance of the proposed SL configuration in different operation modes. Regarding the limited capability of the employed real-time controller board, harmonic analyzation of the proposed topology with proper sampling time and considering both control loops has been performed extensively using Simulink. Therefore,

for demonstrating MPUC5-ES performance and viability experimentally, mitigating PCC voltage fluctuations is the focus of this part. Figures 3.1 and 3.22 illustrate the schematic and the photograph of the experimental setup of the MPUC5-based electric spring implemented in the GRÉPCI Laboratory at ÉTS University, respectively. The experimental parameters of the setup can also be found in Table 3.4.

Figure 3.22 Picture of the experimental setup

Table 3.4 Parameters of the experimental setup

Variable Source (V_g) in Neutral and Inductive	115 V, 121 V RMS
Grid and Switching Frequency (F_g), (F_{sw})	60 Hz, 2 kHz
Range of MPUC5-ES RMS Voltage (V_{es})	0 ~ 70 V_{ac}
Inductor of LC Filter of MPUC5-ES (L_f)	1.5 mH
Capacitance of LC Filter of MPUC5-ES (C_f)	35 µF
DC Voltage Reference (V_{DCr})	100 V
DC Bus Capacitance (C_1) and (C_2)	2500 µF
Source Impedance (Z_g)	0.1+j5.65 Ω
Non-critical and Critical Loads (Z_{ncl}), (Z_{cl})	40 Ω

3.5.2.1 MPUC5-ES performance in various steady-states modes

Firstly, to show the steady-state performance of the proposed configuration, MPUC5-ES voltage, PCC voltage, NCL voltage, and its current are measured and recorded during neutral and inductive operation conditions. In the neutral mode operation of the MPUC5-ES, measured waveforms are illustrated in Figure 3.23. On the other hand, Figure 3.24 shows the equivalent waveforms in the inductive operation mode. In accordance with the simulation results, MPUC5-ES voltage in neutral operation is negligible and thus measured PCC and NCL voltage are almost equal to 110 Vrms (155.6 V Max). Consequently, in this mode injected reactive power to the grid by the MPUC5-ES is around zero. However, as expected in the inductive operation of the SL, the MPUC5-ES injected compensation voltage leads the NCL current by about 90 degrees. Therefore, a positive amount of reactive power is generated to stabilize the PCC voltage of the system at its nominal value (155.6 V Max) by modifying the NCL voltage (from 155.6 V to 136 V) and current (from 3.8 A to 3.4 A). The smooth five-level waveform of the output voltage of the MPUC5-based ES in this condition can be also seen. It should be mentioned that due to limitations of the employed dSPACE controller, the sampling time of the experiment is 60μs, which is more than two times higher than the sampling time of the simulation section. This has a negative impact on the THD and transients settling time of the system.

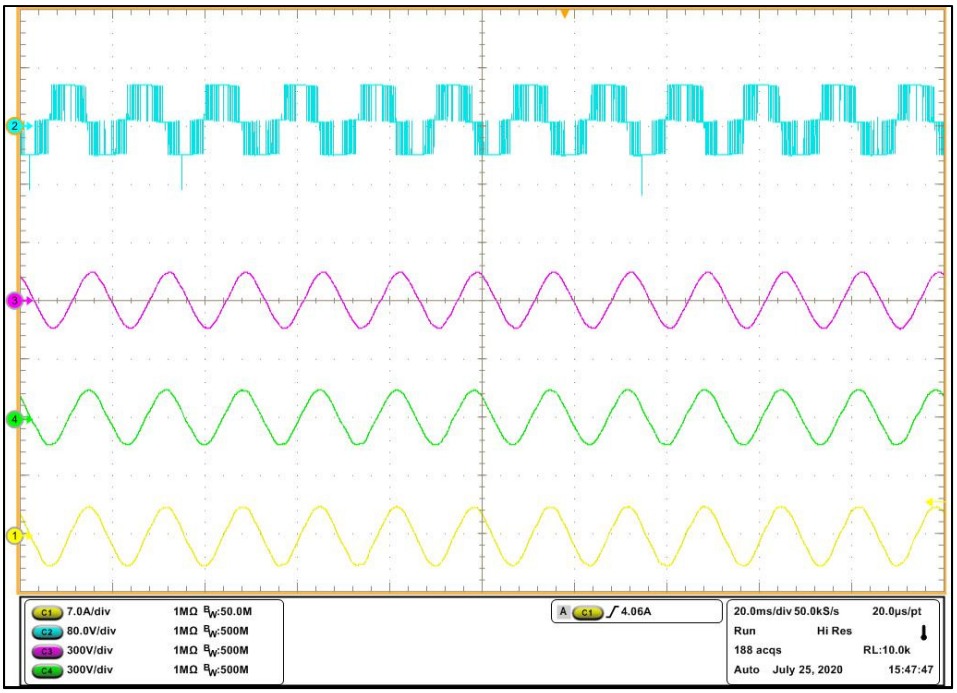

Figure 3.23 Experimental results under the steady-state neutral operation from top to bottom V_{ab}, V_s, V_{ncl}, and I_{ncl}

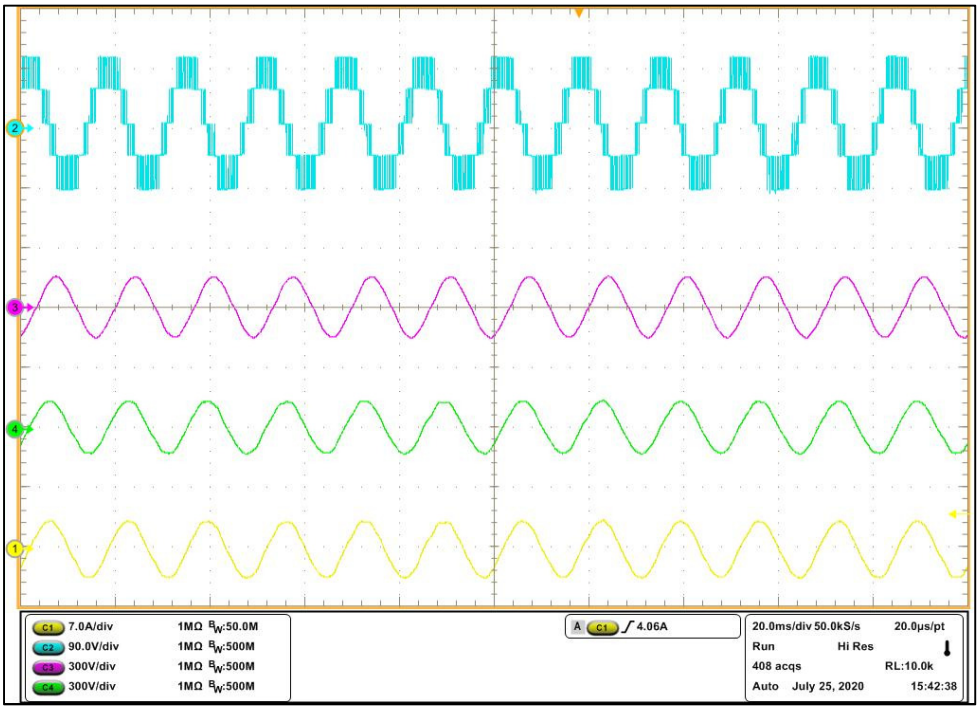

Figure 3.24 Experimental results under the steady-state inductive operation from top to bottom V_{ab}, V_s, V_{ncl}, and I_{ncl}

3.5.2.2 MPUC5-ES dynamic performance

Secondly, in weak grids, variation in the demanded power is one of the main causes of the PCC voltage fluctuations. Thus, to experimentally check the dynamic performance of the proposed SL, in the second experiment during the inductive operation mode, the resistance of the critical load is changed from around 40 Ω to roughly 26 Ω. In Figure 3.25, the measured waveforms of this experiment are depicted. As can be noted, through increasing the NCL voltage and current and reducing the injected MPUC5-ES compensation voltage to the grid, the PCC voltage is stabilized effectively after a sudden reduction in the CL amount by about 35%. Finally, Figure 3.26 shows the recorded DC voltages of both energy storage elements during this transient. And, it is clear that the employed voltage balancing technique has managed to keep the DC-links' voltages constant at around 50 V after the change in the power consumption of the CL.

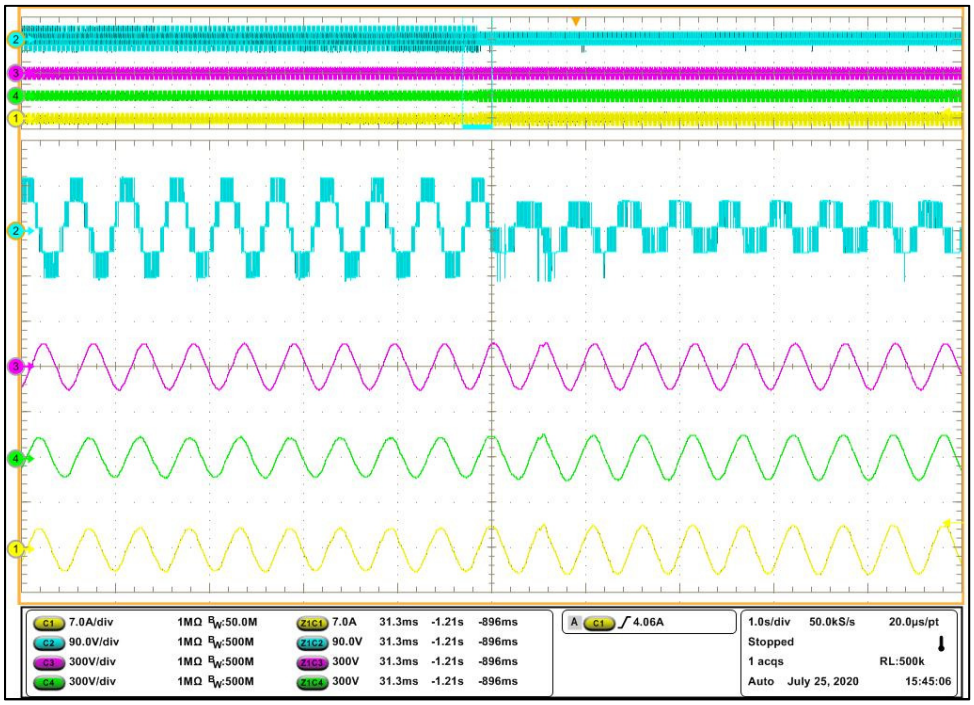

Figure 3.25 Experimental results of respectively V_{ab}, V_s, V_{ncl}, and I_{ncl} under transient

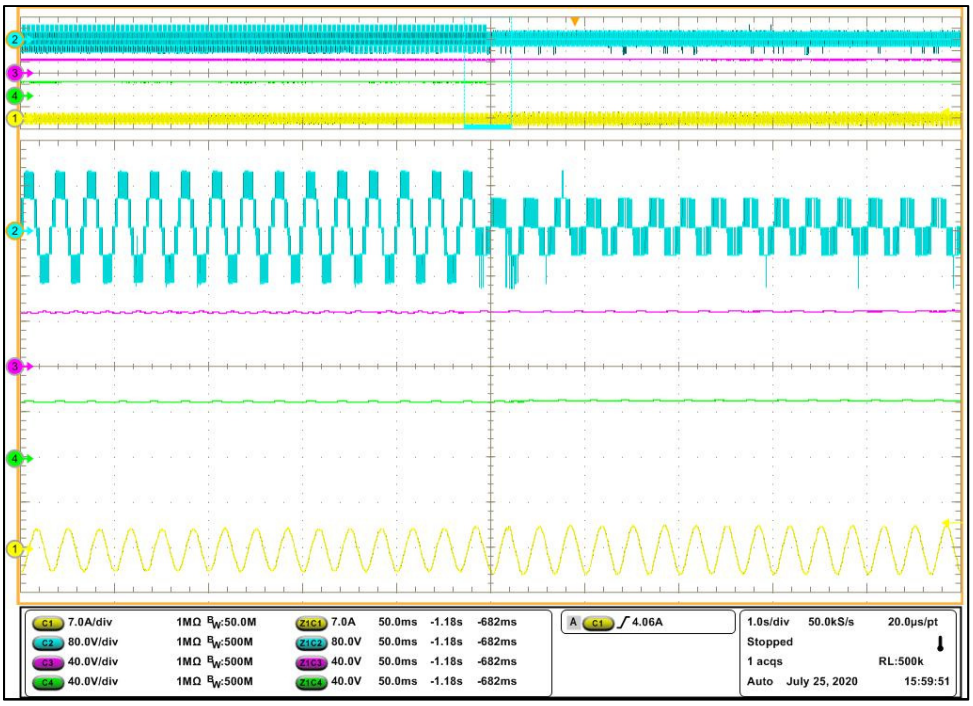

Figure 3.26 Experimental results of respectively V_{ab}, V_1, V_2, and I_{ncl} under the CL resistance variation

3.6 Conclusion

In this chapter, the MPUC5 inverter has been used as a multifunctional single-phase ES for improving voltage stability and power quality of a weak grid for the first time. The principles of the operation and design, configuration, and control method of the proposed MPUC5-based ES are also described. The key advantages of the MPUC5-ES are 1) balancing capacitors' voltage and power without any external controller; 2) five-level voltage waveform in its output with reduced THD and better power quality performance; 3) halved DC links' voltages; 4) plausibility of higher power application in comparison to the full-bridge or half-bridge topologies; 5) no need of bulky output LC filter, and 6) lower switching frequency and voltage stress on the switches. We have also managed to assess the performance of the proposed multilevel ES for automatic regulation of the PCC voltage, harmonics reduction, and load shedding of the NCL in an SL setup. Comprehensive simulation and experimental results verify the superiority of both steady-state and dynamic performance of the introduced MPUC5-

ES configuration in a weak grid with a highly unstable PCC voltage with and without harmonics.

CHAPTER 4

MODEL PREDICTIVE CURRENT CONTROL OF MULTILEVEL SMART LOAD BASED ON MPUC7 CONVERTER

Amirabbas Kaymanesh [a], Mohammad Babaie [a], Ambrish Chandra [a] and Kamal Al-Haddad [a],

[a] Department of Electrical Engineering, École de Technologie Supérieure,
1100 Notre-Dame West, Montreal, Quebec, Canada H3C 1K3

Paper published in *IEEE Access*, September 2021

Abstract

Considering the poor power quality performance of a two-level capacitor-based electric spring (ES1), this article presents a high-power density multilevel ES1 configuration based on a seven-level modified packed U-cell converter (MPUC7-ES1). A novel control strategy based on finite control-set model predictive current control (FCS-MPCC) is also proposed for MPUC7-ES1 application. This algorithm is designed to predict the system behavior for all the conceivable switching vectors based on the discrete models of MPUC7-ES1 that is developed for the first time. To guarantee a desirable operation, the main control objectives are the MPUC7-ES1 current, auxiliary capacitors' voltages, and switching frequency reduction. Compared with the conventional ES1 control methods, the proposed strategy has key merits including considering the dynamic models of ES1 converter, not requiring a modulator, and lower switching frequency. The operation and robustness of MPUC7-ES1 and the introduced nonlinear FCS-MPCC technique are also illustrated through extensive simulation and experimental results.

4.1 Introduction

Increasing the percentage of inverter-based renewable energies in electric power systems seems inevitable to rein in the current global warming trend. Nonetheless, this solution addresses the global warming crisis at the expense of challenging the power systems' stability, reliability, and power quality. More specifically, the intermittent nature of non-synchronous energy resources deteriorates the grid's voltage and frequency instabilities more than the tolerable limits. To alleviate these unfavorable fluctuations, active and reactive power imbalances should be addressed in power systems. Conventionally, spinning and non-spinning reserves are employed to address this issue. However, it leads to requiring more generating capacity from finite resources, which is not following accomplishing the targets of 2030 sustainable development goal 7 ("Transforming Our World: The 2030 Agenda for Sustainable Development | Department of Economic and Social Affairs," n.d.). Non-dispatchable renewable energy resources, such as wind and solar, can also participate in both active and reactive power imbalance mitigation. Nonetheless, in this way, the employed conversion system will not be operational at maximum power point (MPP), which reduces the efficiency of the system. In this regard, demand response management (DRM) methods, as more efficient alternatives, have been vastly investigated in the literature (Muthirayan, Kalathil, Poolla, & Varaiya, 2020).

Among various DRM technologies, electric spring (ES), which is a power electronics-based approach, has notable merits. The real-time operation, high efficiency, and distributed nature are just some of them. Furthermore, unlike most of the reported DRM methods, ES can be operational without depending on information and communications technologies. As a result, recently, different versions of ES technology have been conceptualized for both dc and single/three-phase ac microgrids and power systems applications. Capacitor-based ES (ES1), battery-based ES (ES2), and back-to-back converter-based ES (ES3) are the three main generations of the single-phase AC electric spring (C.-K. Lee et al., 2020). Among these, ES1 is mainly focused on stabilizing the point of common coupling (PCC) voltage via direct reactive power compensation. Nevertheless, ES2 and ES3 are capable of direct active and

reactive power compensation for providing more ancillary services in addition to distributed voltage control. Although compared with ES1, both ES2 and ES3 have extended operating ranges, ES1's main advantage is the simplicity of its structure and controller which is a favorable distinction especially for industries. Moreover, it is investigated that ES1 can also mitigate frequency fluctuations through compensating active power indirectly (Xia Chen, Hou, Tan, Lee, & Hui, 2015). Still, most of the reported works in this area are focused on ES2 and ES3 (C.-K. Lee et al., 2020), (M. Wang et al., 2021). Therefore, the need for more focused research on ES1 is clear.

On the one hand, the initial control method introduced for ES1 is merely based on two conventional proportional-integral (PI) control loops (Hui et al., 2012), (C. K. Lee, Chaudhuri, & Hui, 2013). Interestingly, since then, this controller has been the foundation of several ES1 control schemes employed for mitigation of various power quality issues including voltage/frequency variations (C.-K. Lee et al., 2020), voltage flicker (Sharma et al., 2017), and harmonics (Kaymanesh & Chandra, 2020) in the literature. Droop (C. K. Lee, Chaudhuri, Chaudhuri, et al., 2013) and consensus control (J. Chen, Yan, & Ron Hui, 2017) techniques have been also proposed as the controllers of a group of ES1s distributed in microgrids. These methods are employed as a top-layer controller for providing auto-adjustable PCC voltage references for ES1s regarding their locations in an electrical grid. Nonetheless, control of every single ES1 has been mainly based on the PI controllers in combination with a pulse width modulation (PWM) technique. In all these works, nonlinearities and dynamic models of the employed ES1 converter topologies are not considered in the controller design. Furthermore, shared drawbacks of linear PI controllers for ES1 are requiring a modulator, high switching frequency, noticeable overshoots and undershoots in both dc and ac sides, and steady-state tracking error of the generated voltage. In (Z. Zhang et al., 2019), a novel control technique based on the ES1 operational voltage range is also proposed. Nevertheless, this method is founded on instant modification of the ratio of available loads in a microgrid by a direct load on/off control. Accordingly, numerous extra remote-control switching devices and respective coordinating loads are required that reduce the efficiency and reliability of the system.

On the other hand, regarding single-phase ES1 converter topologies, by far, two-level configurations have been mostly utilized (C.-K. Lee et al., 2020). However, although these half/full-bridge-based ES1s require the least possible passive and active components in their structures, they have intrinsic topological disadvantages especially for higher power commercial and industrial applications. Increased switching frequency and electromagnetic interference, noticeable voltage stress on the ES1 components, notoriously high total harmonic distortion (THD) of the injected voltage/current, and requiring bulky heat sink and harmonic filter are just some of them (Arai, Sekiguchi, Mochikawa, Sano, & Fujita, 2021). In (M.-H. Wang, He, Yang, Jia, & Xu, 2020), for dealing with high power loss and voltage stress on the two-level ES1 active and passive components and reducing the size of the required dc-link capacitor, it is proposed to employ a film capacitor instead of an electrolytic capacitor as the ES1 dc-link energy storage element. Nonetheless, in this work, a full-bridge inverter topology is employed as ES1 that still has poor power quality performance. Flying capacitor (FC) (Taul, Pallo, Stillwell, & Pilawa-Podgurski, 2021), cascaded H-bridge (CHB) (B. Liu, Song, Li, & Zhan, 2021) or active-neutral-point-clamped (ANPC) (Kaymanesh, Rezkallah, Saeedi, et al., 2020), as well-established multilevel converters, can be also developed for ES1 applications. As an instance, in (Kaymanesh, Rezkallah, Saeedi, et al., 2020) an ANPC converter is introduced for multilevel electric spring applications. Nevertheless, by employing this topology, eight transistor switches and four capacitors would be required to develop a five-level ES1. This noticeable amplified number of components in the classical multilevel converter topologies increases the ES1 volume, cost, and complexity that are not favorable features for a distributed voltage control method. It should be noted that various compact multilevel battery-based ES configurations have been also reported in the literature recently. But, they have not been proposed and analyzed for ES1 applications (Kaymanesh, Babaie, Tidjani, et al., 2020). Subsequently, in (Kaymanesh & Chandra, 2020), a novel ES1 topology founded on a reduced component count five-level modified packed u-cell (MPUC5) converter is proposed. This compact MPUC5-based ES1 (MPUC5-ES1) mitigates all the mentioned topological shortcomings. Besides, MPUC5-ES1 has a boost-mode operation that is favorable for higher power/voltage applications. But, in (Kaymanesh & Chandra, 2020), auxiliary capacitors' dynamic models cannot be considered in the proposed linear PI voltage controller

and their voltages are adjusted indirectly using a PWM modulator based on the availability of extra switching states. Therefore, in addition to the aforementioned problems of capacitor-based electric spring PI controllers, capacitors' voltages are tunable only on the same value, and relatively increased-size capacitors are required to have acceptable voltage ripples on them.

However, by employing more system parameters and considering the dc-link capacitors' dynamics and converter nonlinearities in the controller design, it will be possible to mitigate mentioned issues associated with available linear controllers. Besides, the voltage of each one of the auxiliary capacitors will be independently modifiable to any desired level directly. So, not only the power density of MPUC5-ES1 topology will be improved, but also it can be operational in a seven-level mode with an even more improved power quality performance. Considering converters' control techniques especially for power system applications, a wide range of linear and nonlinear methods have been proposed recently. However, due to the merits such as not requiring a modulator, superior transient response, considering the converter constraints and dynamic models, multicriteria optimization performance, and intuitiveness, finite control-set model predictive control (FCS-MPC) stands out among them (Gao, Gong, Li, & Liu, 2020). Besides, regarding any concerns about the computational burden of FCS-MPC, the following points should be highlighted. First, the significant development of microcontrollers acts as a key precursor that encourages employing more advanced controllers, especially for power electronics applications. Second, due to the minimized number of switching vectors and auxiliary dc links, the complexity of an FCS-MPC method designed for a high-power-density multilevel topology is reduced noticeably in comparison to when it is applied to a classical multilevel configuration. As an instance, in (Kaymanesh, Chandra, et al., 2021), it is also proven that computational burden is not an issue regarding applying an autotuned FCS-MPC to a seven-level modified packed U-cell (MPUC7) based static synchronous compensator.

Accordingly, to address the aforementioned issues regarding the already available ES1 configurations and controllers, a novel bidirectional ES1 topology founded on the compact

MPUC7 converter, and its particular nonlinear controller based on a finite control-set model predictive current control (FCS-MPCC) is proposed, and vindicated. Finally, the main novelties of this article are listed as follows:

1. MPUC7 topology is proposed for the capacitor-based electric spring application for the first time.
2. Concerning mentioned demerits of existing ES1 linear PI controllers, a nonlinear hybrid controller based on FCS-MPCC is designed and proposed.
3. The MPUC7-ES1 state-space average model is presented.
4. MPUC7-ES1 and its FCS-MPCC-based controller are extensively analyzed and validated experimentally.

After an Introduction to capacitor-based electric spring configurations and controllers, Section 4.2 presents the proposed MPUC7-ES1 basic performance principles. Section 4.3 introduces the MPUC7-ES1 configuration and topological merits. The designed FCS-MPCC-based controller will be presented in Section 4.4. To validate the operation of the proposed ES1 topology and nonlinear controller, Sections 4.5 and 4.6 are respectively focused on providing simulation and experimental results. Finally, the article is concluded in Section 4.7.

4.2 MPUC7-ES1 Operation Principles

Figure 4.1 illustrates an MPUC7-ES1 integrated into a single-phase AC microgrid. As can be seen, a conventional power plant, which provides a stable output voltage, is connected to the PCC through a low-voltage transmission line with a relatively high impedance to represent a microgrid with low system strength (Xin Chen, Zhang, Wang, Chen, & Gong, 2017). An asynchronous power electronics-based renewable energy source such as wind or solar farm also powers this microgrid. As a result, due to the instabilities of the injected current by the renewable energy source, the PCC voltage fluctuates. Available loads in an electrical grid are categorizable to non-sensitive load (NSL) and sensitive load (SL). NSLs are generally thermostatically controlled loads, like heating, ventilation, and air conditioning (HVAC) systems, and can withstand voltage fluctuations to some extent. Demanded power by NSLs

depends on their input voltage. On the contrary, SLs, for instance, data centers, require a tightly regulated input voltage and power. As depicted in Figure 4.1, to stabilize its input voltage (SL voltage) through modulating its output voltage (NSL voltage), MPUC7-ES1 should be installed between the PCC and NSL. In this regard, it generates a high-power quality seven-level compensation voltage. This setup, which is known as multilevel smart load (MSL), can address power imbalance-related problems in an electrical grid by modulating its demanded power in real-time.

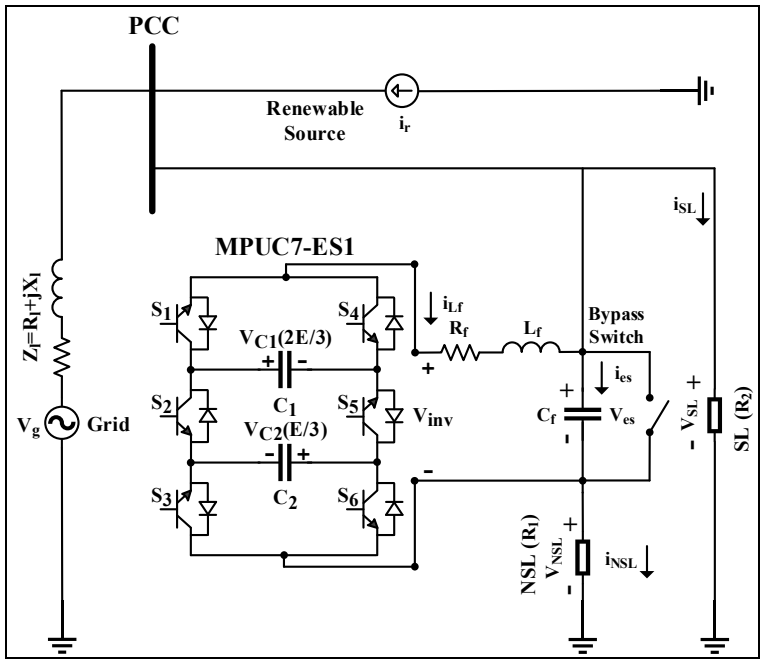

Figure 4.1 MPUC7-ES1 integrated into an AC microgrid

MPUC7-ES1 compensates for reactive power directly and, therefore, its generated voltage should be perpendicular to the NSL current. So, it has three main operation modes, neutral, capacitive, and inductive. In the neutral mode, there is no power imbalance in the system and the MPUC7-ES1 injected voltage should be negligible. When there is an extra amount of injected power into the power system, the SL voltage exceeds its nominal value. Accordingly, MPUC7-ES1 should be operational in the capacitive mode. This means that the MPUC7-ES1 voltage should lag the NSL current by about 90° to increase the NSL voltage and demanded power. Nonetheless, if the consumed power is higher than the power generation, the SL voltage

will be lower than its nominal amount. In this case, MPUC7-ES1 must operate in the inductive mode and its voltage leads the NSL current by around 90˚. Consequently, NSL voltage and power will be decreased to mitigate this power imbalance. As MPUC7-ES1 can only indirectly compensate active power, its capacitive operation range is limited in comparison with its inductive operation. Figure 4.2 depicts phasor diagrams of an MSL with a resistive NSL for all the possible modes.

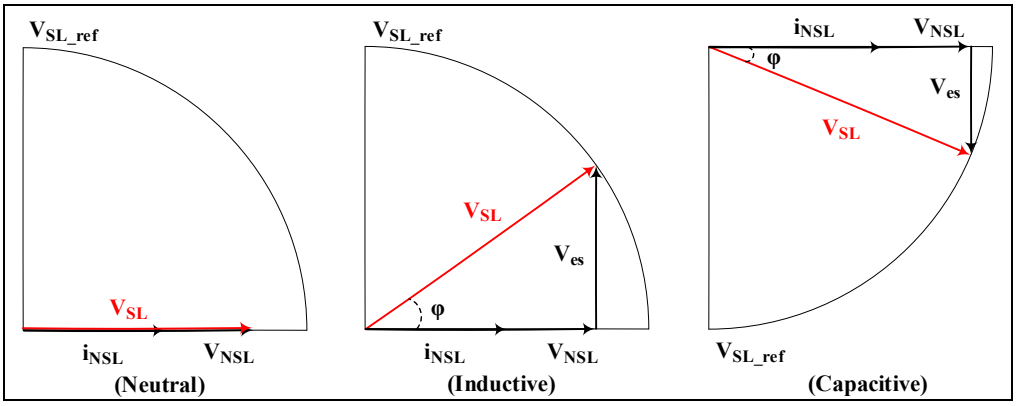

Figure 4.2 Phasor diagrams of a multilevel smart load with a resistive NSL

4.3 MPUC7-ES1 Topology

The proposed high-power density MPUC7-based ES1 is depicted in Figure 4.1. As a seven-level bidirectional ES1 topology with highly reduced component counts, it consists of only six unidirectional semiconductor transistor switches and two auxiliary capacitors. To attain a seven-level voltage waveform, if the peak value of the required compensation voltage equals E, the first capacitor (C_1) and second capacitor (C_2) voltages (V_{C1} and V_{C2}) should be tuned at only *2E/3* and *E/3*, respectively. Furthermore, two upper switches (S_1 and S_4) endure *2E/3*, two middle switches (S_2 and S_5) withstand *E,* and the voltage rating of two remaining switches mounted at the bottom (S_3 and S_6) is only *E/3*. However, the current rating of all the switches must be equal to the NSL maximum current value. The operation of each couple of switches with the same voltage rating is also complementary to prevent short circuits. Switching states and generated voltage levels are also listed in Table 4.1. As can be seen, the only available switching redundancy is at the zero states.

Table 4.1 MPUC7-ES1 switching states

States	S_1	S_2	S_3	Vab	Voltage Level
1	1	0	1	$V_{C1}+V_{C2}$	E
2	1	0	0	V_{C1}	2E/3
3	0	0	1	V_{C2}	E/3
4	0	0	0	0	0
5	1	1	1	0	0
6	1	1	0	$-V_{C2}$	-E/3
7	0	1	1	$-V_{C1}$	-2E/3
8	0	1	0	$-V_{C1}-V_{C2}$	-E

As an instance, in comparison with the widely employed half-bridge capacitor-based two-level electric spring (C. K. Lee, Chaudhuri, & Hui, 2013), four more transistor switches with various voltage ratings are required in the proposed compact seven-level ES1 structure. However, MPUC7-ES1 has several key advantages that can justify this increased number of components. To begin with, the peak value of the generated compensation voltage in a half-bridge ES1 is merely half of its dc-link voltage. Nonetheless, MPUC7-ES1 has a boost operation and its peak output voltage equals the sum of the auxiliary capacitors' voltages ($V_{C1} + V_{C2}$). Consequently, MPUC7-ES1's passive and active components withstand significantly lower voltage stress. This makes MPUC7-ES1 a superior option even for medium-voltage higher-power industrial/commercial applications. In addition, half-bridge ES1 with a conventional controller has a high and uncontrollable switching frequency. While, by the introduced nonlinear FCS-MPCC-based controller, the switching frequency of the MPUC7-ES1 can be controlled and reduced. Moreover, the two-level performance of a half-bridge electric spring increases the SL voltage THD. Therefore, regarding any cost comparisons between the half-bridge ES1 and the proposed MPUC7-ES1 topologies, several points should be noted. First, the discrete semiconductor transistors with reduced drain-source voltage (V_{DSmax}) and decreased switching frequency (cheaper transistors) are required for MPUC7-ES1. Second, due to increased losses, high switching frequency reduces the efficiency of an electric spring topology. Third, it is required to employ a relatively bulky/costly lowpass filter in the half-bridge ES1 output. It will

be also essential to design and utilize a complex controller to add harmonics mitigation capability to the two-level ES1 that also limits its operating voltage range (Q. Wang et al., 2016). However, due to the seven-level symmetrical waveform of the MPUC7-ES1 generated voltage, although a less bulky/costly lowpass filter can be employed, the THD content of the injected voltage and, consequently, SL voltage will be less than the IEEE 1547 standard limit. Last but not least, through the conventional PI controller of a half-bridge ES1 (C. K. Lee, Chaudhuri, & Hui, 2013), the dynamics of the dc-link capacitors are neglected. So, for having an acceptable voltage ripple on capacitors (less than 5 percent), compared with MPUC7-ES1, half-bridge ES1 requires larger size capacitors that are also more expensive. Regarding reliability comparison with a half-bridge ES1, although having a smaller number of components reduces the chance of failure, voltage stress and switching frequency are in direct connection with semiconductor switches' degradation rate (Pu, Ugur, Yang, & Akin, 2020). The notably lower voltage stress on the MPUC7-ES1 capacitors should be also considered regarding reliability comparison. Hence, MPUC7-ES1 can be considered a reliable option.

On the other hand, introduced MPUC7-ES1 has two critical topological merits over the MPUC5-based ES1 (Kaymanesh & Chandra, 2020). Having an increased number of output voltage levels yet requiring the same number of passive/active components is the first crucial advantage. This results in employing a less bulky harmonic filter and reducing the power losses caused by harmonics. Second, through the proposed controller in (Kaymanesh & Chandra, 2020), capacitors' voltages are tuned at the same amount integrated into the switching process without considering their dynamics and nonlinearities. However, by the introduced controller, dynamics models of the auxiliary capacitors are taken into account and their voltages are directly controlled at the required values in a closed-loop manner. So, capacitors' voltage ripple is decreased, and therefore, dc-link capacitors' size/cost can be also reduced. This reduces the size/cost of the proposed MSL. To sum up, MPUC7-ES1 has a better power quality operation with a higher power density. These are critical points for an ES1 configuration as it is a distributed DRM technology.

4.4 MPUC7-ES1 FCS-MPCC-Based Controller

As mentioned before, conventional PI-based ES1 controllers do not consider the nonlinearities of the MPUC7-ES1 converter and its output lowpass filter. Besides, by employing these linear approaches, it is required to employ a modulation technique to generate switching signals indirectly (C.-K. Lee et al., 2020), (Sharma et al., 2017). Considering these issues, an FCS-MPCC-based nonlinear control approach, which is illustrated in Figure 4.3, is designed and proposed. As depicted in the Figure 4.3 block diagram, this method comprises two main control loops, inner and outer. An inner control loop is founded on an FCS-MPCC designed for the MPUC7-ES1 applications. First, it is required to achieve the MPUC7-ES1 state-space average model. By considering the converter losses negligible, regarding active power balance between the MPUC7-ES1 dc and ac sides, (4.1) can be achieved.

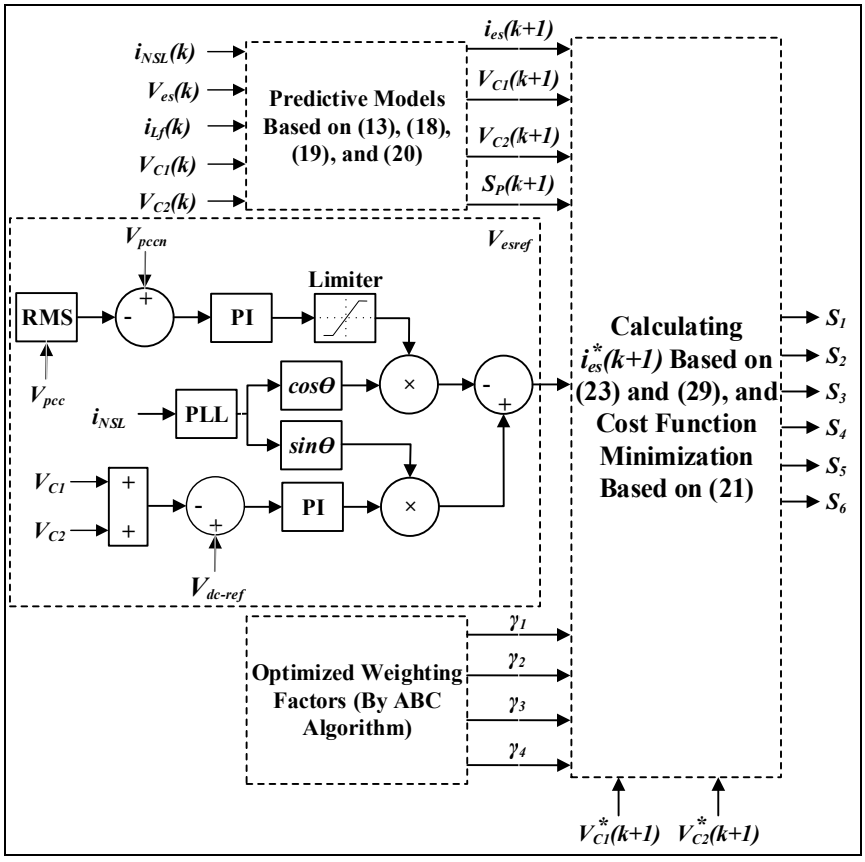

Figure 4.3 FCS-MPCC-based nonlinear controller

$$P_{dc} = P_{ac} \Rightarrow \frac{1}{2} \times (C_1 + C_2) \times \frac{d(V_{dc-link})^2}{dt} = (C_1 + C_2) \times (V_{C1} + V_{C2}) \times \frac{d(V_{C1} + V_{C2})}{dt} = R_f \times {i_{L_f}}^2 \quad (4.1)$$

here P_{dc} and P_{ac} are the real powers of the dc and ac sides, respectively. R_f and i_{L_f} are the parasitic resistance and current of the MPUC7-ES1 output filter inductor (L_f), correspondingly. In addition, $V_{dc-link}$ is the MPUC7-ES1 dc-link voltage. On the other hand, by applying Kirchhoff's Voltage Law and Kirchhoff's Current Law on the MPUC7-ES1 ac side, (4.2) and (4.3) are obtainable.

$$V_{inv} = L_f \times \frac{di_{L_f}}{dt} + R_f \times i_{L_f} + V_{es} \quad (4.2)$$

$$C_f \times \frac{dV_{es}}{dt} = i_{es} = i_{NSL} + i_{L_f} \quad (4.3)$$

where V_{inv} and C_f define the MPUC7-ES1 terminal voltage and the capacitance value of the output LC filter, V_{es} is the MPUC7-ES1 generated and filtered compensation voltage, and i_{NSL} and i_{es} are also the current flowing through the NSL load and C_f, respectively. Furthermore, the tunable voltage across C_f is also achievable as follows:

$$V_{es} = V_{SL} - R_{NSL} \times i_{NSL} \quad (4.4)$$

here V_{SL} and R_{NSL} are the SL voltage and resistance value of the non-sensitive load, respectively. For simplicity, sensitive and non-sensitive loads are considered to be resistive. Regarding the switching vectors provided in Table 4.1, the MPUC7-ES1 terminal voltage discrete model is also calculatable as (4.5).

$$V_{inv} = (S_1 - S_2) \times V_{C1} - (S_2 - S_3) \times V_{C2} \quad (4.5)$$

Considering (4.1) -(4.5), the MPUC7-ES1 state-space average model is derivable as

$$\frac{di_{L_f}}{dt} = -\left(\frac{R_f}{L_f}\right) i_{L_f} - \left(\frac{1}{L_f}\right) V_{es} + \left(\frac{1}{L_f}\right) V_{inv} \tag{4.6}$$

$$\frac{dV_{es}}{dt} = \left(\frac{1}{C_f}\right) i_{L_f} - \left(\frac{1}{R_{NSL} C_f}\right) V_{es} + \left(\frac{1}{R_{NSL} C_f}\right) V_{SL} \tag{4.7}$$

$$\frac{d(V_{C1} + V_{C2})}{dt} = \left(\frac{R_f}{(C_1 + C_2) \times (V_{C1} + V_{C2})}\right) {i_{L_f}}^2 \tag{4.8}$$

As can be noted, the MPUC7-ES1 state-space average model is nonlinear. Accordingly, it is essential to consider its dynamic models in the designed controller. The MPUC7-ES1 FCS-MPCC inner control loop is designed to achieve features that are not attainable by a linear controller. Seven-level performance, reduced capacitors' size and voltage ripples, controllable switching frequency, decreased steady-state error of the injected voltage, and faster transient response are among these characteristics. In this regard, four main control objectives should be defined and achieved. ES1 can be considered as a capacitor that is fed via a controllable current source. Hence, as the first control objective, predictive model of i_{es} for a one-step time-horizon ($i_{es}(k+1)$) should be calculated. Consequently, based on (4.6) and through employing the respective Euler forward approximation presented in (4.9), the predictive model of i_{L_f} ($i_{L_f}(k+1)$) for a sampling period T_s is calculated as (4.10).

$$\frac{di_{L_f}}{dt} = \frac{i_{L_f}(k+1) - i_{L_f}(k)}{T_s} \tag{4.9}$$

$$i_{L_f}(k+1) = \frac{T_s}{L_f} \times (V_{inv} - V_{es}) + \left(1 - \frac{R_f \times T_s}{L_f}\right) \times i_{L_f}(k) \tag{4.10}$$

Variations of the NSL current are also considered negligible for the defined sampling time.

$$i_{NSL}(k+1) = i_{NSL}(k) \tag{4.11}$$

Therefore, considering (4.3), (4.10), and (4.11), $i_{es}(k+1)$ is computed as

$$i_{es}(k+1) = i_{NSL}(k) + i_{L_f}(k+1) \tag{4.12}$$

$$i_{es}(k+1) = i_{NSL}(k) + \frac{T_s}{L_f} \times (V_{inv} - V_{es}) + \left(1 - \frac{R_f \times T_s}{L_f}\right) \times i_{L_f}(k) \tag{4.13}$$

On the other hand, as mentioned earlier and can be noted from Table 4.1, the only extra switching state is available at the zero-voltage level that cannot be employed for tuning the capacitors' voltages. So, to achieve MPUC7-ES1 seven-level operation, auxiliary capacitors' nonlinearities should be integrated into the proposed FCS-MPCC. Consequently, the second and third control objectives are focused on stabilizing V_{C1} and V_{C2} at their references (e.g., *2E/3* and *E/3*) independently. Accordingly, auxiliary capacitors' dynamic models are calculatable through (4.14) and (4.15).

$$i_{C1} = C_1 \times \frac{dV_{C1}}{dt} = (S_2 - S_1) \times i_{L_f} \tag{4.14}$$

$$i_{C2} = C_2 \times \frac{dV_{C2}}{dt} = (S_2 - S_3) \times i_{L_f} \tag{4.15}$$

where i_{C1} and i_{C2} are the currents of the first and second capacitors. As is notable, although V_{C1} and V_{C2} are different, i_{L_f} flows through both of the capacitors. This increases the system's nonlinearity. Accordingly, based on (4.14) and (4.15), Euler forward approximation is employed again to calculate predictive models of the capacitors' voltages as below

$$\frac{dV_{C1}}{dt} = \frac{V_{C1}(k+1) - V_{C1}(k)}{T_s} \tag{4.16}$$

$$\frac{dV_{C2}}{dt} = \frac{V_{C2}(k+1) - V_{C2}(k)}{T_s} \tag{4.17}$$

$$V_{C1}(k+1) = \frac{(S_2 - S_1) \times T_s}{C_1} \times i_{L_f}(k) + V_{C1}(k) \tag{4.18}$$

$$V_{C2}(k+1) = \frac{(S_2 - S_3) \times T_s}{C_2} \times i_{L_f}(k) + V_{C2}(k) \tag{4.19}$$

Regarding (4.13), (4.18), and (4.19), in comparison with the classical linear ES1 controllers (Hui et al., 2012), (C. K. Lee, Chaudhuri, & Hui, 2013), system characteristics and measurement of more parameters, such as $V_{es}(k)$ and $i_{L_f}(k)$, are required in the proposed model-based FCS-MPCC. This is an important point that should be also considered by the designer. Moreover, as noted earlier high and uncontrolled switching frequency is one of the main problems of the conventional ES1 controllers (C. K. Lee, Chaudhuri, & Hui, 2013). Consequently, the fourth control objective is focused on the reduction of the switching frequency. To control switching performance, (4.20) is defined, as follows:

$$\begin{aligned} S_P(k+1) = {} & |S_1(k+1) - S_1(k)| + |S_2(k+1) - S_2(k)| \\ & + |S_3(k+1) - S_3(k)| \end{aligned} \tag{4.20}$$

here $S_P(k+1)$ denotes the predicted switching pattern for the next time step. $S_1(k+1)$, $S_2(k+1)$ and $S_3(k+1)$ represent the next switching vectors for $S_1(k)$, $S_2(k)$ and $S_3(k)$, respectively. Considering the calculated predictive models of the control objectives, cost function ($g(k+1)$) of the designed FCS-MPCC is expressed as (4.21).

$$\begin{aligned} g(k+1) = {} & \gamma_1 |i_{es}(k+1) - i_{es}^*(k+1)| \\ & + \gamma_2 |V_{C1}(k+1) - V_{C1}^*(k+1)| \\ & + \gamma_3 |V_{C2}(k+1) - V_{C2}^*(k+1)| + \gamma_4 \times S_P(k+1) \end{aligned} \tag{4.21}$$

where $\gamma_1, \gamma_2, \gamma_3$ and γ_4 are the weighting coefficients of the control targets. $V_{C1}^*(k+1)$ and $V_{C2}^*(k+1)$ denote desired references for the auxiliary capacitors' voltages (*2E/3* and *E/3*). $i_{es}^*(k+1)$, which represents the reference of i_{es} at $(k+1)$, is attainable by applying the Lagrange extrapolation theory as (Y. Yang et al., 2019):

$$i_{es}^*(k+1) = \sum_{l=0}^{n} (-1)^{n-1} \times \frac{(n+1)!}{l!\,(n+1-l)!} \times i_{es}^*(k+l-n) \tag{4.22}$$

here n is defined to be 2 (second-order), therefore, $i_{es}^*(k+1)$ formula is simplified as (4.23).

$$i_{es}^*(k+1) = 3i_{es}^*(k) - 3i_{es}^*(k-1) + i_{es}^*(k-2) \tag{4.23}$$

where $i_{es}^*(k)$, $i_{es}^*(k-1)$, and $i_{es}^*(k-2)$ are the references for the current flowing through the MPUC7-ES1 output filter capacitor at the instants k, $k-1$, and $k-2$, respectively. In this respect, the outer control loop is designed to generate the MPUC7-ES1 compensation voltage reference magnitude and phase angle. This outer loop contains two discrete PI controllers, ac and dc. The ac PI control loop is responsible to tune the SL voltage at its nominal value through reactive power compensation. On the other hand, during transients the dc-link voltage ($V_{dc-link} = V_{C1} + V_{C2}$) varies, so, dc PI control loop stabilizes $V_{dc-link}$ at its defined reference (V_{dc_ref}) by exchanging a relatively insignificant amount of active power with the grid. Based on the outer control loop, the MPUC7-ES1 reference voltage equation (V_{esref}) can be expressed as follows:

$$\begin{aligned} V_{esref} = &-\left[\left(K_{Pac} + \frac{K_{Iac}}{s}\right) \times \left(V_{pcc_n} - V_{pcc}\right)\right] \times \cos\theta \\ &+ \left[\left(K_{Pdc} + \frac{K_{Idc}}{s}\right) \times \left(V_{dc\_ref} - (V_{C1} + V_{C2})\right)\right] \times \sin\theta \end{aligned} \tag{4.24}$$

where θ, which represents the NSL current phase angle, is determined using a phase-locked loop (PLL). V_{pcc_n} and V_{pcc} denote the RMS values of the defined grid nominal voltage (e.g.

110 V) and the measured PCC voltage, respectively. Moreover, K_{Pac} and K_{Pdc} are the proportional gains of the ac and dc PI control loops and K_{Iac} and K_{Idc} are the integral gains, correspondingly. Besides, considering the MPUC7-ES1 phasor diagram depicted in Figure 4.2, the PCC voltage equation is presented as (4.25). Therefore, for a resistive NSL, the value of V_{dc_ref} can be also computed based on (4.26).

$$V_{pcc}^2 = (V_{NSL}\, cos\, \theta)^2 + (V_{NSL}\, sin\, \theta \pm V_{es})^2 \tag{4.25}$$

$$V_{dc\_ref} = \sqrt{2} \times \sqrt{V_{pcc}^2 - V_{NSL\_min}^2} \tag{4.26}$$

here V_{NSL} and V_{NSL_min} are the non-sensitive load voltage and the minimum amount of voltage that this load can withstand, respectively. Regarding the calculation of C_1 and C_2 capacitance values, (4.27) and (4.28) are also employed.

$$C_1 \geq \frac{|V_{es}||i_{NSL}|}{4\pi f {V_{C1}}^2 V_{ripple}} \tag{4.27}$$

$$C_2 \geq \frac{|V_{es}||i_{NSL}|}{4\pi f {V_{C2}}^2 V_{ripple}} \tag{4.28}$$

where f and V_{ripple} represent the grid frequency and the tolerable percentage of voltage ripple on the capacitors. It should be also indicated that the magnitude of the outer control loop's output signal is limited to the upper and lower saturation amounts (± 1). Therefore, it is multiplied by V_{dc_ref} calculated by (4.26). Considering (4.3), (4.24), and (4.26), it should be indicated that $i_{es}^*(k)$ is also computed as a discrete derivative of the generated reference voltage multiplied by the capacitance value of the output lowpass filter and the reference of the dc-link voltage as (4.29).

$$i_{es}^{*}(k) = V_{dc\_ref} \times C_f \times \frac{dV_{esref}}{dt} \tag{4.29}$$

Finally, to track control objectives accurately and quickly, weighting factors and PI coefficients should be tuned effectively. Consequently, Artificial Bee Colony (ABC) algorithm is recommended in this paper so that desired performance is met. ABC as a metaheuristic optimization algorithm precisely investigates the whole search space, to find the tuned values that are located in the global minimum area. ABC is accurate and reliable because it applies a four-layer optimization over the search space during each iteration of the algorithm. To initialize ABC, *N* vectors called foods with four elements (corresponding to the number of the weighting factors) are randomly set using (4.30).

$$\begin{cases} \varphi_i = \varphi^{min} + rand(\,0,1)(\varphi^{max} - \varphi^{min}) \\ \varphi_i = [\gamma_1, \ldots, \gamma_4] \end{cases} \tag{4.30}$$

φ_i is ith food, which includes the possible best values for the weighting factors. φ^{max} and φ^{min} are the acceptable boundaries of the weighting factors. Afterward, *m* of *M* bees the so-called employed bees are assigned to the initialized foods then they start searching around the candidate foods using (4.31) to find better solutions.

$$\begin{cases} \varphi_i^{*} = \varphi_i + \mu_i(\varphi_i - {\varphi_i}^r) \\ \mu_i = rand(-1,1) \\ {\varphi_i}^r = \varphi_{rand(1,N)} \end{cases} \tag{4.31}$$

φ_i^{*}, μ_i, ${\varphi_i}^r$ are respectively the new position of ith food, a random value, and the food, which is randomly selected among the existing ones. Using (4.31), the employed bees start moving from the assigned food (φ_i) toward another food (${\varphi_i}^r$) in the vicinity to find better solutions (φ_i^{*}). After each movement during the jth iteration, the existing (φ_i) and the updated (φ_i^{*}) foods are applied to the control loop as the weighting factors and then the performance is measured through (4.32) to calculate the cost of the weighting factors modification.

$$\begin{cases} Co_i = \begin{cases} 1/(1+f_i(\Theta_i)) & f_i(\Theta_i) > 0 \\ 1+|f_i(\Theta_i)| & f_i(\Theta_i) < 0 \end{cases} \\ NCo_i = \dfrac{Co_i}{\sum_{i=1}^{N} Co_i} \\ \Theta_i = [\varphi_i^* \ \ \varphi_i] \end{cases} \tag{4.32}$$

Co_i and NCo_i are the cost and the normalized cost of ith food assigned to nth bee, respectively. f_i represents the cost function, which is used to evaluate the optimization performance of ABC. In this paper, Integral Time-weighted Absolute Error (ITAE) is selected as the cost function because it accurately measures the steady-state error of the state variables. Accordingly, ITAE is formed based on the tracking errors of the capacitor voltages and the MPUC7-ES1 current, which are the main control terms, as (4.33).

$$\begin{cases} f_i(\Theta_i) = \int_{t=0}^{t_{ABC}} t(E(t))dt \\ E(t) = (i_{es} - i_{es}^*) + (V_{C1} - V_{C1}^*) + (V_{C2} - V_{C2}^*) \end{cases} \tag{4.33}$$

t_{ABC} is used to indicate the operation time of ABC during each iteration. In the third layer of the ABC, the onlooker bees are assigned to the foods that cost the least. As a result, the best foods have more chances to be investigated by both the employed and the onlooker bees. Notice that the onlooker bees use (4.31) to update the assigned foods. In the fourth layer, the worst foods are abandoned and their bees including employed and onlookers turn into scout ones. The scout bees are assigned to new random foods using (4.30); thus, the fourth layer remarkably helps the ABC algorithm to escape from local minimums. Table 4.2 provides the initial parameters of the ABC algorithm, which were used to train the FCS-MPCC weighting factors. After 40 iterations of ABC, the optimal values of the weighing factors were acquired ($\gamma_1 = 1.23$, $\gamma_2 = 0.89$, $\gamma_3 = 1.15$ and $\gamma_4 = 0.014$). It is worth noting that a similar training loop but with the following cost function and initial parameters that are presented in Table 4.3 was used to adjust the control coefficients of the PI controllers. Integral Squared Error (ISE) as (4.34) is selected as the ABC cost function because it accurately measures the transient effects of the PI controllers during the training process. This time, after 30 iterations of ABC,

the optimum values of the PI coefficients were acquired ($K_{Pac} = 0.15$, $K_{Iac} = 8.18$, $K_{Pdc} = 0.01$, *and* $K_{Idc} = 0.005$).

$$\begin{cases} f_i(\Theta_i) = \int_{t=0}^{t_{ABC}} E(t)^2 dt \\ E(t) = \left(V_{pcc_n} - V_{pcc}\right) + \left(V_{dc\_ref} - (V_{C1} + V_{C2})\right) \end{cases} \tag{4.34}$$

Table 4.2 ABC parameters for tuning weighting factors

N	t_{ABC}	M	Iteration	$[\varphi^{min}, \varphi^{max}]$
200	0.7s	400	40	[0 3]

Table 4.3 ABC parameters for tuning PI coefficients

N	t_{ABC}	M	Iteration	$[\varphi^{min}, \varphi^{max}]$
200	0.5s	400	30	[0 20]

It should be also noted that weighting factors and PI coefficients are not tuned in an online manner. Consequently, the computational burden and complexity of the proposed controller are minimized significantly.

4.5 Simulation Results

A simplified schematic diagram of the simulated MPUC7-ES1-based electric system employing MATLAB/SIMULINK is illustrated in Figure 4.4. Specifications of this system are also presented in Table 4.4. This system is powered through a controlled voltage source to study the operation of the introduced MPUC7-ES1 and controller. To emulate the grid voltage fluctuations, this controlled voltage source is connected to the PCC through a low voltage weak distribution line with a relatively high impedance.

Table 4.4 Specifications of the simulation setup

PCC RMS Nominal Voltage (V_{PCC_n})	110 V
Grid Frequency (F)	60 Hz
Distribution Line Impedance (Z_l)	0.1+j7.54 Ω
Output Filter Inductance (L_f)	2.5 mH
Output Filter Parasitic Resistance (R_f)	0.1 Ω
Output Filter Capacitance (C_f)	30 µF
Maximum Value of Output Voltage (E)	100 V
First Capacitor Voltage ($V_{C1} = 2E/3$)	66.67 V
Second Capacitor Voltage ($V_{C2} = E/3$)	33.3 V
First Capacitor Capacitance (C_1)	1500 µF
Second Capacitor Capacitance (C_2)	1500 µF
Non-Sensitive Load Resistance (R_1)	40 Ω
Sensitive Load Resistances (R_2, R_3)	40 Ω, 80 Ω

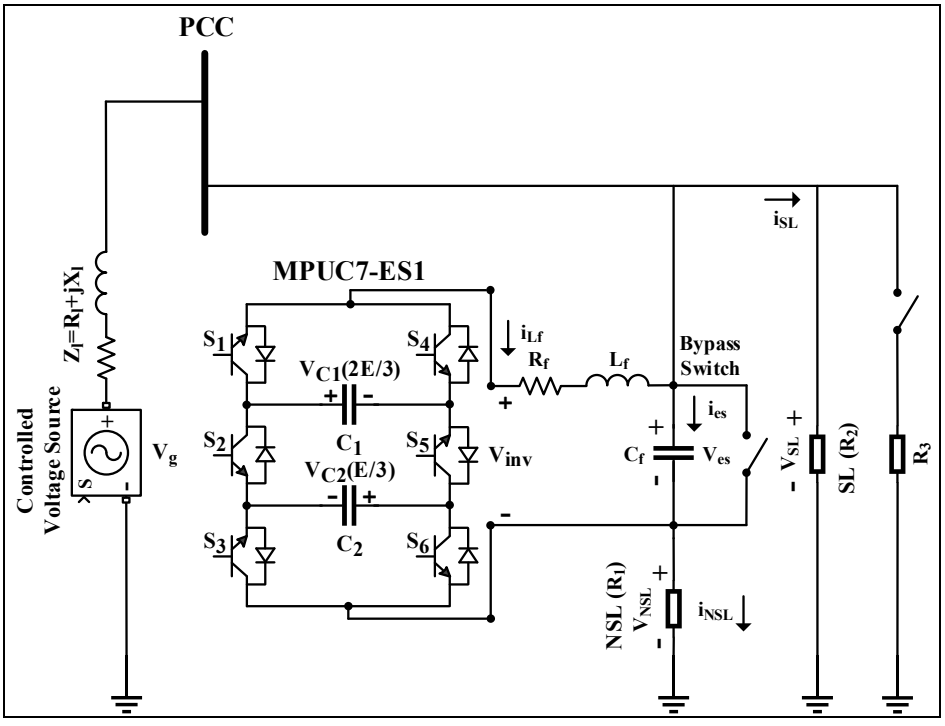

Figure 4.4 Simulated MPUC7-ES1-based electric system

First, the system performance has been analyzed with and without MPUC7-ES1 during steady-state operations when V_{pcc} is equal, higher, and lower than the grid nominal value (110 V RMS). Figure 4.5 illustrates the results for the equal case scenario. As is clear, in this case, the injected voltage by MPUC7-ES1 is negligible, and both V_{SL} and V_{NSL} are stabilized at the nominal value with and without MPUC7-ES1.

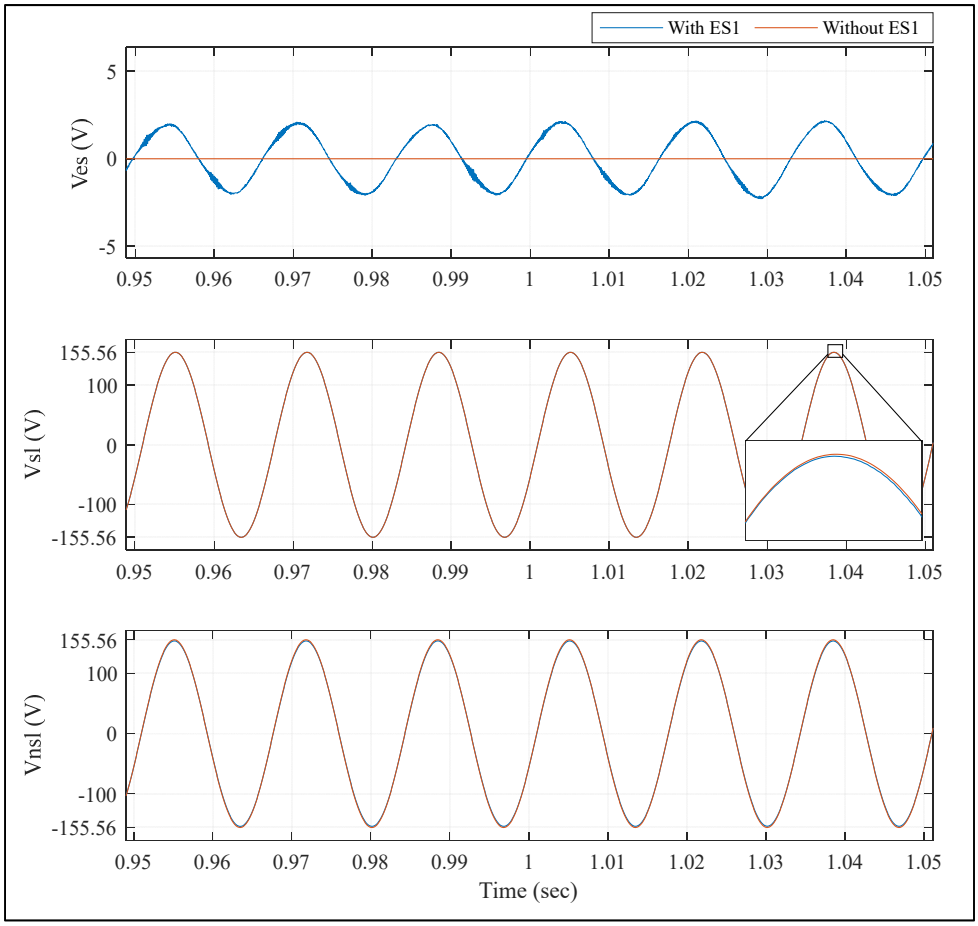

Figure 4.5 Results when the PCC voltage is equal to the grid nominal value

Regarding the higher and lower voltage cases, Figures 4.6 and 4.7 present the respective recorded measurements of the system during these simulations. As can be seen, when MPUC7-ES1 is deactivated, both the SL voltage and NSL voltage are equal with maximum values of 163.4 V and 139.6 V for the high and low voltage scenarios, respectively. Nevertheless, after activating MPUC7-ES1, through the injected compensation voltage, SL voltage is effectively

stabilized at the nominal amount (155.56 V≈110 V RMS). But, this time as expected, the measured NSL voltage maximum value is modified at 140.7 V when the grid voltage is high and 121.6 V for the lower voltage scenario. Voltage fluctuations have been effectively transferred from the SL to the NSL. Considering the phasor diagrams of an MSL presented in Figure 4.2, it can be also noted that the phase difference between the injected compensation voltage and the NSL voltage is following the capacitive (high voltage case) and inductive (low voltage case) operation modes of MPUC7-ES1.

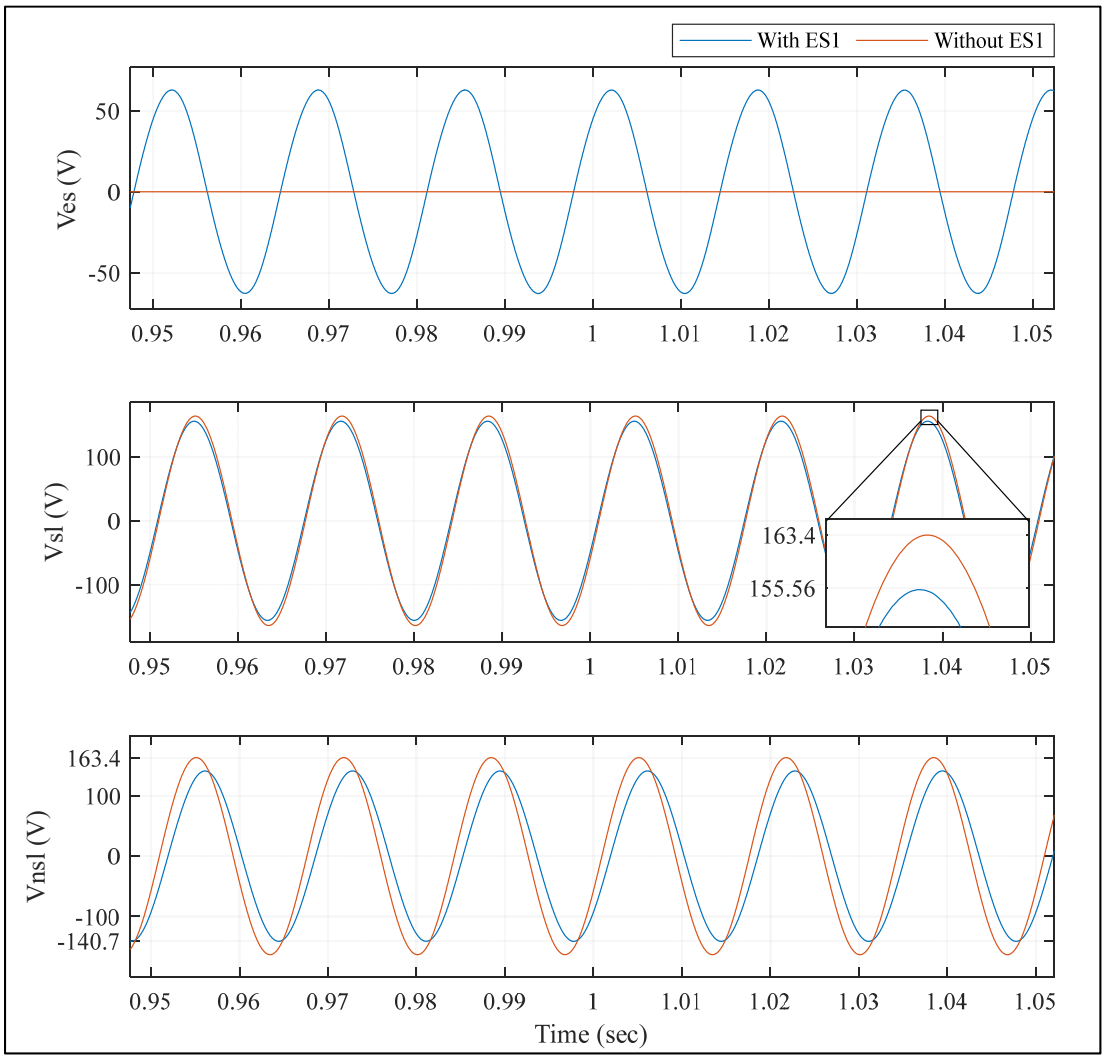

Figure 4.6 Results when the PCC voltage is higher than the grid nominal voltage

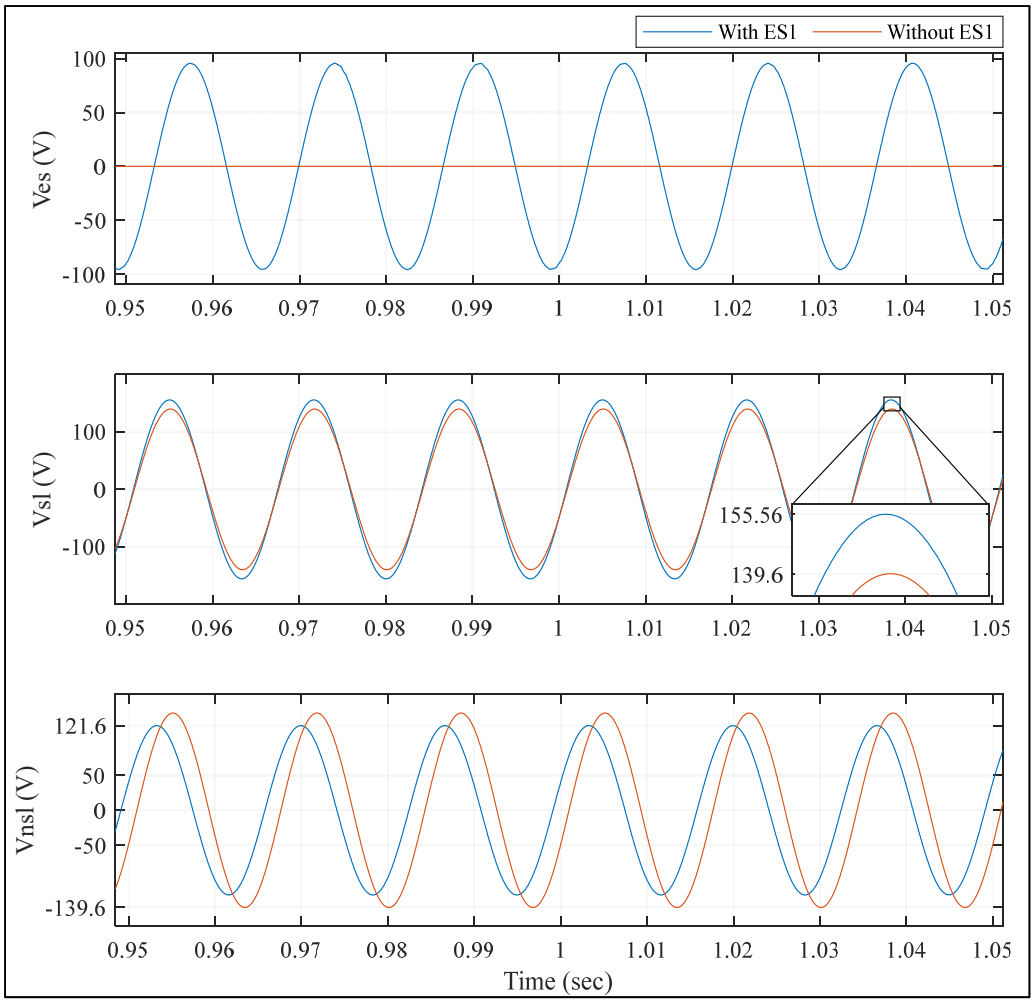

Figure 4.7 Results when the PCC voltage is lower than the grid nominal voltage

Second, the main focus of this part is to demonstrate the enhanced power quality characteristics of MPUC7-ES1, the switching frequency reduction capability, and reduced voltage stress across the employed passive/active components. Hence, the terminal voltage of the proposed seven-level ES1 and voltages of C_1 and C_2 as well as the voltage across S_1, S_2, and S_3 during the lower voltage case of the previous simulation, as an instance, are measured and presented in Figures 4.8 and 4.9, respectively. To better show the capability of the proposed nonlinear controller in reducing the switching frequency of MPUC7-ES1, γ_4 is suddenly changed from 0.014 to 0 at t=2 s during this test. By having a greater γ_4, tracking errors of the other control terms will be increased slightly. However, as is notable in Figure 4.8, both capacitors' voltages are tuned at their references with voltage ripples noticeably less than 5% that is acceptable.

Consequently, MPUC7-ES1 injected seven-level voltage waveform is smooth and symmetrical. As depicted in Figures 4.8 and 4.9, regarding the reduced voltage stress across the components, in this test, the maximum value of the MPUC7-ES1 seven-level terminal voltage equals 100 V. As expected, S_1, S_2, and S_3 endure merely 66.7 V, 100 V and, 33.3 V. Besides, C_1 and C_2 withstand 66.7 V and 33.3 V respectively. So, the boost mode operation of the proposed MPUC7-ES1 is evident. In addition, Figure 4.9 reveals that switches with higher switching frequency operation tolerate less voltage, which leads to less switching loss. Considering the presented results, as is notable with $\gamma_4 = 0.014$, the average switching frequency, which can be also calculated using (4.35), is reduced from around 9.5 kHz to 1.9 kHz.

$$f_{SW} = \frac{f_{S1} + f_{S2} + f_{S3}}{3} \tag{4.35}$$

here f_{SW} represents the averaged switching frequency of the MPUC7-ES1 switches. f_{S1}, f_{S2}, and f_{S3} are the measured average switching frequency of $S1$, $S2$, and $S3$, respectively.

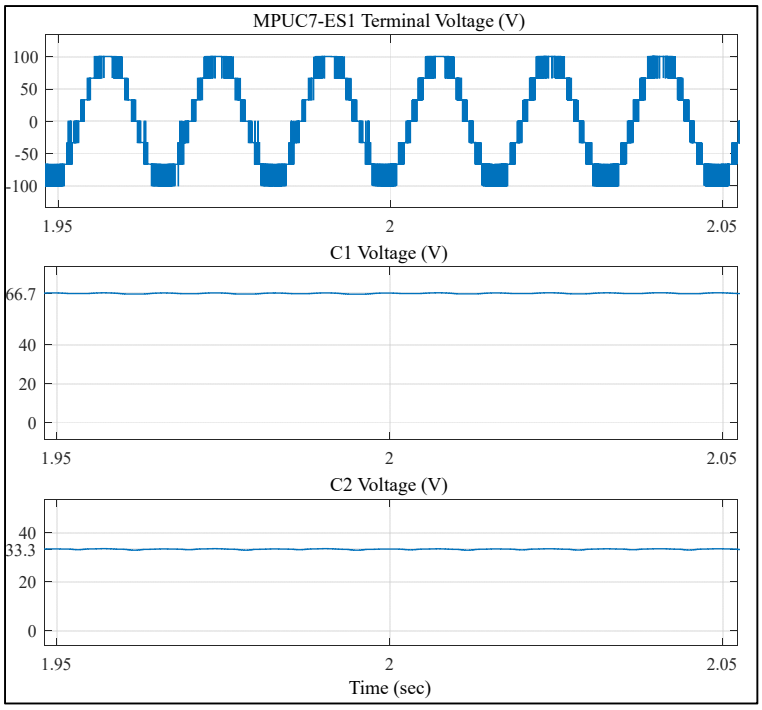

Figure 4.8 MPUC7-ES1 and capacitors' voltages during the lower voltage scenario

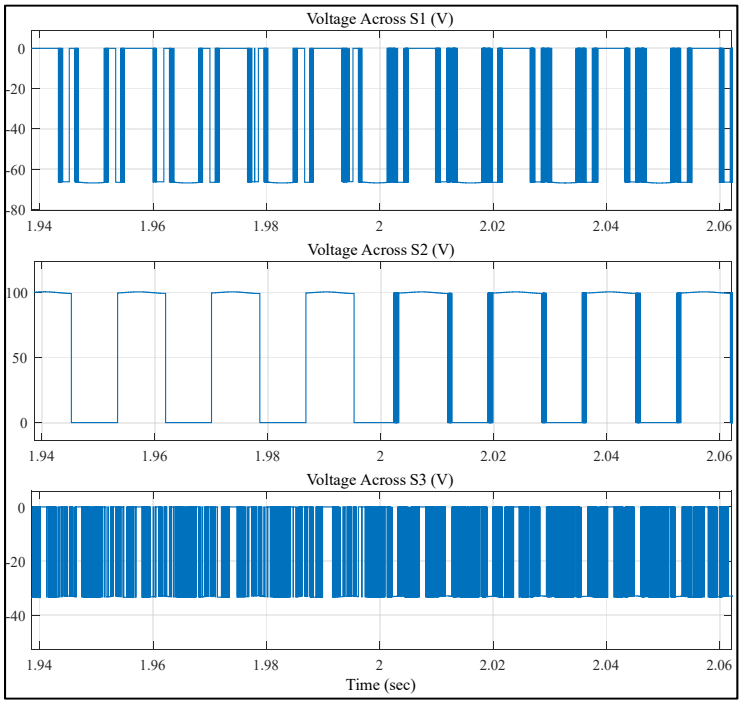

Figure 4.9 The measured voltages across S_1, S_2, and S_3 during the lower voltage scenario

Third, considering power quality performance, to compare these results with a two-level ES1 topology, in this simulated system, MPUC7-ES1 is replaced by a half-bridge ES1 controlled by a PI-based PWM method (C. K. Lee, Chaudhuri, & Hui, 2013). All the system's specifications are selected to be the same as before, except for the switching frequency that is fixed at 20 kHz for the half-bridge ES1 (C. K. Lee, Chaudhuri, & Hui, 2013). Figure 4.10 illustrates the measured parameters of this half-bridge ES1 in the same lower voltage case scenario. As can be seen, this time, instead of a seven-level compensation voltage, a two-level voltage is injected into the system. The auxiliary capacitors and switches of this half-bridge ES1 should also withstand voltages as big as 100 V and 200 V, respectively. Besides, voltage ripples on the capacitors are around 10% that is also increased significantly.

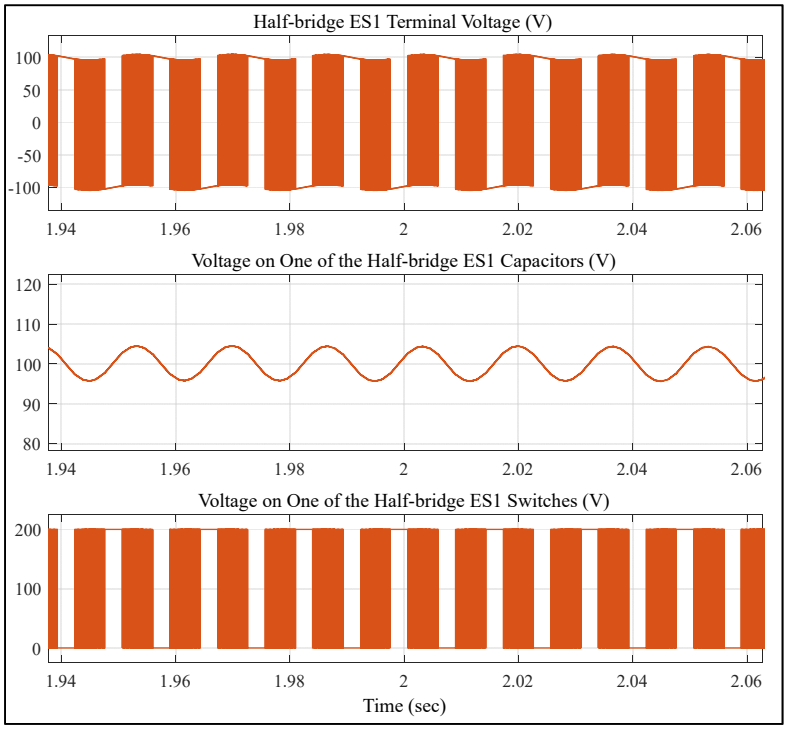

Figure 4.10 Parameters of a simulated half-bridge ES1

Moreover, THD analyzations of the generated seven-level voltage waveform by MPUC7-ES1 with $\gamma_4 = 0.014$ and the two-level voltage by the half-bridge ES1 are presented in Figures 4.11 and 4.12. Measured THD for the MPUC7-ES1 voltage is merely at around 22% for a modulation index of about 0.95. So, in comparison with the two-level ES1 topology and the

five-level MPUC5-based ES1 (Kaymanesh & Chandra, 2020) with the harmonic contents of around 102% and 26%, respectively, the proposed topology has the least THD content of the generated voltage with a reduced switching frequency and voltage stress/ripples on its components.

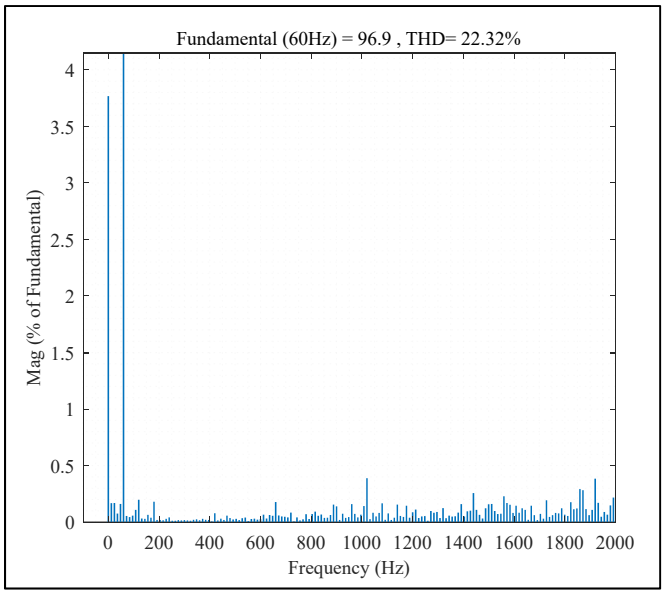

Figure 4.11 THD analysis of the MPUC7-ES1 generated voltage with $\gamma_4 = 0.014$

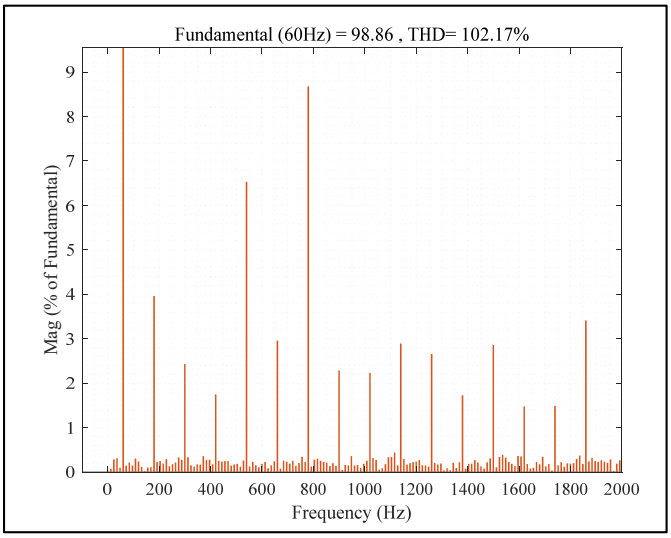

Figure 4.12 THD analysis of the generated voltage waveform by a half-bridge ES1

Fourth, the MPUC7-ES1 performance is evaluated with a conventional linear PI controller (C. K. Lee, Chaudhuri, & Hui, 2013) and the proposed nonlinear FCS-MPCC. The generated voltages and first capacitor voltages, as an instance, during MPUC7-ES1 capacitive operation with the same specifications presented in Table 4.4 have been recorded and presented in Figure 4.13. In addition to the fact that with a PI controller, the proposed topology will be merely operational with a five-level voltage waveform and capacitors' voltages can be regulated only at the same value (Kaymanesh & Chandra, 2020), as can be noted, steady-state tracking errors and voltage ripple (from around 10% to noticeably less than 5%) of the MPUC7-ES1 capacitor are all improved using the proposed FCS-MPCC-based method.

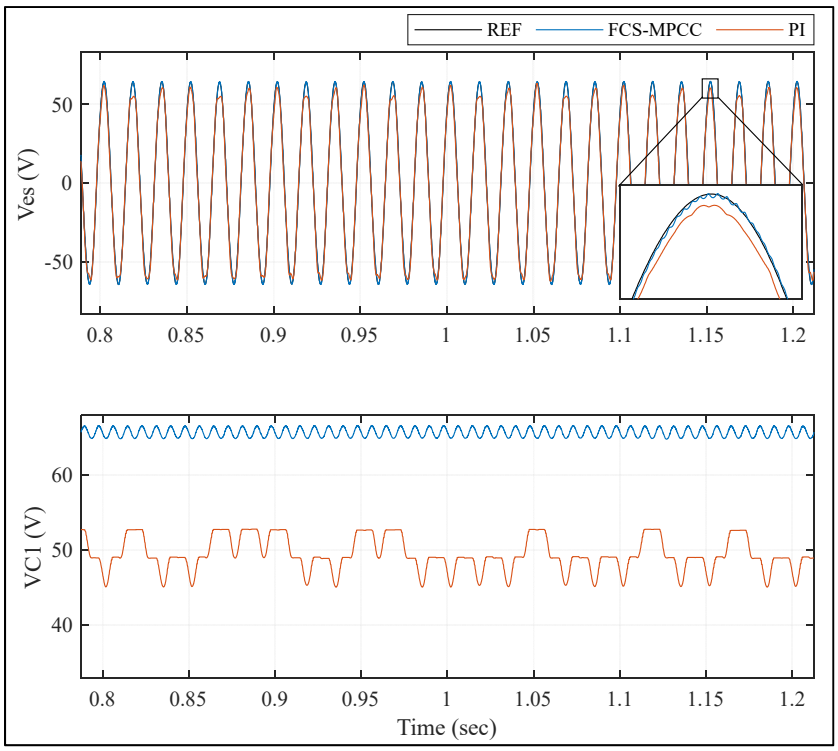

Figure 4.13 Results during MPUC7-ES1 capacitive operation with a linear PI controller and FCS-MPCC

Fifth, the dynamic performance of MPUC7-ES1 and the controller are analyzed. In this regard, when the PCC voltage is less than the nominal value (if MPUC7-ES1 is deactivated), another SL (R_3=80 Ω) is suddenly connected with R_2 at t=3 s with an active MPUC7-ES1. Figure 4.14 illustrates the measurements of the parameters of this system. As illustrated in Figure 4.14,

although the SL current (i_{SL}) is changed instantly from a maximum value of around 3.9 A to 5.8 A due to this transient, MPUC7-ES1 managed to keep the SL voltage stabilized effectively. Moreover, capacitors' voltages are kept regulated adequately.

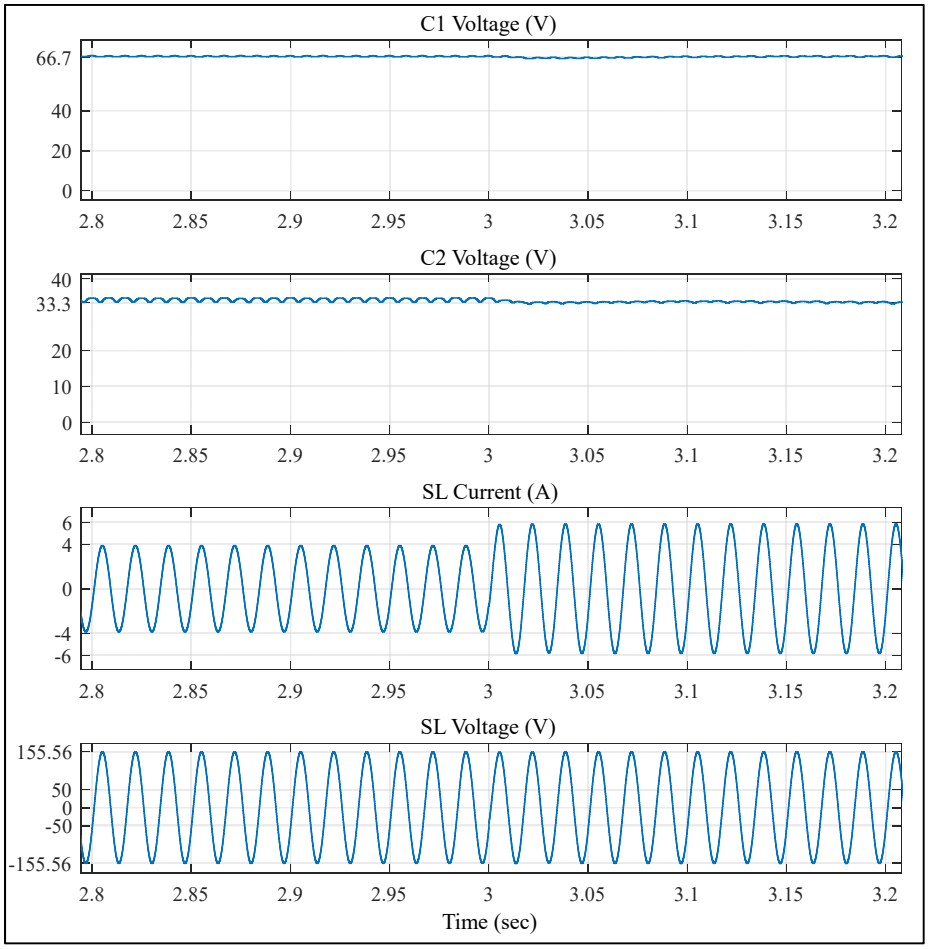

Figure 4.14 Recorded results during transient simulation test

4.6 Experimental Results

To illustrate the operation and viability of the proposed MPUC7-ES1 and the nonlinear current controller, experimental results are also presented. A diagram overview of the implemented real-time experimental setup and its respective laboratory photograph are shown in Figures 4.4 and 4.15, correspondingly. Parameters of this hardware setup are also chosen to be the same as the simulation system presented in Table 4.4. In this experiment, a 28-amp three-phase

variable autotransformer (480V AC input to 0-560V AC output voltage) is acting as a controlled voltage source. Regarding running the designed controller with a fixed sampling time of 35 μs in real-time, MicroLabBox, which is a compact rapid control prototyping (RCP) system, has been utilized. High current/voltage measurements (OP8662), gate drivers, an isolation card, a power analyzer, and an oscilloscope have been also employed. Besides, using FGA30N60LSD IGBT switches, an MPUC7-ES1 prototype is implemented.

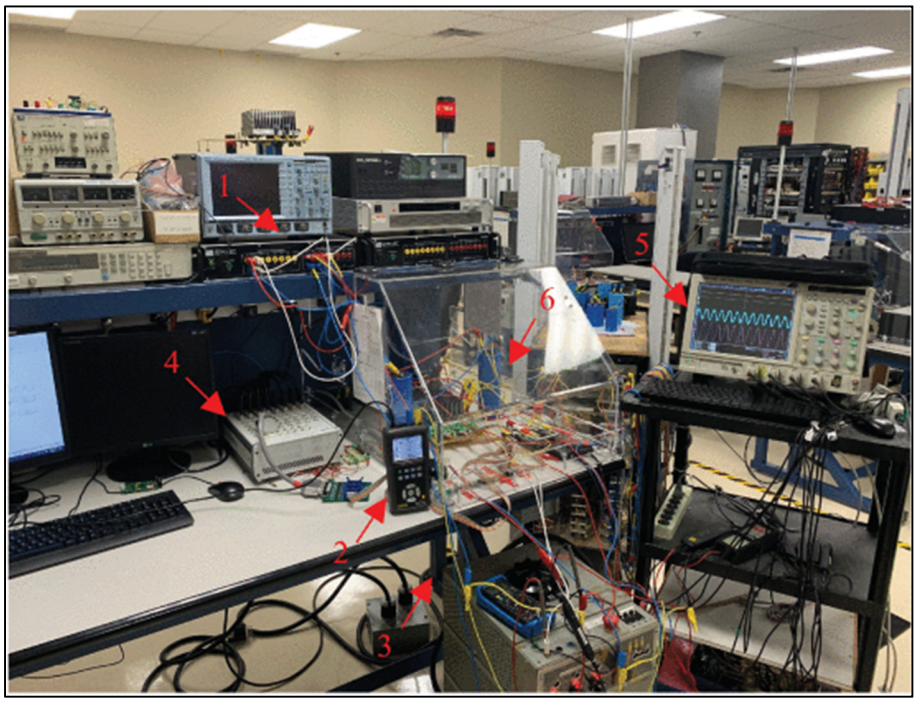

Figure 4.15 Implemented real-time experimental setup:
(1) measurement, (2) power analyzer, (3) autotransformer,
(4) MicroLabBox, (5) oscilloscope, (6) MPUC7-ES1

The main application of the introduced MPUC7-ES1 is to improve the SL voltage stability with an enhanced power quality performance. In this regard, the variable autotransformer is controlled to emulate a low voltage scenario at the PCC with a maximum voltage value of around 139.6 V without the activated MPUC7-ES1. Considering the steady-state operation, measured parameters of this experimental system with an activated MPUC7-ES1, including capacitors' voltages, output terminal voltage, and the SL voltage, are presented in Figure 4.16. As illustrated, through the injected symmetrical seven-level compensation voltage, SL voltage

is regulated at the nominal value (155.56 V). Capacitors' voltages are also tuned effectively with satisfactory voltage ripples (less than 5%).

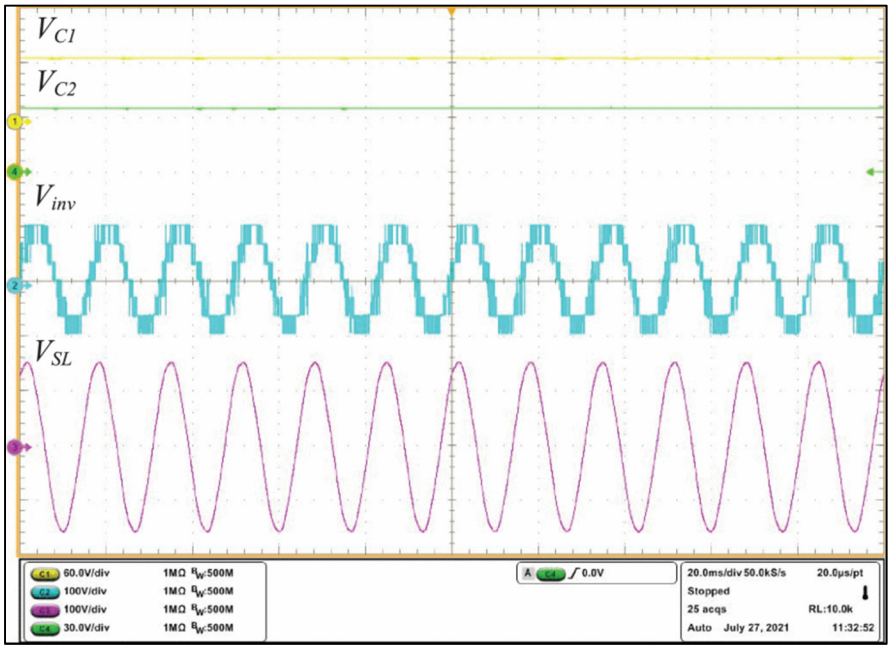

Figure 4.16 Measured parameters of the experimental setup during the steady-state operation

On the other hand, using the power analyzer, harmonic spectrum analysis of the generated seven-level compensation voltage is illustrated in Figure 4.17. The measured signal analyzations of the SL voltage and the MPUC7-ES1 injected voltage are also presented in Figures 4.18 and 4.19, respectively. It is obvious that by the proposed reduced component counts seven-level ES1 topology and controller, the power quality performance of the ES1 is improved tremendously.

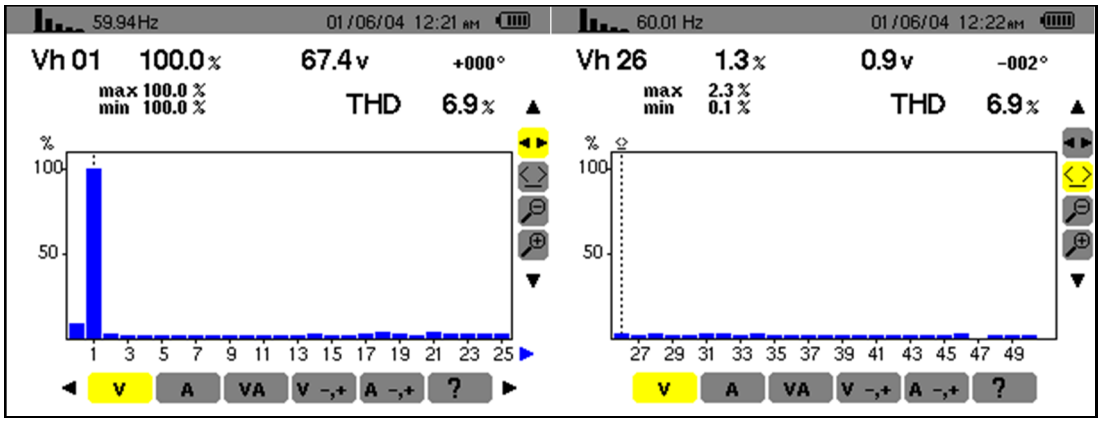

Figure 4.17 Harmonic spectrum analysis of the seven-level voltage

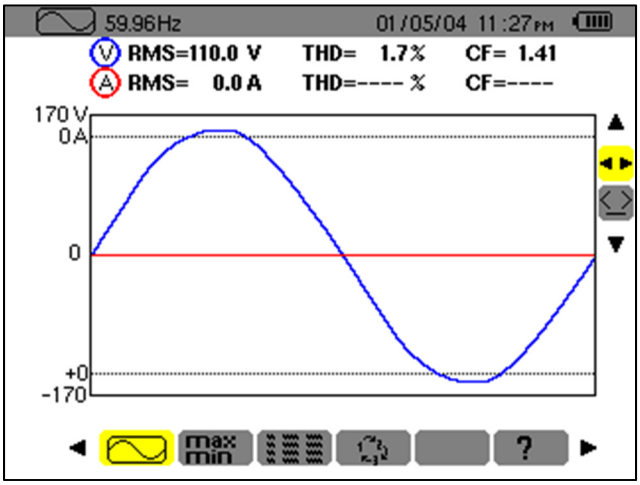

Figure 4.18 SL voltage signal analyzation

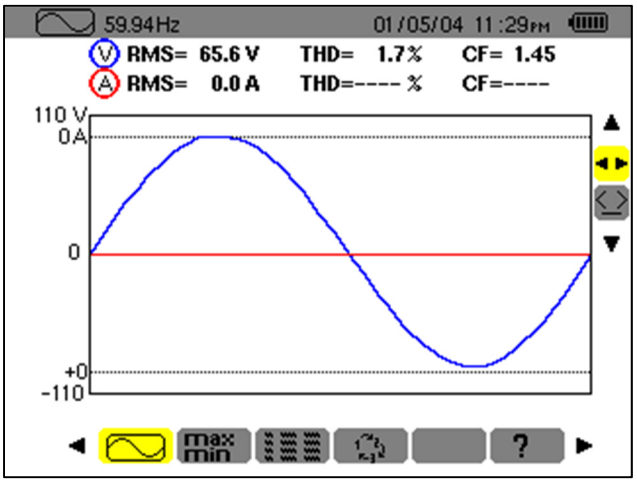

Figure 4.19 MPUC7-ES1 signal analyzation

Considering illustrating the MPUC7-ES1 operation during transients, as an instance, during the inductive operation condition, the total resistance of the SL setup is suddenly changed to around 26.67 Ω by connecting R_3 in parallel with R_2. Figure 4.20 contains the recorded parameters of the experiment during this transient. As is evident, the SL voltage is kept stable effectively. Besides, through the proposed nonlinear controller, MPUC7-ES1 capacitors' voltages remain regulated at their references with an acceptable voltage ripple during this dynamic operation. It is also notable that all the experimental results are in correspondence with the presented simulations and the slight differences are due to the increased sampling time.

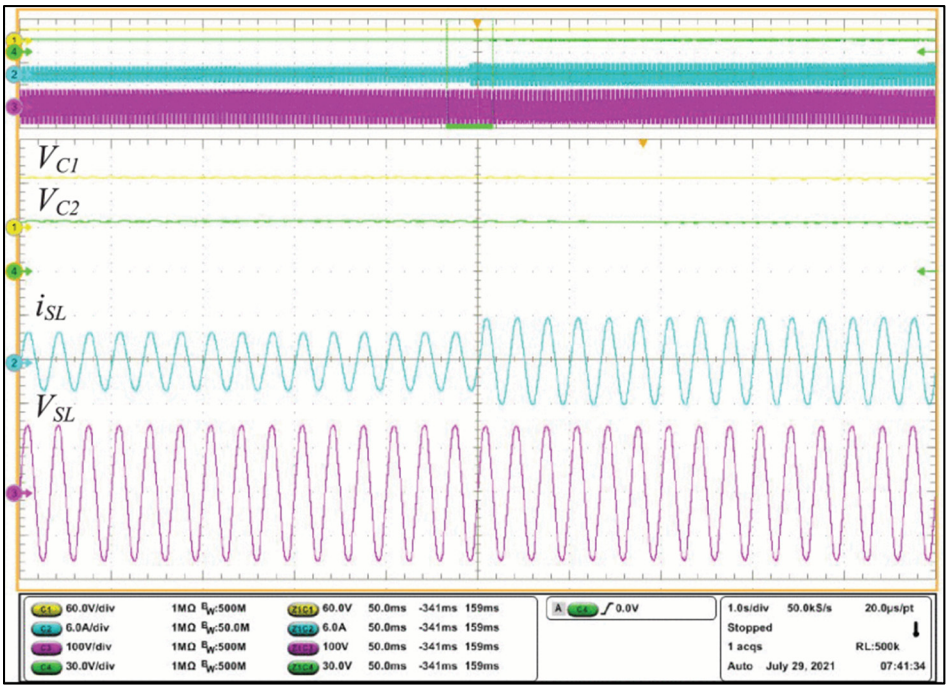

Figure 4.20 Parameters of the experiment during the transient

Finally, to illustrate that MPUC7-ES1 does not require pre-charged capacitors, experimental results of this system during start-up are presented in Figure 4.21. As can be seen, the designed FCS-MPCC managed to keep the system stable effectively until MPUC7-ES1 reaches its operational range.

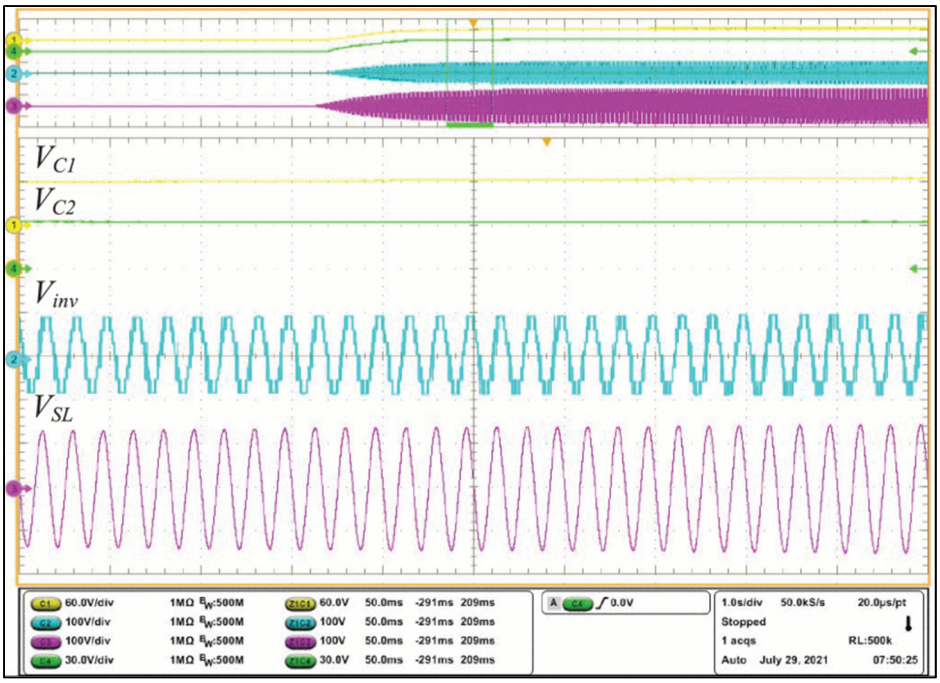

Figure 4.21 Parameters of the experiment during the start-up operation

4.7 Conclusion

High harmonics content of the injected voltage, requiring a bulky harmonic filter, low voltage operation, and increased voltage stress on the components are among the disadvantages of the two-level ES1 topologies. Thus, by introducing a compact seven-level capacitor-based electric spring configuration as a novel distributed reactive power compensator device, power quality operation and reliability of the conventional ES1's topologies are further enhanced. Regarding demerits of the available PI-based PWM ES1 controllers, such as poor transient performance and high steady-state errors, as well as, MPUC7-ES1 requirements, a novel controller founded on the finite control-set model predictive current control is also proposed. This nonlinear control method generates and applies the switching signal directly without requiring any modulation technique. The nonlinearities among the auxiliary capacitors' voltages and the ES1 output current have been considered in the proposed controller for the first time. The switching frequency of the introduced MPUC7-ES1 is also controllable regarding the designer requirements. To support the theoretical framework of the introduced nonlinear controller, extensive mathematical derivations are also presented. Finally, provided simulation and

experimental results illustrate the MPUC7-ES1 and corresponding FCS-MPCC method practicality and superior operation in various modes.

CHAPTER 5

PEC INVERTER FOR INTELLIGENT ELECTRIC SPRING APPLICATIONS USING ANN-BASED CONTROLLER

Amirabbas Kaymanesh [a], Mohammad Babaie [a], Ambrish Chandra [a] and Kamal Al-Haddad [a],

[a] Department of Electrical Engineering, École de Technologie Supérieure,
1100 Notre-Dame West, Montreal, Quebec, Canada H3C 1K3

Paper published in *IEEE Journal of Emerging and Selected Topics in Industrial Electronics*,
July 2021

Abstract

Aiming at delivering power to sensitive loads with an enhanced level of reliability and quality, a compact multilevel battery-based electric spring (ES2) topology founded on the Packed E-Cell (PEC) inverter and an artificial neural network (ANN) based control strategy are introduced. This multilevel ES2 overcomes the limitations of the two-level ES2s and offers key features in the area of electric spring that have not been considered before. From the reliability point of view, the PEC-based ES2 (PEC-ES2) has the capability of instant nine to five-level operation under its bidirectional switch faulty condition. Regarding the power quality, in comparison with the half or full bridge ES2 topologies, PEC-ES2 has switches with halved voltage rating, lower harmonic content in its output current and voltage, considerably lower switching frequency, higher power applications, etc. The proposed intelligent ANN-based controller can also tune and stabilize both the grid voltage and responsive load setup power factor independently with improved dynamic performance. The operation and viability of the proposed ES2 configuration and controller, have been also tested extensively.

5.1 Introduction

The percentage of renewable energies in the electrical grids is increasing dramatically. Due to the stochastic nature of the generated power by these resources, it is imperative to investigate methods for improving the stability, reliability and power quality of the power system. With this regard, recently, through the application of power electronics to demand-side management, electric spring (ES) as a real-time and distributed method has been firstly proposed to mitigate merely voltage fluctuations due to instability of injected power by inverter-based resources (Hui et al., 2012). Through recent advancements, various generations of ES have been proposed for a wide range of smart grid utilizations such as coping with voltage and frequency fluctuations (G. Zhang, Wu, Yu, & Zhang, 2020), (T. Chen, Liu, Lee, & Hui, 2020), reducing required energy storage capacity (Laraki, Kaymanesh, Chandra, Agbossou, & Cardenas, 2019), augmenting the operational flexibility of a microgrid in an islanded mode (Liang, Hou, & Hill, 2019), mitigating harmonics (X. Zhang & Zheng, 2020) and voltage flicker (Sharma et al., 2017), improving power factor (PF) (Mok et al., 2016), etc. Nevertheless, the contribution of all these studies is merely focused on introducing control strategies and different versions of ESs are implemented by a half-bridge/full-bridge inverter.

However, inherent technical limitations of an ES based on these conventional inverters especially for sensitive loads (SLs) in industries are high switching frequency, relatively low efficiency and operational reliability, poor harmonic performance, high dv/dt and voltage stress on components, etc (Omer, Kumar, & Surjan, 2020). To tackle all these technical problems, compact multilevel power inverter topologies suitable for ES applications should be investigated and proposed. Consequently, a reduced switch count five-level single-phase ES based on a modified packed U-cell converter (MPUC5-ES) has been introduced intended for mitigating voltage variations and harmonics (Kaymanesh & Chandra, 2020). Compared to the two-level ESs' topologies, MPUC5-ES is more efficient and has better power quality features. But, it is proposed for a capacitor-based ES (ES1) application (Kaymanesh & Chandra, 2020). Thus, MPUC5-ES can directly compensate only reactive power. Nonetheless, battery-based ES (ES2) uses batteries as its dc source and is capable of direct mitigation of both active and

reactive power mismatches. In this regard, a seven-level high-power-density ES2 based on the modified packed U-cell converter has been also introduced (Kaymanesh, Babaie, Tidjani, et al., 2020). However, it requires two independent dc sources. Hence, it is still required to develop more single-dc-source multilevel ES2s with a reduced number of components.

Due to the expanded industrial applications of multilevel inverters, they have been the focus of a lot of researchers. Nevertheless, among various conventional and recently introduced multilevel voltage source inverters, the Packed E-Cell (PEC) inverter has several major advantages, which make it a suitable option for medium or even low voltage ES2 applications. Requiring merely one independent dc source, reduced number of components, having one dc-link, availability of extra switching states, high reliability concerning its multi-level operation, and noticeable dynamic performance during intensive transients are the main merits of the PEC inverter (Sharifzadeh & Al-Haddad, 2019). PEC inverter configuration has been firstly introduced and vindicated for a standalone mode in (Sharifzadeh & Al-Haddad, 2019). Different linear/nonlinear control techniques have been also proposed for the grid-tied multilevel PEC inverter in the literature (Sebaaly, Sharifzadeh, Kanaan, & Al-Haddad, 2021), (Mehrasa, Sharifzadeh, Babaie, Sebaaly, & Al-Haddad, 2020).

On the other hand, ES2 general control principles have been firstly analyzed in (Tan et al., 2013). Various control strategies such as input current control (Yan, Tan, et al., 2017), δ control (Q. Wang et al., 2015), simple power decoupling (SPD) (Q. Wang et al., 2018) and radial-chordal decomposition (RCD) method (Mok et al., 2016) have been also proposed. Among them, the RCD technique has favorable features like simplicity, direct and autonomous modification of the overall active/reactive power of both ES2 and its associated non-sensitive load (NSL) and multifunctionality (Mok et al., 2016). However, an RCD-based controller requires two conventional linear proportional-integral (PI) control loops to keep both voltage and power factor regulated at their desired amounts. But, utilizing PI control loops for ES2 has critical shortcomings such as poor transient performance with unfavorable under/overshoots and settling time.

Hence, considering both power quality and reliability issues, this paper proposes an artificial neural network (ANN) based control strategy for a compact intelligent multilevel battery-based electric spring founded on the PEC topology (PEC-ES2). Improved harmonic performance and efficiency, noticeable lower switching frequency, the smaller size of the requisite output low-pass filter, and higher voltage and power applications are the general merits of utilizing a multilevel inverter as an electric spring. Nevertheless, compared with the two-level ES2s, the proposed PEC-ES2 and controller have dedicated advantages. First, PEC-ES2 has the capability of five-level operation under faulty bidirectional power switch conditions. Second, PEC-ES2 requires the least possible number of components as a nine-level high power density ES2. Third, switches and capacitors with lower voltage ratings can be employed. Besides, these components withstand lower voltage stress across them. Fourth, adjustment of the PEC-ES2 dc-link voltage does not compel an intricate controller and can be achieved using an active voltage tuning method integrated into the proposed hybrid modulator with only one voltage sensor. Fifth, it has a superior dynamic operation with improved over/undershoots and settling time, especially during start-up. Moreover, the major novelties of this paper have been summarized as follows:

1. This paper presents the design, operating principles and experimental validation of an intelligent PEC-based ES2 concerning the inherent demerits of the two-level ES2 topologies.
2. A multifunctional ES2 controller based on ANN and RCD theory is proposed for concurrent and independent regulation of both SLs voltage and responsive load (RL) power factor with an enhanced transient operation.
3. An extensive comparative study between the proposed PEC-ES2 and the existing ES2s has been performed.

This chapter is organized as follows. In Section 5.2, PEC-ES2 operation principles and design are discussed. PEC-ES2 topology and modulation technique have been explained in Section 5.3. Then, the proposed PEC-ES2 ANN-based control strategy is also detailed in Section 5.4. Furthermore, in Section 5.5, ample simulation results, as well as discussion of the PEC-ES2 in various operation modes, are given. Besides, experimental validation of the PEC-ES2 is achieved in Section 5.6. Finally, in Section 5.7, the conclusions are presented.

5.2 PEC-ES2 Operation Principles and Design

Figure 5.1 illustrates a simplified schematic of a PEC-ES2 mounted in series connection with a non-sensitive load to form a responsive load setup. This setup is in parallel with a sensitive load (SL) and both are connected to a grid with high penetration of renewable energies through a distribution line. First, it should be defined that in this article available loads in an AC grid are categorized into two main classes namely sensitive and non-sensitive loads. SLs are loads that demand reliable and high-quality power such as mining equipment. On the contrary, NSLs can operate effectively even under some extend of voltage variations. As an instance, heat pumps can be categorized as non-sensitive loads. Furthermore, a setup that can modify its demanded active/reactive power concerning the generated power variations instantaneously is known as RL.

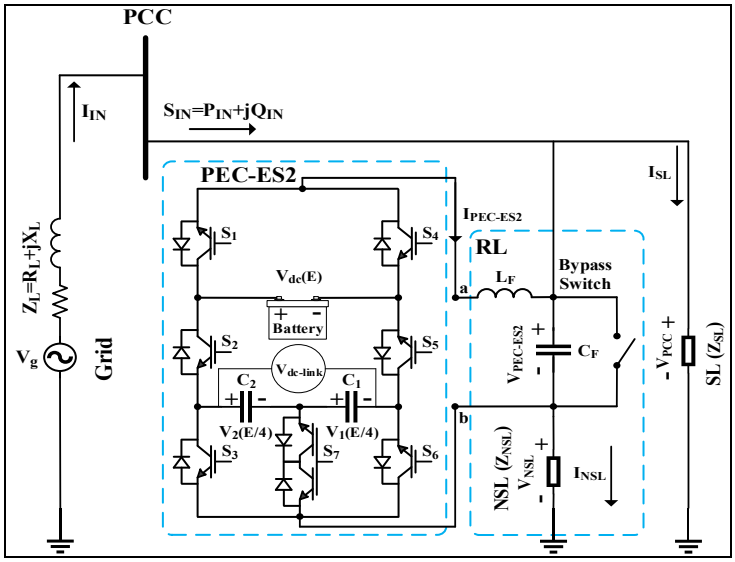

Figure 5.1 PEC-ES2 based responsive load setup

The line voltage of grids with a high percentage of integrated renewable energies fluctuates. Besides, reactive power exchange between the loads and grid should be minimized. Nonetheless, SLs require stabilized voltage and power. So, to explain the basic principles of the PEC-ES2 operation, through producing an up to nine-level AC voltage, PEC-ES2 stabilizes its input voltage (V_{PCC}) by changing its output voltage. As NSL is in series with the PEC-ES2,

its voltage and consequently the RL setup active/reactive power will be modifiable. Thus, RL demanded power can be tuned regarding the availability of renewable energies. So, SL voltage and power will be stabilized and regulated. But, the point of common coupling (PCC) voltage fluctuations will be transmitted to the NSL. The PCC voltage of this system can be calculated as,

$$V_{PCC} = V_{NSL} + V_{PEC-ES2} \tag{5.1}$$

where, V_{PCC}, V_{NSL} and $V_{PEC-ES2}$ define the SL voltage, the NSL voltage, and the PEC-ES2 generated voltage, respectively. Using Kirchhoff's point rule for the input current we have,

$$I_{IN} = I_{NSL} + I_{SL} \tag{5.2}$$

here, I_{IN} is the grid current. Besides, I_{NSL} and I_{SL} are the NSL and SL currents, respectively. Considering (5.1) and (5.2), the input current is calculable as below.

$$I_{IN} = \frac{V_{PCC} - V_{PEC-ES2}}{Z_{NSL}} + \frac{V_{PCC}}{Z_{SL}} \tag{5.3}$$

where, Z_{NSL} and Z_{SL} represent the impedances of the NSL and SL, respectively. Furthermore, employing Kirchhoff's voltage law (KVL) for this closed-loop system we have,

$$V_g = V_{PCC} + Z_L \times I_{IN} \tag{5.4}$$

here, V_g is the grid voltage and Z_L is the line impedance. Via substituting (5.3) into (5.4), PCC voltage can be calculated as,

$$V_{PCC} = \frac{V_g + \frac{Z_L}{Z_{NSL}} \times V_{PEC-ES2}}{1 + \frac{Z_L}{Z_{NSL}} + \frac{Z_L}{Z_{SL}}} \tag{5.5}$$

Finally, regarding (5.3) and (5.5), the input current can be also defined as below (Yan, Tan, et al., 2017).

$$I_{IN} = \left(\frac{\left(\frac{1}{Z_{SL}} + \frac{1}{Z_{NSL}}\right) \times \frac{Z_L}{Z_{NSL}}}{1 + \frac{Z_L}{Z_{NSL}} + \frac{Z_L}{Z_{SL}}} - \frac{1}{Z_{NSL}}\right) \times V_{PEC-ES2} + \left(\frac{\frac{1}{Z_{SL}} + \frac{1}{Z_{NSL}}}{1 + \frac{Z_L}{Z_{NSL}} + \frac{Z_L}{Z_{SL}}}\right) \times V_g \tag{5.6}$$

Based on (5.6), it is demonstrated that for specific amounts of V_g, Z_{SL}, Z_{NSL}, and Z_L by modifying the PEC-ES2 generated voltage ($V_{PEC-ES2}$), I_{IN} can be also adjusted. Thus, the input current (I_{IN}) is compensable. Consequently, employing the PEC-ES2, based on (5.7) and (5.8), both active and reactive power of the considered grid can be compensated.

$$P_{IN} = V_{PCC} \times I_{IN} \times \cos\theta \tag{5.7}$$

$$Q_{IN} = V_{PCC} \times I_{IN} \times \sin\theta \tag{5.8}$$

where, P_{IN}, Q_{IN}, and θ are the input active and reactive powers and phase difference between the SL voltage and input current phase angles. So, the operation principles of the PEC-ES2 for mitigating the SL voltage fluctuations and improving the NSL power factor can be demonstrated theoretically.

To design a PEC-based ES2, the values of the required dc capacitors (C_1, C_2), as well as the components of the output low-pass filter (L_F, C_F), should be calculated. First, concerning the selection of the proper auxiliary capacitors' values, the capacitance value of the dc capacitors is directly proportional to the maximum amount of the PEC-ES2 output current ($I_{MPEC-ES2}$) and their charge/discharge time (Δt) in one cycle and inversely proportional to their acceptable voltage ripple (V_r). Thus, C_1 and C_2 can be calculated as below,

$$C_1 = C_2 = \frac{I_{MPEC-ES2} \times \Delta t}{V_r} \tag{5.9}$$

$$\Delta t = \frac{1}{2 \times F_C} \tag{5.10}$$

where, F_C represents the charging/discharging frequency of C_1 and C_2. Second, regarding calculating PEC-ES2 low-pass filter components' values, (5.11)-(5.13) can be employed (Abarzadeh et al., 2021).

$$L_F = \frac{V_{MPEC-ES2}}{8 \times (n-1) \times \Delta I_{PEC-ES2} \times F_{SW}} \tag{5.11}$$

$$F_{cutoff} = \frac{F_{SW}}{10} \tag{5.12}$$

$$C_F = \frac{1}{\left(2\pi \times F_{cutoff}\right)^2 \times L_F} \tag{5.13}$$

here, $V_{MPEC-ES2}$ and $\Delta I_{PEC-ES2}$ are the maximum value of the PEC-ES2 generated nine-level voltage and its injected current permissible ripple. Besides, n and F_{SW} define the number of the PEC-ES2 voltage levels and its switching frequency. Finally, F_{cutoff} denotes the required low-pass filter cutoff frequency.

5.3 PEC-ES2 Topology and Hybrid Modulator

PEC-ES2 multilevel topology is made up of a battery as its dc source, two capacitors extended in a horizontal manner to constitute its single dc-link, six active switches, and merely one bidirectional switch. PEC-ES2 is tied to the grid through a small-size LC filter. To obtain a nine-level operation, the dc-link voltage should be adjusted to half of the battery voltage and consequently, capacitors' voltages are regulated to one-fourth of the battery voltage. Besides,

by using the PEC-ES2 extra switching states presented in Table 5.1, the voltage/power balance of the capacitors can be achieved conveniently at the same time.

Table 5.1 PEC-ES2 Switching States for Nine-Level Operation

State	S_1	S_2	S_3	S_4	S_5	S_6	S_7	I_{ES2}	V_{ab}	C_1	C_2
1	1	0	0	0	1	1	0	>0	+E	−	−
2	1	0	0	0	1	0	1	>0	+3E/4	↓	−
3	1	0	1	0	1	0	0	>0	+E/2	↓	↓
4	1	1	0	0	0	1	0	>0	+E/2	↑	↑
5	1	1	0	0	0	0	1	>0	+E/4	−	↑
6	0	0	0	1	1	1	0	>0	0	−	−
7	1	1	1	0	0	0	0	>0	0	−	−
8	0	0	0	1	1	0	1	>0	−E/4	↑	−
9	0	1	0	1	0	1	0	>0	−E/2	↓	↓
10	0	0	1	1	1	0	0	>0	−E/2	↑	↑
11	0	1	0	1	0	0	1	>0	−3E/4	−	↓
12	0	1	1	1	0	0	0	>0	−E	−	−
13	1	0	0	0	1	1	0	<0	+E	−	−
14	1	0	0	0	1	0	1	<0	+3E/4	↑	−
15	1	0	1	0	1	0	0	<0	+E/2	↑	↑
16	1	1	0	0	0	1	0	<0	+E/2	↓	↓
17	1	1	0	0	0	0	1	<0	+E/4	−	↓
18	0	0	0	1	1	1	0	<0	0	−	−
19	1	1	1	0	0	0	0	<0	0	−	−
20	0	0	0	1	1	0	1	<0	−E/4	↓	−
21	0	1	0	1	0	1	0	<0	−E/2	↑	↑
22	0	0	1	1	1	0	0	<0	−E/2	↓	↓
23	0	1	0	1	0	0	1	<0	−3E/4	−	↑
24	0	1	1	1	0	0	0	<0	−E	−	−

5.3.1 Comparison with Conventional ES2 topologies

Although in comparison to two-level battery-based electric spring topologies, PEC-ES2 requires more switching components, it has several inherent merits. During the nine-level operation of the PEC-ES2, the THD of the generated voltage waveform is only around 15% that is meaningfully low. Thus, although the switching frequency is low, a reduced size/cost LC filter can be used at its output. Furthermore, the voltage rating of the two upper active switches (S_1, S_4) should be equal to the PEC-ES2 battery nominal voltage. However, they operate at the lowest frequency and switches with a low operating frequency can be employed. Nonetheless, the voltage rating of the remaining active switches (S_2, S_3, S_5, S_6, and S_7) is halved, and are operational at the switching frequency (2 kHz).

If a full-bridge ES2 and the proposed PEC-ES2 are considered to have the same voltage rating switching devices, they would comprise 8 and 9 switches, respectively. However, switches with much lower switching frequency (cheaper switches) can be utilized in the PEC-ES2. Therefore, at the expense of having one more bidirectional switch and two extra capacitors, all the mentioned disadvantages of the full-bridge ES2 configuration will be eliminated. Concerning reliability, PEC-ES2 is capable to continue its operation even after the detection of a fault in its bidirectional switch. Besides, voltage stress and switching frequency of the PEC-ES2 switches are less than the two-level ES2s that results in a lower degradation rate (Nasrin, Khan, & Alam, 2014). Therefore, it also has relatively reliable performance.

Conventional multilevel inverters such as cascaded H-bridge (CHB), flying capacitor (FC) and neutral point clamped (NPC) can be also utilized for ES2 applications. Nonetheless, they require a notably high number of passive/active components which increases the volume and cost of the ES2 and reduces its efficiency. Moreover, as the nonlinearity of these topologies is remarkably high, employing a complex controller will be also inevitable. Employing an increased number of passive/active components in a multilevel ES2 configuration also reduces the reliability of its hardware. Accordingly, a high-density ES2 topology based on a nine-level packed U-cell (PUC9) inverter has been also introduced recently (Kaymanesh, Rezkallah,

Chandra, & El-Bayeh, 2020). But it is not reliable against fault occurrence in any of its switches and requires a relatively complex controller. Finally, Table 5.2 presents the comparison results among nine-level ES2 topologies.

Table 5.2 Comparison among nine-level ES2 topologies

ES2 Type	Battery	Capacitor	Diode	Switch	Controller Complexity
CHB	4	0	0	16	High
NPC	1	8	14	16	High
FC	1	36	0	16	High
PUC9	1	2	0	8	Mid
PEC	1	2	0	7	Low

5.3.2 Fault Detection

Diagnosing switching faults in the bidirectional switch of the proposed PEC-ES2 is of great importance to enable its fault-tolerant performance. The fault detection in the PEC-ES2 bidirectional switch can be simply done via its gate driver by measuring the drain-source voltage (V_{DS}) across S_7. Therefore, for initiating the fault detection procedure integrated into the designed hybrid modulator, the trigger signal is generated based on measured V_{DS} voltage. Concerning other employed switches in the PEC-ES2 topology, after fault detection in any of these switches, PEC-ES2 cannot be reconfigured to continue its operation as a result of reduced switch count.

5.3.3 PEC-ES2 Hybrid Modulation Method

The schematic design of the proposed hybrid modulator for both inverter and converter modes of PEC-ES2 operation can be seen in Figure 5.2. This design is in accordance with integrating PEC-ES2 capacitors' voltage and power modification in the utilized modulator. The proposed design also supports the fault-tolerant operation capability of the PEC-ES2. In the first stage,

for modulating the generated modulation index by the controller in a nine-level operation, eight triangular vertically shifted carriers and comparators have been employed. As indicated in the PEC-ES2 switching states table, there are extra states for the $\pm E/2$ voltage levels. By choosing a suitable state from these redundant states, the voltage/power of the energy storage elements is regulatable. Subsequently, regarding the direction of the PEC-ES2 output current ($I_{PEC-ES2}$) and the magnitude of its dc-link voltage ($V_{dc-link}$) in comparison with half of the battery voltage, suitable states should be selected. Considering the rest of the voltage levels, the number of charge/discharge states for both inverter ($I_{PEC\text{-}ES2}<0$) and converter ($I_{PEC\text{-}ES2}>0$) modes of the PEC-ES2 are equal. In the last stage, the PEC-ES2 competency to operate in a five-level mode during the faulty operation of S_7 is considered. After detecting a fault in S_7, PEC-ES2 resembles a five-level packed U-cell converter and by instant activation of a five-level based modulation method (T_1-T_6) with integrated dc-link voltage regulator (Vahedi et al., 2016), the dc-link voltage will be kept controlled.

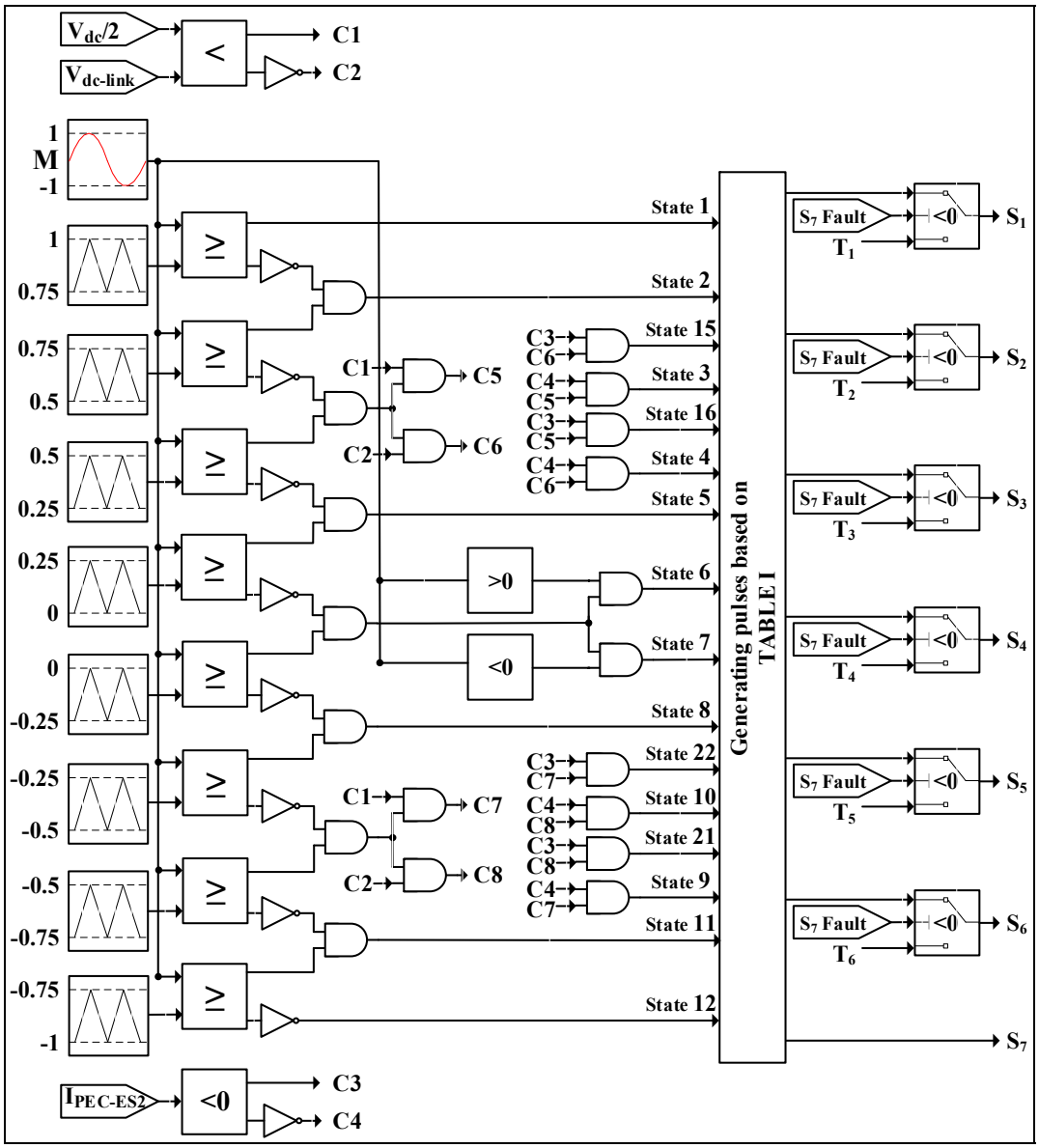

Figure 5.2 Schematic design of the PEC-ES2 modulation technique

5.4 PEC-ES2 ANN-Based Control Method

For catering to the PEC-ES2 multifunctional applications namely stabilizing the sensitive load voltage and improving the responsive load power factor, RCD as a versatile control theory can be employed. This technique is based on controlling the PEC-ES2 voltage and power angle in a decomposed manner. So, modification of the RL active/reactive power concurrently and directly can be achieved. Based on RCD theory, injected multilevel voltage by the PEC-ES2

can be broken down into two main components known as chordal and radial that are responsible for direct modification of the RL power factor and SL voltage, respectively, as below,

$$|V_{PCC}|\angle\theta_{PCC} = |V_{PEC-ES2}|\angle\theta_{PEC-ES2} + |V_{NSL}|\angle\theta_{NSL} \tag{5.14}$$

$$|V_{PEC-ES2}|\angle\theta_{PEC-ES2} = |V_{esc}|\angle\theta_{esc} + |V_{esr}|\angle\theta_{esr} \tag{5.15}$$

here, $|V_{PCC}|$ and $|V_{NSL}|$ denote the magnitudes of SL and NSL voltages. Besides, θ_{PCC} and θ_{NSL} define the SL and NSL voltage phase angles. Also, $|V_{PEC-ES2}|$, $|V_{esc}|$, and $|V_{esr}|$ are magnitudes of the PEC-ES2 voltage and its chordal and radial elements. Moreover, $\theta_{PEC-ES2}$, θ_{esc}, and θ_{esr} represent their respective phase angles. $|V_{esc}|\angle\theta_{esc}$ and $|V_{esr}|\angle\theta_{esr}$ can be also calculated as follows (Mok et al., 2016):

$$V_{esc} = \sqrt{(2 \times |V_{PCC}|^2) \times (1 - cos\,\theta_{NSL})} \tag{5.16}$$

$$\theta_{esc} = -sgn(\theta_{NSL}) \times \frac{\pi - |\theta_{NSL}|}{2} \tag{5.17}$$

$$\theta_{esr} = \begin{cases} \theta_{NSL} & |V_{NSL}| < |V_{PCC}| \\ 0 & |V_{NSL}| = |V_{PCC}| \\ \theta_{NSL} - \pi & |V_{NSL}| > |V_{PCC}| \end{cases} \tag{5.18}$$

$$V_{esr} = \big||V_{NSL}| - |V_{PCC}|\big| \tag{5.19}$$

where, the sign function is demonstrated as sgn. However, in (Mok et al., 2016), PF modification is attained merely in an open-loop manner. To tackle this problem, it would be required to use two autonomous closed-loop PI controllers for stabilizing the PCC voltage and the amount of PF to their desired values. Nonetheless, poor transient performance and low robustness are demerits of utilizing multiple PI controllers.

On the other hand, artificial neural network as an emerging technology has fully proven its effective contribution to solving power system problems such as controlling power converters, fault detection, modeling, estimation and forecasting (Bose, 2007). Multilayer Perceptron (MLP) known as feedforward topology has become the most used ANN in power electronics-based designs due to simple structure, flexibility to extend inputs/outputs and robustness in dealing with unexpected circumstances. Thus, in this paper, MLP is also considered to design an RCD-based model-free but robust control loop for the proposed PEC-ES2. The designed MLP Controller (MLPC) receives tracking errors of V_{PCC} ($e_{V_{pcc}}$) and the RL power angle ($e_{\phi RL}$) besides the root mean square value of V_{PCC} as inputs then generates desired amplitude of the PEC-ES2 voltage as well as its phase angle to stabilize the SL voltage and improve the responsive load PF. Figure 5.3 shows the MLPC structure including input, hidden and output layers. Regarding the control problem, 22 neurons are considered to configure the hidden and output layers. Accordingly, 100 weighting factors and 22 biases are defined among the perceptron neurons to propagate the input signals across the neural network. As (5.20) presents, the activation functions ($f_h(\psi)$) in the hidden layer are sigmoid while output neurons use linear functions for simplification.

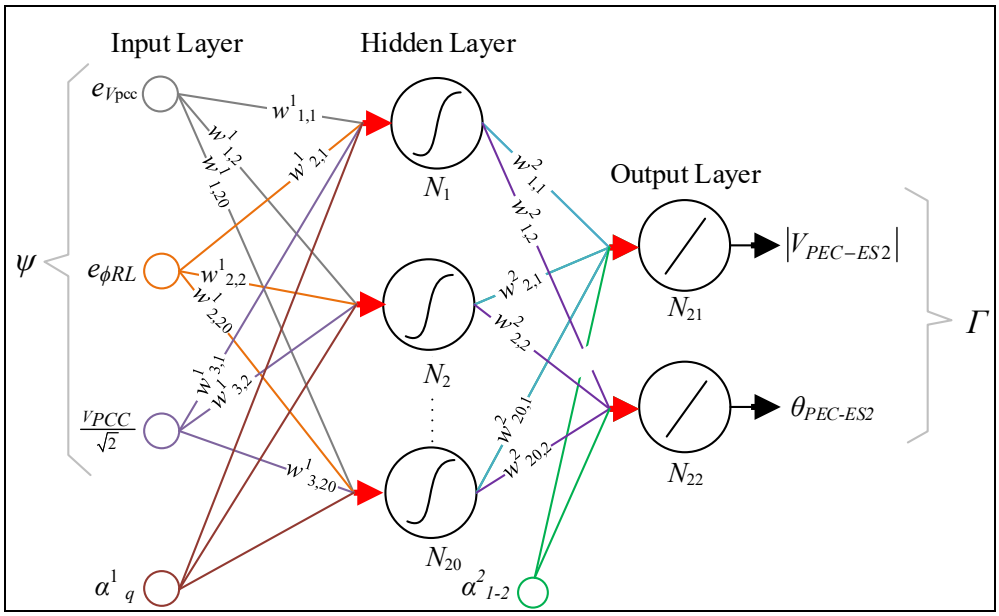

Figure 5.3 Neural network configuration for the proposed MLPC

$$f_h(\psi) = \frac{1}{1 + e^{-\psi}} \tag{5.20}$$

where, ψ is the input vector of the neural network. Since the weighting factors and biases placed among the neurons determine the neural network behavior, they must be properly trained to attain the desired performance expected from MLPC. In this regard, Levenberg-Marquardt (LM) as an effective supervised training strategy is considered to train the MLPC network using training data obtained from the PI-based technique discussed in (Rubio, 2021). LM is a classical optimization algorithm that benefits from the advantages of both Gradient descent and Newton-Gauss techniques to train ANNs with high accuracy in minimum time (Rubio, 2021). As the first step, the mean squared error (ξ) is formalized as (5.21) to measure the training errors between the reference data and MLPC outputs.

$$\xi(y^*, \Gamma) = \frac{1}{Z}\sum_{z=1}^{Z}\left(y^*(z) - \Gamma f_h((\psi), z)\right)^2 \tag{5.21}$$

here, y^*, Z and Γ are respectively, the desired output data obtained from the reference controller, the total number of samples and the MLPC output vector. The mathematical model of the MLPC network shown by Figure 5.3 is obtained as (5.22).

$$\Gamma(\psi) = \begin{bmatrix} \sum_{n=1}^{N}\left(\sum_{q=1}^{Q-2}\sum_{m=1}^{M} f_{h_q}\left(\psi(m)\right)w_{m,q}^{1} + \alpha_q^1\right)w_{1,n}^{2} + \alpha_{Q-1}^{2} \\ \sum_{n=1}^{N}\left(\sum_{q=1}^{Q-2}\sum_{m=1}^{M} f_{h_q}\left(\psi(m)\right)w_{m,q}^{1} + \alpha_q^1\right)w_{2,n}^{2} + \alpha_{Q}^{2} \end{bmatrix} \tag{5.22}$$

where, f_{h_q} is the activation function for q_{th} neuron, $w_{m,q}^{1}$ is q_{th} weighting factor from m_{th} input to q_{th} neuron in the hidden layer and α_q^1 is the bias value for q_{th} neuron in the hidden layer. Besides, $w_{1,n}^{2}$ and $w_{2,n}^{2}$ are respectively n_{th} weighting factor from neurons in the hidden layer

to the first and the second neurons used in the output layer. Finally, α_{Q-1}^{2} and α_{Q}^{2} are biases for the output neurons.

The supervised LM-based training loop is depicted in Figure 5.4. As shown, training data are sampled from the conventional RCD control loop then applied to the neural network and the LM algorithm to train the weighting factors and biases. The training algorithm is initialized by values presented in Table 4.3. It is worth noting that μ in Table 4.3 is used to adjust the convergence rate of the LM optimization algorithm. After 1000 iteration, satisfactory results are obtained; the regression analyses presented in Figure 5.5 for training, validation and test data show that MLPC is properly trained so that the regression index is almost unity.

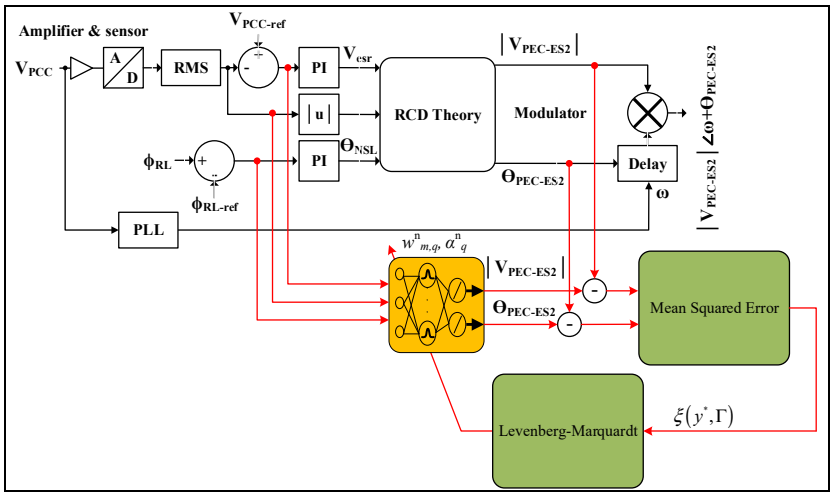

Figure 5.4 MLPC training loop including the RCD

Table 5.3 Initializing the parameters of the LM-based training loop

No. of Iteration	No. of weights	No. of Biases	μ	$w^{n}_{m,q}$	α^{n}_{q}
1000	100	22	0.001	[-50 50]	[-50 150]

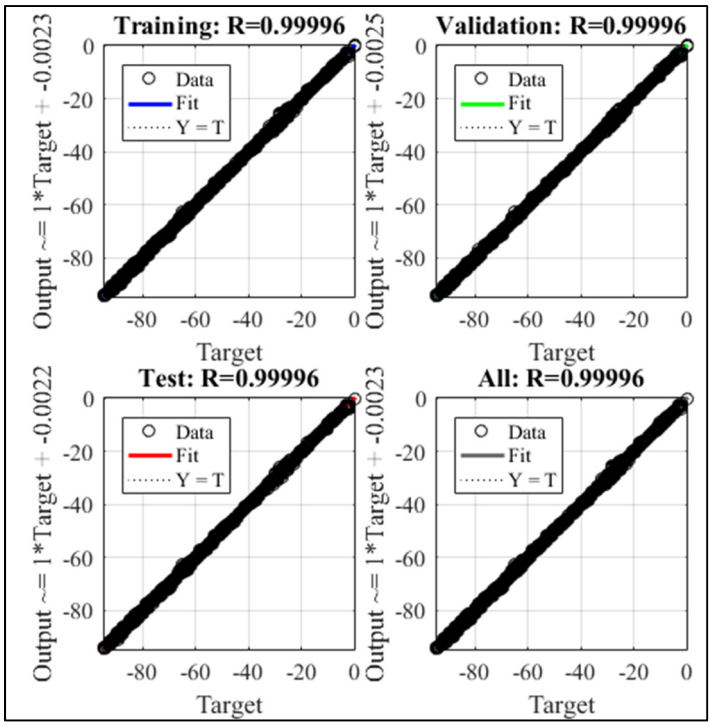

Figure 5.5 Regression analysis for training

An overview of the MLPC control performance in the form of a 3D surface is given in Figure 5.6. This surface demonstrates the variation effects of the errors on the absolute value of the reference voltage generated by MLPC. Since training reports verify MLPC, the training loop and the conventional controller are removed which results in the intelligent control technique depicted in Figure 5.7.

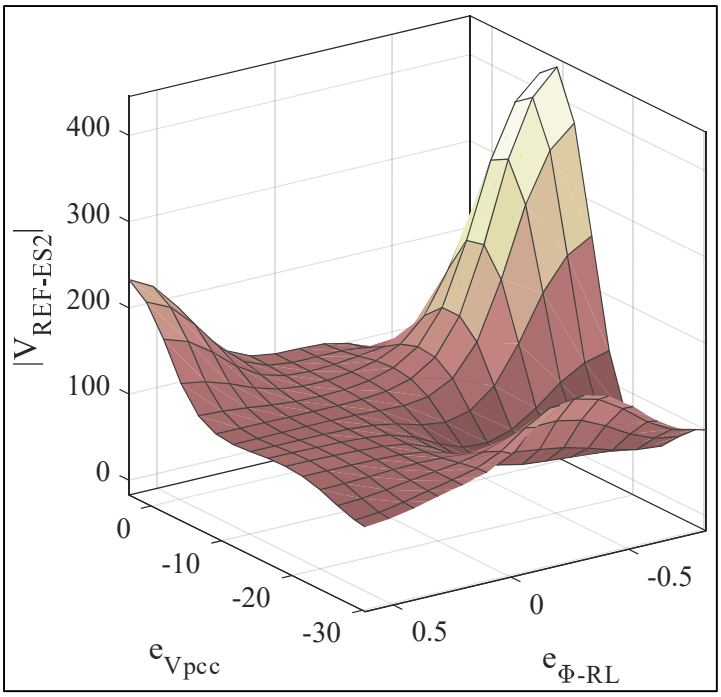

Figure 5.6 Nonlinear behavior of MLPC
regarding the variations of $|V_{REF-ES2}|$, e_{Vpcc} and $e_{\phi-RL}$

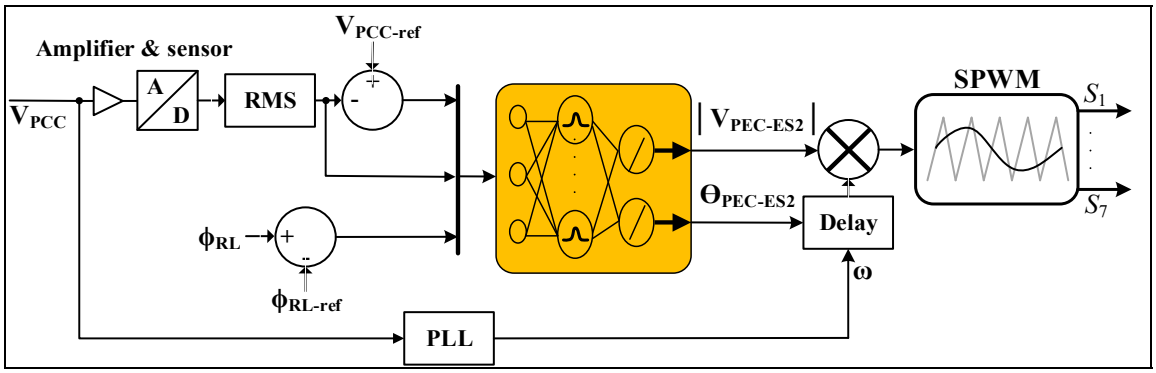

Figure 5.7 Diagram of the proposed ANN based controller for PEC9-ES2

5.5 Extensive Simulation Results

To illustrate the proposed PEC-ES2 and controller performance, this section is divided into five parts. First, the steady-state performance of the PEC-ES2 has been examined. Second, PEC-ES2 reliability has been demonstrated. Third, an analysis of the PEC-ES2 dynamic operation is achieved. Fourth, to justify the superiorities of the PEC-ES2 topology over a two-

level ES2, a comparative study has been presented. Finally, a comparison between the PI-based RCD method and the proposed ANN-based controller regarding their transient performance during PEC-ES2 start-up is presented. The scheme of the simulated system is depicted in Figure 5.8. The simulated system specifications and solar arrays' parameters are also presented in Tables 5.4 and 5.5, respectively. As depicted in Figure 5.8, to harvest energy from different PV panels in this system, a modified seven-level packed u-cell (MPUC7) boost inverter has been utilized (Vahedi, Sharifzadeh, et al., 2018). These solar arrays are connected to the MPUC7 dc-ac inverter by two boost dc-dc converters. To inject the maximum power into the system, two separate maximum power point tracking (MPPT) techniques based on Perturb and Observe (P&O) have been employed to control both of these boost converters independently (Mastromauro, Liserre, & Dell'Aquila, 2012). To have a maximum voltage value of 180 V at the MPUC7 inverter output, its first and second dc bus voltages should be modified at 120 V and 60 V, respectively. Fluctuations in the MPUC7 generated power will cause instabilities in the voltage/power of the sensitive load. On the other hand, for simplicity, the operation of the PEC-ES2 battery is regarded to be ideal with superlative characteristics and its physical limitations including state of charge (SoC) or state of health (SoH) are not considered.

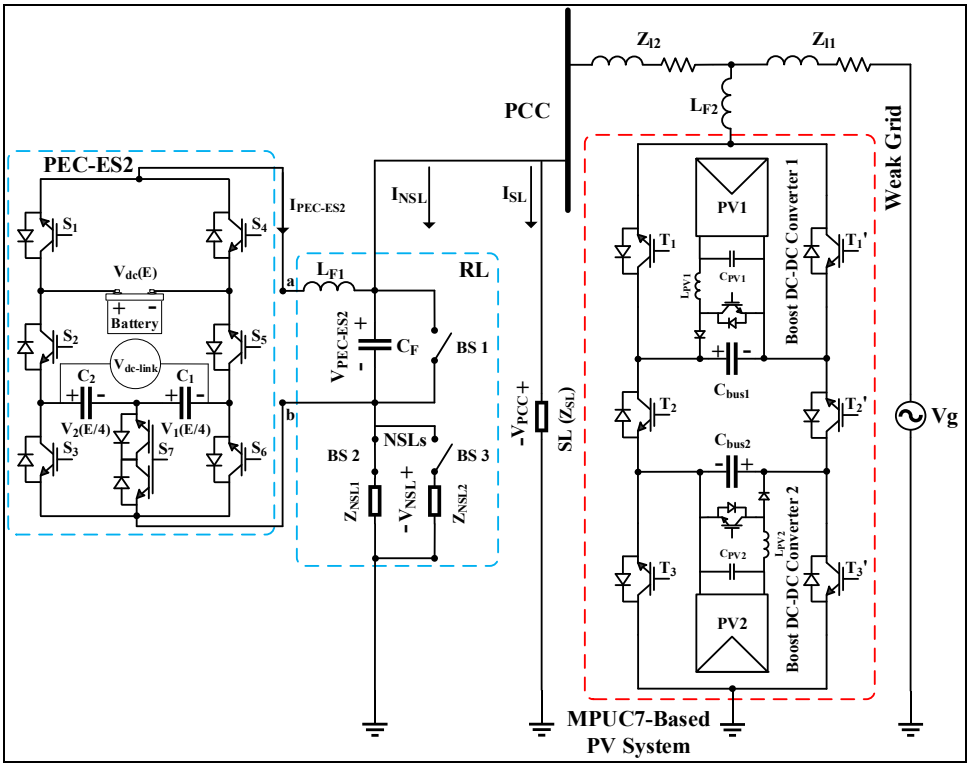

Figure 5.8 Scheme of the designed simulation test system

Table 5.4 Simulated grid's specifications

Grid Voltage (V_g)	110 V rms
Grid and PEC-ES2 Switching Frequencies	60 Hz, 2 kHz
Inductance of the PEC-ES2 LC Filter (L_{F1})	500 µH
Capacitance of the PEC-ES2 LC Filter (C_F)	20 µF
PEC-ES2 Battery Voltage (V_{dc})	200 V
PEC-ES2 Auxiliary Capacitors (C_1, C_2)	2500 µF
First Line Impedance (Z_{l1})	1+j3.13 Ω
Second Line Impedance (Z_{L2})	0.1+j0.37 Ω
NSL1 Impedance (Z_{NSL1})	15+j12 Ω
NSL2 Impedance (Z_{NSL2})	15+j8 Ω
SL Impedance (Z_{SL})	20 Ω

Table 5.5 Solar arrays' parameters

MPUC7 First and Second DC Bus Voltages	120, 60 V
PV1: APOS Energy AP130	2 Series Panel
PV1 Voltage at Maximum Power	2*28.5=57 V
PV2: aleo solar S18.240	1 Panel
PV2 Voltage at Maximum Power	30.1 V
Boost Converter Inductors (L_{PV1}, L_{PV2})	0.8 mH
Output Inductor of the MPUC7 (L_{F2})	2.5 mH
Boost Converter Switching Frequency	5 kHz
MPUC7 Switching Frequency	2 kHz
MPUC7 DC Capacitors (C_{bus1}, C_{bus2})	2500 μF

5.5.1 PEC-ES2 Operation in Steady-State Conditions

In this part, steady-state operation of the PEC-ES2 with an inductive non-sensitive load (Z_{NSL1}), which has a PF of around 0.78 ($\cos(\tan^{-1} X_{NSL1}/R_{NSL1})$), have been investigated. In the simulated system, variations of the harvested power from the MPUC7 inverter destabilizes the sensitive load voltage and power. Nevertheless, Figure 5.9 depicts the results of the grid during the availability of a surplus amount of the PV power with the activated PEC-ES2. As seen, the dc-link voltage is tuned at half of the battery voltage (100 V) and the produced nine-level voltage waveform is acceptable. Thus, through the nine-level generated voltage of the PEC-ES2, SL voltage fluctuations are transmitted to the NSL effectively. Therefore, the SL voltage and power have been stabilized at their nominal values at around 155.6 V (110 V rms) and 605 W ($P_{SL} = V_{SL}^2/R_{SL}$), correspondingly. Besides, the RL setup PF has been also improved to around 0.91. Concerning the defined reference value of the RL power angle (ϕ_{RL-ref}) in the controller, the power factor of the RL can be also modified on any other desired values. Moreover, as can be noted, during one period of the generated nine-level voltage, PEC-ES2 capacitors' currents can be both negative and positive that shows the auxiliary capacitors' energies are being controlled to be tuned at their desired voltages. It should be indicated that for the $\pm E/2$ voltage levels, they are charged and discharged with switching frequency.

However, for the remaining voltage levels, the charging/discharging states of the capacitors are dependent on the generated voltage frequency. This is in accordance with the designed hybrid modulator with integrated capacitors' voltages regulator and switching states presented in Table 5.1.

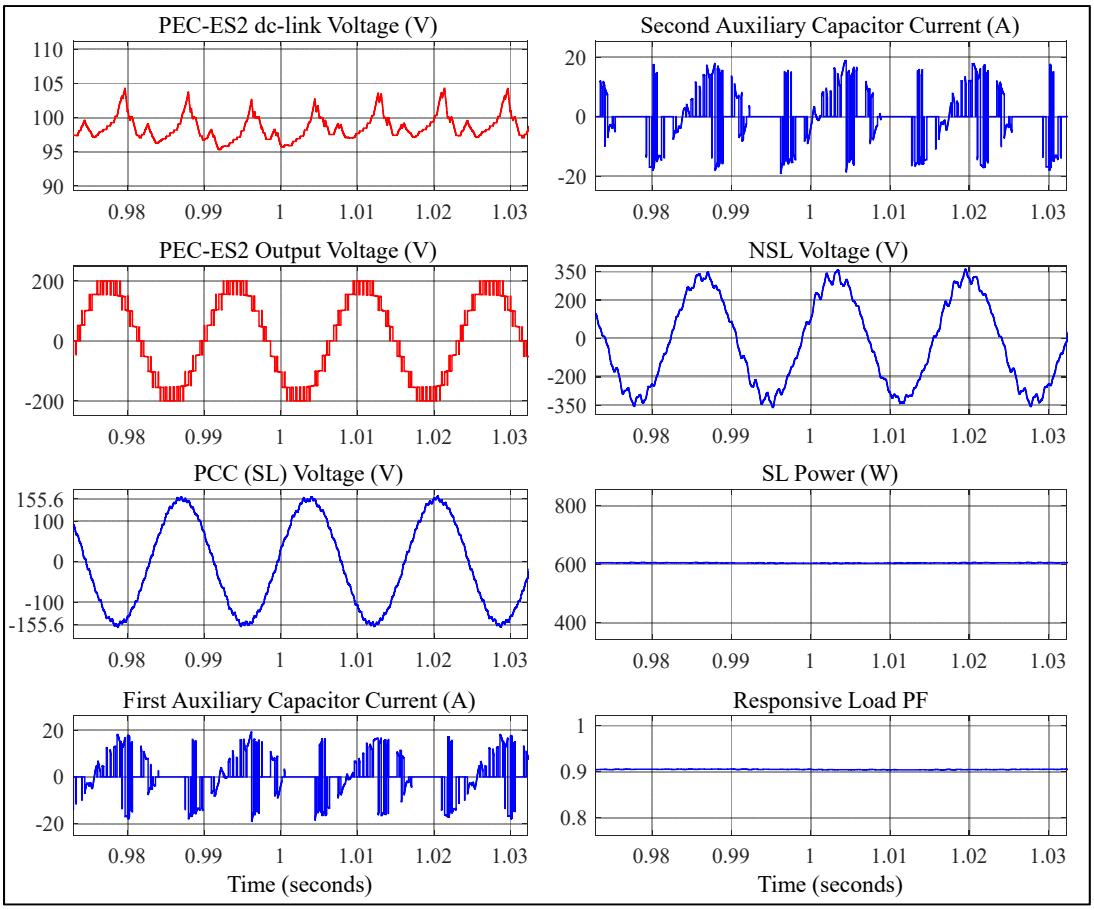

Figure 5.9 Steady-state results of the simulated system

5.5.2 Fault in Switch

The aim is to validate the reliability of the PEC-ES2 in the condition that a fault is detected in S_7. To achieve this, during the previous case, S_7 is suddenly disconnected that emulates its failure. As Figure 5.10 illustrates, after fault detection in S_7 at t=1.5 s, while the dc-link voltage is kept constant (100 V), the PEC-ES2 voltage waveform has transferred from nine-level to five-level operation mode instantaneously without any noticeable transient. Besides, the

control method of the capacitors' energies is changed after the fault which is due to the instant initiation of the post-fault performance approach integrated into the designed hybrid modulator.

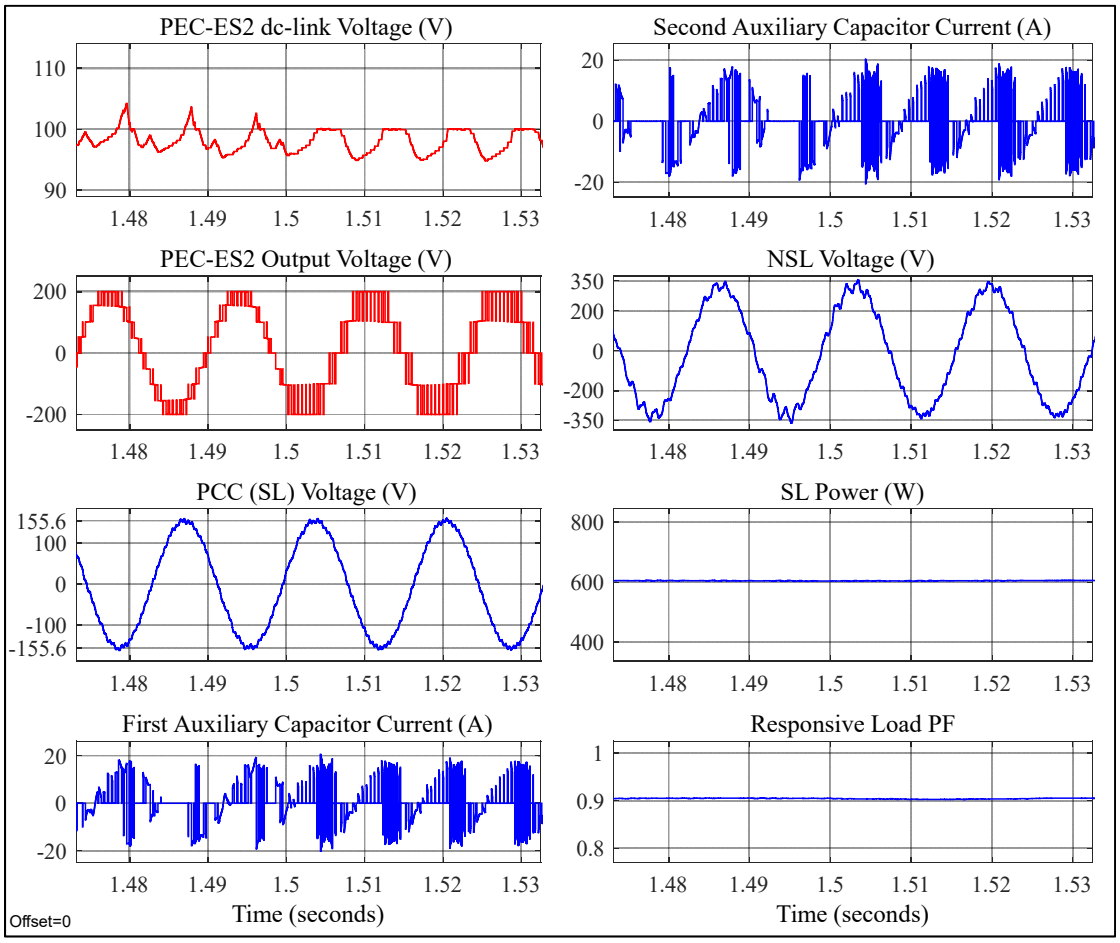

Figure 5.10 Results of the simulated grid during S_7 failure

5.5.3 PEC-ES2 Operation in a Dynamic Condition

To validate the dynamic operation of the PEC-ES2, it is tested during a sudden variation in the NSL impedance and PF. Figure 5.11 presents the measured results during a sudden change in the impedance of the NSL from Z_{NSL1} with PF of around 0.78 to Z_{NSL2} with PF of about 0.88 at t=2 s. As illustrated, by modifying the injected voltage of the PEC-ES2 from the nine-level to seven-level waveform, not only, PF of the RL is kept stabilized at the desired value (0.91)

but also the SL (PCC) voltage and power are fixed at their nominal amounts efficiently. Concerning capacitors' currents, it is clear that the charge and discharge times of both capacitors have been modified instantly to keep their voltage and power balanced.

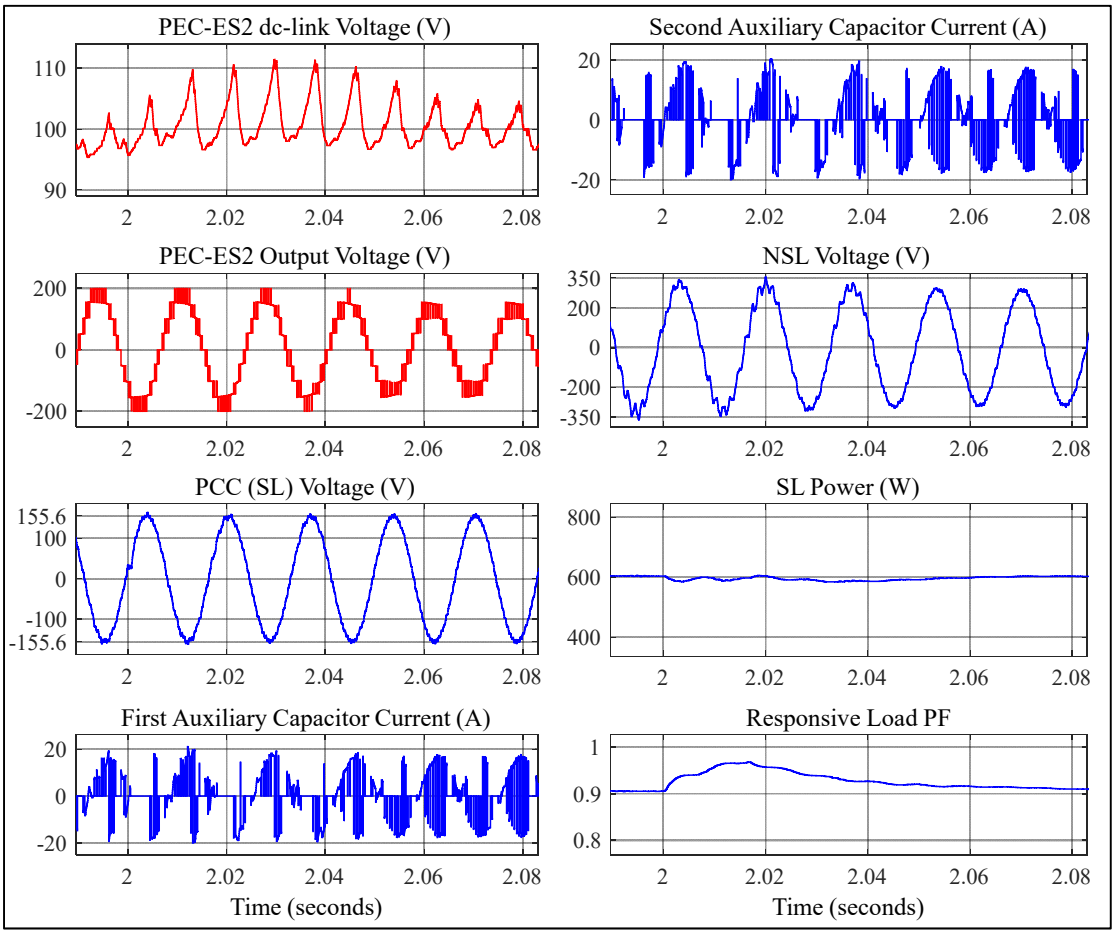

Figure 5.11 Results during a sudden change in the impedance of the NSL

5.5.4 Comparison Between the PEC-ES2 and a Two-level ES2

Two-level ES2 topology, employed in (T. Chen et al., 2020), is used in this section. PEC-ES2 and the two-level ES2 have been utilized in the simulated system with the proposed control technique and same parameters. The only differences are the switching frequency and battery voltage of the two-level ES2 that are 16 kHz and 400 V, respectively (T. Chen et al., 2020). First, generated voltages of the PEC-ES2 and the half-bridge ES2, as well as voltages on their capacitors during steady-state simulation scenario of availability of the extra amount of the

generated power, are presented in Figure 5.12. Moreover, THD analyses of the produced voltages are presented in Figures 5.13 and 5.14. As is clear, due to the nine-level operation of the PEC-ES2 in comparison to the two-level performance of the half-bridge ES2, THD of the generated voltage is improved from around 113% to roughly 15%. Moreover, the voltage on the capacitors is reduced from 200 V in the two-level ES2 to around 50 V in the PEC-ES2.

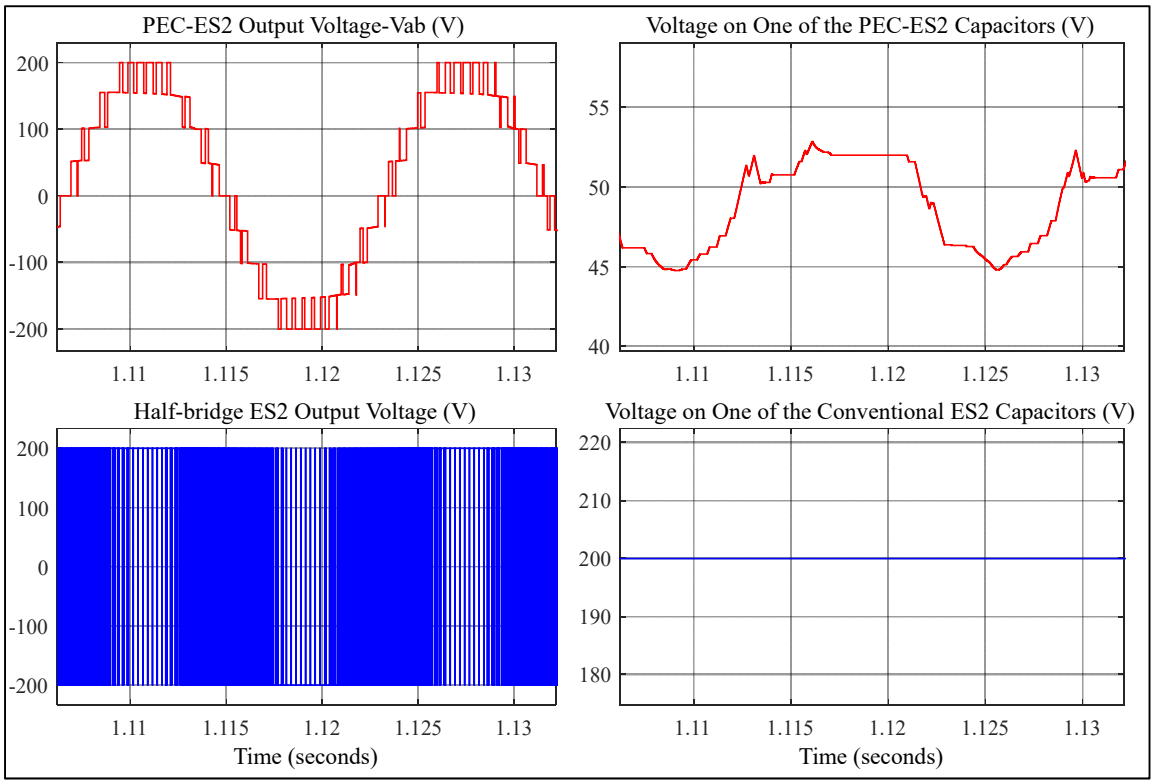

Figure 5.12 Generated voltage by PEC-ES2 and half-bridge ES2 and voltages on their auxiliary capacitors

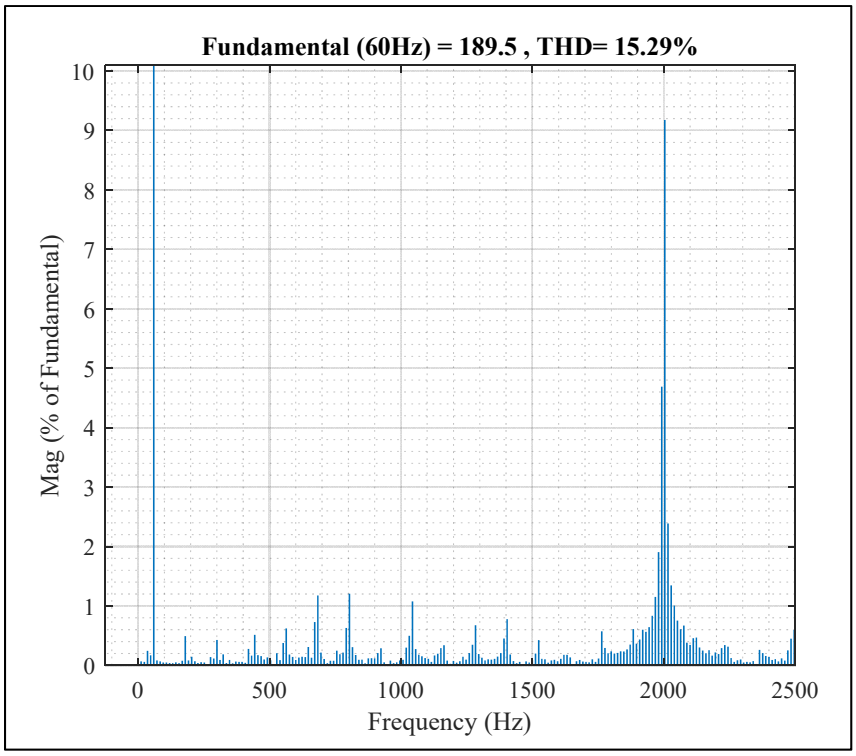

Figure 5.13 Harmonic analysis of the PEC-ES2 voltage

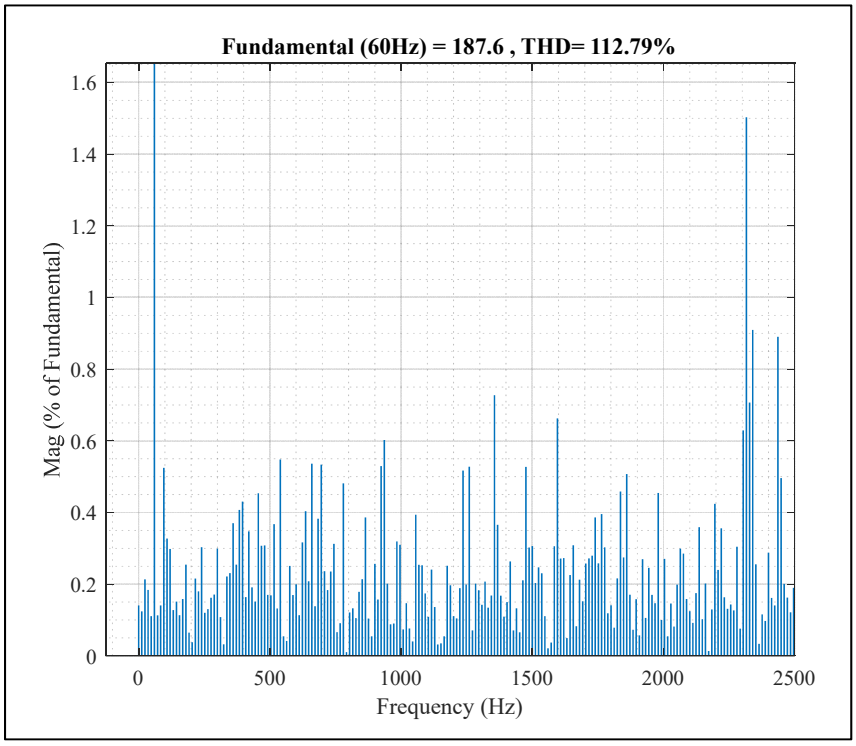

Figure 5.14 Harmonic analysis of the half-bridge ES2 voltage

On the other hand, to show lower switching frequency and voltage rating of the switches of the PEC-ES2, Figure 5.15 depicts voltages on S_1, S_2, S_7 and one of the half-bridge-based ES2 switches throughout the previous test. As seen, S_1, which has the same voltage rating as S_4, withstands a voltage as big as half of the conventional ES2 switches. And, rest of the PEC-ES2 switches have a voltage rating equals to only one-fourth of the two-level ES2 switches. The lower switching frequency of the PEC-ES2 switches, which is on average around 2 kHz, in comparison with two-level ES2 switches (16 kHz) is also noticeable.

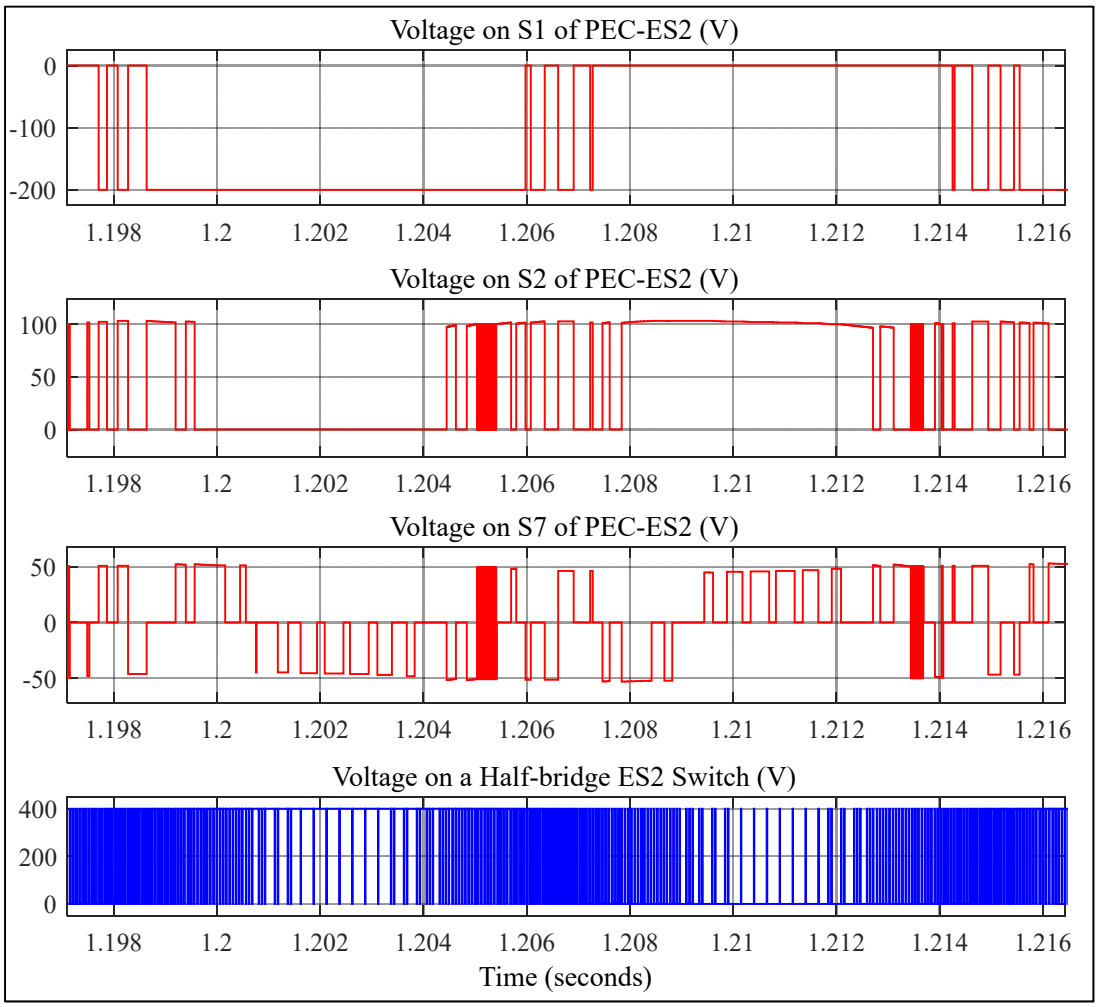

Figure 5.15 Measured voltages on the PEC-ES2 and half-bridge ES2 switches

5.5.5 Comparison Between the PI and ANN-Based Controllers

Figure 5.16 presents the comparison results of the measured parameters of the system during PEC-ES2 start-up when it is controlled by a PI-based method and the proposed intelligent controller. Based on the recorded measurements, utilizing the proposed ANN-based controller notably improves undershoots, overshoots and settling times of the PEC-ES2 dc-link voltage, SL power and responsive load PF during start-up transient. This proves the superior dynamic operation and sturdiness of the introduced control strategy for PEC-ES2 applications.

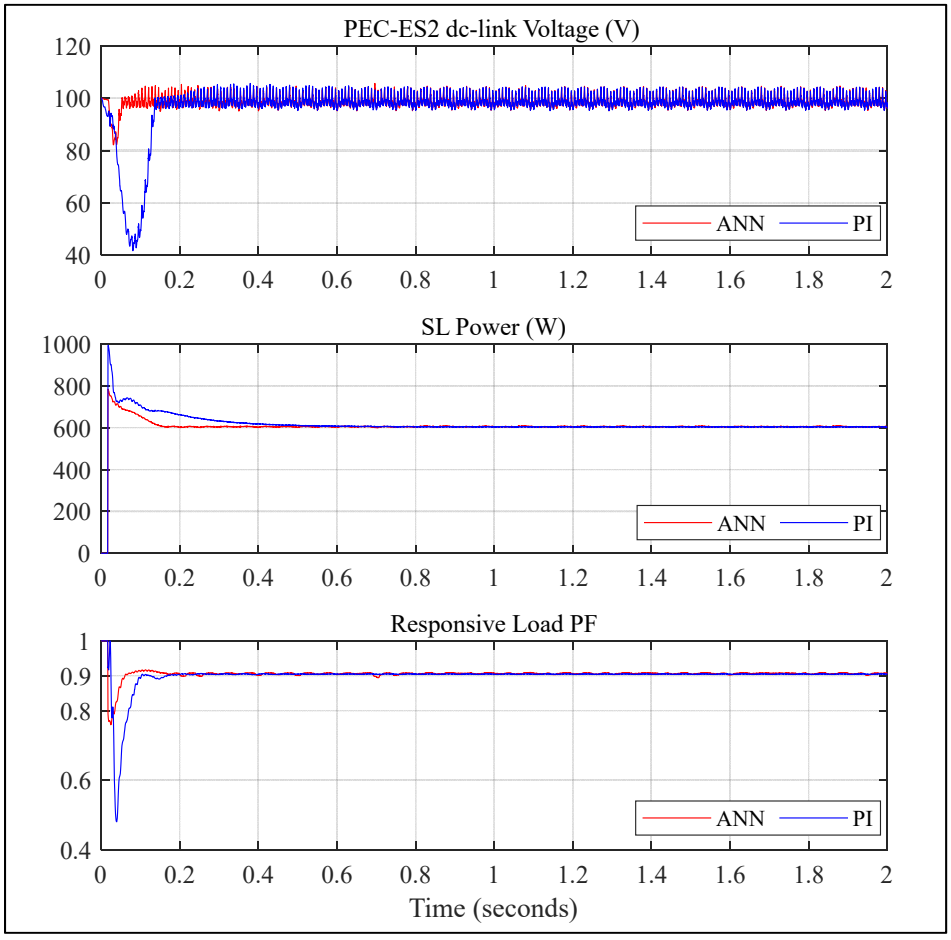

Figure 5.16 Parameters during PEC-ES2 start-up
with the PI-based RCD method and the proposed ANN-based controller

5.6 Experimental Validation

As proposing a multilevel ES2 topology and controller are focused in this article, experimental validation of the PEC-ES2 operation, regarding its reliability during faulty bidirectional switch operation, as well as its steady-state and dynamic performance, is of importance. The scheme of the arranged experimental validation system is demonstrated in Figure 5.1. Moreover, Table 5.6 presents the detailed specifications of this prototype.

Table 5.6 Specifications of the hardware arrangement

PEC-ES2 MOSFET Switches	N-Channel 900V
Nominal PCC Voltage (V_{PCC})	110 V rms
Source Impedance (Z_g)	0.1+j3.8 Ω
Frequencies (F_g), (F_{sw})	60 Hz, 2 kHz
PEC-ES2 DC Power Supply (V_{dc})	200 V
Inductor of the PEC-ES2 LC Filter (L_F)	1.5 mH
Capacitor of the PEC-ES2 LC Filter (C_f)	12 μF
PEC-ES2 Auxiliary Capacitors (C_1, C_2)	2500 μF
Source Impedance (Z_g)	0.1+j5.65 Ω
NSL Impedance (Z_{NSL})	20+j11.3 Ω
SL Impedance (Z_{SL})	80 Ω

The laboratory picture of the implemented hardware setup is also depicted in Figure 5.17. As illustrated, it is composed of OPAL-RT high voltage and current measurement devices, dSPACE 1202 MicroLabBox, variable dc power supply, loads, power analyzer, oscilloscopes, etc. For emulating a grid with unstable PCC voltage, a single-phase adjustable autotransformer has been employed. Moreover, a hardware prototype of the PEC-ES2 has been implemented by silicon carbide (SiC) MOSFET switches (C3M0120090D) and two auxiliary capacitors. As mentioned, it is of crucial importance for power systems to keep the SL's voltage stable. Therefore, firstly, to verify the PEC-ES2 performance in a stable condition, Figure 5.18

illustrates measured $V_{dc-link}$, V_{ab}, and V_{PCC} when the V_g is around 186 V max (131 V rms). This case emulates excess of the generated renewable power in the system. As clearly recorded, PEC-EC2 by generating a nine-level compensation voltage has effectively managed to keep the SL voltage (V_{PCC}) and consequently its power stable at their nominal values around 156 V max (110 V rms) and roughly 151 W ($P_{SL} = V_{SL}^2/R_{SL}$), respectively. Besides, $V_{dc-link}$ is also successfully fixed to half of the employed dc power supply (100 V dc).

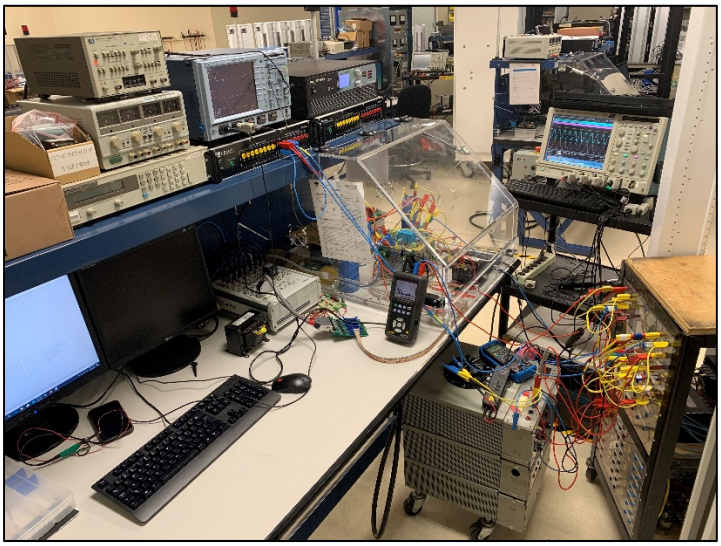

Figure 5.17 Picture of the implemented hardware setup

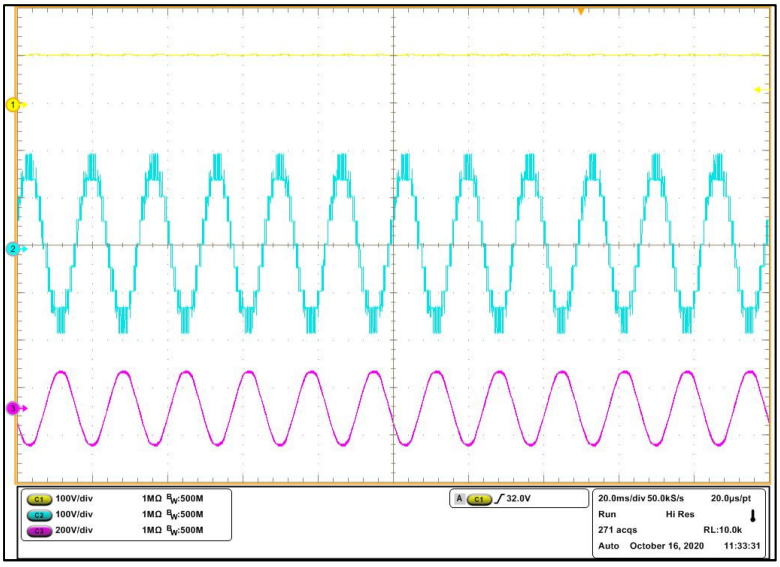

Figure 5.18 Steady-state results of $V_{dc-link}$, V_{ab}, and V_{PCC}

Harmonic analysis of the injected voltage has been also shown in Figure 5.19. A remarkable reduction in the THD of the generated compensation voltage is evident. Secondly, Figure 5.20 presents system results during the faulty operation of S_7 in the previous experimental scenario. It is clear that if S_7 fails, PEC-ES2 can revert to the five-level operation without noticeable transients while keeping the V_{PCC} stable (110 V rms) in the implemented prototype. Furthermore, the PEC-ES2 dc-link voltage is stable (100 V) even after S_7 Failure. Thirdly, for demonstrating the PEC-ES2 transient performance, the SL resistance has been reduced severely by around 67% from approximately 80 to 26.5 ohm in a sudden manner.

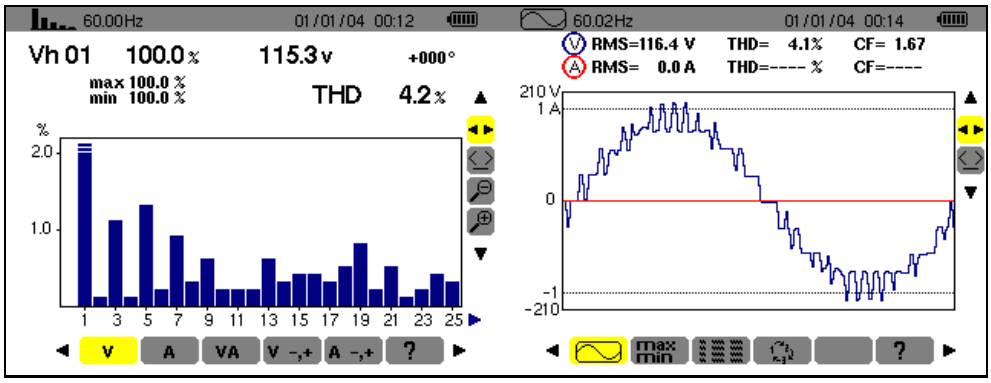

Figure 5.19 PEC-ES2 voltage harmonic spectrum and signal analyzations

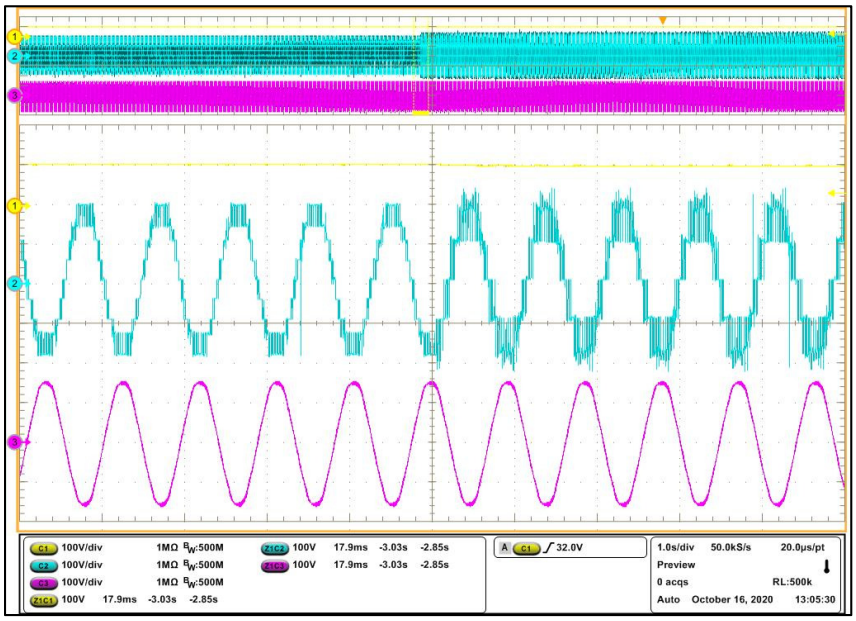

Figure 5.20 Results of $V_{dc\text{-}link}$, V_{ab}, and V_{PCC} during S7 failure

Figure 5.21 depicts the measured results during this case scenario. As seen, multilevel PEC-ES2 not only by reducing its injected voltage from nine-level to seven-level waveform, has efficiently managed to keep the SL voltage regulated without any considerable transients but also its dc-link voltage is kept constant at the required reference value. As can be noted, presented experimental results regarding the PEC-ES2 multi-level performance and its steady-state/dynamic responses are in accordance with the simulation tests.

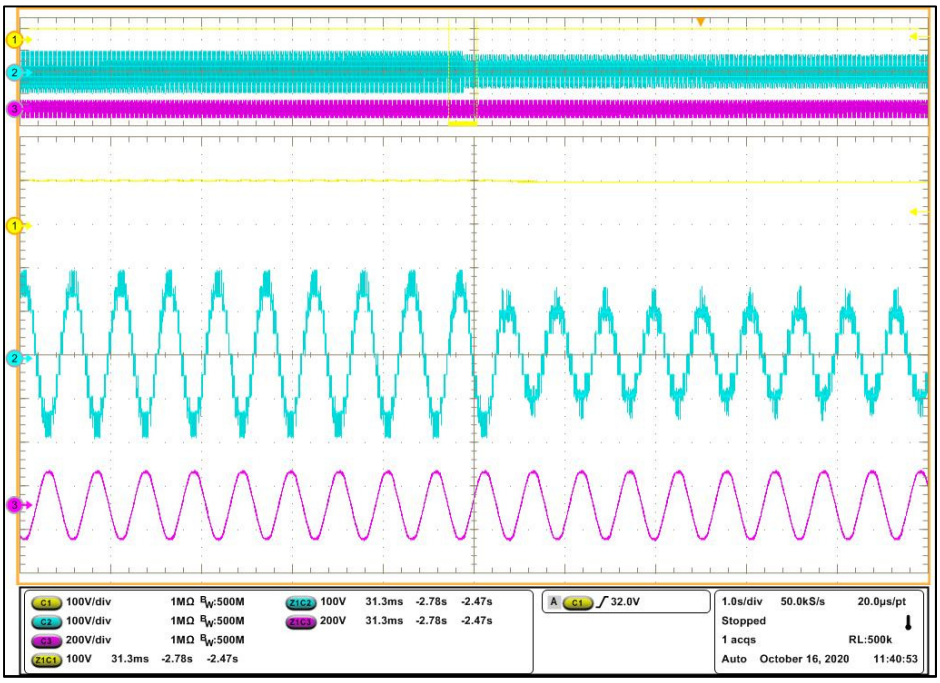

Figure 5.21 Results of $V_{dc\text{-}link}$, V_{ab}, and V_{PCC} during a change in the SL

5.7 Conclusion

A compact multilevel PEC-based ES2 and an intelligent ANN-based control strategy are introduced and explicated for tuning and stabilizing both the grid voltage and responsive load setup power factor. To reveal the higher power quality operation and reliability of the PEC-ES2 and proposed controller, extensive analysis and comparison among the existing ES2s and the PEC-ES2 have been performed. Regarding the power quality, it is demonstrated that by utilizing the introduced ES2 topology and controller, dynamic performance is enhanced and THD of the generated compensation voltage is improved from around 113% to merely 15%.

Besides, switching frequency is reduced from 16 kHz to only 2 kHz, while voltages of the employed battery and required auxiliary capacitors can be decreased to one-half and one-fourth, respectively. Moreover, voltages on the switches are decreased to at least one-half. Considering the improved reliability, it is proved that the PEC-ES2 is competent to continue its operation even if there is a fault in its S_7 switch. Finally, simulation and experimental results are presented.

CONCLUSION

Recently, computing and electronic equipment are being employed by electrical consumers more than ever. Besides, the percentage of electricity generated by renewable energy sources jumps to a new high every year. Consequently, power quality issues have become increasingly more important. Voltage sags/swells, transients, and low power factors are among the most critical power quality problems, which should be mitigated in an online, reliable, and efficient manner. Accordingly, a wide range of STATCOM and electric spring devices have been proposed and utilized in the literature. In this regard, various multilevel converters and linear/nonlinear controllers have been studied and developed. On the one hand, it has been illustrated that classical topologies like CHB and NPC are mostly employed for higher power/voltage industrial applications. Nonetheless, requiring more transistor switches, increased number of employed dc capacitors, being costly/bulky are some of the major topological demerits of these conventional configurations for STATCOM and ES applications. On the other hand, due to the high number of switching vectors and dependent dc links that need to be controlled, especially for STATCOM and ES as mainly real-time reactive power compensator devices, the complexity and computational burden of the applied controllers on these topologies are conspicuous. Therefore, it is required to model, control, and implement various compact multilevel STATCOM and ES configurations with superior features, including, multifunctionality, fast transient response, reduced complexity, and improved reliability.

As a result, to concisely present the conclusion of this dissertation, it can be noted that a highly compact seven-level STATCOM configuration with a boost-mode performance, as well as a reduced complexity model predictive controller using autotuned weighing factors, have been developed. Furthermore, a five-level capacitor-based electric spring with reduced component count and complexity and its multifunctional controller have been presented for dealing with harmonics and voltage stability problems in weak power systems. Moreover, considering problems associated with already available capacitor-based ES (first generation) topologies and controllers, model predictive current control of a multilevel smart load based on the

MPUC7 topology is proposed. Finally, to enhance power quality characteristics, reliability, and operation of the second generation of ES technology, an intelligent high-power-density nine-level PEC-based electric spring, which employs batteries as its energy storage elements, has been also designed and validated. PEC-ES2 has been also controlled by a novel ANN-based method for multifunctional applications in a decoupled manner.

The conclusions of each one of the five main chapters of this dissertation have been also highlighted below:

In CHAPTER 1, a thorough literature review on various versions of already available single/three-phase two/multi-level STATCOM and ES converter topologies as well as their controllers and applications has been performed. This extensive literature review revealed several important points in this area. First, developed half/full-bridge-based STATCOM/ES configurations suffer from inherent topological demerits like high harmonic content of the generated compensation voltage waveforms and increased voltage stress on their components. Second, considering the classical multilevel topologies such as CHB that are proposed to address some of the problems associated with two-level STATCOM/ES topologies, increased component count, cost, volume, and complexity are among their main shortcomings. Third, available STATCOM/ES PI-based controllers have some considerable demerits. Having multiple closed-loop controllers (outer/inner) with different dynamic response times that require precise tuning of several PI coefficients and poor transient performance with noticeable under/overshoots and settling times are among their disadvantages. Fourth, increased complexity and computational burden are the main disadvantages of most of the designed nonlinear controllers applied to conventional multilevel STATCOM/ES configurations. Fifth, the multifunctional operation of STATCOM and ES equipment can increase their efficiency and system reliability. Consequently, compact multilevel STATCOM/ES converters, as well as the required simplified nonlinear controllers, for multifunctional applications should be designed and developed.

CHAPTER 2 contains the development of a high-power-density seven-level STATCOM converter based on MPUC7 topology for applications in single-phase electrical systems. Moreover, a simplified finite control set model predictive-based controller with auto tunable weighting factors is also designed and applied to the proposed MPUC7-based STATCOM. Since a five-level STATCOM converter based on MPUC5 configuration with a linear PI-based controller has been previously introduced, it is studied and compared with the proposed topology and controller. Consequently, it has been proven that MPUC7-STATCOM has several merits. First, as dynamic models and nonlinearity of MPUC7-STATCOM have been considered in the proposed controller, its capacitors' voltages and generated current are all controlled in an accurate and separated manner. Second, considering its seven-level voltage waveform, the proposed MPUC7-STATCOM with the same number of passive and active components and reduced-size dependent dc links has improved power quality performance. Third, although the designed controller has superior steady-state and dynamic operations, it does not require any modulator or adjustment of several PI coefficients. On the other hand, compared to the already available seven-level CHB-based STATCOM, a highly reduced number of employed active and passive components and improved complexity/computational burden of the designed controller are two of the main advantages of the introduced MPUC7-STATCOM and its auto tunable FCS-MPC controller. Finally, extensive simulation and experimental results have been also presented for different stable and variable conditions.

As a remedy to the two-level ES topologies (half-bridge or full-bridge) with limited applications, a compact five-level capacitor-based ES founded on the MPUC5 converter, as well as its novel controller and modulation technique, for weak power systems have been proposed in CHAPTER 3. The introduced MPUC5-ES has multifunctional applications, including mitigation of PCC voltage fluctuations and harmonics. Moreover, the operating principles and design procedure of this high-power-density five-level electric spring have been also presented. Indirect adjustment of the auxiliary capacitors' voltages using a PWM modulator based on the availability of additional switching states, boost-mode operation, five-level voltage waveform, and lower/fixed switching frequency are among the main merits of the introduced MPUC5-based ES and control method. Regarding validating MPUC5-ES

performance for regulating the PCC voltage and reducing its harmonics content automatically and instantly, as well as its load-shedding capability, comprehensive simulation and experimental results have been also presented for both steady-state and dynamic conditions.

CHAPTER 4 illustrated the topological disadvantages of two-level capacitor-based ES converters such as demanding a relatively bulky harmonic filter, low voltage/power performance, and poor power quality characteristics. Moreover, problems associated with PI-based ES controllers, including high steady-state errors and poor dynamic operation are also highlighted. Moreover, improving the power density of the recently introduced MPUC5-ES has been also focused on in this chapter. Therefore, a seven-level capacitor-based electric spring configuration, which requires only six semiconductor switches and two capacitors, known as MPUC7-ES1 has been developed with highly enhanced power density, power quality, and reliability characteristics. Considering the presented MPUC7-ES1 state-space average model and related mathematical derivations, an innovative finite control set model predictive current control approach has been also designed and applied on the proposed topology for the first time. For achieving a superior operation, the key control aims of the MPUC7-ES1 nonlinear FCS-MPCC-based controller are defined as the generated current, capacitors' voltages, and reduction of commutation frequency. In comparison with a PI-based ES controller, the nonlinearities among the voltages of energy storage elements (capacitors) and the MPUC7-ES1 injected current has been also considered in the proposed FCS-MPCC method. Finally, MPUC7-ES1 performance and its FCS-MPCC controller are demonstrated by both simulation and experimental tests.

Eventually, CHAPTER 5 has presented an intelligent multilevel battery-based electric spring topology with a controller founded on artificial neural network and radial-chordal decomposition theory for modification and stabilization of the PCC voltage and power factor in an instantaneous and autonomous manner. Superior features of the proposed battery-based ES configuration founded on the PEC converter are compactness, fault-tolerant operation, the lower voltage stress on its switches and capacitors, decreased switching frequency from about 16 kHz to only 2 kHz, and improved harmonic content in its output current/voltage from about

113% in a two-level electric spring topology to merely 15%. Furthermore, multifunctionality and enhanced transient and start-up operations are among the merits of the proposed ANN-based controller. A hybrid modulator that supports both inverter and converter modes of PEC-ES2 operation and its fault-tolerant feature is also developed in this chapter. Detailed analysis and comparison among the available battery-based ESs and PEC-ES2 as well as simulation and experimental results are also presented to validate the performance and viability of the proposed PEC-ES2 topology and ANN-based controller.

Future Works

Considering real-time mitigation of power quality issues, this thesis has mainly focused on modeling, control, and implementation of compact multilevel converters for STATCOM and ES applications. Although this dissertation has reached its key goals, it can be considered as a preliminary phase and continued for years of research and development in this area. In this regard, some ideas have been concisely highlighted as below:

Developing single-phase compact multilevel STATCOM configurations and controllers with fault-tolerant operations

As indicated in CHAPTER 2, although the proposed seven-level MPUC7-based STATCOM topology and MPC-based nonlinear controller have several superior features such as boost-mode operation and reduced voltage on its components, it lacks fault-tolerant operation. This is due to its highly reduced component counts as a seven-level STATCOM topology. Therefore, new high-power-density multilevel STATCOM configurations with fault-tolerant performance can be also designed and proposed. Besides, novel nonlinear controllers that support this fault-tolerant feature should be also developed and applied to them.

Designing three-phase high-power-density multilevel STATCOM and ES topologies and controllers

Several single-phase compact multilevel STATCOM/ES configurations and controllers with superior features have been developed and experimentally validated in this thesis. However,

having a higher power density at the same amperage is one of the critical merits of a three-phase circuit over a single-phase one. Therefore, compact multilevel STATCOM/ES topologies and their respective controllers suitable for three-phase system applications can be also investigated. It is worth mentioning that considering proposing three-phase configurations and controllers for ES applications, various generations of this technology, for instance, capacitor and battery-based ESs, should be also considered.

Development of novel compact multilevel topologies and controllers for other generations of ES technology

As also indicated in the first chapter of this dissertation, capacitor and battery-based ESs are the two primary versions of this demand response management-based approach. Most of the available works in this area are focused on these two ES types. However, back-to-back ES, hybrid ES with renewable energy, and DC ES are recently introduced as the newer generations of this technology in the literature. More specifically, over the capacitor-based ES and battery-based ES, back-to-back ES and hybrid ES have two common favorable features, namely extended operating ranges and multifunctionality. Moreover, considering extending ES technology applications to dc microgrids, DC ES is also proposed. Nevertheless, still, half/full-bridge converters with PI-based controllers have mostly been employed as their topologies and control methods. Consequently, considering back-to-back ES, hybrid ES with renewable energy, and DC ES applications, multilevel converter topologies could be developed with merits like boost-mode operation, reduced voltage stress on their passive and active components, compactness, fault-tolerant performance, etc. Besides, as a response to shortcomings of the already available PI-based control methods, respective nonlinear controllers with superior steady-state and dynamic performances should be designed and applied to them.

LIST OF REFERENCES

Abarzadeh, M., Peyghami, S., Al-Haddad, K., Weise, N., Chang, L., & Blaabjerg, F. (2021). Reliability and Performance Improvement of PUC Converter Using a New Single-Carrier Sensor-Less PWM Method With Pseudo Reference Functions. *IEEE Transactions on Power Electronics*, *36*(5), 6092–6105. https://doi.org/10.1109/TPEL.2020.3030698

Abarzadeh, M., Vahedi, H., & Al-Haddad, K. (2019). Fast Sensor-Less Voltage Balancing and Capacitor Size Reduction in PUC5 Converter Using Novel Modulation Method. *IEEE Transactions on Industrial Informatics*, *15*(8), 4394–4406. https://doi.org/10.1109/TII.2019.2893739

Abughalieh, K. M., & Alawneh, S. G. (2019). A Survey of Parallel Implementations for Model Predictive Control. *IEEE Access*, *7*, 34348–34360. https://doi.org/10.1109/ACCESS.2019.2904240

Akhtar, Z., Chaudhuri, B., & Hui, S. Y. R. (2017). Smart Loads for Voltage Control in Distribution Networks. *IEEE Transactions on Smart Grid*, *8*(2), 937–946. https://doi.org/10.1109/TSG.2015.2486139

Akhtar, Z., Chaudhuri, B., & Ron Hui, S. Y. (2015). Primary Frequency Control Contribution From Smart Loads Using Reactive Compensation. *IEEE Transactions on Smart Grid*, *6*(5), 2356–2365. https://doi.org/10.1109/TSG.2015.2402637

Arai, T., Sekiguchi, K., Mochikawa, H., Sano, K., & Fujita, H. (2021). Evaluation of Required Energy Storage in Neutral-Point-Clamped Modular Multilevel Converter for Downsizing Low-Voltage Grid Converters. *IEEE Transactions on Power Electronics*, *36*(6), 6774–6786. https://doi.org/10.1109/TPEL.2020.3037936

Babaie, M., Sharifzadeh, M., & Al-Haddad, K. (2020). Proportional Integral Finite Set Model Predictive Control for a Transformer-Less Compact Multilevel Active Power Filter. *2020 IEEE Energy Conversion Congress and Exposition (ECCE)*, 5898–5903. https://doi.org/10.1109/ECCE44975.2020.9235394

Babaie, M., Sharifzadeh, M., Mehrasa, M., Chouinard, G., & Al-Haddad, K. (2021). Supervised Learning Model Predictive Control Trained by ABC Algorithm for Common-Mode Voltage Suppression in NPC Inverter. *IEEE Journal of Emerging and Selected Topics in Power Electronics*, *9*(3), 3446–3456. https://doi.org/10.1109/JESTPE.2020.2984674

Barrena, J. A., Marroyo, L., Rodriguez Vidal, M. Á., & Torrealday Apraiz, J. R. (2008). Individual Voltage Balancing Strategy for PWM Cascaded H-Bridge Converter-Based STATCOM. *IEEE Transactions on Industrial Electronics*, *55*(1), 21–29. https://doi.org/10.1109/TIE.2007.906127

Bose, B. K. (2007). Neural Network Applications in Power Electronics and Motor Drives—An Introduction and Perspective. *IEEE Transactions on Industrial Electronics*, *54*(1), 14–33. https://doi.org/10.1109/TIE.2006.888683

Canada, N. R. (2017, October 6). Energy-facts. Retrieved October 5, 2021, from https://www.nrcan.gc.ca/science-and-data/data-and-analysis/energy-data-and-analysis/energy-facts/20061

Caseiro, L. M. A., Mendes, A. M. S., & Cruz, S. M. A. (2019). Dynamically Weighted Optimal Switching Vector Model Predictive Control of Power Converters. *IEEE Transactions on Industrial Electronics*, *66*(2), 1235–1245. https://doi.org/10.1109/TIE.2018.2829689

Chaudhuri, N. R., Lee, C. K., Chaudhuri, B., & Hui, S. Y. R. (2014). Dynamic Modeling of Electric Springs. *IEEE Transactions on Smart Grid*, *5*(5), 2450–2458. https://doi.org/10.1109/TSG.2014.2319858

Chen, J., Yan, S., & Ron Hui, S. Y. (2017). Using consensus control for reactive power sharing of distributed electric springs. *2017 IEEE Energy Conversion Congress and Exposition (ECCE)*, 3741–3746. https://doi.org/10.1109/ECCE.2017.8096661

Chen, J., Yan, S., Yang, T., Tan, S.-C., & Hui, S. Y. (2019). Practical Evaluation of Droop and Consensus Control of Distributed Electric Springs for Both Voltage and Frequency Regulation in Microgrid. *IEEE Transactions on Power Electronics*, *34*(7), 6947–6959. https://doi.org/10.1109/TPEL.2018.2874495

Chen, T., Liu, H., Lee, C.-K., & Hui, S. Y. R. (2020). A Generalized Controller for Electric-Spring-Based Smart Load With Both Active and Reactive Power Compensation. *IEEE Journal of Emerging and Selected Topics in Power Electronics*, *8*(2), 1454–1465. https://doi.org/10.1109/JESTPE.2019.2908730

Chen, Xia, Hou, Y., Tan, S.-C., Lee, C.-K., & Hui, S. Y. R. (2015). Mitigating Voltage and Frequency Fluctuation in Microgrids Using Electric Springs. *IEEE Transactions on Smart Grid*, *6*(2), 508–515. https://doi.org/10.1109/TSG.2014.2374231

Chen, Xin, Zhang, Y., Wang, S., Chen, J., & Gong, C. (2017). Impedance-Phased Dynamic Control Method for Grid-Connected Inverters in a Weak Grid. *IEEE Transactions on Power Electronics*, *32*(1), 274–283. https://doi.org/10.1109/TPEL.2016.2533563

Chivite-Zabalza, J., Izurza-Moreno, P., Madariaga, D., Calvo, G., & Rodríguez, M. A. (2013). Voltage Balancing control in 3-Level Neutral-Point Clamped Inverters Using Triangular Carrier PWM Modulation for FACTS Applications. *IEEE Transactions on Power Electronics*, *28*(10), 4473–4484. https://doi.org/10.1109/TPEL.2012.2237415

Ciobotaru, M., Teodorescu, R., & Blaabjerg, F. (2006). A new single-phase PLL structure based on second order generalized integrator. *2006 37th IEEE Power Electronics Specialists Conference*, 1–6. https://doi.org/10.1109/pesc.2006.1711988

Cupertino, A. F., Farias, J. V. M., Pereira, H. A., Seleme, S. I., & Teodorescu, R. (2019). Comparison of DSCC and SDBC Modular Multilevel Converters for STATCOM Application During Negative Sequence Compensation. *IEEE Transactions on Industrial Electronics*, *66*(3), 2302–2312. https://doi.org/10.1109/TIE.2018.2811361

Cupertino, A. F., Pereira, H. A., Seleme, S. I., & Teodorescu, R. (2020). On Inherent Redundancy of MMC-Based STATCOMs in the Overmodulation Region. *IEEE Transactions on Power Delivery*, *35*(3), 1169–1179. https://doi.org/10.1109/TPWRD.2019.2936784

Donoso, F., Mora, A., Cárdenas, R., Angulo, A., Sáez, D., & Rivera, M. (2018). Finite-Set Model-Predictive Control Strategies for a 3L-NPC Inverter Operating With Fixed Switching Frequency. *IEEE Transactions on Industrial Electronics*, *65*(5), 3954–3965. https://doi.org/10.1109/TIE.2017.2760840

Farivar, G., Hredzak, B., & Agelidis, V. G. (2016). Decoupled Control System for Cascaded H-Bridge Multilevel Converter Based STATCOM. *IEEE Transactions on Industrial Electronics*, *63*(1), 322–331. https://doi.org/10.1109/TIE.2015.2472358

Farivar, G., Townsend, C. D., Hredzak, B., Pou, J., & Agelidis, V. G. (2017). Low-Capacitance Cascaded H-Bridge Multilevel StatCom. *IEEE Transactions on Power Electronics*, *32*(3), 1744–1754. https://doi.org/10.1109/TPEL.2016.2557351

Gao, J., Gong, C., Li, W., & Liu, J. (2020). Novel Compensation Strategy for Calculation Delay of Finite Control Set Model Predictive Current Control in PMSM. *IEEE Transactions on Industrial Electronics*, *67*(7), 5816–5819. https://doi.org/10.1109/TIE.2019.2934060

Gautam, S. P., Kumar, L., & Gupta, S. (2018). Single-phase multilevel inverter topologies with self-voltage balancing capabilities. *IET Power Electronics*, *11*(5), 844–855. https://doi.org/10.1049/iet-pel.2017.0401

Gavagsaz-Ghoachani, R., Phattanasak, M., Martin, J.-P., Nahid-Mobarakeh, B., Pierfederici, S., & Riedinger, P. (2019). Observer and Lyapunov-Based Control for Switching Power Converters With LC Input Filter. *IEEE Transactions on Power Electronics*, *34*(7), 7053–7066. https://doi.org/10.1109/TPEL.2018.2877180

Ge, X., & Gao, F. (2018). Flexible Third Harmonic Voltage Control of Low Capacitance Cascaded H-Bridge STATCOM. *IEEE Transactions on Power Electronics*, *33*(3), 1884–1889. https://doi.org/10.1109/TPEL.2017.2738778

Hackl, C. M., & Landerer, M. (2020). Modified Second-Order Generalized Integrators With Modified Frequency Locked Loop for Fast Harmonics Estimation of Distorted Single-Phase Signals. *IEEE Transactions on Power Electronics*, *35*(3), 3298–3309. https://doi.org/10.1109/TPEL.2019.2932790

Haw, L. K., Dahidah, M. S. A., & Almurib, H. A. F. (2014). SHE–PWM Cascaded Multilevel Inverter With Adjustable DC Voltage Levels Control for STATCOM Applications. *IEEE Transactions on Power Electronics*, *29*(12), 6433–6444. https://doi.org/10.1109/TPEL.2014.2306455

Hui, S. Y., Lee, C. K., & Wu, F. F. (2012). Electric Springs—A New Smart Grid Technology. *IEEE Transactions on Smart Grid*, *3*(3), 1552–1561. https://doi.org/10.1109/TSG.2012.2200701

Isobe, T., Shiojima, D., Kato, K., Hernandez, Y. R. R., & Shimada, R. (2016). Full-Bridge Reactive Power Compensator With Minimized-Equipped Capacitor and Its Application to Static Var Compensator. *IEEE Transactions on Power Electronics*, *31*(1), 224–234. https://doi.org/10.1109/TPEL.2015.2412954

Karamanakos, P., & Geyer, T. (2020). Guidelines for the Design of Finite Control Set Model Predictive Controllers. *IEEE Transactions on Power Electronics*, *35*(7), 7434–7450. https://doi.org/10.1109/TPEL.2019.2954357

Kaymanesh, A., Babaie, M., Chandra, A., & Al-Haddad, K. (2021a). Model Predictive Current Control of Multilevel Smart Load Based on MPUC7 Converter. *IEEE Access*, 1–1. https://doi.org/10.1109/ACCESS.2021.3113630

Kaymanesh, A., Babaie, M., Chandra, A., & Al-Haddad, K. (2021b). PEC Inverter for Intelligent Electric Spring Applications Using ANN-Based Controller. *IEEE Journal of Emerging and Selected Topics in Industrial Electronics*, 1–1. https://doi.org/10.1109/JESTIE.2021.3095018

Kaymanesh, A., Babaie, M., Tidjani, F. S., Chandra, A., & Al-Haddad, K. (2020). Modified Seven-Level Pack U-Cell Inverter for Electric-Spring-Based Smart Load Applications. *IECON 2020 The 46th Annual Conference of the IEEE Industrial Electronics Society*, 4221–4226. https://doi.org/10.1109/IECON43393.2020.9254299

Kaymanesh, A., & Chandra, A. (2020). Electric Spring Using MPUC5 Inverter for Mitigating Harmonics and Voltage Fluctuations. *IEEE Journal of Emerging and Selected Topics in Power Electronics*, 1–1. https://doi.org/10.1109/JESTPE.2020.3028586

Kaymanesh, A., Chandra, A., & Al-Haddad, K. (2021). Model Predictive Control of MPUC7-Based STATCOM Using Autotuned Weighting Factors. *IEEE Transactions on Industrial Electronics*, 1–1. https://doi.org/10.1109/TIE.2021.3070502

Kaymanesh, A., Rezkallah, M., Chandra, A., & El-Bayeh, C. Z. (2020). Nine-Level Packed U-Cell Converter for Electric Spring Applications. *2020 IEEE Electric Power and Energy Conference (EPEC)*, 1–6. https://doi.org/10.1109/EPEC48502.2020.9320081

Kaymanesh, A., Rezkallah, M., Saeedi, M., & Chandra, A. (2020). Industrial Smart Load Using Five-Level ANPC Converter with Sensorless Modulation Method. *2020 IEEE International Conference on Power Electronics, Drives and Energy Systems (PEDES)*, 1–6. https://doi.org/10.1109/PEDES49360.2020.9379474

Khamis, A. K., Zakzouk, N. E., Abdelsalam, A. K., & Lotfy, A. A. (2019). Decoupled Control Strategy for Electric Springs: Dual Functionality Feature. *IEEE Access*, *7*, 57725–57740. https://doi.org/10.1109/ACCESS.2019.2914141

Kolluri, S., Gorla, N. B. Y., & Panda, S. K. (2020). Capacitor Voltage Ripple Suppression in a Modular Multilevel Converter Using Frequency-Adaptive Spatial Repetitive-Based Circulating Current Controller. *IEEE Transactions on Power Electronics*, *35*(9), 9839–9849. https://doi.org/10.1109/TPEL.2020.2971737

Laraki, M.-H., Kaymanesh, A., Chandra, A., Agbossou, K., & Cardenas, A. (2019). A New Configuration to Mitigate Load Transients for FUEL Cell Using Electric Springs. *2019 IEEE 2nd International Conference on Renewable Energy and Power Engineering (REPE)*, 73–77. https://doi.org/10.1109/REPE48501.2019.9025119

Lee, C. K., Chaudhuri, B., & Hui, S. Y. (2013). Hardware and Control Implementation of Electric Springs for Stabilizing Future Smart Grid With Intermittent Renewable Energy Sources. *IEEE Journal of Emerging and Selected Topics in Power Electronics*, *1*(1), 18–27. https://doi.org/10.1109/JESTPE.2013.2264091

Lee, C. K., Chaudhuri, N. R., Chaudhuri, B., & Hui, S. Y. R. (2013). Droop Control of Distributed Electric Springs for Stabilizing Future Power Grid. *IEEE Transactions on Smart Grid*, *4*(3), 1558–1566. https://doi.org/10.1109/TSG.2013.2258949

Lee, C. K., & Hui, S. Y. (2013). Reduction of energy storage requirements in future smart grid using electric springs. *IEEE Transactions on Smart Grid*, *4*(3), 1282–1288. https://doi.org/10.1109/TSG.2013.2252208

Lee, C.-K., Liu, H., Tan, S.-C., Chaudhuri, B., & Hui, S. Y. (2020). Electric Spring and Smart Load: Technology, System-level Impact and Opportunities. *IEEE Journal of Emerging and Selected Topics in Power Electronics*, 1–1. https://doi.org/10.1109/JESTPE.2020.3004164

Li, X., Zhang, H., Shadmand, M. B., & Balog, R. S. (2017). Model Predictive Control of a Voltage-Source Inverter With Seamless Transition Between Islanded and Grid-Connected Operations. *IEEE Transactions on Industrial Electronics*, *64*(10), 7906–7918. https://doi.org/10.1109/TIE.2017.2696459

Liang, L., Hou, Y., & Hill, D. J. (2019). Enhancing Flexibility of an Islanded Microgrid With Electric Springs. *IEEE Transactions on Smart Grid*, *10*(1), 899–909. https://doi.org/10.1109/TSG.2017.2754545

Liang, L., Hou, Y., Hill, D. J., & Hui, S. Y. R. (2018). Enhancing Resilience of Microgrids With Electric Springs. *IEEE Transactions on Smart Grid*, *9*(3), 2235–2247. https://doi.org/10.1109/TSG.2016.2609603

Liu, B., Song, W., Li, Y., & Zhan, B. (2021). Performance Improvement of DC Capacitor Voltage Balancing Control for Cascaded H-Bridge Multilevel Converters. *IEEE Transactions on Power Electronics*, *36*(3), 3354–3366. https://doi.org/10.1109/TPEL.2020.3012540

Liu, H., Ng, W. M., Lee, C.-K., & Ron Hui, S. Y. (2020). Integration of Flexible Loads and Electric Spring Using a Three-Phase Inverter. *IEEE Transactions on Power Electronics*, *35*(8), 8013–8024. https://doi.org/10.1109/TPEL.2019.2953603

Liu, X., Wang, D., & Peng, Z. (2019). Cascade-Free Fuzzy Finite-Control-Set Model Predictive Control for Nested Neutral Point-Clamped Converters With Low Switching Frequency. *IEEE Transactions on Control Systems Technology*, *27*(5), 2237–2244. https://doi.org/10.1109/TCST.2018.2839091

Luo, X., Akhtar, Z., Lee, C. K., Chaudhuri, B., Tan, S.-C., & Hui, S. Y. R. (2015). Distributed Voltage Control with Electric Springs: Comparison with STATCOM. *IEEE Transactions on Smart Grid*, *6*(1), 209–219. https://doi.org/10.1109/TSG.2014.2345072

Mastromauro, R. A., Liserre, M., & Dell'Aquila, A. (2012). Control Issues in Single-Stage Photovoltaic Systems: MPPT, Current and Voltage Control. *IEEE Transactions on Industrial Informatics*, *8*(2), 241–254. https://doi.org/10.1109/TII.2012.2186973

Mehrasa, M., Sharifzadeh, M., Babaie, M., Sebaaly, F., & Al-Haddad, K. (2020). Virtual Admittance Compensator (VAC)-based Control Method for PEC9 Inverter. *2020 IEEE International Conference on Industrial Technology (ICIT)*, 872–877. https://doi.org/10.1109/ICIT45562.2020.9067222

Mok, K.-T., Ho, S.-S., Tan, S.-C., & Hui, S. Y. (2017). A Comprehensive Analysis and Control Strategy for Nullifying Negative- and Zero-Sequence Currents in an Unbalanced Three-Phase Power System Using Electric Springs. *IEEE Transactions on Power Electronics*, *32*(10), 7635–7650. https://doi.org/10.1109/TPEL.2016.2636226

Mok, K.-T., Tan, S.-C., & Hui, S. Y. R. (2016). Decoupled Power Angle and Voltage Control of Electric Springs. *IEEE Transactions on Power Electronics*, *31*(2), 1216–1229. https://doi.org/10.1109/TPEL.2015.2424153

Mok, K.-T., Wang, M.-H., Tan, S.-C., & Hui, S. Y. R. (2017). DC Electric Springs—A Technology for Stabilizing DC Power Distribution Systems. *IEEE Transactions on Power Electronics*, *32*(2), 1088–1105. https://doi.org/10.1109/TPEL.2016.2542278

Muthirayan, D., Kalathil, D., Poolla, K., & Varaiya, P. (2020). Mechanism Design for Demand Response Programs. *IEEE Transactions on Smart Grid*, *11*(1), 61–73. https://doi.org/10.1109/TSG.2019.2917396

Nami, A., Wang, L., Dijkhuizen, F., & Shukla, A. (2013). Five level cross connected cell for cascaded converters. *2013 15th European Conference on Power Electronics and Applications (EPE)*, 1–9. https://doi.org/10.1109/EPE.2013.6631941

Nasiri, M. R., Farhangi, S., & Rodríguez, J. (2019). Model Predictive Control of a Multilevel CHB STATCOM in Wind Farm Application Using Diophantine Equations. *IEEE Transactions on Industrial Electronics*, *66*(2), 1213–1223. https://doi.org/10.1109/TIE.2018.2833055

Nasrin, M. S., Khan, F. H., & Alam, M. K. (2014). Quantifying Device Degradation in Live Power Converters Using SSTDR Assisted Impedance Matrix. *IEEE Transactions on Power Electronics*, *29*(6), 3116–3131. https://doi.org/10.1109/TPEL.2013.2273556

Omer, P., Kumar, J., & Surjan, B. S. (2020). A Review on Reduced Switch Count Multilevel Inverter Topologies. *IEEE Access*, *8*, 22281–22302. https://doi.org/10.1109/ACCESS.2020.2969551

Ounejjar, Y., Al-Haddad, K., & Gregoire, L.-A. (2011). Packed U Cells Multilevel Converter Topology: Theoretical Study and Experimental Validation. *IEEE Transactions on Industrial Electronics*, *58*(4), 1294–1306. https://doi.org/10.1109/TIE.2010.2050412

Pachauri, R. K., Mayer, L., & Intergovernmental Panel on Climate Change (Eds.). (2015). *Climate change 2014: Synthesis report*. Geneva, Switzerland: Intergovernmental Panel on Climate Change.

Patil, T., Pawar, R., Jangade, C., Fuke, P., Gawande, S. P., & Kadwane, S. G. (2017). Cascaded multilevel inverter based electric spring for smart grid applications. *2017 Innovations in Power and Advanced Computing Technologies (i-PACT)*, 1–7. https://doi.org/10.1109/IPACT.2017.8245154

Pu, S., Ugur, E., Yang, F., & Akin, B. (2020). In situ Degradation Monitoring of SiC MOSFET Based on Switching Transient Measurement. *IEEE Transactions on Industrial Electronics*, *67*(6), 5092–5100. https://doi.org/10.1109/TIE.2019.2924600

Rubio, J. de J. (2021). Stability Analysis of the Modified Levenberg–Marquardt Algorithm for the Artificial Neural Network Training. *IEEE Transactions on Neural Networks and Learning Systems*, *32*(8), 3510–3524. https://doi.org/10.1109/TNNLS.2020.3015200

Saeedifard, M., Nikkhajoei, H., & Iravani, R. (2007). A Space Vector Modulated STATCOM Based on a Three-Level Neutral Point Clamped Converter. *IEEE Transactions on Power Delivery*, *22*(2), 1029–1039. https://doi.org/10.1109/TPWRD.2007.893448

Sajadi, R., Iman-Eini, H., Bakhshizadeh, M. K., Neyshabouri, Y., & Farhangi, S. (2018). Selective Harmonic Elimination Technique With Control of Capacitive DC-Link Voltages in an Asymmetric Cascaded H-Bridge Inverter for STATCOM Application. *IEEE Transactions on Industrial Electronics*, *65*(11), 8788–8796. https://doi.org/10.1109/TIE.2018.2811365

Sebaaly, F., Sharifzadeh, M., Kanaan, H. Y., & Al-Haddad, K. (2021). Multilevel Switching-Mode Operation of Finite-Set Model Predictive Control for Grid-Connected Packed E-Cell Inverter. *IEEE Transactions on Industrial Electronics*, *68*(8), 6992–7001. https://doi.org/10.1109/TIE.2020.3003627

Shadmand, M. B., Jain, S., & Balog, R. S. (2019). Autotuning Technique for the Cost Function Weight Factors in Model Predictive Control for Power Electronic Interfaces. *IEEE Journal of Emerging and Selected Topics in Power Electronics*, *7*(2), 1408–1420. https://doi.org/10.1109/JESTPE.2018.2849738

Sharifzadeh, M., & Al-Haddad, K. (2019). Packed E-Cell (PEC) Converter Topology Operation and Experimental Validation. *IEEE Access*, *7*, 93049–93061. https://doi.org/10.1109/ACCESS.2019.2924009

Sharma, S. K., Chandra, A., Saad, M., Lefebvre, S., Asber, D., & Lenoir, L. (2017). Voltage Flicker Mitigation Employing Smart Loads With High Penetration of Renewable Energy in Distribution Systems. *IEEE Transactions on Sustainable Energy*, *8*(1), 414–424. https://doi.org/10.1109/TSTE.2016.2603512

Shen, X., Liu, J., Luo, W., Leon, J. I., Vazquez, S., Alcaide, A. M., … Wu, L. (2020). High-Performance Second-Order Sliding Mode Control for NPC Converters. *IEEE Transactions on Industrial Informatics*, *16*(8), 5345–5356. https://doi.org/10.1109/TII.2019.2960550

Shukla, A., Ghosh, A., & Joshi, A. (2007). Hysteresis Current Control Operation of Flying Capacitor Multilevel Inverter and Its Application in Shunt Compensation of Distribution Systems. *IEEE Transactions on Power Delivery*, *22*(1), 396–405. https://doi.org/10.1109/TPWRD.2006.877100

Singh, B., Chandra, A., & Al-Haddad, K. (2014). *Power Quality: Problems and Mitigation Techniques*. John Wiley & Sons.

Song, W., & Huang, A. Q. (2010). Fault-Tolerant Design and Control Strategy for Cascaded H-Bridge Multilevel Converter-Based STATCOM. *IEEE Transactions on Industrial Electronics*, *57*(8), 2700–2708. https://doi.org/10.1109/TIE.2009.2036019

Sundar, N. S., Philip, L., Tapasvi, P., Akash, M., & Hiraj, D. (2016). Multilevel inverter based electric spring for voltage regulation and active reactive power control. *2016 IEEE 1st International Conference on Power Electronics, Intelligent Control and Energy Systems (ICPEICES)*, 1–5. https://doi.org/10.1109/ICPEICES.2016.7853410

Tan, S.-C., Lee, C. K., & Hui, S. Y. (2013). General Steady-State Analysis and Control Principle of Electric Springs With Active and Reactive Power Compensations. *IEEE Transactions on Power Electronics*, *28*(8), 3958–3969. https://doi.org/10.1109/TPEL.2012.2227823

Taul, M. G., Pallo, N., Stillwell, A., & Pilawa-Podgurski, R. C. N. (2021). Theoretical Analysis and Experimental Validation of Flying-Capacitor Multilevel Converters Under Short-Circuit Fault Conditions. *IEEE Transactions on Power Electronics*, *36*(11), 12292–12308. https://doi.org/10.1109/TPEL.2021.3075447

Townsend, C. D., Summers, T. J., Vodden, J., Watson, A. J., Betz, R. E., & Clare, J. C. (2013). Optimization of Switching Losses and Capacitor Voltage Ripple Using Model Predictive Control of a Cascaded H-Bridge Multilevel StatCom. *IEEE Transactions on Power Electronics*, *28*(7), 3077–3087. https://doi.org/10.1109/TPEL.2012.2219593

Transforming our world: The 2030 Agenda for Sustainable Development | Department of Economic and Social Affairs. (n.d.). Retrieved October 7, 2021, from https://sdgs.un.org/2030agenda

Vahedi, H., & Al-Haddad, K. (2016a). A Novel Multilevel Multioutput Bidirectional Active Buck PFC Rectifier. *IEEE Transactions on Industrial Electronics*, *63*(9), 5442–5450. https://doi.org/10.1109/TIE.2016.2555279

Vahedi, H., & Al-Haddad, K. (2016b). PUC5 inverter—A promising topology for single-phase and three-phase applications. *IECON 2016 - 42nd Annual Conference of the IEEE Industrial Electronics Society*, 6522–6527. https://doi.org/10.1109/IECON.2016.7793810

Vahedi, H., Dehghanzadeh, A., & Al-Haddad, K. (2018). Static VAr compensator using packed U-cell based multilevel converter. *2018 IEEE 12th International Conference on Compatibility, Power Electronics and Power Engineering (CPE-POWERENG 2018)*, 1–5. https://doi.org/10.1109/CPE.2018.8372576

Vahedi, H., Labbé, P.-A., & Al-Haddad, K. (2016). Sensor-Less Five-Level Packed U-Cell (PUC5) Inverter Operating in Stand-Alone and Grid-Connected Modes. *IEEE Transactions on Industrial Informatics*, *12*(1), 361–370. https://doi.org/10.1109/TII.2015.2491260

Vahedi, H., Sharifzadeh, M., & Al-Haddad, K. (2018). Modified Seven-Level Pack U-Cell Inverter for Photovoltaic Applications. *IEEE Journal of Emerging and Selected Topics in Power Electronics*, *6*(3), 1508–1516. https://doi.org/10.1109/JESTPE.2018.2821663

Vahedi, H., Shojaei, A. A., Dessaint, L.-A., & Al-Haddad, K. (2018). Reduced DC-Link Voltage Active Power Filter Using Modified PUC5 Converter. *IEEE Transactions on Power Electronics*, *33*(2), 943–947. https://doi.org/10.1109/TPEL.2017.2727325

Villarroel, F., Espinoza, J. R., Rojas, C. A., Rodriguez, J., Rivera, M., & Sbarbaro, D. (2013). Multiobjective Switching State Selector for Finite-States Model Predictive Control Based on Fuzzy Decision Making in a Matrix Converter. *IEEE Transactions on Industrial Electronics*, *60*(2), 589–599. https://doi.org/10.1109/TIE.2012.2206343

Wang, M., He, Y., Xu, X., Dong, Z., & Lei, Y. (2021). A Review of AC and DC Electric Springs. *IEEE Access*, *9*, 14398–14408. https://doi.org/10.1109/ACCESS.2021.3051340

Wang, M.-H., He, Y., Yang, T., Jia, Y., & Xu, Z. (2020). Cascaded Voltage Control for Electric Springs With DC-Link Film Capacitors. *IEEE Journal of Emerging and Selected Topics in Power Electronics*, *8*(4), 3982–3994. https://doi.org/10.1109/JESTPE.2019.2962238

Wang, M.-H., Yan, S., Tan, S.-C., & Hui, S. Y. (2018). Hybrid-DC Electric Springs for DC Voltage Regulation and Harmonic Cancellation in DC Microgrids. *IEEE Transactions on Power Electronics*, *33*(2), 1167–1177. https://doi.org/10.1109/TPEL.2017.2681120

Wang, Q., Cheng, M., Chen, Z., & Wang, Z. (2015). Steady-State Analysis of Electric Springs With a Novel δ Control. *IEEE Transactions on Power Electronics*, *30*(12), 7159–7169. https://doi.org/10.1109/TPEL.2015.2391278

Wang, Q., Cheng, M., & Jiang, Y. (2016). Harmonics Suppression for Critical Loads Using Electric Springs With Current-Source Inverters. *IEEE Journal of Emerging and Selected Topics in Power Electronics*, *4*(4), 1362–1369. https://doi.org/10.1109/JESTPE.2016.2591942

Wang, Q., Cheng, M., Jiang, Y., Zuo, W., & Buja, G. (2018). A Simple Active and Reactive Power Control for Applications of Single-Phase Electric Springs. *IEEE Transactions on Industrial Electronics*, *65*(8), 6291–6300. https://doi.org/10.1109/TIE.2018.2793201

World Energy Outlook-2017. (2017). 782.

Yan, S., Lee, C.-K., Yang, T., Mok, K.-T., Tan, S.-C., Chaudhuri, B., & Hui, S. Y. R. (2017). Extending the Operating Range of Electric Spring Using Back-To-Back Converter: Hardware Implementation and Control. *IEEE Transactions on Power Electronics*, *32*(7), 5171–5179. https://doi.org/10.1109/TPEL.2016.2606128

Yan, S., Tan, S.-C., Lee, C.-K., Chaudhuri, B., & Hui, S. Y. R. (2015). Electric Springs for Reducing Power Imbalance in Three-Phase Power Systems. *IEEE Transactions on Power Electronics*, *30*(7), 3601–3609. https://doi.org/10.1109/TPEL.2014.2350001

Yan, S., Tan, S.-C., Lee, C.-K., Chaudhuri, B., & Hui, S. Y. R. (2017). Use of Smart Loads for Power Quality Improvement. *IEEE Journal of Emerging and Selected Topics in Power Electronics*, *5*(1), 504–512. https://doi.org/10.1109/JESTPE.2016.2637398

Yan, S., Wang, M.-H., Yang, T.-B., Tan, S.-C., Chaudhuri, B., & Hui, S. Y. R. (2018). Achieving Multiple Functions of Three-Phase Electric Springs in Unbalanced Three-Phase Power Systems Using the Instantaneous Power Theory. *IEEE Transactions on Power Electronics*, *33*(7), 5784–5795. https://doi.org/10.1109/TPEL.2017.2748221

Yang, T., Liu, T., Chen, J., Yan, S., & Hui, S. Y. R. (2018). Dynamic Modular Modeling of Smart Loads Associated With Electric Springs and Control. *IEEE Transactions on Power Electronics*, *33*(12), 10071–10085. https://doi.org/10.1109/TPEL.2018.2794516

Yang, T., Mok, K.-T., Ho, S.-S., Tan, S.-C., Lee, C.-K., & Hui, R. S. Y. (2019). Use of Integrated Photovoltaic-Electric Spring System as a Power Balancer in Power Distribution Networks. *IEEE Transactions on Power Electronics*, *34*(6), 5312–5324. https://doi.org/10.1109/TPEL.2018.2867573

Yang, Y., Wen, H., Fan, M., Xie, M., Chen, R., & Wang, Y. (2019). A Constant Switching Frequency Model Predictive Control Without Weighting Factors for T-Type Single-Phase Three-Level Inverters. *IEEE Transactions on Industrial Electronics*, *66*(7), 5153–5164. https://doi.org/10.1109/TIE.2018.2868290

Yuan, C., Feng, J., Tong, M., Yang, D., & Tang, N. (2019). Piecewise control strategy for electric spring. *IET Generation, Transmission & Distribution*, *13*(12), 2496–2506. https://doi.org/10.1049/iet-gtd.2018.7027

Zhang, G., Wu, Z., Yu, S. S., & Zhang, Y. (2020). A Novel Impedance-Network-Based Electric Spring. *IEEE Access*, *8*, 129123–129135. https://doi.org/10.1109/ACCESS.2020.3009320

Zhang, X., & Zheng, Z. (2020). Application of Repetitive Control in Electric Spring. *IEEE Access*, *8*, 216607–216616. https://doi.org/10.1109/ACCESS.2020.3041648

Zhang, Y., Wu, X., & Yuan, X. (2017). A Simplified Branch and Bound Approach for Model Predictive Control of Multilevel Cascaded H-Bridge STATCOM. *IEEE Transactions on Industrial Electronics*, *64*(10), 7634–7644. https://doi.org/10.1109/TIE.2017.2698360

Zhang, Y., Yuan, X., Wu, X., Yuan, Y., & Zhou, J. (2020). Parallel Implementation of Model Predictive Control for Multilevel Cascaded H-Bridge STATCOM With Linear Complexity. *IEEE Transactions on Industrial Electronics*, *67*(2), 832–841. https://doi.org/10.1109/TIE.2019.2901647

Zhang, Z., Xie, C., Tong, R., & Gao, S. (2019). Identification and Control of Electric Elasticity Limit for Electric-Spring-Based Flexible Loads. *IEEE Transactions on Industrial Informatics*, *15*(11), 6001–6010. https://doi.org/10.1109/TII.2019.2900196

Zheng, Y., Hill, D. J., Meng, K., & Hui, S. Y. (2017). Critical Bus Voltage Support in Distribution Systems With Electric Springs and Responsibility Sharing. *IEEE Transactions on Power Systems*, *32*(5), 3584–3593. https://doi.org/10.1109/TPWRS.2016.2645940

Zheng, Y., Hill, D. J., Song, Y., Zhao, J., & Hui, S. Y. R. (2020). Optimal Electric Spring Allocation for Risk-Limiting Voltage Regulation in Distribution Systems. *IEEE Transactions on Power Systems*, *35*(1), 273–283. https://doi.org/10.1109/TPWRS.2019.2933240

Zhou, J., & Cheng, P.-T. (2019). Modulation Methods for 3L-NPC Converter Power Loss Management in STATCOM Application. *IEEE Transactions on Industry Applications*, *55*(5), 4965–4973. https://doi.org/10.1109/TIA.2019.2924407